

University of Alberta

A generalized valence bond basis for the half-filled Hubbard model

by

Christopher B. Graves

A thesis submitted to the Faculty of Graduate Studies and Research
in partial fulfillment of the requirements for the degree of

Master of Science

Department of Physics

©Christopher B. Graves

Fall 2011

Edmonton, Alberta

Permission is hereby granted to the University of Alberta Libraries to reproduce single copies of this thesis and to lend or sell such copies for private, scholarly or scientific research purposes only. Where the thesis is converted to, or otherwise made available in digital form, the University of Alberta will advise potential users of the thesis of these terms.

The author reserves all other publication and other rights in association with the copyright in the thesis and, except as herein before provided, neither the thesis nor any substantial portion thereof may be printed or otherwise reproduced in any material form whatsoever without the author's prior written permission.

Dedication

I dedicate my thesis to God and His Son, Jesus Christ, whom I serve.

Abstract

I present a non-orthogonal and overcomplete set of states that spans the $S_{tot} = 0$ Hilbert subspace for a fermionic system with four possible spin configurations per site, on a half-filled lattice with an even number of sites. This set consists of possible pairing of the spins into three bond types: singlet bonds and positive and negative charge bonds. Although I present the specific case for the half-filled Hubbard model in one-dimension, these sets of states can be trivially extended to higher dimensions. The overlap of these generalized valence bond states form closed loops with properties that are related to operator expectation values in this basis. I verify the correctness of this basis by solving the model via exact diagonalization and comparing with known results. There is evidence of structure in the ground state that may be useful to simulations using variational wave functions.

Acknowledgements

I would like to acknowledge my supervisor for all his help in guiding and directing my research and I am proud to share the title of his first graduate student. I would also like to thank my thesis defense committee members for identifying important issues with my thesis and, in doing so, encouraging me to write a better thesis.

Table of Contents

1 – Introduction.....	1
2 - Valence Bond Basis and the Heisenberg Model.....	12
3 – Generalized Valence Bond Basis.....	19
3.1 – GVB overcompleteness.....	20
3.2 – GVB overlaps.....	22
4 – Solving the Hubbard Model.....	28
4.1 – Update rules	29
4.2 – Matrix elements	30
4.3 – Exact diagonalization.....	33
4.4 – Construction and storage of GVB states	34
4.5 – Test for loop purity	35
5 – Determining Expectation Values	37
5.1 – Structure factor.....	38
5.2 – Charge-density-wave order	39
5.3 – Dimer operator	41
6 – Comparison to Known Models/Methods	44
6.1 – Hubbard model and the occupation basis.....	45
6.2 – Heisenberg model and the VB basis	52
6.3 – Tight-binding model (analytical)	59
7 – Results.....	69
7.1 – Phase diagram	69
7.2 – Ground state structure	77
8 – Conclusion	94
Bibliography	96

Appendix A.....	98
A1 – Commutation Relations.....	98
A1.1 – Summary of commutation relations	98
A1.2 – Work for commutation relations	100
A2 – Linear dependence	102
Appendix B.....	103
B1 – Update rules for Hubbard Hamiltonian	103
B1.1 – Summary of update rules.....	103
B1.2 – Work for update rules.....	104
B2 – Update rules for $\vec{S}_i \cdot \vec{S}_j$	106
B2.1 – Summary of update rules.....	106
B2.2 – Work for update rules.....	106
B3 – Other update rules	108
Appendix C.....	109
C1 – Ground state energy.....	110
C2 – Structure factor.....	111

List of Tables

Table 1 – Sizes of the $S_{tot}^z = 0$ and $S_{tot} = 0$ subsectors for an even number of sites between 2 and 16. 8

Table 2 – List of the update rules involving $\chi_{ij}^{VB\dagger} \chi_{ij}^{VB}$ acting upon states in the VB basis. 18

Table 3 – This table summarizes the update rules when the Hubbard- U term acts on each type of bond of the GVB basis. 29

Table 4 – This table summarizes all update rules when the hopping term acts on a single bond. Under this condition, the hopping term effectively changes the bond type. 29

Table 5 – This table summarizes all update rules when the hopping term acts between bonds. Under this condition, the hopping term rearranges the bonds and changes the bond types. 30

Table 6 – Bond types are represented by integers in the range 0-5. 35

Table 7 – This table lists the update rules for $\vec{S}_i \cdot \vec{S}_j$ acting on and between the different bond types of our GVB basis. 38

Table 8 – This table summarizes the update rules for $(n_i - 1)$ and $(n_i - 1)(n_j - 1)$ 40

List of Figures

Figure 1 – These are examples of common lattices in one and two spatial dimensions: (a) the linear chain, (b) the square lattice, and (c) the triangular lattice.	1
Figure 2 – (a) Classical 1D <i>ferromagnet</i> with all spins <i>aligned</i> and (b) classical 1D <i>antiferromagnet</i> with spins <i>anti-aligned</i> . Spins are either “up” (red) or “down” (blue)....	2
Figure 3 – Assignments of (a) vacancy, (b) spin “up”, (c) spin “down”, and (d) double occupancy for a given site.....	2
Figure 4 – (a) Electron may hop from one site to another. (b) The likelihood that an electron will hop depends on the overlap between the orbitals.....	3
Figure 5 – The virtual hopping process. The end configuration may be the same as original (top right) or the two spins may be switched (bottom right).	4
Figure 6 – A singlet connecting sites i and j is defined as a linear superposition of a spins “up” and “down” on sites i and j (respectively) and spins “down” and “up” on sites i and j (respectively). As a convention, singlet bonds are represented by a solid blue line.	4
Figure 7 – The VB state (b) is a linear superposition of many states in the S^z basis; the S^z state shown (a) is one of these states.	5
Figure 8 – Illustration of the block diagonal nature of the Hubbard model Hilbert space with respect to spin sector.....	6
Figure 9 – A charge bond (represented by a double solid line) connecting sites i and j is defined as a linear superposition of a double occupancy and a vacancy on sites i and j (respectively) and a vacancy and a double occupancy on sites i and j (respectively). A PCB is the addition of the two states and a NCB is the subtraction between the two states. As a convention, I use a double solid line to represent a charge bond, distinguishing the two types of charge bonds by an arrow on the NCB (red) (as these bonds have a sense of “direction,” see Chapter 3) and no arrow on the PCB (green).....	7
Figure 10 – The GVB state (b) is a linear superposition of many states in the occupation basis; the state shown in (a) is one of these states.....	8
Figure 11 – I solved the Hubbard model on the 1D chain with periodic boundary conditions and nearest- and next-nearest-neighbour hopping. Also, I used the zero-based numbering convention with the rightmost lattice site as my starting site.	9
Figure 12 – The triangular lattice (a) is a common example of geometric frustration. Spins prefer to be anti-aligned with nearest-neighbours, but with the triangular lattice not all nearest neighbours can be anti-aligned. When one considers next-nearest-neighbour interactions along with nearest-neighbours (b), not all nearest- and next-nearest-neighbours can be anti-aligned.	10

Figure 13 – The crossing state (left-hand-side) is related to the sum of the non-crossing states (right-hand-side). Note the arrows on the singlet bonds; these arrows come from the sense of direction that VB singlet have (in contrast the GVB singlets do not share this sense of direction, as they are defined using fermion operators). 13

Figure 14 – Example visually showing the overlap between two VB states $|P\rangle$ and $|Q\rangle$, that form a total of five loops (1 – 5). 14

Figure 15 – Single solid (blue) lines represent singlet bonds, double solid (green) lines represent PCBs, and double solid (red) lines represent NCBs. We can clearly see that “crossing” bonds (of similar type, these are the states in the middle) are linearly dependent on states without crossings. Also, note that the charge bond crossings have two linear dependence relations for each crossing. This suggests that restricting ourselves to “non-crossing” states is not enough, we will need one or more rules to further restrict the number of states to obtain the correct counting. 20

Figure 16 – An example of a six-site state with two bonds that cross and a bond being enclosed by another bond. I only use singlet bonds for the example since the concept of *crossing* and *enclosing* does not change with bond type. 21

Figure 17 – Illustration showing how a 4x4 square lattice is reduced to a 1D problem via choosing a numbering scheme. Our example shows a *snake-like* numbering scheme. ... 21

Figure 18 - Same example as Figure 14; however, singlets are defined in terms of fermions instead of bosons, and as a result, the bonds no longer have direction. We expect both methods to be equivalent. 22

Figure 19 – Same bond orientations as Figures 14 and 18, but now some singlet bonds are replaced by PCBs and NCBs and we wish to determine when the overlap is non-zero, and what that non-zero value might be. 23

Figure 20 – As mixed loops gave zero overlap, we replaced the mixed loop (loop 4) with a pure charge bond loop. Now we would like to know if this overlap is non-zero and, if so, what that value might be..... 25

Figure 21 – The block tridiagonal nature of the Hubbard Hamiltonian matrix elements is apparent when the basis states are grouped with respect to the number of charge bonds in the state (i.e. charge sector). The hopping term can either change the number of charge bonds by one or zero. In the figure, I label each block as ‘0’ if all elements in block are zero, ‘U’ if the Hubbard- U term can be non-zero, ‘T’ if the hopping term can be non-zero, or ‘UT’ if both terms can be non-zero. 32

Figure 22 – This diagram illustrates the concept of elevation, how I determined whether a state is “well-formed” or not, and how I determined the location of the bond partner. . 34

Figure 23 – This figure shows a singlet loop with labelling of the *loop* sublattice (ABAB...) along with the traditional sublattice labelling of the underlying lattice (*closed* and *open* circles). 39

Figure 24 – An arbitrary VBC state in 2D with both horizontal and vertical nearest-neighbour singlets is shown in (a). The horizontally-aligned VBC state that is preferred by our dimer order operator $\langle \widehat{D}^2 \rangle$ is shown in (b). The Majumdar-Ghosh chain, shown in (c), is the 1D VBC. 41

Figure 25 – Diagram showing the four cases (a-d) when $\langle Q | (\vec{S}_i \cdot \vec{S}_j) (\vec{S}_k \cdot \vec{S}_l) | P \rangle$ is non-zero. All loops in the diagram (represented by circles) are pure singlet loops. By nature of the problem, indices i and j are linked via $\vec{S}_i \cdot \vec{S}_j$ and k and l are linked via $\vec{S}_k \cdot \vec{S}_l$. I consider these links as “virtual” bonds and these bonds are drawn as dotted grey lines in the figure. 43

Figure 26 – This figure shows that for 6 sites (or any odd $N/2$), the next-nearest-neighbour antiferromagnetic ordering is disrupted through periodic boundary conditions. This is not true for 8 sites (or any even $N/2$). 45

Figure 27 – For each case ($N = 4, 6,$ and 8) there is one cusp where the ground state transitions from the $\uparrow\downarrow\uparrow\downarrow \dots$ antiferromagnetic ordered state (left of cusp, independent on t_2/t_1) to the $\uparrow\uparrow\downarrow\downarrow \dots$ antiferromagnetic ordered state (right of cusp, depends linearly on t_2/t_1). 46

Figure 28 – The cusps are still visible and we begin to see the transition between the two antiferromagnetic states becoming smoother as N and U are increased. We clearly see the discrepancy for $N = 6$ when using the occupation basis (spanning the $S_{tot}^z = 0$ spin sector) and the GVB basis (spanning the $S_{tot} = 0$ spin sector). 46

Figure 29 – As U/t_1 is large now, the ground state energies obtained with either basis are now equal for $N = 6$ 47

Figure 30 – With $U/t_1 = 200$, it is significantly large enough to be considered as the large- U limit and we have complete agreement between the ground state energies using the occupation basis and the GVB basis. Not obvious in this particular plot, there are actually three unique states for $N = 8$ and $U/t_1 = 200$ instead of the two seen at small U (it is seen much more clearly in the staggered magnetization plots). 47

Figure 31 – For $t_2/t_1 < 1$, there is a clear instability issue when using either the occupation or the GVB basis; although, the GVB basis appears to be less affected by this instability. For $t_2/t_1 > 1$, there is no issue whatsoever. 48

Figure 32 – There is no instability issue for any value of t_2/t_1 and $N = 6$. Notice that $S(\pi)$ is larger for $t_2/t_1 < 1$, which corresponds the expectation of $\uparrow\downarrow\uparrow\downarrow \dots$ antiferromagnetic ordering in this region. For $t_2/t_1 > 1$, we expect $\uparrow\uparrow\downarrow\downarrow \dots$

antiferromagnetic ordering; but even with this ordering, half the *nearest-neighbours* are anti-aligned as well, which is why $S(\pi)$ is non-zero in this region. 49

Figure 33 – Similar to $N = 4$, we see an instability again using either basis, but this time for $t_2/t_1 < 1/2$; after which, the instability disappears. 49

Figure 34 – As we saw in the ground state energies for $U/t_1 = 2$ (Figure 28), there is complete agreement for $N = 4$ and 8 and the same discrepancy for $N = 6$ 50

Figure 35 – There is complete agreement seen in the range $0 < t_2/t_1 < 2$ (above which I did not make any measurements) for $N = 4, 6,$ and 8 sites. Notice that, for $N = 8$, there are clearly three different states. 51

Figure 36 – There is complete agreement again for $N = 4, 6,$ and 8. The middle state seen for $N = 8$ is actually the 1D VBC as we will see in Chapters 6.2 and 7. 51

Figure 37 – This is an illustration of how the hopping term t_{ij} affects a pair of singly occupied sites. 53

Figure 38 – This is an illustration of how the exchange term J_{ij} affects a pair of singly occupied sites. The exchange term J_{ij} is conceptually equivalent to acting with the hopping term t_{ij} twice with an energy cost U for creating a doubly occupied site in the process. 53

Figure 39 – The process of virtual hopping can be described with the GVB basis as well. 54

Figure 40 – The ground state energy for 4 sites has one cusp at $J_2/J_1 = 1$ (or $(t_2/t_1)^2 = 1$) separating the nearest-neighbour antiferromagnetically ordered $\uparrow\downarrow\uparrow\downarrow \dots$ state and the next-nearest-neighbour antiferromagnetically ordered $\uparrow\uparrow\downarrow\downarrow \dots$ state (see Figure 43). The “1/2” coefficient in front of the $(t_2/t_1)^2$ term compensates for double counting the next-nearest-neighbours in the $N = 4$ case. With scaling (according to the expression in the figure) the Hubbard ground state energies agree completely with the Heisenberg ground state energies. 55

Figure 41 – For $N = 6$, there is one cusp at $J_2/J_1 = 0.5$ where there is a level crossing and there is complete agreement between the Heisenberg and Hubbard ground state energies. 56

Figure 42 – This figure has two cusps, one at $J_2/J_1 = 0.5$ and the other at $J_2/J_1 = 0.75$. For $0 < J_2/J_1 < 0.5$ the ground state has $\uparrow\downarrow\uparrow\downarrow \dots$ antiferromagnetic ordering and for $J_2/J_1 > 0.75$, the ground state has $\uparrow\uparrow\downarrow\downarrow \dots$ antiferromagnetic ordering. Between the two cusps is when the ground state has the frustrated 1D VBC ordering (see Figure 45). 56

Figure 43 – Other than at the cusp points, there is complete agreement between the spin correlation functions calculated on the ground state of the Heisenberg model and the Hubbard model at $U/t_1 = 200$ 57

Figure 44 – Oddly enough dimer order is dominant for $J_2/J_1 > 0.5$ (with M2D close behind). This is most likely the cause of the increased frustration due to the periodic boundary conditions when next-nearest-neighbour antiferromagnetic interactions are large on odd $N/2$ 1D lattices. 58

Figure 45 – There are three regions in which each of the spin correlation functions dominate. For small J_2/J_1 , M2 ($\uparrow\downarrow\uparrow\downarrow \dots$) order dominates, for large J_2/J_1 , M2D ($\uparrow\uparrow\downarrow\downarrow \dots$) order dominates, and in the frustrated regime in between, the dimer order dominates. ... 58

Figure 46 – The tight-binding energy spectrum is plotted with respect to ‘ ka ’ for five different values of the parameter t_2/t_1 60

Figure 47 – This figure plots the energy levels for the 8 possible k -states when $N = 8$ with respect to t_2/t_1 . Each state can hold two electrons (one spin up and one spin down). 61

Figure 48 – This figure is a plot of the ground state energies per site for the tight-binding-model (TBM) and the Hubbard model (using the GVB basis)..... 62

Figure 49 – The ground state energy of the tight-binding model for $N = 8$ and $N = 100$. The energy is constant with respect to t_2/t_1 for $t_2/t_1 < 0.5$ in the large- N limit, just as it was for $N = 8$. However, for large N and large t_2/t_1 , the slope of the energy is steeper. This suggests 8 sites is a decent approximation (in terms of capturing the ground state properties) for small t_2/t_1 , but not for larger t_2/t_1 63

Figure 50 – Like the 8-site case, when $N = 4$, there is the degeneracy between states $\pm\pi/2$ at the Fermi level for $t_2/t_1 < 1$. It appears that the $(\uparrow\downarrow, 0)$ arrangement (TBM 1) in states $(+\pi/2, -\pi/2)$ agrees with the GVB results (TBM 2 is the staggered magnetization for the arrangement (\uparrow, \downarrow)). Unfortunately, because there definitely is an instability issue with the GVB results (recall that this instability issue is seen with the occupation basis results as well) I cannot state this conclusively. Note that the two degenerate states at the Fermi level is separated by π and I am measuring $S(\pi)$; I believe this relation to be important. 64

Figure 51 – For $N = 6$, there is no instability issue; however, there is a degeneracy between states $\pm\pi/3$ for $t_2/t_1 > 1$ (see Figure 53) but this does not alter the staggered magnetization $S(\pi)$. Note that in this case the degenerate states are separated by $2\pi/3$, not π 65

Figure 52 – We see the instability issue again, but only in the region where we have the $+\pi/2$ and $-\pi/2$ degeneracy at the Fermi level. And again, it appears that the $(\uparrow\downarrow, 0)$ arrangement (TBM 1) is the preferred arrangement. 65

Figure 53 – For $t_2/t_1 < 1$, states $ka = 0$ and $ka = \pm\pi/3$ are filled completely with the six available electrons. For $t_2/t_1 > 1$, states $ka = 0$ and $ka = \pi$ are filled completely, and states $ka = \pm\pi/3$ are half-filled with only two electrons. 66

Figure 54 – For $U/t_1 = 10^{-4}$, there is a clear difference between the GVB results and the TBM results (TBM 1 is the $(\uparrow\downarrow, 0)$ electron arrangement for the degenerate $(+\pi/2, -\pi/2)$ states).....	67
Figure 55 – No change with respect to Figure 51 ($U = 0$ exactly) for $N = 6$	67
Figure 56 – Like the 4-site case, there is a clear shift in the $(+\pi/2, -\pi/2)$ degenerate region, otherwise the plot remains unchanged. The occupation basis shows the same shift as well.	68
Figure 57 – Phase diagram for the ground state of the half-filled Hubbard model when $N = 8$. I divide the phase diagram into three main regions: I, II, and III.	70
Figure 58 – The $\uparrow\downarrow\uparrow\downarrow \dots$ ordering (M2S) is clearly dominant in region I when $U/t_1 = 10^{-4}$, with non-zero $\uparrow\downarrow\uparrow\downarrow \dots$ (M2D) and dimer ordering (D2). In region II, $\uparrow\downarrow\uparrow\downarrow \dots$ is the dominant ordering, but there is still a significant amount of M2S order. This suggests that for small U there are other types of order that the ground state has in region II—in particular I suspect some sort of order pertaining to charge bonds, since U is small (also see Figures 64-66).....	71
Figure 59 – This figure is similar to Figure 58 ($U/t_1 = 10^{-4}$), but D2 begins to surpass M2D in region I.	71
Figure 60 – We begin to see D2 contributing more in the frustrated regime of region II (next to region I).	72
Figure 61 – Region III clearly has $\uparrow\downarrow\uparrow\downarrow \dots$ as its dominant ordering, with little to no M2S and D2 ordering. Region II, between region I and III, clearly has the competing order between M2S and M2D, but now with the dimer order as well.....	72
Figure 62 – With $U/t_1 = 20$, we are very near the large- U limit where we see $\uparrow\downarrow\uparrow\downarrow \dots$ order in region I, $\uparrow\downarrow\uparrow\downarrow \dots$ in region III, and dimer order in region II.....	73
Figure 63 – Very similar behaviour to Figure 62 ($U/t_1 = 20$).....	73
Figure 64 – Singlet bonds always contribute the most to the ground state, except in region II at $U/t_1 = 10^{-4}$, where the contribution from singlets and charge bonds (both PCBs and NCBs) are equal.	74
Figure 65 – For $U/t_1 = 2$, we begin to see an increase in charge bond contribution in region II as t_2/t_1 increases (however, singlet bonds always have over 50% contribution).	75
Figure 66 – With $U/t_1 = 5$, we see a more prominent increase in charge bond contribution with t_2/t_1	75
Figure 67 – Oddly enough, with the introduction of region III, the concavity of the charge bond contribution changes (though I believe the concavity changes back for large	

enough t_2/t_1 , suggesting that at some value of t_2/t_1 there is an inflection point). In region I, we see almost complete suppression of NCB contribution. 76

Figure 68 – There are no discontinuities in the fraction of bond type plots between regions..... 76

Figure 69 – At $U/t_1 = 200$, the charge bonds are completely suppressed in the range $0 < t_2/t_1 < 2$. As I show in Chapter 7.2, the contribution does increase for larger values of t_2/t_1 (see Figure 91). 77

Figure 70 – With each axis with a logarithmic scale, the Heisenberg ground state is nearly linearly dependent on the product of bond lengths. This, in turn, implies that the ground state weights depend on the product of bond lengths according to some power law. 78

Figure 71 – The pure singlet states decay with the product of bond lengths. Note the *asymmetry* with translation of the most contributing state with only nearest-neighbour bonds (upper-left-most labelled state). Also note the translational *symmetry* of the pure NCB state indicated in the figure, as Figures 73 and 74 show translational *asymmetry* in region II..... 79

Figure 72 – Since we know the ground state does not change (in each region) in the tight-binding limit, this figure is exactly the same as Figure 71..... 79

Figure 73 – In region II, we see the translational *asymmetry* between the pure NCB state indicated. Also, the pure PCB state indicated contributes significantly to the ground state, whereas, in region I, it did not contribute at all. Note the change in the pure singlet state weights, the two longer bond states have the same magnitude, with the nearest-neighbour pure singlet state having exactly twice that magnitude..... 80

Figure 74 – The ground state weights are exactly the same as Figure 73, since we are in the same region and in the tight-binding limit. 80

Figure 75 – Even with a small value of U/t_1 , the pure singlet states contribute more (and there is still a similar decay with bond length) than most of the mixed states. Many of the states that have many charge bonds do not contribute nearly as much as when $U/t_1 = 0$ 81

Figure 76 – This state is very similar to the one in the previous figure. This is because we are in the same region (region I). 82

Figure 77 – Notice that the pure charge bond states indicated still significantly contribute to the ground state. This supports Figure 65 where the charge bond contribution increases in region II..... 82

Figure 78 – Despite being in the same region as the previous figure, this state appears quite different than when $t_2/t_1 = 0.75$. For example, the nearest-neighbour pure singlet

state no longer has the largest contribution. This also supports the fact that charge bonds are not as easily suppressed for large t_2/t_1 83

Figure 79 – The contribution of the states with charge bonds are further suppressed as U/t_1 is increased from 2 to 5. We still see, however, that the state with one PCB indicated still contributes a significant amount. 83

Figure 80 – Almost the same as the previous figure (the charge bond states are suppressed a little more, as the pure singlet states contribute a little more). 84

Figure 81 – With $U/t_1 = 5$, we now see more suppression of charge bond states in region II. 84

Figure 82 – As t_2/t_1 is increased from 0.75 to 1.5, the charge bond states contribute more to the ground state. 85

Figure 83 – With $U/t_1 = 20$, we expect almost all the charge bond states to be suppressed by this large on-site interaction. 85

Figure 84 – Again, in region I, we do not much change to the ground state (the charge bond states are a little more suppressed again when changing t_2/t_1 from 0 to 0.25). 86

Figure 85 – This is the first time we take a look at region II in between regions I and III. There is a significant change to the ground state. The Majumdar-Ghosh chain (nearest-neighbour singlets) is nearly the only state that contributes to the ground state. 86

Figure 86 – In region III and at $U/t_1 = 20$, many of the charge bond states are suppressed. Also, the pure singlet states do not decay in the same fashion as region I. 87

Figure 87 – We are now in the Heisenberg limit. We clearly see the full suppression of states with charge bonds as only the pure singlet states contribute to the ground state. ... 87

Figure 88 – Very similar, in shape to the previous figure. 88

Figure 89 – In the frustrated regime of region II, we see that the Majumdar-Ghosh chain is nearly the only contributing state. 88

Figure 90 – In region III and at $t_2/t_1 = 1.5$, we see that most of the charge bond states are sufficiently suppressed. 89

Figure 91 – This figure suggests that even at a large value of $U/t_1 = 200$, it is still very hard to suppress states with charge bonds for very large values of t_2/t_1 89

Figure 92 – With 10 sites, there are 19404 states in the GVB basis, and we can see a nice decay envelope as the product of bond lengths increases. 90

Figure 93 – Both this figure and the last, plotted the ground state weights on the y-axis relative to the ground state weight of the pure singlet state with the longest possible bonds (indicated in the figure). In the tight-binding limit, the pure singlet state with the longest

possible bonds always has the lowest, non-zero contribution to the ground state. This can also be seen in Figures 71 – 74 for $N = 8$ in the same limit. 91

Figure 94 – This is a plot of only the pure singlet state weights. Notice that the pure singlet states follow the nice power law decay even in the tight-binding limit (we already know it will in the Heisenberg limit). 91

Figure 95 – Three examples of states with equivalent weights, but with different bond lengths. States are equivalent for all tested data points. 92

Chapter 1

Introduction

In the simplest models of electrons in a solid, the regular arrangement of constituent atoms is represented by a lattice of sites, and each site is endowed with a single orbital that can accommodate up to two electrons. For example, the three low-dimensional lattices shown in **Figure 1** may be realized in layered or highly anisotropic materials.

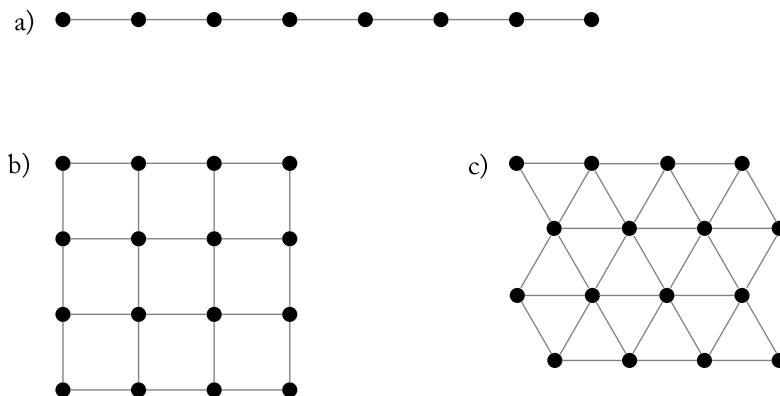


Figure 1 – These are examples of common lattices in one and two spatial dimensions: (a) the linear chain, (b) the square lattice, and (c) the triangular lattice.

The Hubbard, Heisenberg, and Ising models are the simplest, nontrivial lattice models. The Heisenberg [1] and Ising [2] models are used to describe ferromagnetic (**Figure 2a**) and antiferromagnetic (**Figure 2b**) ordering. Both models require a set of states that have exactly one spin per site (corresponding to the situation where one electron is localized at each site and charge fluctuations are quenched) and each spin assigned as an “up” or “down” (these spin assignments are also seen in **Figure 2**). Physically, each spin represents a lone valence electron of the atom with that particular spin configuration. The main and crucial difference between the two models is that the Ising model is a classical spin model (or a quantum one in the limit of strong spin anisotropy along an easy axis) and the Heisenberg model is a quantum spin model.

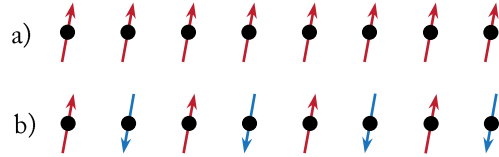


Figure 2 – (a) Classical 1D *ferromagnet* with all spins *aligned* and (b) classical 1D *antiferromagnet* with spins *anti-aligned*. Spins are either “up” (red) or “down” (blue).

The Hubbard model describes the electronic and magnetic properties of a lattice of interest. The Hubbard Hamiltonian consists of a tight-binding term augmented by local Coulomb repulsion and requires one to work with a more general set of states than was needed in the case of the Heisenberg and Ising models. The Hubbard model relaxes the condition of exactly one electron per site, allowing from zero up to two electrons on a single site with the condition that these two electrons must have opposite spin (i.e. one electron is spin “up” and other is spin “down”). This is a requirement of the Pauli exclusion principle, which states that electrons with the same spin may not be in the same quantum state. As a result there are four possible spin configurations for a given site (**Figure 3**).



Figure 3 – Assignments of (a) vacancy, (b) spin “up”, (c) spin “down”, and (d) double occupancy for a given site.

The pure tight-binding model is a free electron model in the sense that it does not include Coulomb interactions between electrons. It does include Pauli exclusion principle, which is arguably a fundamental electron-electron interaction; in this sense, the electron is not completely free. Nevertheless, this model describes freely-wandering (i.e. itinerant) electrons as is the case with simple metals. This model describes electron motion by invoking the idea of electrons “hopping” between atoms. Physically, electrons can “hop” between atoms because of quantum tunnelling [3][4]. And the probability that an electron will “hop” from its atomic orbital to an atomic orbital of another atom is a consequence of the overlap between the two atomic orbitals. As a result, hopping between nearest-neighbour lattice sites dominates (as the atomic orbitals between these two atoms usually have the largest overlap). Sometimes nearest-neighbour and next-nearest-neighbour hopping are allowed if the overlap between atomic orbitals between next-nearest-neighbours is large enough to consider. Usually, there is no need to add hopping between lattice sites that are separated any more than next-nearest-neighbours, since the hopping amplitudes drop off exponentially with distance. The following figure illustrates the concept of hopping.

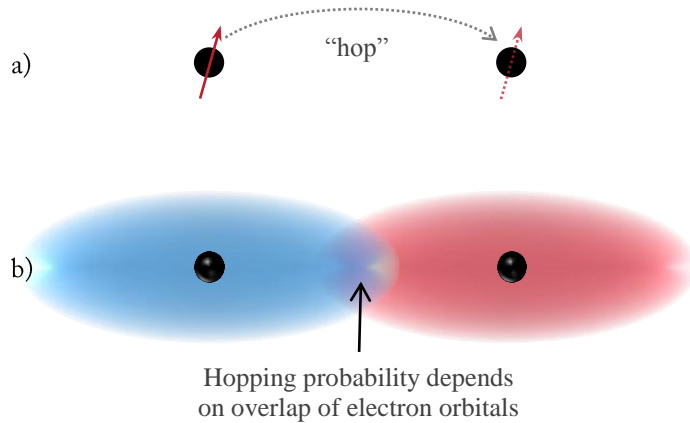


Figure 4 – (a) Electron may hop from one site to another. (b) The likelihood that an electron will hop depends on the overlap between the orbitals.

The Hubbard model is the tight-binding model with an additional term that captures the Coulomb repulsion between electrons. As a result of this electron-electron interaction term, the Hubbard model is what we call a strongly correlated electron model.

In the simplest case, the Coulomb repulsion term has an associated energy cost of U for every doubly occupied site (i.e. spin up and down electrons on same site) in a state. The bare Coulomb interaction is long ranged and inversely proportional to the distance between charged particles (in our case electrons). However, because of screening effects from all other charges in the system, valence electrons on different atoms effectively do not “see” each other [1][5]. Hence, we may keep only the on-site Coulomb term as an appropriate approximation.

The on-site Coulomb term favours localized electronic states and competes directly with the kinetic energy term in the Hamiltonian. This is seen most clearly at large U for a half-filled system. A system that is half-filled has an equal number of electrons and lattice sites. Recall that there can be a maximum of two electrons per site (of opposite spin); so a system that is fully filled has $2N$ electrons (where N is defined as the number of lattice sites). At large U , this on-site term favours systems with one electron per site. If an electron wished to hop to another site, it would create a double occupancy, which is energetically unfavourable because of the large energy cost U .

In the limit when U is the largest energy scale by far, the half-filled Hubbard model has the Heisenberg model as its low-energy effective theory [1][5]; the electrons behave as fixed local magnetic moments, interacting with their neighbour via exchange-interactions. These exchange interactions are viewed as electrons “virtually” hopping from its site to another, which is already occupied by an electron of opposite spin (recall that the Heisenberg model requires the set of states with *exactly* one electron per site); then one of the two electrons on this doubly occupied site will hop back to the vacant site. The process is considered “virtual” since the electron in motion will never linger at another

site because of the infinite energy cost of creating a double occupancy. **Figure 5** illustrates the concept of virtual hopping.

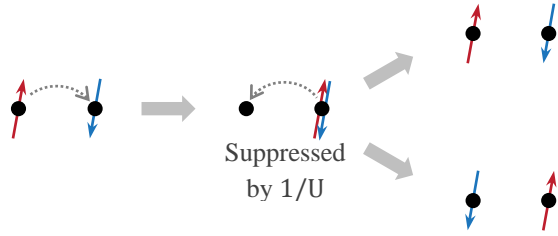


Figure 5 – The virtual hopping process. The end configuration may be the same as original (top right) or the two spins may be switched (bottom right).

So far, we have been working implicitly in the so-called occupation basis—representing each state as an assignment of “vacant”, spin “up” or “down”, or “doubly occupied” to a given lattice site (**Figure 3**). There is another way of representing a state, which is with *bonds* between lattice sites. In the 1930s, Rumer and Pauling [6][7] proposed a bond basis (see next paragraph for more information about the definition of a basis; for now, consider it as a set of states) that was named the valence bond basis. This basis was applied to the Heisenberg model, which only uses the assignments of spin “up” or “down”. The valence bond (VB) basis required one to work in a system with an *even* number of sites and consisted of “pairing” a spin “up” with a spin “down” into a singlet; hence, requires one to also work with a system that has an equal number of “up” spins as “down” spins. A singlet is a special linear superposition (**Figure 6**) of the spin “up” and “down” electrons.

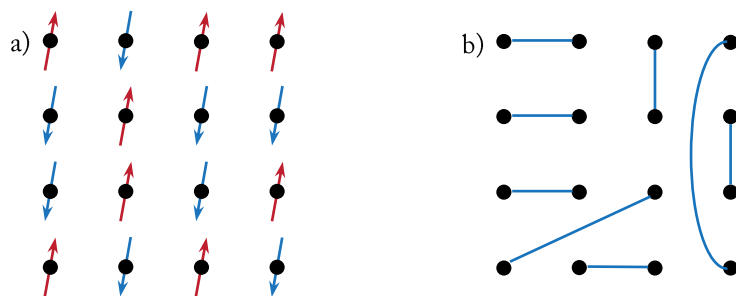


Figure 6 – A singlet connecting sites i and j is defined as a linear superposition of a spins “up” and “down” on sites i and j (respectively) and spins “down” and “up” on sites i and j (respectively). As a convention, singlet bonds are represented by a solid blue line.

For our purposes, a basis is a set of states that, together, contain all possible configurations. Hence, the assignment of a “vacancy”, spin “up” or “down”, or “double occupancy” to each lattice site is a state. If we consider all possible configurations, these states form a basis that is called the *occupation* basis. The subset of states in the occupation basis that contain a spin “up” or a spin “down” but no vacancies or double occupancies is a suitable basis for the Heisenberg model. This basis, containing all possible configurations of spin “up” and “down”, is referred to as the S^z basis, since $|\uparrow\rangle$ and $|\downarrow\rangle$ are the eigenstates of the S^z operator.

There are two main properties that a basis can have that we are interested in: *orthogonality* and *completeness*. A basis that is orthogonal has the convenient property

that the overlap between distinct states in the basis is zero; otherwise the basis is considered *non-orthogonal*. A complete basis is one in which each state in the basis is *linearly independent* of all other states in the basis, and the number of states is equal to the dimension of the Hilbert space. A state that is linearly independent of other states *cannot* be written as a linear superposition of those states. If a basis spans the Hilbert space but has states that are linearly dependent (opposite of linearly independent) on other states, then this basis is referred to as *overcomplete*. The occupation basis and the S^z basis are both orthogonal and complete. The valence bond basis is non-orthogonal (with the special property that *every* two states in the basis have a non-zero overlap) and overcomplete. Fortunately, a subset of the VB basis that is complete can be formed if we choose to keep only the “non-crossing” VB states [6] (“non-crossing” is defined and explained in detail in [Chapter 2](#)). [Figure 7](#) shows an arbitrary state in the S^z basis and a similar state in the VB basis.



[Figure 7](#) – The VB state (b) is a linear superposition of many states in the S^z basis; the S^z state shown (a) is one of these states.

The occupation basis without any restrictions spans the full Hilbert space of the system. The Hubbard model is *block diagonal* in this representation with respect to the z component of the total spin (See [Figure 8](#)). Spin is an angular momentum-like quantity; and therefore, is a vector with x -, y -, and z -components, represented by

$$\vec{S} = S^x \hat{x} + S^y \hat{y} + S^z \hat{z}.$$

The “hat” over the x , y , and z indicates that they are unit vectors. Spins are, by convention, represented by the z -component of their spin S^z as “up,” if $S^z = +\hbar/2$, or “down,” if $S^z = -\hbar/2$ (for simplicity, \hbar is usually set to one). Thus, the total spin in the z -direction (denoted S_{tot}^z), when there are multiple spins, can be written as a sum over every spin in a state,

$$S_{tot}^z = \sum_i S_i^z$$

where i represents an index for the lattice sites. Commonly (especially when working with the occupation or S^z basis), the spin sectors are divided into the possible values of S_{tot}^z . An example of a common spin sector is when we choose the set of states with an equal number of spins “up” and “down;” these states have a total spin $S_{tot}^z = 0$. If we

select one of these states and flip any spin from down to up, then the new state would have a total spin of $S_{tot}^z = 1$. The various spin sectors (having quantum numbers $S_{tot}^z = 0, 1, 2, \dots, N/2$ where N is the even number of lattice sites) are *independent* for the Hubbard model, as there is no possible way that a state in one spin sector can change into a state in another spin sector via the hopping term (the on-site interaction term does not ever change the state, so we do not need to consider it). As a result, one can solve the Hubbard model in each spin sector independently.

$S_{tot}^z = 0$	0	0		0
0	$S_{tot}^z = 1$	0	...	0
0	0	$S_{tot}^z = 2$		0
	⋮		⋱	0
0	0	0	0	$S_{tot}^z = \frac{N}{2}$

Figure 8 – Illustration of the block diagonal nature of the Hubbard model Hilbert space with respect to spin sector.

There are other spin sectors that one could consider; specifically, sectors with different values of total spin (denoted S_{tot}) may also be independently solved. The occupation basis and S^z basis cannot be trivially restricted to span these sectors. In fact, to restrict the S^z basis so that it may span the $S_{tot} = 0$ sector is to transform this basis into the VB basis. The valence bond basis does not span the full Hilbert space, only the $S_{tot} = 0$ sector of the Hilbert space. The $S_{tot} = 0$ spin sector contains the ground state of the Heisenberg model [8][9], the ground state being the lowest energy state that the system prefers to be in. This, in turn, implies that the ground state is also in the $S_{tot}^z = 0$ spin sector. The main advantage of working in the $S_{tot} = 0$ (or singlet) sector is that the size of this sector is smaller than the $S_{tot}^z = 0$ sector.

The main advantage of using the VB basis comes from introducing the notion of a “bond” between lattice sites, as a bond has spatial extent (e.g. a length) associated with it. Physically, the notion of a bond is useful as long bonds imply long-range correlations between the two electrons (one on each of the sites that the bond connects), and short bonds imply short-range correlations. In 1988, a variational method was proposed by Liang, Doucot, and Anderson [10] that uses a singlet product wave function for the square lattice Heisenberg model, in which the weights associated with each valence bond

configuration depend only on the bond lengths. In 2009, Beach [11] developed a master equation technique for computing the bond amplitudes. The schemes developed by [10] and [11] began to break down in the presence of frustrating interactions (the concept of frustration is explained later in this chapter and is illustrated in Figure 12). They operate in a domain only slightly less restricted than quantum Monte Carlo.

Since the Heisenberg model is a special case of the Hubbard model (infinite- U limit at half-filling), one would suspect that the valence bond basis used with the Heisenberg model may be extended or generalized in some way to span the $S_{tot} = 0$ sector of the Hubbard model. The generalization of the valence bond basis to create a new bond basis for the half-filled Hubbard model is the core of what this thesis is about. Singlet bonds in the VB basis connect *singly occupied* sites and fully span the $S_{tot} = 0$ sector (for the Heisenberg model). A natural extension to include *doubly occupied* and *vacant* sites would be to include a new bond type that connects a double occupancy with a vacancy. This new bond type is called a charge bond. Upon examining how the hopping term affects singlet and charge bonds in a state (see Chapter 4.1), it turns out that we will need to have two species of charge bonds: labelled *positive* and *negative* charge bonds, PCBs and NCBs respectively (see Figure 9); these correspond to symmetric and antisymmetric linear combinations.

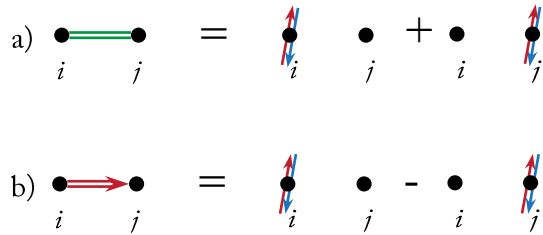


Figure 9 – A charge bond (represented by a double solid line) connecting sites i and j is defined as a linear superposition of a double occupancy and a vacancy on sites i and j (respectively) and a vacancy and a double occupancy on sites i and j (respectively). A PCB is the addition of the two states and a NCB is the subtraction between the two states. As a convention, I use a double solid line to represent a charge bond, distinguishing the two types of charge bonds by an arrow on the NCB (red) (as these bonds have a sense of “direction,” see Chapter 3) and no arrow on the PCB (green).

With these three bond types (singlet, positive and negative charge bonds), I constructed a basis that spans the singlet ($S_{tot} = 0$) sector of the Hilbert space for the Hubbard model (see Table 1 for a comparison of the sizes of the $S_{tot} = 0$ and $S_{tot}^z = 0$ sectors). I call this basis the generalized valence bond (GVB) basis, and it consists of states with all possible bond configurations and all bond varieties (see Figure 10 for a comparison between an occupation basis state and a GVB basis state). Like the valence bond basis, the GVB basis is overcomplete and non-orthogonal, but a subset can be chosen that is

complete (see [Chapter 3.1](#)). Also, upon analyzing the ground state of the Hubbard model (see [Chapter 7.2](#)), there appears to be a dependence on bond lengths, similar to what is seen with the VB basis and the Heisenberg model. This dependence is, however, non-trivial and likely depends on other factors, such as bond type, number of charge bonds, and crossing states (as the complete GVB basis may have singlets crossing with charge bonds). Nevertheless, the dependence is not well understood and requires more research to determine if trial wave functions could be constructed that take advantage of this dependence.

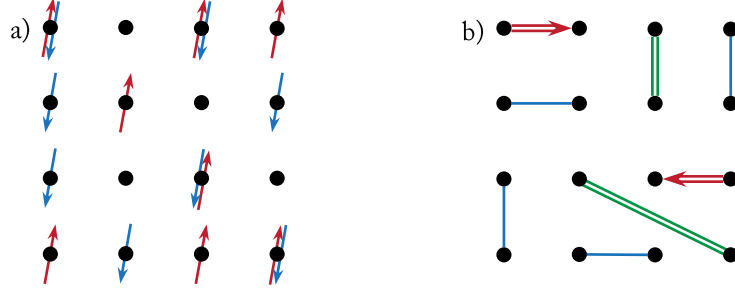


Figure 10 – The GVB state (b) is a linear superposition of many states in the occupation basis; the state shown in (a) is one of these states.

Table 1 – Sizes of the $S_{tot}^z = 0$ and $S_{tot} = 0$ subsectors for an even number of sites between 2 and 16.

N	$D_1 (S_{tot}^z = 0)$	$D_2 (S_{tot} = 0)$	D_2/D_1
2	4	3	0.7500
4	36	20	0.5556
6	400	175	0.4375
8	4900	1764	0.3600
10	63504	19404	0.3056
12	853776	226512	0.2653
14	11778624	2760615	0.2344
16	165636900	34763300	0.2099

$$D_1 = \binom{N}{N/2}^2 = \frac{(N!)^2}{((N/2)!)^4}$$

$$D_2 = \frac{(N+2)^2((N+1)!)^2}{4(N+1)((N/2+1)!)^4}$$

$$\frac{D_2}{D_1} = \frac{4(N+1)}{(N+2)^2} \sim \frac{4}{N} \text{ for large } N$$

The size of the $S_{tot}^z = 0$ sector (D_1) for the half-filled Hubbard model can be determined by counting the number of total possible combinations of assigning vacancies, spins “up” and “down”, and double occupancies on each lattice site, with the constraint that the system is half-filled and there is an equal number of spin “up” and spin “down” electrons.

The size of the $S_{tot} = 0$ sector (D_2) can be determined in a series of steps. First is to count the total number of possible configurations of $N/2$ double occupancies and $N/2$ vacancies. Then replace a double occupancy and a vacancy with a singlet bond and count the total number of possible configurations. Then replace another double occupancy and vacancy with a singlet bond (there are now two singlet bonds) and count the number of possible configurations with the added constraint that singlet bonds cannot cross. Continue to remove one double occupancy and one vacancy and add a singlet in its place and count the number of possible configurations (remembering that singlet bonds cannot cross each other) until there are only singlet bonds in the state. Add each number of

possible configurations to obtain D_2 . Note that it is not necessary to define charge bonds in order to span the $S_{tot} = 0$ sector; it is the singlet bonds that are necessary.

As our basis is non-orthogonal, we need to be able to construct a set of rules that allow us to be able to determine the value of the overlap between states. Also, in order to solve the model, we need to be able to construct a set of rules that tells us how the Hubbard Hamiltonian affects a GVB state. I successfully constructed rules for these two important cases as well as many other rules for other cases.

In order to verify and test the rules of the GVB basis, I used exact diagonalization to determine all the eigenvalues (physically, these are the quantized energy levels of the system) and the eigenvectors for the system. I compared the ground state energies, as well as ground state staggered magnetization with results obtained using the occupation basis with exact diagonalization. Exact diagonalization requires generating the Hamiltonian and overlap matrices (these matrices store all possible overlap values between states in our complete basis) that, in turn, are numerically diagonalized using LAPACK via a generalized eigenvalue solver (see [Chapter 4](#) for more details on exact diagonalization). Unfortunately, exact diagonalization scales as $O(D^3)$ [12], where D is the size of the working Hilbert space (this is a good reason why one would want to use a basis that spans the smaller $S_{tot} = 0$ over the $S_{tot}^Z = 0$). This, along with the exponential increase in D with system size N (as the number of states is a combinatorial problem), limits us to small lattice sizes of approximately 8 or 10 sites. For this reason, I restrict myself to one-dimension, despite the fact that our basis may be used in arbitrary dimensions (as any higher dimensional system is mapped onto a non-trivial one-dimensional system). I considered the *frustrated* Hubbard model with hopping between nearest- and next-nearest-neighbours (this model is referred to in literature as the t_1 - t_2 Hubbard model). Unlike the model with nearest-neighbour hopping only (which is amenable to a Bethe Ansatz treatment), this model cannot be solved analytically. [Figure 11](#) shows a typical one-dimensional chain, along with the definition for nearest- and next-nearest-neighbours, my lattice labelling scheme and periodic boundary conditions.

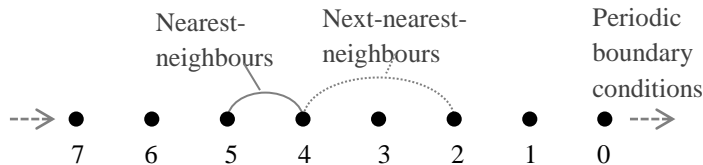


Figure 11 – I solved the Hubbard model on the 1D chain with periodic boundary conditions and nearest- and next-nearest-neighbour hopping. Also, I used the zero-based numbering convention with the rightmost lattice site as my starting site.

There are two types of frustration that can occur in models of this kind: frustration introduced by the natural geometry of the lattice, or frustration introduced by a

competition between interactions (normally between nearest- and next-nearest-neighbour interactions). **Figure 12** provides an illustration of the two types of frustration.

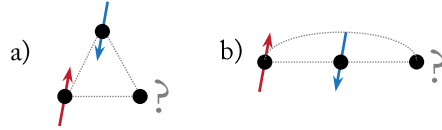


Figure 12 – The triangular lattice (a) is a common example of geometric frustration. Spins prefer to be anti-aligned with nearest-neighbours, but with the triangular lattice not all nearest neighbours can be anti-aligned. When one considers next-nearest-neighbour interactions along with nearest-neighbours (b), not all nearest- and next-nearest-neighbours can be anti-aligned.

Since the size of the Hilbert space limits exact diagonalization to small system sizes, there has been considerable effort in developing approximate methods in order to treat larger lattices (and, in turn, consider higher dimensional systems).

A considerably powerful method to solve one-dimensional Heisenberg and Hubbard models is the density matrix renormalization group (DMRG). This method was developed in the 1990s by White [13][14] and was originally tested using the Heisenberg model. The construction is recursive but was later shown to be variational within the class of matrix product states. The method was later extended to 2D in 2001 by Xiang et al. [15] and tested with the Heisenberg model, where they were able to go up to a lattice size of 12x12. Nonetheless, it is only well-behaved in 1D, or close to, as DMRG has also been shown to work well for ladder lattices [16]. Exact diagonalization has no such restriction.

As DMRG is exact in one dimension, dynamical mean-field theory (DMFT) is exact in infinite spatial dimensions, or infinite lattice coordination¹ [17] because it is a local impurity solver. Many lattices in three-dimensions have a large coordination number, such as the face-centred cubic, which has 12 (the simple cubic has 6, and the body-centred cubic has 8). For this reason, DMFT's most practical applications are 3D crystals with large coordination numbers [18]. DMFT provides the most insight into the electronic structure of a material [19], such as a Mott metal-insulator transition [20].

A common method to obtain a good approximation for the lowest-lying eigenvalues and eigenvectors of a real symmetric matrix is the method developed by Lanczos in 1950 [21].

¹ The coordination number of a Bravais lattice is the number of nearest-neighbours of each site. The regularity of a Bravais lattice ensures that each site has the same number of nearest-neighbours.

This method tridiagonalizes² the matrix and is particularly useful for sparse matrices [22][23]. Once tridiagonalized, the matrix is then diagonalized using the appropriate routine in LAPACK, which, today, can scale up to $O(D^2)$ [12]. The Lanczos method has been found to be more useful when determining the ground state of the Heisenberg and Hubbard models than using exact diagonalization with the traditional occupation bases [24][25], as Lanczos can handle a few more lattice sites.

The goal of this thesis is to show that my new generalized valence bond basis, which spans the singlet sector of the Hilbert space, gives the correct ground state through the use of exact diagonalization. In doing this, I show that the overlap and update rules are correct and can then be used in methods other than exact diagonalization; perhaps some variational techniques that take advantage of the ground state's dependence on bond length. I determined that our ground state was correct by successfully comparing my results with results from the following three models: the Hubbard model, solved through exact diagonalization using the occupation basis, the Heisenberg model, solved through exact diagonalization using the valence bond basis, and the tight-binding model, solved analytically in the micro-canonical ensemble. A phase diagram for the Hubbard model, for 8 sites, is shown, determined from calculating the staggered magnetization on the ground state. I also show the existence of a correlation of ground state weights and bond length (and bond type).

This thesis is organized as follows. In **Chapter 2** I discuss the properties of the valence bond basis and the Heisenberg model. Then I introduce my new generalized valence bond basis for the half-filled Hubbard model in **Chapter 3**. I explain how to deal with the overcomplete nature of the GVB basis and how to determine the overlaps between two GVB states. In **Chapter 4** I go into detail about how to solve the Hubbard model using the GVB basis, including the update rules needed to determine the Hamiltonian matrix element overlaps. In this chapter I also provide details about the numerical aspects to solving the Hubbard model through exact diagonalization. The following chapter (**Chapter 5**) I present details about computing observable expectation values (such as structure factor, dimer order, and charge-density-wave order) on the ground state. In doing this I provide the update rules needed to compute these observables. In **Chapter 6** I present my results with the purpose of comparing them with results of other models. First I compare it to the Hubbard model results obtained using the traditional occupation basis. Next I compare my results in the limit of large U with results from the Heisenberg model using the VB basis. Finally, in this chapter, I compare my results when $U = 0$ with the tight-binding model analytically solved in the micro-canonical ensemble. In **Chapter 7** I present results for 8 sites, such as the phase diagram and how I obtained the phase diagram. I also present results demonstrating the existence of a correlation between the ground state weights and the bond lengths and bond type. We then conclude in **Chapter 8**.

² A tridiagonal matrix is one with non-zero values along the main diagonal and the first diagonals above and below the main diagonal.

Chapter 2

Valence Bond Basis and the Heisenberg Model

As described in the first chapter, the VB basis consists of all possible pairings (forming bonds) of a spin up electron (on one site) and a spin down electron (on another site) into a singlet. Singlet creation (χ_{ij}^\dagger) and annihilation (χ_{ij}) operators are defined such that, when acting on a state, they create or annihilate a singlet on sites i and j [26]. Due to the nature of the Heisenberg problem and the concept of the bond basis, these singlet creation and annihilation operators may be defined in terms of *boson* creation ($b_{i\sigma}^\dagger$) or annihilation ($b_{i\sigma}$) operators (i represents the lattice site, and σ represents the spin), despite the problem inherently dealing with *fermions* (i.e. electrons) [26], which would normally require the use of fermion creation ($c_{i\sigma}^\dagger$) and annihilation ($c_{i\sigma}$) operators. At a physical level, fermions differ from bosons because fermions have half-integer spin (i.e. $\frac{1}{2}, \frac{3}{2}, \frac{5}{2}, \dots$) and are required to obey Pauli exclusion principle [27]; whereas, bosons have integer spin (i.e. 1, 2, 3...) and are not required to obey Pauli exclusion principle [27]. At a mathematical level, fermion operators anticommute ($\{c_{i\sigma}^\dagger, c_{j\sigma'}\} = \delta_{ij}\delta_{\sigma\sigma'}$), whereas bosons commute ($[b_{i\sigma}^\dagger, b_{j\sigma'}] = \delta_{ij}\delta_{\sigma\sigma'}$) [27]. In the valence bond basis, the singlet operators are usually defined in terms of boson operators for simplicity; in doing so, the electrons are treated as pseudo-*bosons* that carry spin-1/2 and obey Pauli exclusion principle. In general, it is easier to deal with operators that commute than those that anticommute. The singlet creation and annihilation operators of the valence bond basis are defined as

$$\chi_{ij}^{VB\dagger} \equiv \frac{1}{\sqrt{2}}(b_{i\uparrow}^\dagger b_{j\downarrow}^\dagger - b_{i\downarrow}^\dagger b_{j\uparrow}^\dagger)$$
$$\chi_{ji}^{VB} \equiv \frac{1}{\sqrt{2}}(b_{j\downarrow} b_{i\uparrow} - b_{j\uparrow} b_{i\downarrow})$$

Note that the VB singlet has a sense of “direction” associated with it, as a negative sign is introduced when the lattice indices are swapped (i.e. $\chi_{ij}^{VB\dagger} = -\chi_{ji}^{VB\dagger}$).

A VB state is defined as the product of all the singlet bonds that make up the state,

$$|VB\rangle = \left(\prod_{ij} \chi_{ij}^{VB\dagger} \right) |vac\rangle$$

with each site label (i, j) appearing only once (as a single site cannot have multiple bonds connecting to it), and where $|vac\rangle$ is the quantum vacuum state with no electrons.

With the VB basis being overcomplete (i.e. too many states), some states in the basis are linearly dependent on others [28]. It is often desirable, and sometimes necessary, to work with a set of states that is complete. For example, exact diagonalization cannot be carried out unless the working basis is complete. VB states that contain a singlet bond crossing another singlet bond are eliminated to obtain a subset that holds no linear dependencies [26]. At the level of two bonds, the crossing state can be written as a linear superposition of two non-crossing states (Figure 13).

$$-\chi_{ik}^{VB\dagger} \chi_{lj}^{VB\dagger} = \chi_{il}^{VB\dagger} \chi_{jk}^{VB\dagger} + \chi_{ij}^{VB\dagger} \chi_{kl}^{VB\dagger}$$

Figure 13 – The crossing state (left-hand-side) is related to the sum of the non-crossing states (right-hand-side). Note the arrows on the singlet bonds; these arrows come from the sense of direction that VB singlet have (in contrast the GVB singlets do not share this sense of direction, as they are defined using fermion operators).

As every two states in the VB basis has a non-zero overlap, it is useful to develop a set of rules to determine the value of the overlap. The concept of a bond basis introduces an alternate way of looking at the overlaps that is not obvious in a basis that uses representations of spin up and down like the occupation basis. If we pictorially overlay two bond states (Figure 14), their bonds join together to form *loops*.

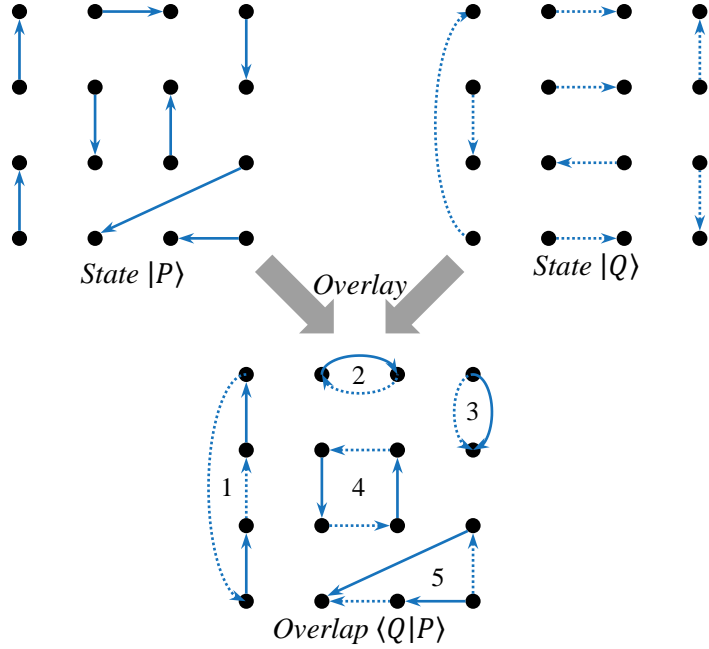


Figure 14 – Example visually showing the overlap between two VB states $|P\rangle$ and $|Q\rangle$, that form a total of five loops (1 – 5).

As shown in **Figure 14**, when two arbitrary VB states $|P\rangle$ and $|Q\rangle$ are overlaid, they form loops (the number of loops formed can range from 1 to $N/2$). In our example, the overlap forms five loops (labelled 1 – 5). It is important to note that the directions of the singlet bonds in state $|Q\rangle$ switch when the transformation $|Q\rangle \rightarrow \langle Q|$ is applied in order to determine the overlap $\langle Q|P\rangle$.

The magnitude of an overlap is related to the size of each loop. The size of a loop depends on the number of bonds that make up the loop. In our example, loops 1, 4, and 5 are of size *two*, since each contain four bonds ($size \equiv (number\ of\ bonds)/2$) and loops 2 and 3 are of size *one*. Each loop contributes a magnitude of 2^{1-size} , these factors of $1/2$ come from the normalization factors $1/\sqrt{2}$ for every singlet. When considering the loops collectively, the magnitude of the overlap $|\langle Q|P\rangle|$ is related to the total number of loops ($N_{\mathcal{L}}$) and total number of bonds ($N/2$) [26] and is expressed as

$$|\langle Q|P\rangle| = 2^{N_{\mathcal{L}} - N/2}.$$

The overall sign of the overlap depends on the directional *alignment* of the VB singlet bonds in a particular loop. A negative sign is obtained every time the direction of a singlet bond is switched so that it may be aligned with the direction of the other singlet bonds in the loop [26]. Our example in **Figure 14** shows loops 1, 2, and 4 already aligned; therefore, there is an overall positive sign contributed by these loops. Loops 3 and 5 have unaligned bonds: loop 3 has one unaligned bond, and loop 5 has two unaligned bonds. As a result, loop 3 contributes an overall negative sign (odd number of unaligned bonds) and loop 5 contributes an overall positive sign (even number of

unaligned bonds). Considering all five loops in the overlap, there is an overall negative sign for the overlap; thus for our example,

$$\langle Q|P\rangle = -2^{N_G - N/2} = -2^{5-8} = -\frac{1}{8}.$$

Since a VB state is written as a product of singlets ($\chi_{ij}^{VB\dagger}$), the overlap $\langle Q|P\rangle$ is written as

$$\langle Q|P\rangle = \langle vac|\chi_{iN,jQN}^{VB} \cdots \chi_{i2,jQ2}^{VB} \chi_{i1,jQ1}^{VB} \chi_{i1,jP1}^{VB\dagger} \chi_{i2,jP2}^{VB\dagger} \cdots \chi_{iN,jPN}^{VB\dagger}|vac\rangle.$$

In order to determine the overlap, it is useful to know the commutation relations for the singlet creation and annihilation operators. For VB singlets, the following commutation rules,

$$[\chi_{ij}^{VB}, \chi_{kl}^{VB}] = 0$$

$$[\chi_{ij}^{VB\dagger}, \chi_{kl}^{VB\dagger}] = 0$$

$$[\chi_{ij}^{VB}, \chi_{kl}^{VB\dagger}] = 0 \quad \text{if } (i \neq k \text{ and } j \neq l) \text{ or } (i \neq l \text{ and } j \neq k)$$

allow singlet creation and annihilation operators to be shuffled past one another, so long as they do not share any indices in common. When indices are shared between creation and annihilation operators, the following commutation rules are used [26] (note that these rules act on a vacuum state).

$$[\chi_{ji}^{VB}, \chi_{ij}^{VB\dagger}]|vac\rangle = |vac\rangle$$

$$[\chi_{ji}^{VB}, \chi_{kj}^{VB\dagger} \chi_{il}^{VB\dagger}]|vac\rangle = \frac{1}{2} \chi_{kl}^{VB\dagger} |vac\rangle$$

A decimation scheme can be used to show that the overlap depends on the number of loops [26].

For an example, consider the two states $|P\rangle$ and $|Q\rangle$ from **Figure 14**. These states written in terms of VB singlet creation operators are (a snake-like numbering scheme is used and talked about in **Chapter 3.1** and **Figure 17**):

$$|P\rangle = \chi_{0,7}^{VB\dagger} \chi_{4,1}^{VB\dagger} \chi_{3,2}^{VB\dagger} \chi_{5,10}^{VB\dagger} \chi_{9,6}^{VB\dagger} \chi_{8,15}^{VB\dagger} \chi_{12,11}^{VB\dagger} \chi_{14,13}^{VB\dagger} |vac\rangle$$

$$|Q\rangle = \chi_{0,15}^{VB\dagger} \chi_{1,2}^{VB\dagger} \chi_{4,3}^{VB\dagger} \chi_{5,6}^{VB\dagger} \chi_{8,7}^{VB\dagger} \chi_{9,10}^{VB\dagger} \chi_{11,12}^{VB\dagger} \chi_{14,13}^{VB\dagger} |vac\rangle.$$

The overlap $\langle Q|P\rangle$ is then written as,

$$\begin{aligned} \langle Q|P\rangle &= \langle vac|(\chi_{13,14}^{VB} \chi_{12,11}^{VB} \chi_{10,9}^{VB} \chi_{7,8}^{VB} \chi_{6,5}^{VB} \chi_{3,4}^{VB} \chi_{2,1}^{VB} \chi_{15,0}^{VB})(\chi_{0,7}^{VB\dagger} \chi_{4,1}^{VB\dagger} \chi_{3,2}^{VB\dagger} \chi_{5,10}^{VB\dagger} \chi_{9,6}^{VB\dagger} \chi_{8,15}^{VB\dagger} \chi_{12,11}^{VB\dagger} \chi_{14,13}^{VB\dagger})|vac\rangle. \end{aligned}$$

We can always shuffle the singlet operators around (since operators that do not share indices commute) so that the singlet operators are grouped into groups corresponding to the loops (we organize it so that the loop labelled 1 is on the far right, then 2, 3, 4 and loop 5 on the far left).

$$\begin{aligned}
& \langle Q|P\rangle \\
&= \langle vac | (\chi_{3,4}^{VB} \chi_{2,1}^{VB} \chi_{4,1}^{VB\dagger} \chi_{3,2}^{VB\dagger}) (\chi_{10,9}^{VB} \chi_{6,5}^{VB} \chi_{5,10}^{VB\dagger} \chi_{9,6}^{VB\dagger}) (\chi_{12,11}^{VB} \chi_{12,11}^{VB\dagger}) (\chi_{13,14}^{VB} \chi_{14,13}^{VB\dagger}) (\chi_{7,8}^{VB} \chi_{15,0}^{VB} \chi_{0,7}^{VB\dagger} \chi_{8,15}^{VB\dagger}) | vac \rangle \\
&= \langle vac | (\chi_{3,4}^{VB} \chi_{2,1}^{VB} \chi_{4,1}^{VB\dagger} \chi_{3,2}^{VB\dagger}) (\chi_{10,9}^{VB} \chi_{6,5}^{VB} \chi_{5,10}^{VB\dagger} \chi_{9,6}^{VB\dagger}) (\chi_{12,11}^{VB} \chi_{12,11}^{VB\dagger}) (\chi_{13,14}^{VB} \chi_{14,13}^{VB\dagger}) \left(\chi_{7,8}^{VB} \left(\frac{1}{2} \chi_{8,7}^{VB\dagger} \right) \right) | vac \rangle \\
&= \langle vac | (\chi_{3,4}^{VB} \chi_{2,1}^{VB} \chi_{4,1}^{VB\dagger} \chi_{3,2}^{VB\dagger}) (\chi_{10,9}^{VB} \chi_{6,5}^{VB} \chi_{5,10}^{VB\dagger} \chi_{9,6}^{VB\dagger}) (\chi_{12,11}^{VB} \chi_{12,11}^{VB\dagger}) (\chi_{13,14}^{VB} \chi_{14,13}^{VB\dagger}) \left(\frac{1}{2} \cdot 1 \right) | vac \rangle \\
&= \langle vac | (\chi_{3,4}^{VB} \chi_{2,1}^{VB} \chi_{4,1}^{VB\dagger} \chi_{3,2}^{VB\dagger}) (\chi_{10,9}^{VB} \chi_{6,5}^{VB} \chi_{5,10}^{VB\dagger} \chi_{9,6}^{VB\dagger}) (\chi_{12,11}^{VB} \chi_{12,11}^{VB\dagger}) (1) \left(\frac{1}{2} \cdot 1 \right) | vac \rangle \\
&= \langle vac | (\chi_{3,4}^{VB} \chi_{2,1}^{VB} \chi_{4,1}^{VB\dagger} \chi_{3,2}^{VB\dagger}) (\chi_{10,9}^{VB} \chi_{6,5}^{VB} \chi_{5,10}^{VB\dagger} \chi_{9,6}^{VB\dagger}) (-1)(1) \left(\frac{1}{2} \cdot 1 \right) | vac \rangle \\
&= \langle vac | (\chi_{3,4}^{VB} \chi_{2,1}^{VB} \chi_{4,1}^{VB\dagger} \chi_{3,2}^{VB\dagger}) \left(\chi_{10,9}^{VB} \left(\frac{1}{2} \chi_{9,10}^{VB\dagger} \right) \right) (-1)(1) \left(\frac{1}{2} \cdot 1 \right) | vac \rangle \\
&= \langle vac | (\chi_{3,4}^{VB} \chi_{2,1}^{VB} \chi_{4,1}^{VB\dagger} \chi_{3,2}^{VB\dagger}) \left(\frac{1}{2} \cdot 1 \right) (-1)(1) \left(\frac{1}{2} \cdot 1 \right) | vac \rangle \\
&= \langle vac | \left(\chi_{3,4}^{VB} \left(-\frac{1}{2} \chi_{3,4}^{VB\dagger} \right) \right) \left(\frac{1}{2} \cdot 1 \right) (-1)(1) \left(\frac{1}{2} \cdot 1 \right) | vac \rangle \\
&= \langle vac | \left(\left(-\frac{1}{2} \right) (-1) \right) \left(\frac{1}{2} \cdot 1 \right) (-1)(1) \left(\frac{1}{2} \cdot 1 \right) | vac \rangle = -\frac{1}{8}
\end{aligned}$$

We can see the negative signs arising from switching the direction of the singlets (or switching the indices of the singlet operators). Also, we begin to see how larger loops affect the magnitude of the overlap.

The sign of the overlap may be eliminated altogether when working with the “non-crossing” set of states and directing all singlet bonds in a particular manner. A bipartite lattice (such as the 1D chain and square lattice) can be separated into two *sublattices*, namely sublattice *A* and sublattice *B*, such that a lattice site in *A* always has nearest neighbours in *B*, and vice versa (this is related to the concept of frustration). If all singlet bonds in a non-crossing state are directed from *A* to *B* (or equivalently *B* to *A*), then the overlap will *always* be positive [26].

It is useful to understand how VB states behave when acted upon by the antiferromagnetic Heisenberg Hamiltonian, as we see similar characteristic displayed by our GVB basis used to solve the Hubbard model in [Chapter 4](#). This Hamiltonian is expressed as

$$\hat{\mathcal{H}} = \sum_{ij} J_{ij} \vec{S}_i \cdot \vec{S}_j$$

where,

J_{ij} denotes the antiferromagnetic exchange coupling amplitude between sites i and j , and

\vec{S}_i is a vector consisting of the three spin operators S_i^x , S_i^y , and S_i^z as its x -, y -, and z -components.

The spin operator S_i^z , when acting on a spin state $|v\rangle$ (a state in the S^z basis), will be $+\frac{\hbar}{2}|v\rangle$ if there is a spin up at site i , or $-\frac{\hbar}{2}|v\rangle$ if there is a spin down at site i [27]. S_i^x and S_i^y are usually, and more conveniently, written in terms of the raising and lowering spin operators S_i^+ and S_i^- [27] as $S_i^x = \frac{1}{2}(S_i^+ + S_i^-)$ and $S_i^y = \frac{1}{2i}(S_i^+ - S_i^-)$. The raising operator S_i^+ converts a spin *down* at site i to a spin *up*; however, if there is a spin up at site i , then it is zero. The lowering operator S_i^- converts a spin *up* at site i to a spin *down*, unless, there is a spin down there, in which case, it is zero. Therefore, the exchange interaction $\vec{S}_i \cdot \vec{S}_j$ may be written

$$\vec{S}_i \cdot \vec{S}_j = S_i^z S_j^z + \frac{1}{2}(S_i^+ S_j^- + S_i^- S_j^+),$$

which is useful to use in the S^z basis.

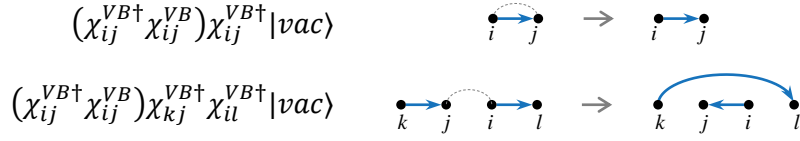
However, for the VB basis (which is closely related to our proposed GVB basis), it is more favourable to write the exchange interaction in terms of the VB singlet creation $\chi_{ij}^{VB\dagger}$ and annihilation χ_{ij}^{VB} operators as [26]

$$\vec{S}_i \cdot \vec{S}_j = \frac{1}{4} n_i n_j - \chi_{ij}^{VB\dagger} \chi_{ij}^{VB}.$$

n_i is the number operator and counts the number of electrons at site i . Since the Heisenberg model only deals with the case of exactly one electron per site, $n_i = 1$ for any site i .

In the VB language, the exchange interaction $\vec{S}_i \cdot \vec{S}_j$ involves annihilating, then creating, a singlet between sites i and j . When $\chi_{ij}^{VB\dagger} \chi_{ij}^{VB}$ acts *between* two singlets (i.e. site i belongs to one singlet bond and site j another), this term *rearranges* the bond configuration such that the new configuration contains a singlet *connecting* sites i and j [26]. The following update rules listed in [Table 2](#) show this.

Table 2 – List of the update rules involving $\chi_{ij}^{VB\dagger} \chi_{ij}^{VB}$ acting upon states in the VB basis.



This rearrangement of bonds is also seen in our GVB basis ([Chapter 4.1](#)) when an operator acts between bonds. As well, the exchange interaction $\vec{S}_i \cdot \vec{S}_j$ is a useful operator to consider when calculating observables, such as the staggered magnetization.

Consider matrix elements of the form $\langle Q | \chi_{ij}^{VB\dagger} \chi_{ij}^{VB} | P \rangle$ and how the loop configurations change after $\chi_{ij}^{VB\dagger} \chi_{ij}^{VB}$ act on state $|P\rangle$. If $\chi_{ij}^{VB\dagger} \chi_{ij}^{VB}$ acts within a loop (i.e. both i and j belong to the same loop), then the bonds in that loop are rearranged or that loop is split into two loops. If i and j belong to the same sublattice, then the bonds in the loop will be rearranged. If i and j are on different sublattices, then the loop will split into two loops. However, if $\chi_{ij}^{VB\dagger} \chi_{ij}^{VB}$ acts between two loops (i.e. i and j belong to different loops), then the two loops always join together to form a single loop. This rearrangement, splitting, and joining of loops is seen with our GVB basis as well and plays an important role in determining the matrix elements ([Chapter 4.2](#)).

The matrix elements of the type $\langle Q | \vec{S}_i \cdot \vec{S}_j | P \rangle$ have rules based on the overlay of both states bond configuration. The rules can be expressed in mathematical form as [\[26\]](#)

$$\frac{\langle Q | \vec{S}_i \cdot \vec{S}_j | P \rangle}{\langle Q | P \rangle} = \frac{3}{4} \epsilon_{ij} \delta^{\alpha_i \alpha_j}$$

where,

α_i is the loop that contains lattice site i and

$$\epsilon_{ij} = \begin{cases} -1 & \text{if } i, j \text{ are in different sublattices,} \\ +1 & \text{otherwise.} \end{cases}$$

Thus, lattice sites i and j must belong to the same loop.

Chapter 3

Generalized Valence Bond Basis

In this chapter, I go into detail about my newly proposed basis to solve the half-filled Hubbard model. As the name suggests, the GVB basis is a generalization of the valence bond basis used to solve the Heisenberg model. Keeping the singlet bonds that connect two single occupancies (of opposite spin), the GVB basis introduces two types of charge bonds that connect a double occupancy and a vacancy, namely the positive and negative charge bonds (PCB and NCB respectively). In turn, the GVB basis spans the singlet ($S_{tot} = 0$) sector of the Hilbert space. Creation and annihilation operators for each bond type are defined in terms of *fermion* creation ($c_{i\sigma}^\dagger$) and annihilation ($c_{i\sigma}$) operators that create (or annihilate) an electron of spin σ on site i . Formally, I define the *bond* creation and annihilation operators as,

$$\chi_{ij}^\dagger \equiv \frac{1}{\sqrt{2}}(c_{i\uparrow}^\dagger c_{j\downarrow}^\dagger - c_{i\downarrow}^\dagger c_{j\uparrow}^\dagger)$$

$$\chi_{ij} \equiv \frac{1}{\sqrt{2}}(c_{j\downarrow} c_{i\uparrow} - c_{j\uparrow} c_{i\downarrow})$$

For GVB singlets and

$$\eta_{ij}^{u\dagger} \equiv \frac{1}{\sqrt{2}}(c_{i\uparrow}^\dagger c_{i\downarrow}^\dagger + u c_{j\uparrow}^\dagger c_{j\downarrow}^\dagger)$$

$$\eta_{ij}^u \equiv \frac{1}{\sqrt{2}}(c_{i\downarrow} c_{i\uparrow} + u c_{j\downarrow} c_{j\uparrow})$$

for charge bonds of type u ($u = +1$ for PCBs and $u = -1$ for NCBs). The NCBs are interpreted to have “direction” as there is an introduction of a negative sign when the indices are swapped ($\eta_{ij}^{-\dagger} = -\eta_{ji}^{-\dagger}$). The singlets and the PCBs do not share this sense of direction as $\chi_{ij}^\dagger = \chi_{ji}^\dagger$ and $\eta_{ij}^{+\dagger} = \eta_{ji}^{+\dagger}$ (recall that VB singlets $\chi_{ij}^{VB\dagger}$ do have a sense of direction since they are defined in terms of *boson* operators).

A single GVB state is defined as the product of all bonds that make up the state,

$$|GVB\rangle = \left(\prod_{ij}^{N_{si}} \chi_{ij}^\dagger \right) \left(\prod_{ij}^{N_{pc}} \eta_{ij}^{+\dagger} \right) \left(\prod_{ij}^{N_{nc}} \eta_{ij}^{-\dagger} \right) |vac\rangle$$

with each site label (i, j) appearing only once and where,

$N_{si} \equiv$ total number of singlet bonds,

$N_{pc} \equiv$ total number of PCBs, and

$N_{nc} \equiv$ total number of NCBs in the GVB state, with

$|vac\rangle$ is defined as the quantum vacuum state with no electrons.

It must be true that the total number of bonds ($N/2$, with N defined as the number of lattice sites) is equal to $N_{si} + N_{pc} + N_{nc}$.

3.1 – GVB overcompleteness

As the VB basis is overcomplete, so is the GVB basis. To obtain the correct number of states, I have worked out a set of rules to restrict certain states, to ensure that we are left with a set of states without any linear dependencies. Consider the four-site (two-bond) case. The following figure shows an exhaustive list of all the states that are linearly dependent on other states when $N = 4$ (see [Appendix A2](#) for detailed work).

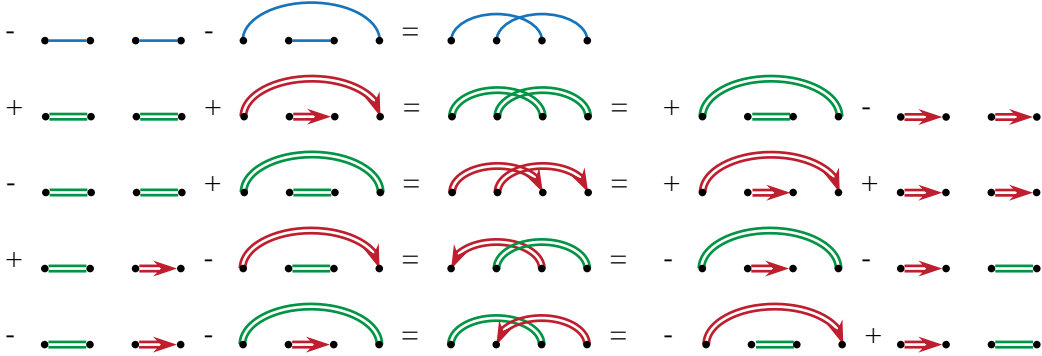


Figure 15 – Single solid (blue) lines represent singlet bonds, double solid (green) lines represent PCBs, and double solid (red) lines represent NCBs. We can clearly see that “crossing” bonds (of similar type, these are the states in the middle) are linearly dependent on states without crossings. Also, note that the charge bond crossings have two linear dependence relations for each crossing. This suggests that restricting ourselves to “non-crossing” states is not enough, we will need one or more rules to further restrict the number of states to obtain the correct counting.

Using the four-site linear dependence relations, I extrapolated rules that would provide the correct counting of states for 6, 8, and 10 sites (above this I was unable to test). The rules to obtain a complete set of states are as follows,

1. Singlet bonds may not cross another single bond
2. Charge bonds may not cross another charge bond (regardless the type)
3. PCBs may not be enclosed by another charge bond (regardless the type)

The VB basis, which contains only singlet bonds, also have the “non-crossing” rule for singlet bonds (as discussed in [Chapter 2](#)). For this reason, and as [Figure 15](#) suggests, I expected the complete set of states to exclude states with “crossing” charge bonds. The third rule, which states that PCBs may not be enclosed by another charge bond, is not intuitive. Through testing of which set of rules gave the correct counting, only the set of rules listed above (with one exception) worked. The exception occurs as a result of symmetry; we could equivalently state the third rule as ‘*NCBs* may not be enclosed by another charge bond.’ The concept of “crossing” or “enclosed” (see [Figure 16](#)) does not change as we increase the dimensionality of our system.

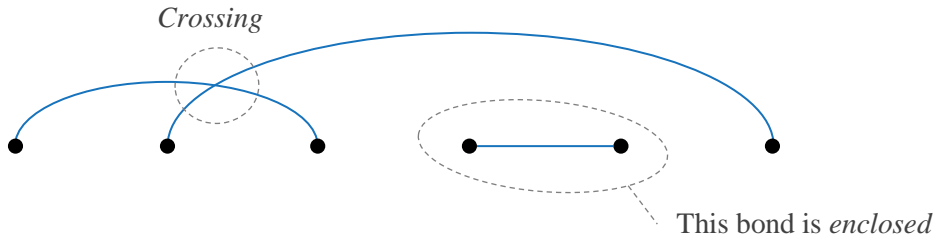


Figure 16 – An example of a six-site state with two bonds that cross and a bond being enclosed by another bond. I only use singlet bonds for the example since the concept of *crossing* and *enclosing* does not change with bond type.

Any higher dimensional system is mapped onto a 1D system via an arbitrary numbering scheme. Consider the 4x4 square lattice in which we number the lattice in a “snake-like” pattern (see [Figure 17](#)). The advantage of using the snake-like numbering scheme is that the nearest-neighbours of even-labelled sites are always odd-labelled sites; and as a result, non-crossing bonds connect an even site to an odd site. In principle, one may solve the system regardless of the numbering scheme used. In numbering the lattice sites, the system is effectively reduced to a 1D system with non-trivial boundary conditions and definitions of nearest- and next-nearest-neighbours. It is in this effective 1D system where the concept of *crossing* and *enclosing* is applicable.

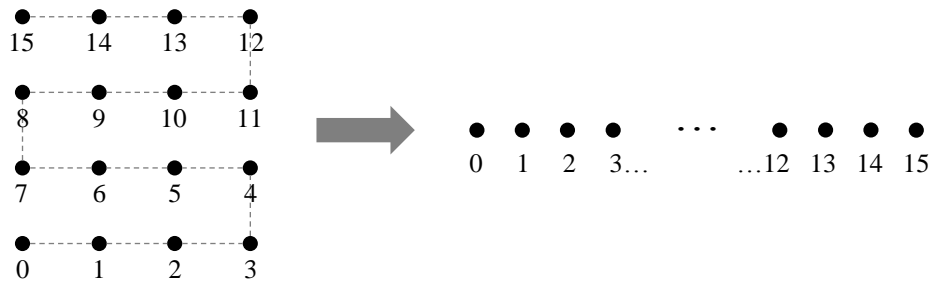


Figure 17 – Illustration showing how a 4x4 square lattice is reduced to a 1D problem via choosing a numbering scheme. Our example shows a *snake-like* numbering scheme.

3.2 – GVB overlaps

Not only is the GVB basis overcomplete, but it is also inconveniently non-orthogonal. As a result, we need to know when two states have non-zero overlap and, for non-zero overlap, what that value is. Like the VB states, overlaps involving GVB states form loops and the magnitude of the overlap may be expressed in terms of the number of loops. In fact, when a GVB overlap is non-zero, it has the same magnitude as its VB equivalent (replacing all charge bonds with singlets). First, let us consider our example in [Chapter 2 \(Figure 14\)](#); however, the singlets will be defined in terms of *fermions* (GVB singlets) instead of bosons (VB singlets) ([Figure 18](#)).

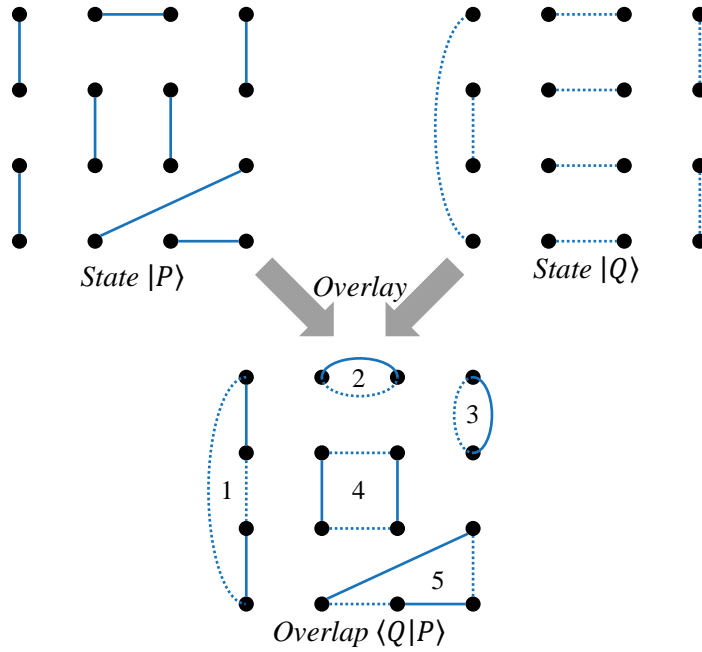


Figure 18 - Same example as [Figure 14](#); however, singlets are defined in terms of fermions instead of bosons, and as a result, the bonds no longer have direction. We expect both methods to be equivalent.

The magnitude is the same as before ($2^{N_\sigma - N/2} = 1/8$). We expect the overlaps obtained using either method to be equivalent; since using boson operators is considered appropriate in defining VB singlets. Since GVB singlets do not have direction; the sign change must come from elsewhere. In fact, the sign associated with GVB singlets depends on the size of the singlet loops (just as the magnitude did). Recall the example worked out in [Chapter 2](#)—in particular, the commutation rule

$$[\chi_{ji}^{VB}, \chi_{kj}^{VB\dagger}, \chi_{il}^{VB\dagger}]|vac\rangle = \frac{1}{2}\chi_{kl}^{VB\dagger}|vac\rangle$$

for VB singlets. The equivalent commutation rule for GVB singlets is

$$[\chi_{ij}, \chi_{kj}^\dagger, \chi_{il}^\dagger] = -\frac{1}{2}\chi_{kl}^\dagger.$$

Thus, there is an alternating sign depending on the size of each singlet loop.

Of course, our GVB basis consists of more than just singlet bonds, let us now add our two types of charge bonds and consider the overlap. Replacing some of the singlet bonds in example states with charge bonds, we obtain two new states in our GVB basis (**Figure 19**).

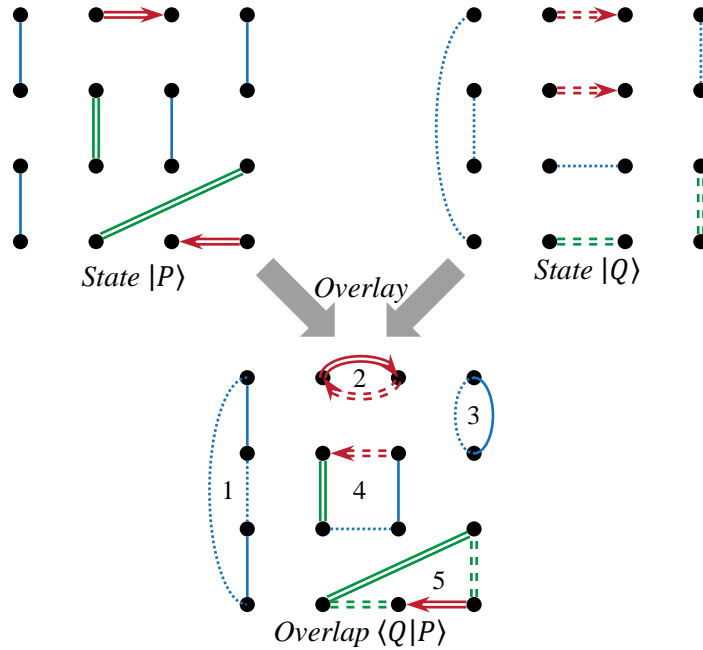


Figure 19 – Same bond orientations as **Figures 14 and 18**, but now some singlet bonds are replaced by PCBs and NCBs and we wish to determine when the overlap is non-zero, and what that non-zero value might be.

As the bond orientations did not change (only the bond types changed), there are still five loops labelled in the same fashion as before. To introduce some terminology, I define a “pure” loop as one that exclusively contains either singlets *or* charge bonds. Thus, loops 1, 2, 3, and 5 are all *pure* loops, with loops 1 and 3 being pure singlet loops, and 2 and 5 pure charge bond loops. Loop 5 is classified as a “mixed” loop, as it contains *both* singlets and charge bonds. Mixed loops always contain an even number of “transition points;” these are locations of the lattice sites where, in a loop, there is a transition from a singlet to a charge bond. Loop 4 has two transition points, one on the bottom left corner and the other on the top left corner of the loop itself. A loop with two transition points has a special name, a “half-pure” loop; this distinguishing feature becomes important in the next chapter when we discuss the *hopping* term matrix elements.

The overlap $\langle Q|P\rangle$ shown in **Figure 19** is zero because it contains a mixed loop. To show how mixed loops force a zero overlap, we will look at how states $|P\rangle$ and $|Q\rangle$ are defined using the GVB creation and annihilation operators, the appropriate commutation rules for our operators, and the snake-like numbering scheme.

$$|P\rangle = \chi_{0,7}^\dagger \eta_{4,1}^{+\dagger} \eta_{3,2}^{-\dagger} \chi_{5,10}^\dagger \eta_{9,6}^{+\dagger} \chi_{8,15}^\dagger \chi_{12,11}^\dagger \eta_{14,13}^{-\dagger} |vac\rangle$$

$$|Q\rangle = \chi_{0,15}^\dagger \eta_{1,2}^{+\dagger} \eta_{4,3}^{+\dagger} \chi_{5,6}^\dagger \chi_{8,7}^\dagger \eta_{9,10}^{-\dagger} \chi_{11,12}^\dagger \eta_{14,13}^{-\dagger} |vac\rangle$$

Therefore, the overlap is expressed as,

$$\begin{aligned} \langle Q|P\rangle &= \langle vac | \eta_{13,14}^- \chi_{11,12} \eta_{10,9}^- \chi_{8,7} \chi_{5,6} \eta_{4,3}^+ \eta_{1,2}^+ \chi_{0,15} \chi_{0,7}^\dagger \eta_{4,1}^{+\dagger} \eta_{3,2}^{-\dagger} \chi_{5,10}^\dagger \eta_{9,6}^{+\dagger} \chi_{8,15}^\dagger \chi_{12,11}^\dagger \eta_{14,13}^{-\dagger} |vac\rangle \end{aligned}$$

Since singlet operators χ , PCB operators η^+ and NCB operators η^- all commute with each other (as long as they do not share indices), these operators may be shuffled such that they may be grouped according to the loop to which they belong. For an exhaustive list of all the appropriate commutation rules regarding these three operators, see [Appendix A1.1](#).

$$\langle Q|P\rangle = \langle vac | (\eta_{4,3}^+ \eta_{1,2}^+ \eta_{4,1}^{+\dagger} \eta_{3,2}^{-\dagger}) (\eta_{10,9}^- \chi_{5,6} \chi_{5,10}^\dagger \eta_{9,6}^{+\dagger}) (\chi_{11,12} \chi_{12,11}^\dagger) (\eta_{13,14}^- \eta_{14,13}^{-\dagger}) (\chi_{8,7} \chi_{0,15} \chi_{0,7}^\dagger \chi_{8,15}^\dagger) |vac\rangle$$

Again the loops are ordered with loop 5 on the left, then 4, 3, 2, and 1 on the right. Using the commutation rule $[\chi_{ij}, \chi_{kj}^\dagger \eta_{li}^{u\dagger}] |vac\rangle = -\frac{u}{2} \chi_{ik}^\dagger |vac\rangle$ on loop 4, we obtain

$$\langle Q|P\rangle = \langle vac | (\eta_{4,3}^+ \eta_{1,2}^+ \eta_{4,1}^{+\dagger} \eta_{3,2}^{-\dagger}) \left(\eta_{10,9}^- \left(-\frac{1}{2} \chi_{6,10}^\dagger \right) \right) (\chi_{11,12} \chi_{12,11}^\dagger) (\eta_{13,14}^- \eta_{14,13}^{-\dagger}) (\chi_{8,7} \chi_{0,15} \chi_{0,7}^\dagger \chi_{8,15}^\dagger) |vac\rangle.$$

It is also true that singlet operators χ commute with charge bond operators η^u even if they share *one* or *both* indices in common according to the commutation rule $[\chi_{ij}, \eta_{kl}^{u\dagger}] |vac\rangle = 0$. Therefore, the *annihilation* operator $\eta_{10,9}^-$ may be shuffled to the right-hand-side to force the overlap to zero.

Let us fix the mixed loop issue by replacing both singlets in loop 4 with a PCB and a NCB as shown in [Figure 20](#).

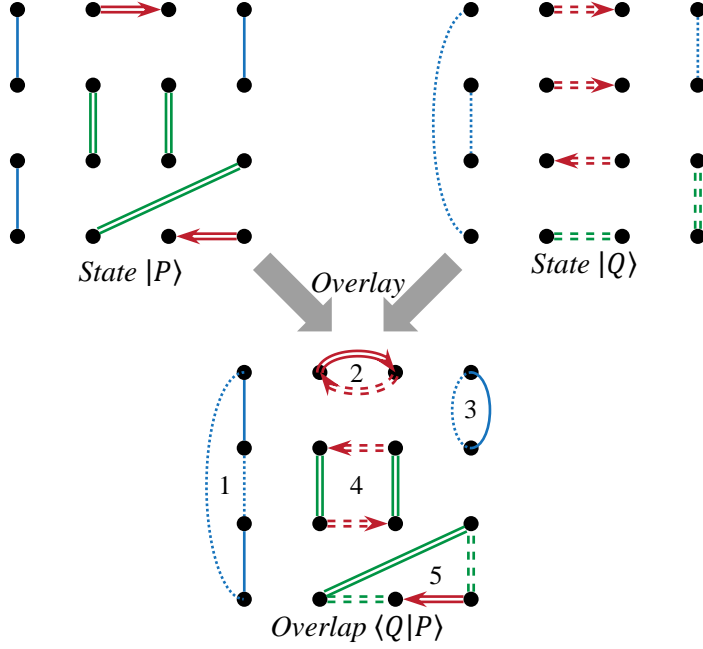


Figure 20 – As mixed loops gave zero overlap, we replaced the mixed loop (loop 4) with a pure charge bond loop. Now we would like to know if this overlap is non-zero and, if so, what that value might be.

It turns out that this overlap is also zero, because there is an odd number of NCBs in the pure charge bond loop 5. Let us consider the new states and the resulting overlap $\langle Q|P\rangle$ (organized according the loops again) and focus on loop 5.

$$|P\rangle = \chi_{0,7}^\dagger \eta_{4,1}^{++} \eta_{3,2}^{-\dagger} \eta_{5,10}^{++} \eta_{9,6}^{++} \chi_{8,15}^\dagger \chi_{12,11}^\dagger \eta_{14,13}^{-\dagger} |vac\rangle$$

$$|Q\rangle = \chi_{0,15}^\dagger \eta_{1,2}^{++} \eta_{4,3}^{++} \eta_{5,6}^{-\dagger} \chi_{8,7}^\dagger \eta_{9,10}^{-\dagger} \chi_{11,12}^\dagger \eta_{14,13}^{-\dagger} |vac\rangle$$

$$\langle Q|P\rangle = \langle vac | (\eta_{4,3}^\dagger \eta_{1,2}^\dagger \eta_{4,1}^\dagger \eta_{3,2}^\dagger) (\eta_{10,9}^- \eta_{6,5}^- \eta_{5,10}^+ \eta_{9,6}^+) (\chi_{11,12}^\dagger \chi_{12,11}^\dagger) (\eta_{13,14}^- \eta_{14,13}^-) (\chi_{8,7} \chi_{0,15} \chi_{0,7}^\dagger \chi_{8,15}^\dagger) |vac\rangle$$

$$\text{Using the commutation rule } [\eta_{ij}^u, \eta_{kj}^{v\dagger} \eta_{li}^{w\dagger}] |vac\rangle = \frac{1}{2} (w \eta_{kj}^{v\dagger} + uv \eta_{li}^{w\dagger}) |vac\rangle,$$

$$\langle Q|P\rangle = \langle vac | \left(\eta_{4,3}^\dagger \frac{1}{2} (-\eta_{4,1}^{++} + \eta_{3,2}^{-\dagger}) \right) \cdot (\eta_{10,9}^- \eta_{6,5}^- \eta_{5,10}^+ \eta_{9,6}^+) (\chi_{11,12}^\dagger \chi_{12,11}^\dagger) (\eta_{13,14}^- \eta_{14,13}^-) (\chi_{8,7} \chi_{0,15} \chi_{0,7}^\dagger \chi_{8,15}^\dagger) |vac\rangle$$

along with the commutation rules $[\eta_{ij}^u, \eta_{ik}^{v\dagger}] |vac\rangle = \frac{1}{2} |vac\rangle$ and $[\eta_{ji}^u, \eta_{ik}^{v\dagger}] = \frac{u}{2} |vac\rangle$, the overlap now becomes

$$\langle Q|P\rangle = \langle vac | \left(\frac{1}{2} \left(-\frac{1}{2} + \frac{1}{2} \right) \right) \cdot (\eta_{10,9}^- \eta_{6,5}^- \eta_{5,10}^+ \eta_{9,6}^+) (\chi_{11,12}^\dagger \chi_{12,11}^\dagger) (\eta_{13,14}^- \eta_{14,13}^-) (\chi_{8,7} \chi_{0,15} \chi_{0,7}^\dagger \chi_{8,15}^\dagger) |vac\rangle = 0$$

which is zero, because the terms cancel. When there is an even number of NCBs in a loop, there will not be any cancellation.

Let us change the diagonal PCB of loop 5 in state $|P\rangle$ to a NCB (directed to the left), so that there are an even number of NCBs in each pure charge bond loop.

$$|P\rangle = \chi_{0,7}^\dagger \eta_{4,1}^- \eta_{3,2}^- \eta_{5,10}^{++} \eta_{9,6}^{++} \chi_{8,15}^\dagger \chi_{12,11}^\dagger \eta_{14,13}^- |vac\rangle$$

$$|Q\rangle = \chi_{0,15}^\dagger \eta_{1,2}^{++} \eta_{4,3}^{++} \eta_{5,6}^- \chi_{8,7}^\dagger \eta_{9,10}^- \chi_{11,12}^\dagger \eta_{14,13}^- |vac\rangle$$

The overlap is *non-zero* with a magnitude equal to $|\langle Q|P\rangle| = 2^{N_G - N/2} = 1/8$. This is shown below using various commutation rules found in [Appendix A1.1](#).

$$\begin{aligned} \langle Q|P\rangle &= \langle vac | (\eta_{4,3}^\dagger \eta_{1,2}^\dagger \eta_{4,1}^- \eta_{3,2}^-) (\eta_{10,9}^- \eta_{6,5}^- \eta_{5,10}^{++} \eta_{9,6}^{++}) (\chi_{11,12}^\dagger \chi_{12,11}^\dagger) (\eta_{13,14}^- \eta_{14,13}^-) (\chi_{8,7} \chi_{0,15} \chi_{0,7}^\dagger \chi_{8,15}^\dagger) |vac\rangle \\ &= \langle vac | (\eta_{4,3}^\dagger \eta_{1,2}^\dagger \eta_{4,1}^- \eta_{3,2}^-) (\eta_{10,9}^- \eta_{6,5}^- \eta_{5,10}^{++} \eta_{9,6}^{++}) (\chi_{11,12}^\dagger \chi_{12,11}^\dagger) (\eta_{13,14}^- \eta_{14,13}^-) \left(\chi_{8,7} \left(-\frac{1}{2} \chi_{7,8}^\dagger \right) \right) |vac\rangle \\ &= \langle vac | (\eta_{4,3}^\dagger \eta_{1,2}^\dagger \eta_{4,1}^- \eta_{3,2}^-) (\eta_{10,9}^- \eta_{6,5}^- \eta_{5,10}^{++} \eta_{9,6}^{++}) (\chi_{11,12}^\dagger \chi_{12,11}^\dagger) (\eta_{13,14}^- \eta_{14,13}^-) \left(-\frac{1}{2} \right) |vac\rangle \\ &= \langle vac | (\eta_{4,3}^\dagger \eta_{1,2}^\dagger \eta_{4,1}^- \eta_{3,2}^-) (\eta_{10,9}^- \eta_{6,5}^- \eta_{5,10}^{++} \eta_{9,6}^{++}) (1)(1) \left(-\frac{1}{2} \right) |vac\rangle \\ &= \langle vac | \left(\eta_{4,3}^\dagger \frac{1}{2} (-\eta_{4,1}^- - \eta_{3,2}^-) \right) \left(\eta_{10,9}^- \frac{1}{2} (\eta_{5,10}^{++} - \eta_{9,6}^{++}) \right) (1)(1) \left(-\frac{1}{2} \right) |vac\rangle \\ &= \langle vac | \left(\frac{1}{2} \left(-\frac{1}{2} - \frac{1}{2} \right) \right) \left(\frac{1}{2} \left(\frac{1}{2} - \left(-\frac{1}{2} \right) \right) \right) (1)(1) \left(-\frac{1}{2} \right) |vac\rangle \\ &= \langle vac | \left(-\frac{1}{2} \right) \left(\frac{1}{2} \right) (1)(1) \left(-\frac{1}{2} \right) |vac\rangle = \frac{1}{8} \end{aligned}$$

The sign of the overlap $\langle Q|P\rangle$ comes from the size of the pure singlet loops, and the realignment of the directional NCBs. The sign (ϕ_S) from the singlets can be written in closed form as

$$\phi_S = (-1)^{N_G^S - N_P^S}$$

where, N_G^S is the number of pure singlet loops and N_P^S is the number of singlet bonds in state $|P\rangle$, which, for non-zero overlap, is equal to the N_Q^S , the number of singlet bonds in state $|Q\rangle$. I could not determine a way write the sign from the realignment of NCBs in closed form. However, if we work in our complete basis, using the rule that ‘PCBs may not be enclosed by another charge bond’ (enclosed NCBs does not work) *and* with the additional constraint that we direct all NCBs in a state towards the lower numbered lattice site, then we can write the overlap in a simple, closed form (recall that we define a numbering scheme to the lattice, and if a NCB connects two lattice sites, say 7 and 2

$(\eta_{7,2}^{-\dagger})$, then the bond would be directed from 7 to 2). Under these conditions the overlap $\langle Q|P\rangle$ may be rewritten as

$$\langle Q|P\rangle = (-2)^{N_G - N/2}.$$

However, the expression that must be used for an arbitrary state in the overcomplete GVB basis is

$$\langle Q|P\rangle = \phi_{NCB} (-1)^{N_G^S - N_P^S} 2^{N_G - N/2}$$

defining ϕ_{NCB} to be the sign associated with the realignment of the NCBs. This, of course, is the value of the overlap when it is non-zero. As suggested by the examples I presented above, the following rules must be satisfied for non-zero overlap:

1. All loops must of pure and
2. All pure charge bond loops must have an even number of NCBs in each loop.

Chapter 4

Solving the Hubbard Model

The Hubbard Hamiltonian, with hopping between arbitrary sites i and j , is given by

$$\hat{\mathcal{H}} = - \sum_{ij,\sigma} t_{ij} (c_{i\sigma}^\dagger c_{j\sigma} + c_{j\sigma}^\dagger c_{i\sigma}) + U \sum_i n_{i\uparrow} n_{i\downarrow}$$

where,

t_{ij} is the hopping amplitude (between sites i and j),

σ is the spin (either up \uparrow or down \downarrow),

$c_{i\sigma}^\dagger$ and $c_{i\sigma}$ are fermion creation and annihilation operators respectively,

$n_{i\sigma} \equiv c_{i\sigma}^\dagger c_{i\sigma}$ counts the number of electrons on site i with spin σ and,

U is the energy cost associated with a double occupancy.

Two terms are clearly seen in the Hamiltonian, with

$$\hat{\mathcal{T}} \equiv - \sum_{ij,\sigma} t_{ij} (c_{i\sigma}^\dagger c_{j\sigma} + c_{j\sigma}^\dagger c_{i\sigma})$$

as the tight-binding, hopping (kinetic energy) term and

$$\hat{\mathcal{U}} \equiv U \sum_i n_{i\uparrow} n_{i\downarrow}$$

as the on-site Coulomb repulsion (potential energy) term.

In the hopping term the combination of creation and annihilation operators, $c_{i\sigma}^\dagger c_{j\sigma}$ and $c_{j\sigma}^\dagger c_{i\sigma}$, allow an electron of spin σ to hop from sites j to i and i to j , respectively. Both number operators $n_{i\uparrow} n_{i\downarrow}$ in the on-site interaction term, together, count the number of spin up electrons *and* spin down electrons on a single site. Of course, Pauli exclusion principle prohibits more than one electron of the same spin. When we sum over the lattice sites, the term $\sum_i n_{i\uparrow} n_{i\downarrow}$ counts total number of double occupancies in a state. This description is provided with respect to the *occupation* basis and is expected to change with the use the GVB basis.

4.1 – Update rules

Update rules describe how each term in the Hamiltonian affects a basis state. Let us first consider the on-site Coulomb term \hat{U} and how this term affects the GVB states. A charge bond connects a double occupancy with a vacancy and a singlet connects two single occupancies. Therefore, our expectation is that, in a GVB state, \hat{U} will count the number of charge bonds and apply an energy cost of U for each charge bond. Our expectations were verified when I worked out the update rules for this term (see [Appendix B1.2](#)). Defining $\hat{U}_l \equiv n_{l\uparrow}n_{l\downarrow}$, the following table shows the update rules involving the on-site interaction term.

Table 3 – This table summarizes the update rules when the Hubbard- U term acts on each type of bond of the GVB basis.

$$\begin{aligned} \hat{U}_i \chi_{ij}^\dagger |vac\rangle &= 0 & \begin{array}{c} \circ \text{---} \bullet \\ i \quad j \end{array} &\rightarrow 0 \\ (\hat{U}_i + \hat{U}_j) \eta_{ij}^{u\dagger} |vac\rangle &= \eta_{ij}^{u\dagger} |vac\rangle & \begin{array}{c} \bullet \text{---} \bullet \\ i \quad j \end{array} &\rightarrow \begin{array}{c} \bullet \text{---} \bullet \\ i \quad j \end{array} \\ & & \begin{array}{c} \circ \text{---} \circ \\ i \quad j \end{array} &\rightarrow \begin{array}{c} \circ \text{---} \circ \\ i \quad j \end{array} \end{aligned}$$

The Hubbard- U term is the simplest term in the Hamiltonian to deal with as it does not alter the state on which it acts. The hopping term, however, does alter the state. Consider the example of two sites, i and j , site i with a spin up and site j with a spin down (this is similar to a singlet). If the spin up electron in site i hops to site j , it creates a vacancy on site i and a double occupancy on site j (this is similar to a charge bond). In this way, when the hopping term $\hat{T}_{ij} \equiv \sum_{\sigma} (c_{i\sigma}^\dagger c_{j\sigma} + c_{j\sigma}^\dagger c_{i\sigma})$ acts on each end of a singlet bond $\chi_{ij}^\dagger |vac\rangle$, we expect the term to change the bond from a singlet to a particular charge bond $\eta_{ij}^{u\dagger} |vac\rangle$. Our reasoning turns out to be correct when I worked out the update rules for \hat{T}_{ij} acting on each end of the three bonds (see [Appendix B1.2](#)) and [Table 4](#) shows the corresponding update rules.

Table 4 – This table summarizes all update rules when the hopping term acts on a single bond. Under this condition, the hopping term effectively changes the bond type.

$$\begin{aligned} \hat{T}_{ij} \chi_{ij}^\dagger |vac\rangle &= 2 \eta_{ij}^{+\dagger} |vac\rangle & \begin{array}{c} \bullet \text{---} \bullet \\ i \quad j \end{array} &\rightarrow 2 \begin{array}{c} \bullet \text{---} \bullet \\ i \quad j \end{array} \\ \hat{T}_{ij} \eta_{ij}^{u\dagger} |vac\rangle &= (1 + u) \chi_{ij}^\dagger |vac\rangle & \begin{array}{c} \bullet \text{---} \bullet \\ i \quad j \end{array} &\rightarrow 2 \begin{array}{c} \bullet \text{---} \bullet \\ i \quad j \end{array} \\ & & \begin{array}{c} \circ \text{---} \circ \\ i \quad j \end{array} &\rightarrow 0 \end{aligned}$$

From the update rules in [Table 4](#), we see that the hopping term \hat{T}_{ij} changes a *singlet* bond into a *positive* charge bond (and vice versa), when i and j are lattice sites at either end of the bonds and destroys the *negative* charge bond under the same conditions.

When the hopping term \hat{T}_{ij} acts between two bonds it rearranges the bonds (similar to what was seen in [Chapter 2](#) with the VB basis and the Heisenberg Hamiltonian update rules) and changes the bond type (the change is not always from a singlet to a charge bond or vice versa; sometimes, only the charge bond type changes). This is seen in [Table 5](#) showing all possible update rules for when \hat{T}_{ij} acts between two bonds (the work is shown in [Appendix B1.2](#)).

Table 5 – This table summarizes all update rules when the hopping term acts between bonds. Under this condition, the hopping term rearranges the bonds and changes the bond types.

$\hat{T}_{ij}\chi_{kj}^\dagger\chi_{il}^\dagger vac\rangle = -\eta_{ij}^{++}\chi_{kl}^\dagger vac\rangle$	
$\hat{T}_{ij}\eta_{kj}^{++}\eta_{il}^{++} vac\rangle = +\chi_{ij}^\dagger\eta_{kl}^{++} vac\rangle$	
$\hat{T}_{ij}\eta_{kj}^{-+}\eta_{il}^{-+} vac\rangle = +\chi_{ij}^\dagger\eta_{kl}^{++} vac\rangle$ If head-to-tail, then +	
$\hat{T}_{jl}\eta_{kj}^{-+}\eta_{il}^{-+} vac\rangle = -\chi_{jl}^\dagger\eta_{ik}^{++} vac\rangle$ If head-to-head (or tail-to-tail), then -	
$\hat{T}_{ij}\eta_{kj}^{++}\eta_{il}^{-+} vac\rangle = +\chi_{ij}^\dagger\eta_{kl}^{-+} vac\rangle$ The resulting NCB maintains the same head or tail as it started with.	
$\hat{T}_{ij}\chi_{kj}^\dagger\eta_{il}^{++} vac\rangle = +\chi_{ik}^\dagger\eta_{lj}^{-+} vac\rangle$ The resulting NCB always points towards lattice site in the subscript of \hat{T}_{ij} .	
$\hat{T}_{ij}\chi_{kj}^\dagger\eta_{il}^{-+} vac\rangle = -\chi_{ik}^\dagger\eta_{lj}^{++} vac\rangle$ If singlet-to-tail of NCB, then -	
$\hat{T}_{jl}\chi_{kj}^\dagger\eta_{il}^{-+} vac\rangle = +\chi_{kl}^\dagger\eta_{ij}^{++} vac\rangle$ If singlet-to-head of NCB, then +	

4.2 – Matrix elements

Combining the update rules from the previous sub-chapter and the overlap rules (for $\langle Q|P\rangle$) from [Chapter 3.2](#), I determined the necessary rules for the matrix elements (of the type $\langle Q|\hat{\mathcal{H}}|P\rangle$). The matrix element $\langle Q|\hat{\mathcal{H}}|P\rangle$ may be written

$$\langle Q|(\hat{\mathcal{T}} + \hat{\mathcal{U}})|P\rangle = \langle Q|\hat{\mathcal{T}}|P\rangle + \langle Q|\hat{\mathcal{U}}|P\rangle.$$

As a result we may consider the overlaps for each term independently.

Since number operators ($n_{i\sigma}$) do not change the state on which they act, $\hat{\mathcal{U}}|P\rangle = UN_P^{CB}|P\rangle$ associates an energy cost U with each charge bond in state $|P\rangle$ ($N_P^{CB} \equiv$ number of charge bonds in state $|P\rangle$) and the state $|P\rangle$ is left unaltered. Thus, the matrix elements

$$\langle Q|\hat{U}|P\rangle = UN_{\bar{P}}^{CB}\langle Q|P\rangle$$

have the same conditions for when the overlap $\langle Q|P\rangle$ is non-zero.

The hopping term matrix elements $\langle Q|\hat{T}|P\rangle$ are not as trivially determined. Consider $\langle Q|\hat{T}_{ij}|P\rangle$ and how hopping affects the loop configuration. If \hat{T}_{ij} acts within a loop, then it either rearranges the bonds in the loop or splits the loop into two loops. If \hat{T}_{ij} acts between two loops, then it will join the loops and form a single loop. Since \hat{T}_{ij} changes the bond types of the bonds involved, according to the update rules, any loop rearrangement or joining of two loops will always result in a mixed loop. Thus, the matrix elements $\langle Q|\hat{T}_{ij}|P\rangle$ involving lattice sites i and j that rearrange the bonds in a loop or join two loops together will be zero. In fact, there is only one circumstance in which $\langle Q|\hat{T}_{ij}|P\rangle$ will be non-zero. Consider a half-pure loop (a loop with two transition points, see [Chapter 2](#)), if \hat{T}_{ij} act on the two transition points of the half-pure loop, then, in this case (and this case only), \hat{T}_{ij} will split the half-pure loop into two pure loops (a pure singlet loop and a pure charge bond loop). Since there is only one possible pair of indices that can possibly give a non-zero overlap, the conclusion that

$$\langle Q|\hat{T}|P\rangle = \langle Q|\hat{T}_{ij}^*|P\rangle$$

is made; where * indicates that the indices i and j act on the two transition points of the half-pure loop (if one exists). Also, because of the condition of the half-pure loop, the hopping term matrix element $\langle Q|\hat{T}|P\rangle$ is zero when $\langle Q|\hat{U}|P\rangle$ is non-zero and vice versa.

All loops, other than the half-pure loop, must be pure, with pure charge bond loops containing an even number of NCBs, for the matrix element $\langle Q|\hat{T}_{ij}^*|P\rangle$ to possibly be non-zero. To establish a set of rules in which matrix elements of the form $\langle Q|\hat{T}|P\rangle$ are non-zero, we need to add one more rule to ensure that the resulting pure charge bond loop (from the splitting of the half-pure loop) has an *even* number of NCBs. This condition is ensured when there is an *odd* number of PCBs in the half-pure loop. The rules to ensure non-zero $\langle Q|\hat{T}|P\rangle$ overlap are summarized as

1. All loops must be pure, except for one half-pure loop
2. Each pure charge bond loop must contain an even number of NCBs
3. The half-pure loop must contain an odd number of PCBs
4. The hopping term must act on the two transition points of the half-pure loop.

The magnitude of the non-zero matrix element $|\langle Q|\hat{T}_{ij}^*|P\rangle|$ is

$$|\langle Q|\hat{T}_{ij}^*|P\rangle| = 2^{N_{\cup}+1-N/2}$$

since the number of loops increases by one. The sign associated with the pure singlet loops ϕ_S^T is expressed as

$$\phi_S^T = (-1)^{N_S+1-\max(N_P^S, N_Q^S)}.$$

The number of pure singlet loops increases by one ($N_S + 1$) and $\max(N_P^S, N_Q^S)$ will give the correct number of singlets *after* we act with the hopping term \hat{T}_{ij}^* . Like the overlap $\langle Q|P\rangle$, the sign from the realignment of NCBS ϕ_{NCB}^T cannot be expressed in closed form. The non-zero matrix element $\langle Q|\hat{T}_{ij}^*|P\rangle$ is written as

$$\langle Q|\hat{T}_{ij}^*|P\rangle = \phi_{NCB}^T (-1)^{N_S+1-\max(N_P^S, N_Q^S)} 2^{N_S+1-N/2}.$$

An interesting feature of the Hubbard Hamiltonian matrix elements is that it is naturally block tridiagonalized (see **Figure 21**) with each block along the diagonal representing a charge sector (similarly, the overlap matrix is block diagonal).

	0 CB	1 CB	2 CB	3 CB	4 CB		$(\frac{N}{2} - 1)$ CB	$\frac{N}{2}$ CB
0 CB	0	T_{01}	0	0	0		0	0
1 CB	T_{10}	UT_{11}	T_{12}	0	0		0	0
2 CB	0	T_{21}	UT_{22}	T_{23}	0	• • •	0	0
3 CB	0	0	T_{32}	UT_{33}	T_{34}		0	0
4 CB	0	0	0	T_{43}	UT_{44}		0	0
			•				$T_{\frac{N}{2}-2, \frac{N}{2}-1}$	0
			•					
			•					
$(\frac{N}{2} - 1)$ CB	0	0	0	0	0	$T_{\frac{N}{2}-1, \frac{N}{2}-2}$	$UT_{(\frac{N}{2}-1)}$	$T_{\frac{N}{2}-1, \frac{N}{2}}$
$\frac{N}{2}$ CB	0	0	0	0	0	0	$T_{\frac{N}{2}, \frac{N}{2}-1}$	$U_{\frac{N}{2}}$

Figure 21 – The block tridiagonal nature of the Hubbard Hamiltonian matrix elements is apparent when the basis states are grouped with respect to the number of charge bonds in the state (i.e. charge sector). The hopping term can either change the number of charge bonds by one or zero. In the figure, I label each block as ‘0’ if all elements in block are zero, ‘U’ if the Hubbard- U term can be non-zero, ‘T’ if the hopping term can be non-zero, or ‘UT’ if both terms can be non-zero.

Note that each charge sector is not of equal size, so the block matrices are not square. Potentially, one could take advantage of this structure and *block diagonalize* the matrix and perform an exact diagonalization procedure on each of the resulting block diagonal matrices individually. However, block diagonalizing a block tridiagonal matrix has only been done when the matrix blocks are *square* [29].

4.3 – Exact diagonalization

Since the GVB basis is non-orthogonal we need to solve the generalized eigenvalue problem $H\psi = ES\psi$, where H and S are matrices of the overlap values $\langle Q|\hat{\mathcal{H}}|P\rangle$ and $\langle Q|P\rangle$ respectively, E is the eigenvalue and ψ is the eigenvector. For an orthonormal basis (such as the occupation basis), the overlap matrix S would be the identity matrix, and we would have the regular eigenvalue problem $H\psi = E\psi$.

Until recently, there were two routines that LAPACK provided to solve and obtain the eigenvalues and eigenvectors of the real symmetric matrix H ; the traditional method using QR and LQ factorization [30] and Cuppen’s divide-and-conquer (CDC) method [31]. The divide-and-conquer method is faster than QR (especially for larger matrices), but uses more workspace [12]. In each case, LAPACK solves the regular eigenproblem for a real symmetric matrix H in two steps; the reduction of H to a tridiagonal matrix T , then the diagonalization of T to obtain all the eigenvalues and, optionally, the eigenvectors of H . LAPACK has only one routine to reduce H (of size D) to a tridiagonal matrix and the number of operations needed to do so is $O(D^3)$ [12]. The two routines mentioned above differ in the second step of obtaining the eigenvalues and eigenvectors of T . Using QR factorization, the number of operations needed to obtain the eigenvalues and eigenvectors of T is $O(D^2)$ and $O(D^3)$ respectively [12]. With the CDC method, the number of operations needed to obtain the eigenvectors is also $O(D^3)$ [12] (though it is still faster than QR factorization). I use the divide-and-conquer routine in all of my exact diagonalization programs.

As of June 2010, with the release of version 3.2.2, LAPACK included a new routine to solve the regular eigenvalue problem of a real symmetric matrix. This routine included a method, called the relatively robust representation (RRR), used for obtaining the eigenvalues/eigenvectors of a symmetric tridiagonal matrix. It was first presented in the Ph.D. dissertation of Dhillon in 1997 [32] and LAPACK added it (as a prototype) to its routine list in 1999 when version 3.0 was released. This method scales as $O(D^2)$ and, in most cases, is the fastest routine LAPACK provides to eigensolve a symmetric tridiagonal matrix and it requires the least amount of space [12]. However, at the moment, this routine is not available to solve the generalized eigenproblem. Also, with RRR, one can choose to solve for a subset of eigenvalues/eigenvectors, which will also speed up the diagonalization process.

4.4 – Construction and storage of GVB states

Let's consider the VB basis, which deals with only one bond type (singlets). A single VB state can be stored as a 32-bit integer, with each bit representing a lattice site (so with a 32-bit integer we are limited to a maximum of 32 sites, but it is trivial to go beyond 32 sites by concatenating multiple 32-bit integers). However, this bit representation is only unique when we restrict ourselves to the complete VB basis of “non-crossing” states. Each bond is represented by a pair of bits (not necessarily adjacent bits), with one bit set and the other cleared (1 and 0, respectively). By convention, the 1 is always more significant³ than its partnered 0. Also, for any given cleared bit (in our range of N bits) there must never be more 1's than 0's in the bits that are less significant than itself. The opposite is true for any given set bit; there can never be more 0's than 1's in the bits that are more significant than itself.

A helpful picture that I use to determine whether or not a given integer is a “well-formed” state is the concept of elevation. First, we start with an elevation of zero. Then we traverse the bits of the integer, starting from the least significant bit (LSB) and ending with the most significant bit (MSB). As we traverse the bits, we add one to the elevation when a 0 is encountered and we subtract one when a 1 is encountered. If the elevation ever is negative or is not zero when we pass the MSB, then the state is not “well-formed.” The following figure illustrates the concept of elevation and provides an example of a well-formed state.

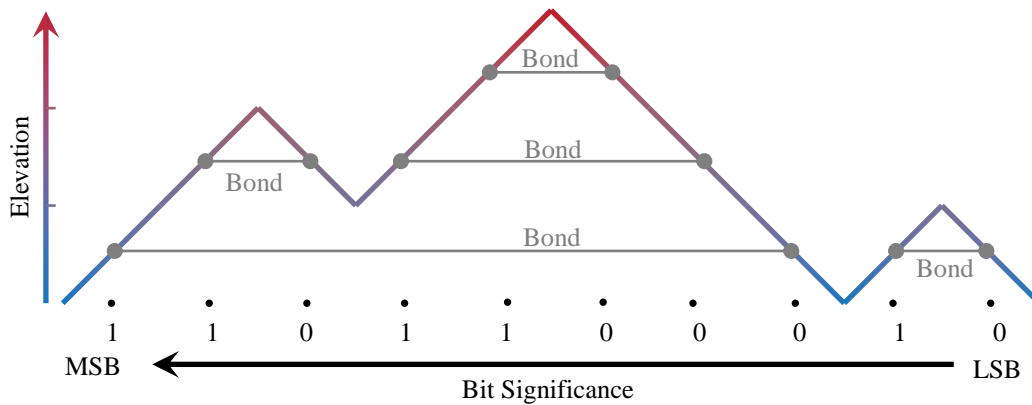


Figure 22 – This diagram illustrates the concept of elevation, how I determined whether a state is “well-formed” or not, and how I determined the location of the bond partner.

The problem of counting the number of “non-crossing” states is well known. The number of non-crossing states (which correspond to so-called Catalan objects) is given by the Catalan number [33]. This number is the solution to many different counting problems (of similar nature as ours) in combinatorics.

³ More significant in the sense that the most significant bit (MSB) is the leftmost set bit of the integer, and the least significant bit (LSB) is the rightmost bit of the integer. Therefore, a bit which is more significant than another means it is relatively closer to the MSB. Example of an integer in bit representation: (MSB \rightarrow 101100100 \leftarrow LSB).

A GVB state can be stored in a similar manner as the VB state, but now require three bits in order to represent a single lattice site. A GVB state can have up to three bond types, which means we need six distinguishable elements to represent the bonds. A single bit can only represent two distinguishable elements; three bits can represent up to $2^3 = 8$ distinguishable elements. We use the bit representation of integers 0-5 to make up our six elements (**Table 6**).

Table 6 – Bond types are represented by integers in the range 0-5.

Singlets	000	0
	001	1
PCBs	010	2
	011	3
NCBs	100	4
	101	5

With this representation, we can uniquely construct states with the restriction that bonds of the same type may not cross. The pairing works in the same way as in the VB basis; but a “well-formed” state requires three elevations (one for each bond type) in order to test the validity. However, unlike VB states, a “well-formed” GVB state is not necessarily a state in the complete GVB basis. As a result, further pruning of these “well-formed” GVB states is needed in order to obtain the subset of GVB states which form the complete basis. Although this pruning process is not trivial, it was done during the elevation test stage with some modifications.

4.5 – Test for loop purity

There is a simple method to test these three possible cases:

1. All loops in an overlap are pure
2. All loops in an overlap are pure except for one half-pure loop
3. Neither of the above two.

This method involves comparing the bond types associated with a given lattice site of the two states which are being overlapped; if the two bond types are different, then we have a transition point. So, this test actually reveals the locations of all the transition points in a set of loops. However, we do not care if there is a transition between the two charge bond types, so from now on we will consider transition points between singlets and charge bonds. If all loops are pure, then there will be no transition points. If there are exactly two transition points (note: there cannot be an odd number of transitions in a loop) in the overlap, then those two transition points must belong to the same loop and this loop is half-pure (the rest will be pure). If there are more than two transition points then the overlap must be zero and so must the hopping term matrix elements.

Consider the following example, let

$$|P\rangle = \chi_{78}^\dagger \chi_{46}^\dagger \eta_{53}^{-\dagger} \eta_{92}^{-\dagger} \eta_{01}^{+\dagger} |vac\rangle \text{ and}$$

$$|Q\rangle = \chi_{67}^\dagger \chi_{48}^\dagger \eta_{32}^{-\dagger} \eta_{15}^{+\dagger} \eta_{90}^{-\dagger} |vac\rangle.$$

These states represented as integers are,

$$|P\rangle = 101 \quad 001 \quad 000 \quad 001 \quad 101 \quad 000 \quad 100 \quad 100 \quad 011 \quad 010 = 688294170$$

$$|Q\rangle = 101 \quad 001 \quad 001 \quad 000 \quad 011 \quad 000 \quad 101 \quad 100 \quad 010 \quad 100 = 690064148$$

To test for purity, we compare bond types for each lattice site.

$ P\rangle =$	101	001	000	001	101	000	100	100	011	010
	↑	↑	↑	↑	↑	↑	↑	↑	↑	↑
$ Q\rangle =$	101	001	001	000	011	000	101	100	010	100
	↓	↓	↓	↓	↓	↓	↓	↓	↓	↓
	Same	Same	Same	Same	Same	Same	Same	Same	Same	Same

There are no transition points; therefore, all loops are pure and the overlap may exist. Let us switch the non-crossing singlet in state P into a charge bond (say a PCB).

$ P\rangle =$	101	011	010	001	101	000	100	100	011	010
	↑	↑	↑	↑	↑	↑	↑	↑	↑	↑
$ Q\rangle =$	101	001	001	000	011	000	101	100	010	100
	↓	↓	↓	↓	↓	↓	↓	↓	↓	↓
	Same	Transition	Transition	Same	Same	Same	Same	Same	Same	Same

Now we have two transitions and the overlap has a half-pure loop with the rest remaining pure.

Chapter 5

Determining Expectation Values

After we solve the Hubbard model and obtain its eigenenergies E^n and eigenstates $|\psi^n\rangle$ (n is the index for all the eigenstates, ordered according to energy levels, with $n = 0$ associated with the lowest energy state) we can then determine expectation values from each eigenstate. According to linear algebra, an eigenstate is written as a linear superposition of the basis states that make up the system. For our system, the an arbitrary eigenstate is written as

$$|\psi^n\rangle = \sum_P c_P^n |P\rangle$$

where, c_P^n is the weight associated to each basis state $|P\rangle$ and energy level n . From this the expectation value of an operator \hat{O} may be expressed as

$$\langle \hat{O} \rangle^n = \frac{\langle \psi^n | \hat{O} | \psi^n \rangle}{\langle \psi^n | \psi^n \rangle} = \frac{\sum_{P,Q} c_Q^n c_P^n \langle Q | \hat{O} | P \rangle}{\sum_{P,Q} c_Q^n c_P^n \langle Q | P \rangle}.$$

So far, I have covered rules for the overlap $\langle Q | P \rangle$ and the matrix elements for the Hubbard Hamiltonian $\langle Q | \hat{\mathcal{H}} | P \rangle$; it is necessary to determine overlap rules $\langle Q | \hat{O} | P \rangle$ for a particular operator \hat{O} .

A particularly important operator is the structure factor, which contains the spin exchange term $\vec{S}_i \cdot \vec{S}_j$ seen in the Heisenberg Hamiltonian in [Chapter 2](#). The structure factor depends on a vector \vec{q} defined in k -space. The structure factor $S(\vec{q})$ is expressed as

$$S(\vec{q}) \equiv \langle \psi | \sum_{ij} e^{-i\vec{q} \cdot \vec{r}_{ij}} \vec{S}_i \cdot \vec{S}_j | \psi \rangle.$$

The vector \vec{r}_{ij} is the “distance” between sites i and j and is equal to $\vec{r}_{ij} = \vec{r}_j - \vec{r}_i$ where, \vec{r}_i is the vector location of lattice site i . It is similar to how matrix elements are labelled with *column* as the “ x -component” and *row* as the “ y -component.”

The structure factor $S(\pi)$ is the one-dimensional staggered magnetization and it is one of the measurements that I make on the ground state of the 1D Hubbard model. The analogous structure factor for the charge-density-wave order is

$$S_{CDW}(\vec{q}) = \langle \psi | \sum_{ij} e^{-\vec{q} \cdot \vec{r}_{ij}} (n_i - 1)(n_j - 1) | \psi \rangle.$$

We also make measurements for the expectation value of the dimer order operator $\langle \hat{D}^2 \rangle$

$$\langle \hat{D}^2 \rangle = \sum_{ij} (-1)^{r_i^x + r_j^x} \langle \psi | (\vec{S}_{\vec{r}_i} \cdot \vec{S}_{\vec{r}_i + \hat{x}}) (\vec{S}_{\vec{r}_j} \cdot \vec{S}_{\vec{r}_j + \hat{x}}) | \psi \rangle.$$

5.1 – Structure factor

The structure factor measures the magnetic order of a state. Classically, the staggered magnetization ($S(\pi)$ in 1D) measures the *antiferromagnetic* ordering of *nearest-neighbour* anti-aligned spins ($\uparrow, \downarrow, \uparrow, \downarrow, \uparrow, \downarrow, \dots$). $S(0)$ measures the one-dimensional *ferromagnetic* ordering of aligned spins ($\uparrow, \uparrow, \uparrow, \uparrow, \dots$). $S(\pi/2)$ measures the one-dimensional *antiferromagnetic* ordering of *next-nearest-neighbour* anti-aligned spins ($\uparrow, \uparrow, \downarrow, \downarrow, \uparrow, \uparrow, \dots$).

To make measurements using the structure factor, we need to be able to develop rules the matrix elements $\langle Q | \vec{S}_i \cdot \vec{S}_j | P \rangle$. To do so, we need to first determine the update rules $\vec{S}_i \cdot \vec{S}_j | P \rangle$. Since the spin operator \vec{S}_i operates on lone spin up or spin down electrons only, we expect $\vec{S}_i \cdot \vec{S}_j | P \rangle$ to be non-zero only when it acts on the singlets in state $|P\rangle$. This is verified algebraically in [Appendix B2.2](#) and the following table summarizes these update rules.

Table 7 – This table lists the update rules for $\vec{S}_i \cdot \vec{S}_j$ acting on and between the different bond types of our GVB basis.

$$\begin{aligned} (\vec{S}_i \cdot \vec{S}_j) \chi_{ij}^\dagger |vac\rangle &= -\frac{3}{4} \chi_{ij}^\dagger |vac\rangle & \begin{array}{c} \text{---} \text{---} \\ \text{---} \end{array} &\rightarrow -\frac{3}{4} \begin{array}{c} \text{---} \\ \text{---} \end{array} \\ (\vec{S}_i \cdot \vec{S}_j) \eta_{ij}^{u\dagger} |vac\rangle &= 0 & \begin{array}{c} \text{---} \text{---} \\ \text{---} \end{array} &\rightarrow 0 \\ (\vec{S}_i \cdot \vec{S}_j) \chi_{kj}^\dagger \chi_{il}^\dagger |vac\rangle &= \frac{1}{4} \chi_{kj}^\dagger \chi_{il}^\dagger |vac\rangle + \frac{1}{2} \chi_{ij}^\dagger \chi_{kl}^\dagger |vac\rangle \\ & \begin{array}{c} \text{---} \text{---} \text{---} \\ \text{---} \end{array} &\rightarrow \frac{1}{4} \begin{array}{c} \text{---} \text{---} \\ \text{---} \end{array} \begin{array}{c} \text{---} \text{---} \\ \text{---} \end{array} + \frac{1}{2} \begin{array}{c} \text{---} \text{---} \\ \text{---} \end{array} \\ (\vec{S}_i \cdot \vec{S}_j) \chi_{kj}^\dagger \eta_{il}^{u\dagger} |vac\rangle &= 0 & \begin{array}{c} \text{---} \text{---} \text{---} \\ \text{---} \end{array} &\rightarrow 0 \\ (\vec{S}_i \cdot \vec{S}_j) \eta_{kj}^{u\dagger} \eta_{il}^{v\dagger} |vac\rangle &= 0 & \begin{array}{c} \text{---} \text{---} \text{---} \\ \text{---} \end{array} &\rightarrow 0 \end{aligned}$$

According to the update rules listed in [Table 7](#), $\vec{S}_i \cdot \vec{S}_j$ only acts on singlet bonds and the bond types do not change. This suggests that, when considering the loop structure of the overlap $\langle Q | \vec{S}_i \cdot \vec{S}_j | P \rangle$, $\vec{S}_i \cdot \vec{S}_j$ must act within a pure singlet loop. The overlap rules are very similar to those of the VB basis and the Heisenberg model and are:

1. The overlap $\langle Q|P\rangle$ must be non-zero with at least one singlet loop
2. $\vec{S}_i \cdot \vec{S}_j$ must act within the same loop

The matrix elements $\langle Q|\vec{S}_i \cdot \vec{S}_j|P\rangle$ is summarized in the mathematical expression

$$\langle Q|\vec{S}_i \cdot \vec{S}_j|P\rangle = \frac{3}{4}\beta_{ij}\delta^{\alpha_i\alpha_j}\langle Q|P\rangle.$$

α_i is the loop identifier for the loop that contains lattice site i and β_{ij} is defined as

$$\beta_{ij} = \begin{cases} -1, & \text{if } i \text{ and } j \text{ are on opposite } \textit{loop} \text{ sublattices,} \\ +1, & \text{if } i \text{ and } j \text{ are on the same } \textit{loop} \text{ sublattice.} \end{cases}$$

β_{ij} is similar to the sign term ϵ_{ij} defined in [Chapter 2](#) for the same matrix elements using the VB basis; however, β_{ij} introduces a concept of *loop* sublattice, which I define as an ABAB... alternating pattern (see [Figure 23](#)) as the loop is traversed (“A” labels one sublattice and “B” labels the other sublattice). This loop sublattice is not necessarily coincident with the sublattice labelling of the underlying lattice.

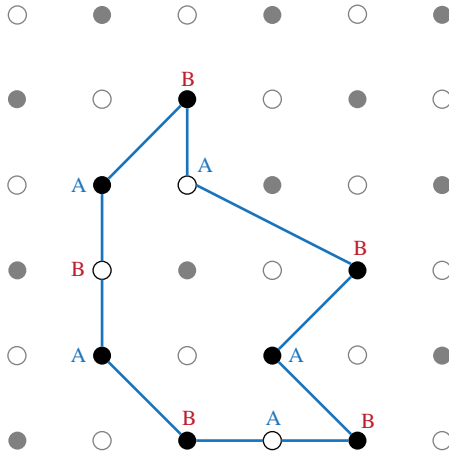


Figure 23 – This figure shows a singlet loop with labelling of the *loop* sublattice (ABAB...) along with the traditional sublattice labelling of the underlying lattice (closed and open circles).

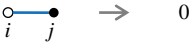










5.2 – Charge-density-wave order

The charge-density-wave (CDW) order is similar, in concept, to the structure factor involving spins up and down, except the CDW ordering involves double occupancies and vacancies. Classically, $S_{CDW}(\pi)$ measures the $\uparrow\downarrow, 0, \uparrow\downarrow, 0, \uparrow\downarrow, 0, \dots$ type ordering of the system, $S_{CDW}(0)$ measures the $\uparrow\downarrow, \uparrow\downarrow, \uparrow\downarrow, \uparrow\downarrow, \dots$ ordering and $S_{CDW}(\pi/2)$ measures the $\uparrow\downarrow, \uparrow\downarrow, 0, 0, \uparrow\downarrow, \uparrow\downarrow, 0, 0, \dots$ ordering.

The CDW structure factor involves $(n_i - 1)(n_j - 1)$ operators; in order to perform measurements on a state we need to be able to determine the corresponding update rules and matrix elements.

First we will consider the update rules for the operator $(n_i - 1)$ acting on each type of bond in our GVB basis. I worked these rules out in [Appendix B3](#) and they are summarized in [Table 8](#) below. $(n_i - 1)$ is zero if it acts on a singlet and it changes the charge bond type ($u \rightarrow \bar{u}$) if it acts on a charge bond. In our ensemble, which imposes half-filling strictly and not just on average, the Hubbard-U term $U \sum_i n_{i\uparrow} n_{i\downarrow}$ may be rewritten as $\frac{U}{2} \sum_i (n_i - 1)^2$. So the latter also counts the number of charge bonds in a given state. By compounding the rules for $(n_i - 1)$ I determined update rules for $(n_i - 1)(n_j - 1)$ (worked out in [Appendix B3](#) and summarized in [Table 8](#)).

Table 8 – This table summarizes the update rules for $(n_i - 1)$ and $(n_i - 1)(n_j - 1)$.

$(n_i - 1)\chi_{ij}^\dagger vac\rangle = 0$	
$(n_i - 1)\eta_{ij}^{u\dagger} vac\rangle = \eta_{ij}^{\bar{u}\dagger} vac\rangle$	
	
$(n_j - 1)\eta_{ij}^{u\dagger} vac\rangle = -\eta_{ij}^{\bar{u}\dagger} vac\rangle$	
	
$(n_i - 1)(n_j - 1)\eta_{ij}^{u\dagger} vac\rangle = -\eta_{ij}^{u\dagger} vac\rangle$	
	
$(n_i - 1)(n_j - 1)\eta_{kj}^{u\dagger} \eta_{il}^{v\dagger} vac\rangle = -\eta_{kj}^{\bar{u}\dagger} \eta_{il}^{v\dagger} vac\rangle$	
	
	
	

Using these update rules, I determined a possible (I have not verified these rules) set of rules to determine when the matrix elements $\langle Q|(n_i - 1)(n_j - 1)|P\rangle$ are non-zero. These matrix elements are non-zero when the following rules are satisfied.

1. All loops must be pure.
2. If sites i, j act within the same pure charge bond loop, then that loop must have an even number of NCBs.
3. If sites i, j act between two pure charge bond loops, then each of those two loops must have an odd number of NCBs.

5.3 – Dimer operator

Unlike the previous two structure factors, dimer ordering is not best described using the spins up and down. It is more natural to use singlets to describe the ordering, as a dimerized state (also known as a valence bond crystal or VBC [34][35][36]) is one with nearest-neighbour singlets (Figure 24a). $\langle \hat{D}^2 \rangle$ written at the beginning of the chapter describes as specific type of VBC in which the singlets are preferred to align horizontally in 2D (Figure 24b) (this is a result of the $(-1)^{r_i^x + r_j^x}$ term in $\langle \hat{D}^2 \rangle$), but can be trivially made to prefer vertical alignment (by changing the sign term to $(-1)^{r_i^y + r_j^y}$). In one dimension, this dimerized state is called the Majumdar-Ghosh chain [37][38] and consists of a chain of nearest-neighbour singlets (Figure 24c).

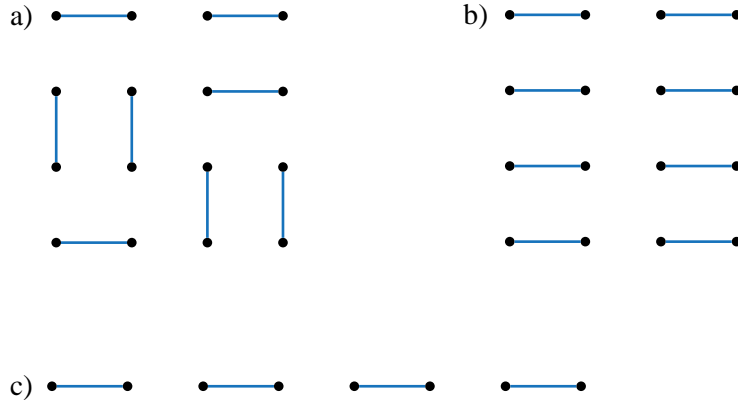


Figure 24 – An arbitrary VBC state in 2D with both horizontal and vertical nearest-neighbour singlets is shown in (a). The horizontally-aligned VBC state that is preferred by our dimer order operator $\langle \hat{D}^2 \rangle$ is shown in (b). The Majumdar-Ghosh chain, shown in (c), is the 1D VBC.

The dimer order is seen largely in frustrated regimes where there is competition between nearest- and next-nearest-neighbour antiferromagnetic interactions. In fact, the Majumdar-Ghosh chain is known to be the exact solution for the ground state of the Heisenberg model with the special condition that the next-nearest-neighbour exchange

amplitude (traditionally labelled J_2) is half the strength as the nearest-neighbour exchange amplitude (traditionally labelled J_1) [37][38], or alternately written $J_2/J_1 = 1/2$.

Consider the following example for insight of how a VBC in 1D is a natural way of representing a system with frustration from nearest- and next-nearest-neighbour interactions. Let

$$\begin{aligned}
|P\rangle &= \chi_{01}^\dagger \chi_{23}^\dagger |vac\rangle \\
&= \frac{1}{2} (|\uparrow_0\downarrow_1\rangle - |\downarrow_0\uparrow_1\rangle)(|\uparrow_2\downarrow_3\rangle - |\downarrow_2\uparrow_3\rangle) \\
&= \frac{1}{2} (|\uparrow_0\downarrow_1\uparrow_2\downarrow_3\rangle - |\uparrow_0\downarrow_1\downarrow_2\uparrow_3\rangle - |\downarrow_0\uparrow_1\uparrow_2\downarrow_3\rangle + |\downarrow_0\uparrow_1\downarrow_2\uparrow_3\rangle)
\end{aligned}$$

The two nearest-neighbour singlets is actually a linear superposition of nearest-neighbour antiferromagnetic ordering ($\uparrow\downarrow\uparrow\downarrow \dots$) and next-nearest-neighbour antiferromagnetic ordering ($\uparrow\uparrow\downarrow\downarrow \dots$). One would expect that, in the frustrated regime, the ground state would be some non-trivial superposition of the two types of antiferromagnetic ordering; and the VB basis does this naturally.

To obtain measurements of the dimer order to an eigenstate described using our GVB basis, we need to develop update rules for $(\vec{S}_i \cdot \vec{S}_j)(\vec{S}_k \cdot \vec{S}_l)$. These update rules can be thought out by applying $\vec{S}_i \cdot \vec{S}_j$ twice; however, there are many combinations so I will not write them down. The matrix elements $\langle Q | (\vec{S}_i \cdot \vec{S}_j)(\vec{S}_k \cdot \vec{S}_l) | P \rangle$ have been determined using the VB basis [26], so the rules for our basis are very similar. For these matrix elements to be non-zero:

1. The overlap $\langle Q | P \rangle$ must be non-zero with at least one pure singlet loop.
2. Two of the four indices need to belong to one singlet loop with the other two indices belonging to either the same loop or a different singlet loop.

If the matrix elements are non-zero, their values are given by (see [Figure 25](#) as well),

- a) $\frac{9}{16} \beta_{ij} \beta_{kl}$, if indices i, j, k, l belong to the same loop and the “virtual” bond connecting sites i and j *does not cross* the “virtual” bond connecting sites k and l .
- b) $\frac{3}{16} \beta_{ij} \beta_{kl}$, if indices i, j, k, l belong to the same loop and the “virtual” bond connecting sites i and j *does cross* the “virtual” bond connecting sites k and l .
- c) $\frac{9}{16} \beta_{ij} \beta_{kl}$, if indices i, j belong to one loop and indices k, l belong to another loop.
- d) $\frac{3}{16} \beta_{ik} \beta_{jl}$ (or $\frac{3}{16} \beta_{il} \beta_{jk}$), if indices i, k (or i, l) belong to one loop and indices j, l (or j, k) belong to another loop.

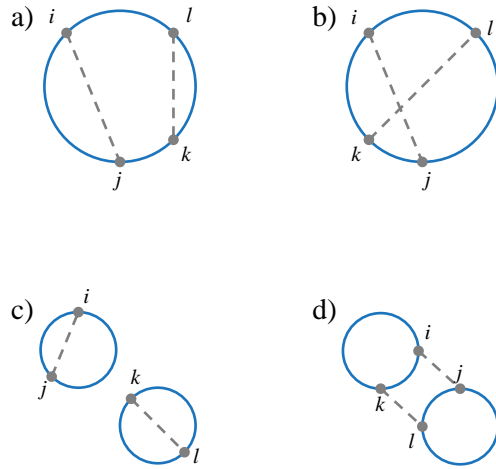


Figure 25 – Diagram showing the four cases (a-d) when $\langle Q | (\vec{S}_i \cdot \vec{S}_j) (\vec{S}_k \cdot \vec{S}_l) | P \rangle$ is non-zero. All loops in the diagram (represented by circles) are pure singlet loops. By nature of the problem, indices i and j are linked via $\vec{S}_i \cdot \vec{S}_j$ and k and l are linked via $\vec{S}_k \cdot \vec{S}_l$. I consider these links as “virtual” bonds and these bonds are drawn as dotted grey lines in the figure.

Chapter 6

Comparison to Known Models/Methods

Since we are limited to only a small number of lattice sites, due to the size of the singlet sector of the Hilbert space, I limited myself to a 1D chain with periodic boundary conditions. I solved the half-filled Hubbard model using our GVB basis via exact diagonalization with nearest- and next-nearest-neighbour hopping,

$$\hat{\mathcal{H}} = -t_1 \sum_{\substack{\langle i,j \rangle \\ \sigma}} (c_{i\sigma}^\dagger c_{j\sigma} + c_{j\sigma}^\dagger c_{i\sigma}) - t_2 \sum_{\substack{\langle\langle i,j \rangle\rangle \\ \sigma}} (c_{i\sigma}^\dagger c_{j\sigma} + c_{j\sigma}^\dagger c_{i\sigma}) + U \sum_i n_{i\uparrow} n_{i\downarrow}.$$

t_1 and t_2 are the nearest- and next-nearest-neighbour hopping amplitudes respectively, and I adopt the traditional notation for the representation of nearest- and next-nearest-neighbour lattice sites as $\langle i, j \rangle$ and $\langle\langle i, j \rangle\rangle$ (as seen in the summations), respectively. When I solve the model, I divide through by t_1 , such that everything is measured in units of t_1 (this can also be effectively thought as setting $t_1 = 1$),

$$\frac{\hat{\mathcal{H}}}{t_1} = - \sum_{\substack{\langle i,j \rangle \\ \sigma}} (c_{i\sigma}^\dagger c_{j\sigma} + c_{j\sigma}^\dagger c_{i\sigma}) - \frac{t_2}{t_1} \sum_{\substack{\langle\langle i,j \rangle\rangle \\ \sigma}} (c_{i\sigma}^\dagger c_{j\sigma} + c_{j\sigma}^\dagger c_{i\sigma}) + \frac{U}{t_1} \sum_i n_{i\uparrow} n_{i\downarrow}.$$

The parameters that I varied are $0 \leq t_2/t_1 \leq 2$ and $0 \leq U/t_1 \leq 200$; each set of values $(t_2/t_1, U/t_1)$ comprises a *data point*.

Once solved and I obtain the eigenenergies and eigenstates, for various data points, I measured the staggered magnetization $S(\pi)$ (labelled M2 in the plots), the doubly staggered magnetization $S(\pi/2)$ (labelled M2D in the plots) and the dimer order $\langle \hat{D}^2 \rangle$ (labelled D2 in the plots) for each data point.

I compared my ground state energies and staggered magnetizations (for various values of t_2/t_1 and U/t_1) with those I obtained using the traditional occupation basis (solving the Hubbard model via exact diagonalization still, though restricting the occupation basis to the $S^z = 0$ sector of the Hilbert space). This comparison is done in order to verify that my basis (and all the rules I developed) are correct.

Then I compare my ground state energies at $U/t_1 = 200$ (for various values of t_2/t_1) with those I obtained solving the Heisenberg model via exact diagonalization using the VB basis. This comparison was, in part, to further verify my basis, and to establish that,

in the limit of large U , the Heisenberg model and the half-filled Hubbard model are equivalent.

In the opposite limit, when $U/t_1 = 0$, the Hubbard model becomes the tight-binding model, and I compare my ground state energies (for various values of t_2/t_1) with those obtained from the tight-binding model solved analytically in the micro-canonical ensemble. This comparison was also done, in part, to verify my basis, but also to ensure that the tight-binding model and the Hubbard model (using the GVB basis) are equivalent.

6.1 – Hubbard model and the occupation basis

When I compared the ground state energies using the GVB basis with those using the occupation basis, there was complete agreement for $N = 4$ and $N = 8$ (See **Figures 27 – 30**). However, for $N = 6$, there is disagreement for large $t_2/t_1 (>1)$ and small $U (\sim 2)$ (**Figures 27 – 30**). This disagreement is due to the natural next-nearest-neighbour frustration that occurs for one dimensional, $N/2$ odd, lattices through periodic boundary conditions. This frustration forces the ground state outside the $S = 0$ sector of the Hilbert space (into the $S = 1$ spin sector). The GVB basis, restricted to the $S = 0$ sector, cannot detect this; whereas, the occupation basis can. Consider of the following figure to see how this frustration occurs.

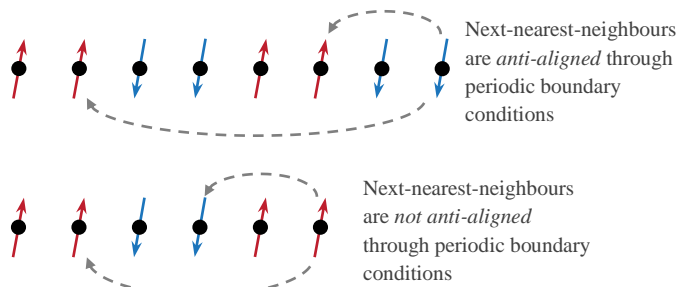


Figure 26 – This figure shows that for 6 sites (or any odd $N/2$), the next-nearest-neighbour antiferromagnetic ordering is disrupted through periodic boundary conditions. This is not true for 8 sites (or any even $N/2$).

The following four figures (**Figures 27 – 30**) show the ground state energy per site (E^0/Nt_1) for four values of U/t_1 (0, 2, 20, and 200) and $0 \leq t_2/t_1 \leq 2$ (“Occ” denotes the occupation basis).

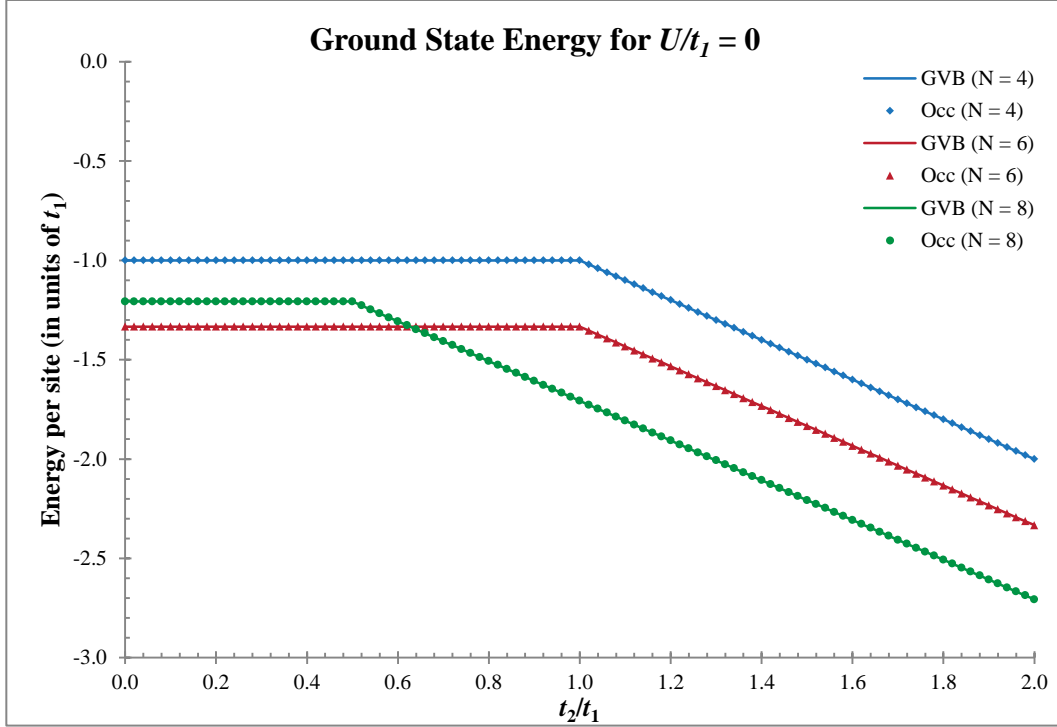


Figure 27 – For each case ($N = 4, 6,$ and 8) there is one cusp where the ground state transitions from the $\uparrow\downarrow\uparrow\downarrow \dots$ antiferromagnetic ordered state (left of cusp, independent on t_2/t_1) to the $\uparrow\uparrow\downarrow\downarrow \dots$ antiferromagnetic ordered state (right of cusp, depends linearly on t_2/t_1).

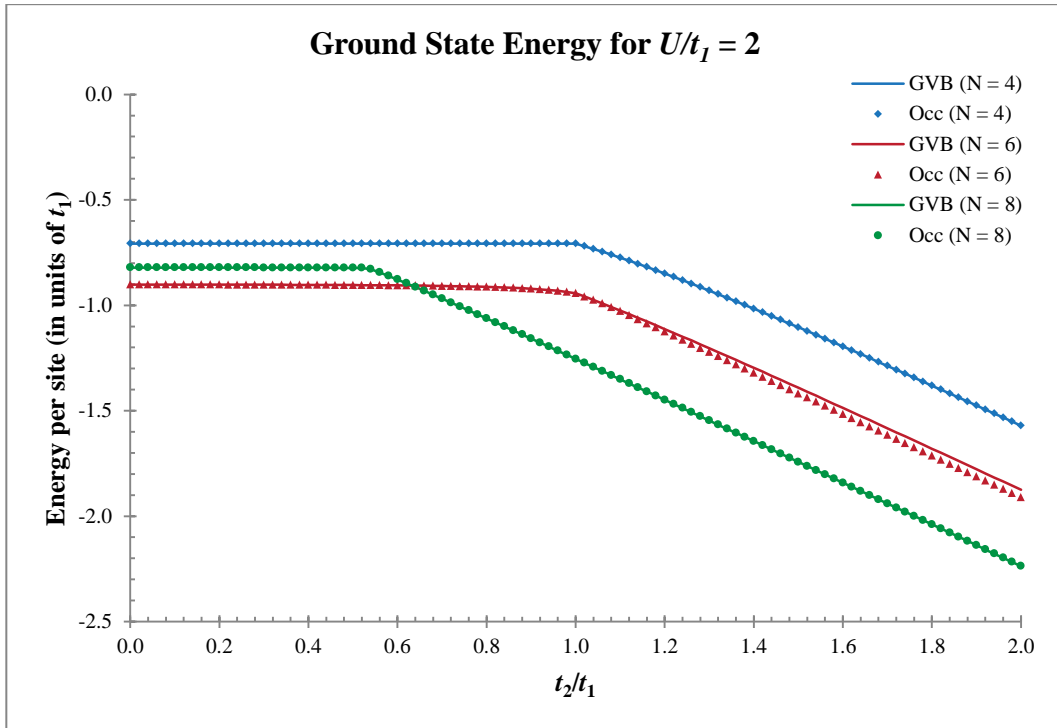


Figure 28 – The cusps are still visible and we begin to see the transition between the two antiferromagnetic states becoming smoother as N and U are increased. We clearly see the discrepancy for $N = 6$ when using the occupation basis (spanning the $S_{tot}^z = 0$ spin sector) and the GVB basis (spanning the $S_{tot} = 0$ spin sector).

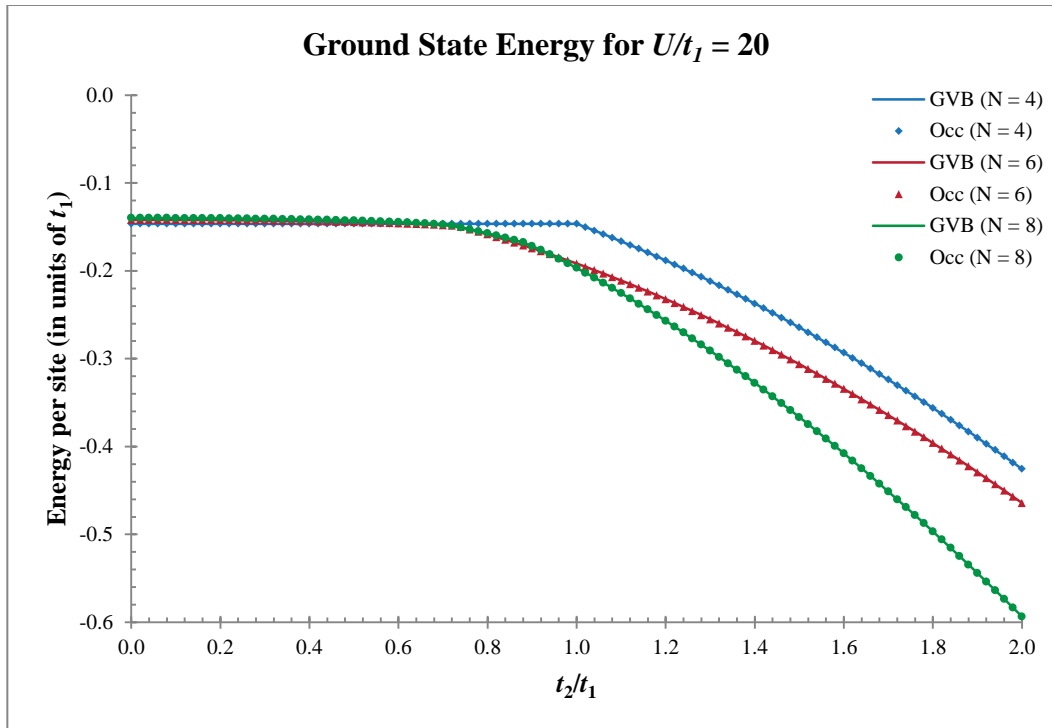


Figure 29 – As U/t_1 is large now, the ground state energies obtained with either basis are now equal for $N = 6$.

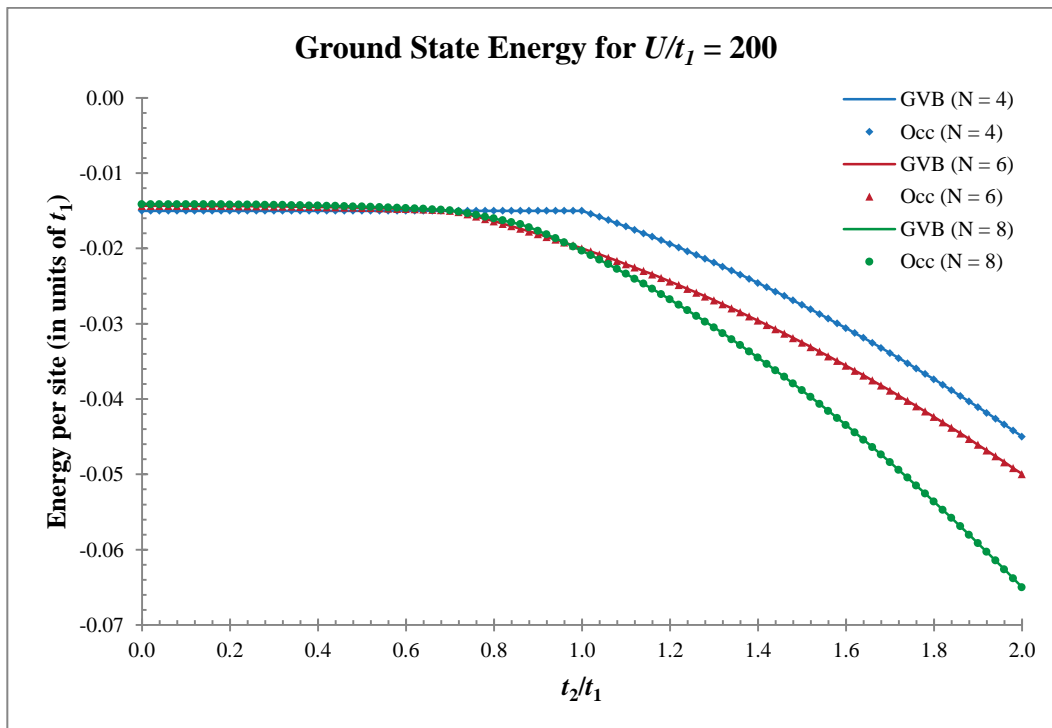


Figure 30 – With $U/t_1 = 200$, it is significantly large enough to be considered as the large- U limit and we have complete agreement between the ground state energies using the occupation basis and the GVB basis. Not obvious in this particular plot, there are actually three unique states for $N = 8$ and $U/t_1 = 200$ instead of the two seen at small U (it is seen much more clearly in the staggered magnetization plots).

Disregarding the $N = 6$, large t_2/t_1 discrepancy, due to frustration through periodic boundary conditions, there is complete agreement between the ground state energies obtained (via exact diagonalization) using the traditional occupation basis and our newly proposed GVB basis. This supports the conclusion that the GVB basis and the update rules used to obtain the overlaps $\langle Q|P\rangle$ and matrix elements $\langle Q|\hat{\mathcal{H}}|P\rangle$ are correct. The $N = 6$ discrepancy (or I believe odd $N/2$ discrepancy) forces the ground state out of the $S = 0$ spin sector into the $S = 1$ spin sector for large t_2/t_1 and small U , which means, by construction, that our GVB basis cannot capture this $S = 1$ ground state as the GVB basis only spans the $S = 0$ spin sector.

The next set of plots (**Figures 31 – 33**) show that staggered magnetization $S(\pi)$ calculated on the occupation basis ground state and the GVB basis ground state for $U/t_1 = 0$ for $N = 4, 6$, and 8 . Recall that the staggered magnetization measures the nearest-neighbour antiferromagnetic ordering $\uparrow\downarrow\uparrow \dots$ so we expect it to be large for small values of t_2/t_1 . **Figures 31 and 33** ($N = 4$ and 8 respectively) show a clear instability, seen using *either* basis, for values of t_2/t_1 left of the cusp. When these instabilities occur is related to a degeneracy seen at $U/t_1 = 0$ and we will look at this in more detail with the tight-binding model in **Chapter 6.3**. Nevertheless, since these instabilities occur with either basis, I do not consider it an issue with the GVB basis or the appropriate update and overlap rules; but I expect it to be a numerical issue with LAPACK that occurs whenever there is this “degeneracy” as described in **Chapter 6.3**.

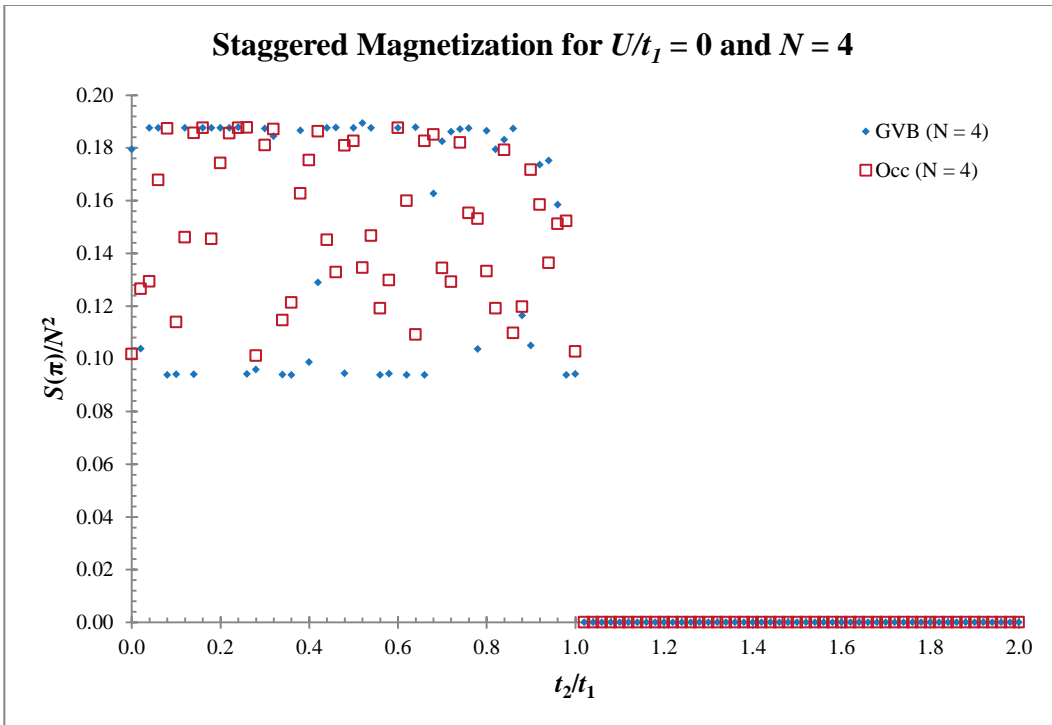


Figure 31 – For $t_2/t_1 < 1$, there is a clear instability issue when using either the occupation or the GVB basis; although, the GVB basis appears to be less affected by this instability. For $t_2/t_1 > 1$, there is no issue whatsoever.

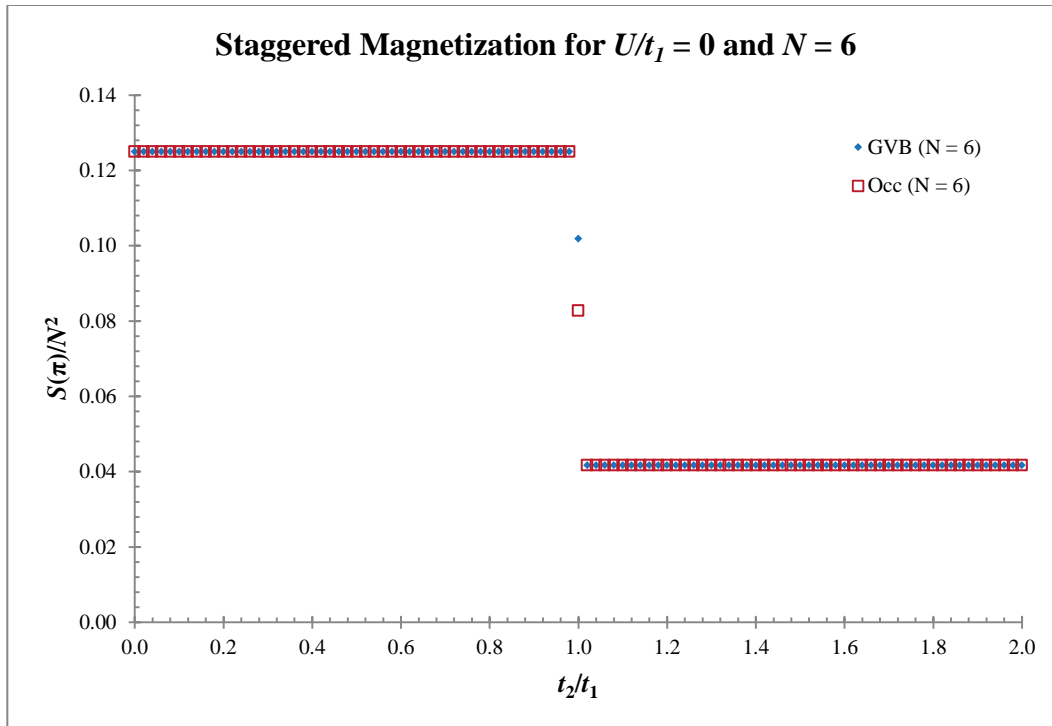


Figure 32 – There is no instability issue for any value of t_2/t_1 and $N = 6$. Notice that $S(\pi)$ is larger for $t_2/t_1 < 1$, which corresponds the expectation of $\uparrow\downarrow\downarrow \dots$ antiferromagnetic ordering in this region. For $t_2/t_1 > 1$, we expect $\uparrow\downarrow\downarrow \dots$ antiferromagnetic ordering; but even with this ordering, half the *nearest-neighbours* are anti-aligned as well, which is why $S(\pi)$ is non-zero in this region.

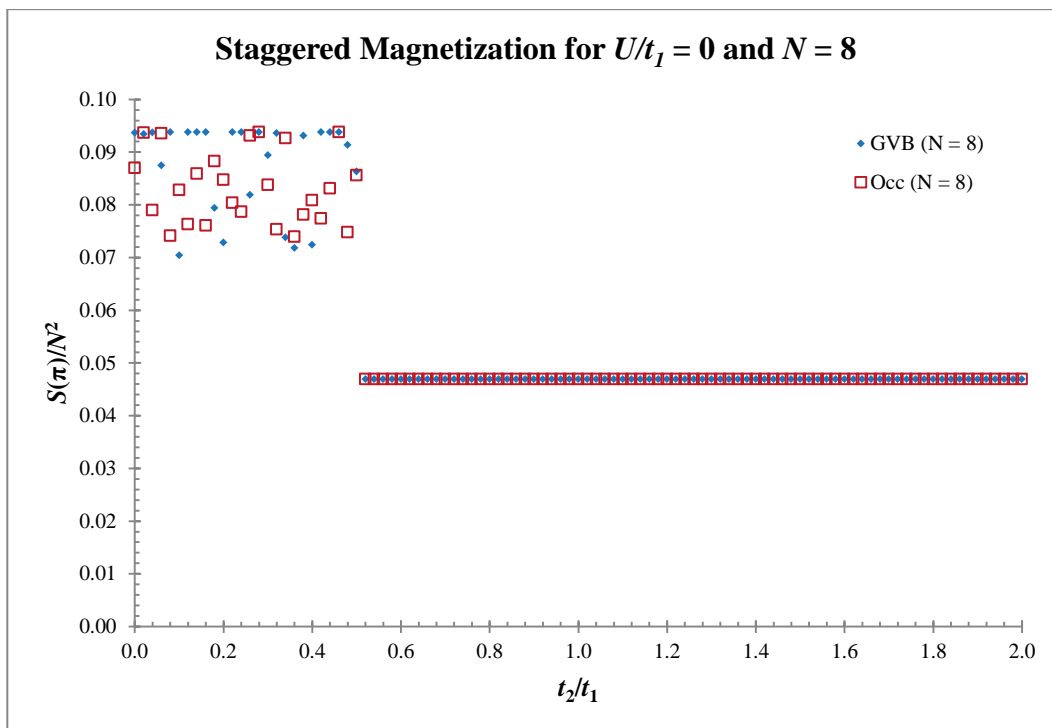


Figure 33 – Similar to $N = 4$, we see an instability again using either basis, but this time for $t_2/t_1 < 1/2$; after which, the instability disappears.

The cusps seen in the ground state energy plots (Figures 27 – 30) are seen as discontinuities in the staggered magnetization plots. As we will see when we look at the staggered magnetization for $U/t_1 = 20$ and 200 (Figures 35 and 36), there are actually three states (two cusps) other than the apparent two (one cusp) seen in the ground state energies for the same values of U/t_1 .

For $U/t_1 = 2, 20,$ and 200 and $N = 4$ and 8, there is complete agreement between the staggered magnetization calculated using occupation states as the basis and GVB states as the basis. The instability seen at $U/t_1 = 0$ disappears (using either basis) when we increase U/t_1 ; in fact, the instability disappears for $U/t_1 = 10^{-4}$ (see Chapter 6.3). The discrepancy seen for $N = 6, t_2/t_1 > \sim 1.06,$ and $U/t_1 = 2$ is because of same reason as the discrepancy seen in the ground state energies at the same point.

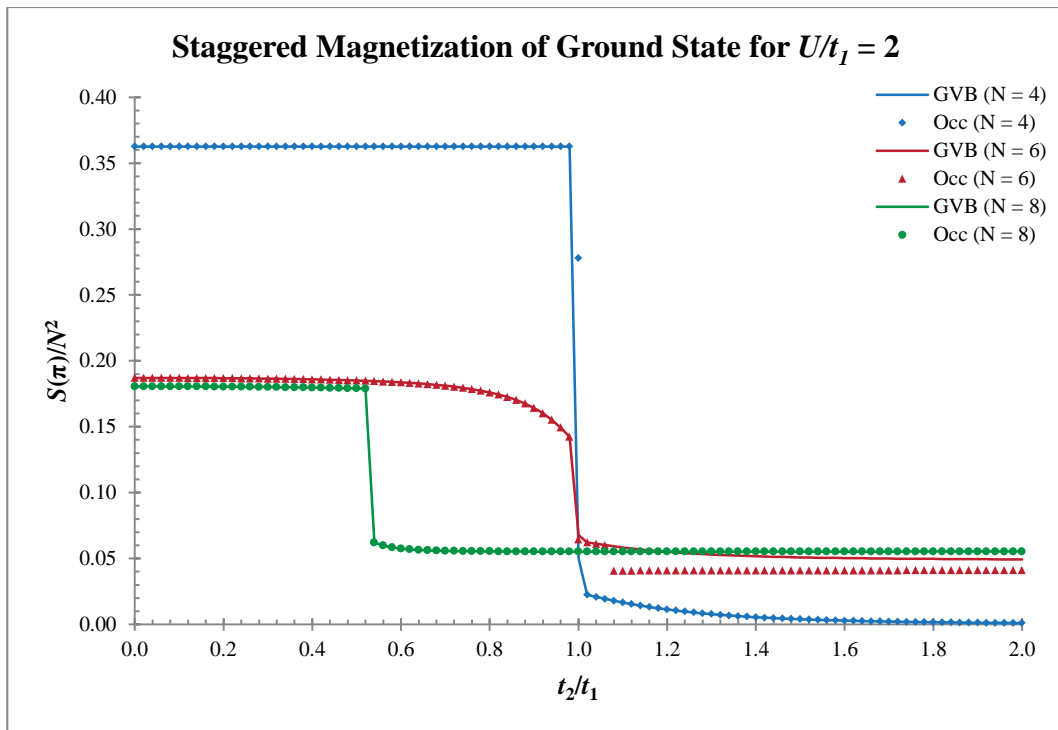


Figure 34 – As we saw in the ground state energies for $U/t_1 = 2$ (Figure 28), there is complete agreement for $N = 4$ and 8 and the same discrepancy for $N = 6$.

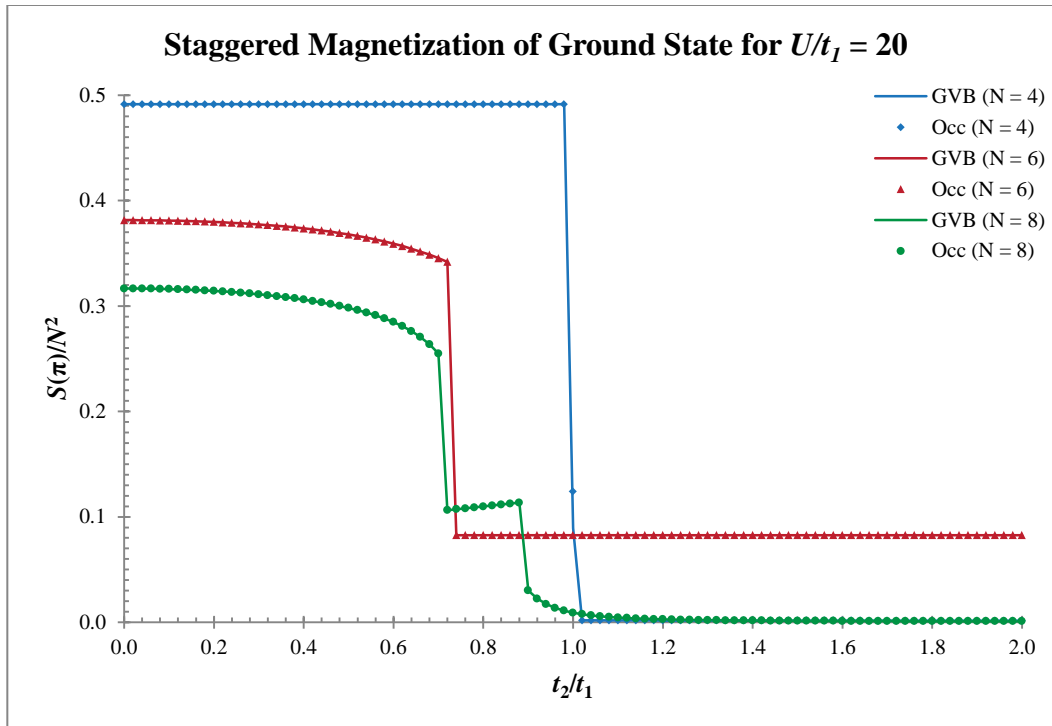


Figure 35 – There is complete agreement seen in the range $0 < t_2/t_1 < 2$ (above which I did not make any measurements) for $N = 4, 6,$ and 8 sites. Notice that, for $N = 8$, there are clearly three different states.

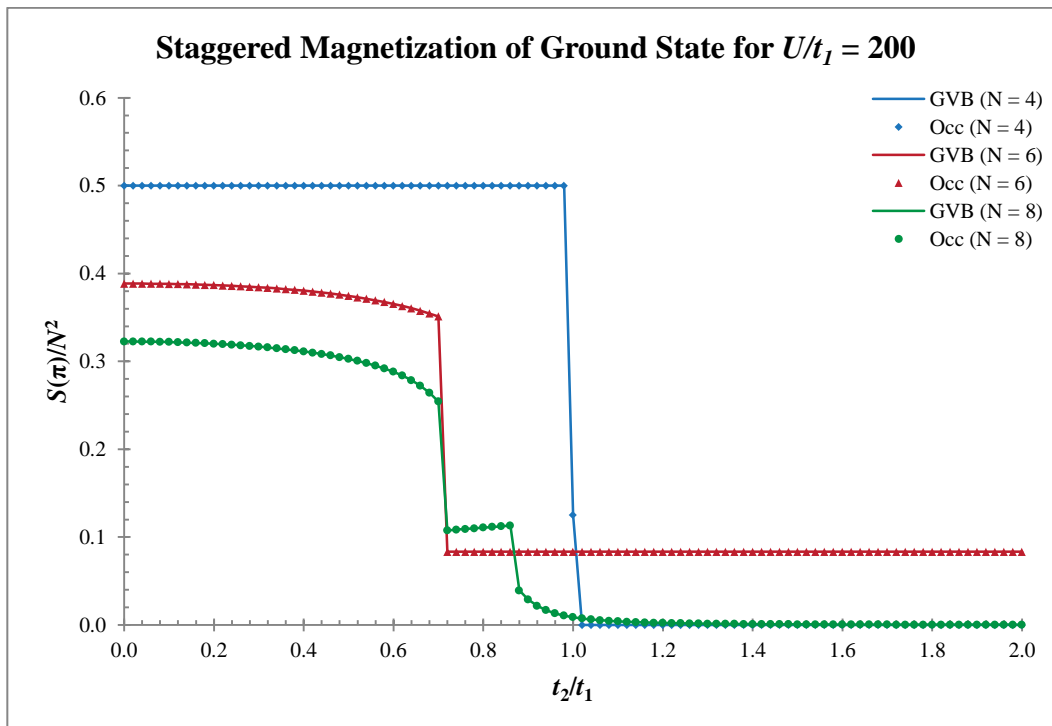


Figure 36 – There is complete agreement again for $N = 4, 6,$ and 8 . The middle state seen for $N = 8$ is actually the 1D VBC as we will see in [Chapters 6.2 and 7](#).

From these comparisons of the ground state energies and staggered magnetizations between the GVB basis and the occupation basis, there does not appear to be any issue with the update rules or the overlap rules themselves. The discrepancy seen at $N = 6$, large t_2/t_1 , and small U/t_1 seen is because of frustration, through periodic boundary condition, for next-nearest-neighbour interactions. The instabilities at $U/t_1 = 0$ exactly are seen when using either basis and localized to a particular region of t_2/t_1 as well. As a result, it is unlikely that these instabilities would be caused by inappropriate update or overlap rules.

6.2 – Heisenberg model and the VB basis

As mentioned in previous chapters, the Heisenberg model can be derived from the Hubbard model in the limit as $U \rightarrow \infty$ [1]. As an additional check to make sure that the GVB basis is correct and works according to the update and overlap rules that I developed, I will compare my results from solving the Hubbard model at $U/t_1 = 200$ via exact diagonalization using the GVB basis with results I obtained from solving the Heisenberg model via exact diagonalization using the VB basis. As **Figures 40 – 42** show us, the ground state energies for the Hubbard model (at $U/t_1 = 200$) and the Heisenberg model are the same; the Hubbard model ground state energies require scaling (according to the expression in the graphs) and plotting with respect to $(t_2/t_1)^2$. This comes from the fact that the exchange amplitude J_{ij} of the Heisenberg model is related to the square of the hopping amplitude t_{ij} of the Hubbard model at large U [1],

$$J_{ij} = \frac{4t_{ij}^2}{U}.$$

This can be shown using the occupation basis or the GVB basis. First consider the occupation basis and the hopping term t_{ij} acting between two spins (see **Figure 37**). If sites i and j contain a spin up (or down) each, then, because of Pauli exclusion principle, there can be no hopping between the two sites. If one site contains a spin up and the other a spin down, then an electron can hop from one site to the other creating a double occupancy and a vacancy (it actually creates a charge bond) with an energy cost of U because of the double occupancy. Since a double occupancy is energetically unfavourable (since U is considered to be large), an electron in the doubly occupied site will hop to the vacant site, creating a singlet. This process, called virtual hopping, involves two hops, hence t_{ij}^2 , with one energy cost U .

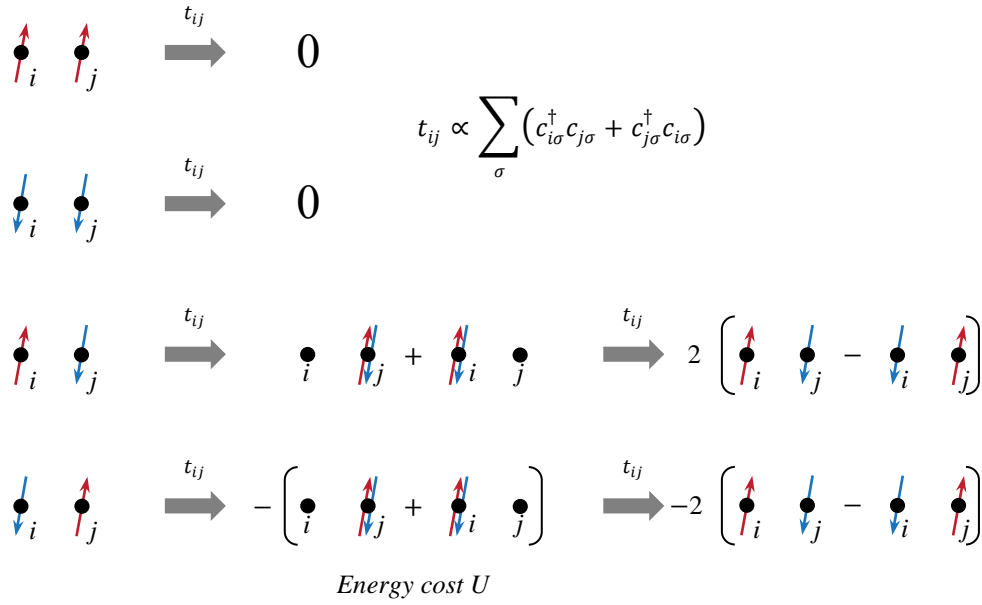


Figure 37 – This is an illustration of how the hopping term t_{ij} affects a pair of singly occupied sites.

Now consider the same spin states, except using the exchange term J_{ij} to operate on them (**Figure 38**). We obtain, in the end, the same states, except off by a factor of 4.

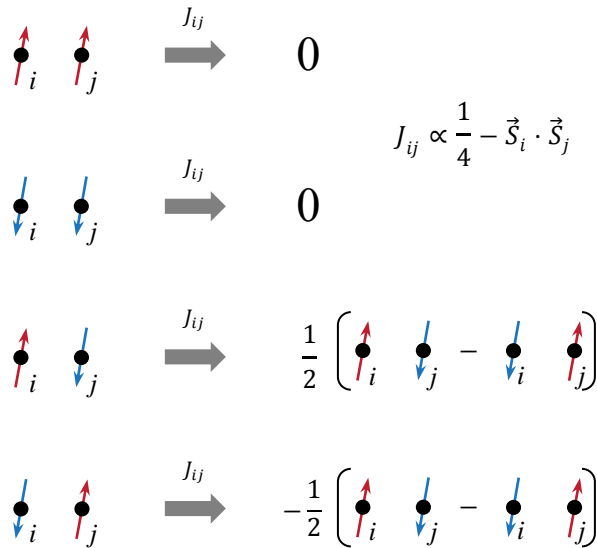


Figure 38 – This is an illustration of how the exchange term J_{ij} affects a pair of singly occupied sites. The exchange term J_{ij} is conceptually equivalent to acting with the hopping term t_{ij} twice with an energy cost U for creating a doubly occupied site in the process.

Notice that despite starting with a state that is just a spin up on one site and spin down on the other, whenever that state is acted on with the exchange term J_{ij} or hopping term t_{ij} a singlet or charge bond is created. This implies that singlets and charge bonds are perhaps

a more natural language to use to describe a state. We can also describe virtual hopping in terms of the GVB basis (**Figure 39**) as changing the bond from a singlet to a PCB and then back to a singlet.

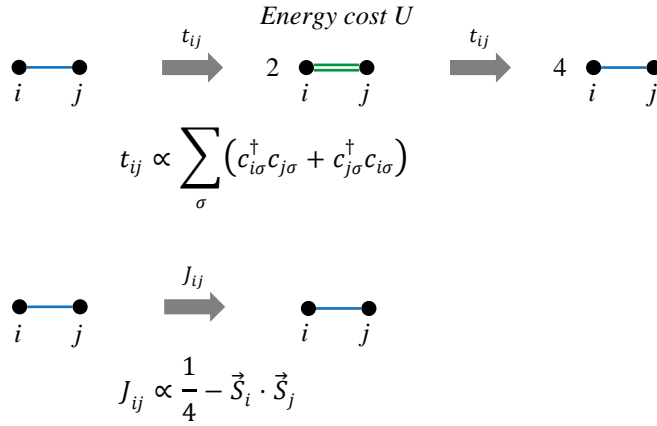


Figure 39 – The process of virtual hopping can be described with the GVB basis as well.

The following three plots (**Figures 40 – 42**) compare the ground state energies obtained through solving the Heisenberg model and the Hubbard model with $U/t_1 = 200$ and nearest- and next-nearest-neighbour interactions; such that the Heisenberg Hamiltonian can be written in terms of the nearest- (J_1) and next-nearest-neighbour (J_2) exchange terms.

$$\hat{\mathcal{H}} = J_1 \sum_{\langle i,j \rangle} \vec{S}_i \cdot \vec{S}_j + J_2 \sum_{\langle\langle i,j \rangle\rangle} \vec{S}_i \cdot \vec{S}_j.$$

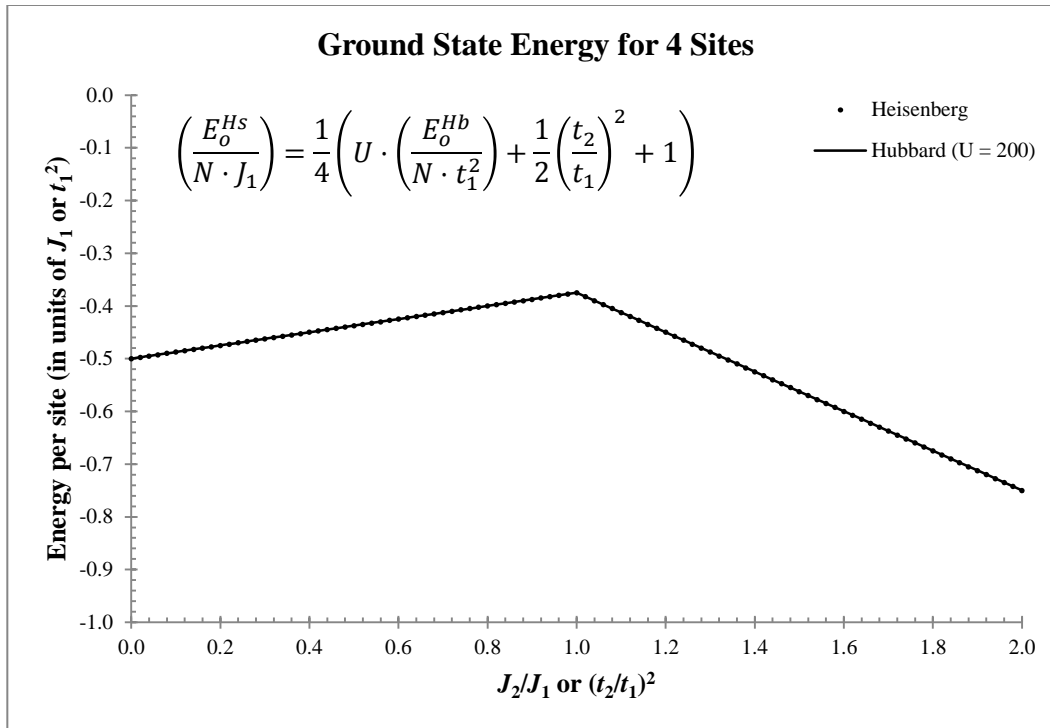


Figure 40 – The ground state energy for 4 sites has one cusp at $J_2/J_1 = 1$ (or $(t_2/t_1)^2 = 1$) separating the nearest-neighbour antiferromagnetically ordered $\uparrow\downarrow\uparrow\downarrow \dots$ state and the next-nearest-neighbour antiferromagnetically ordered $\uparrow\uparrow\downarrow\downarrow \dots$ state (see **Figure 43**). The “1/2” coefficient in front of the $(t_2/t_1)^2$ term compensates for double counting the next-nearest-neighbours in the $N = 4$ case. With scaling (according to the expression in the figure) the Hubbard ground state energies agree completely with the Heisenberg ground state energies.

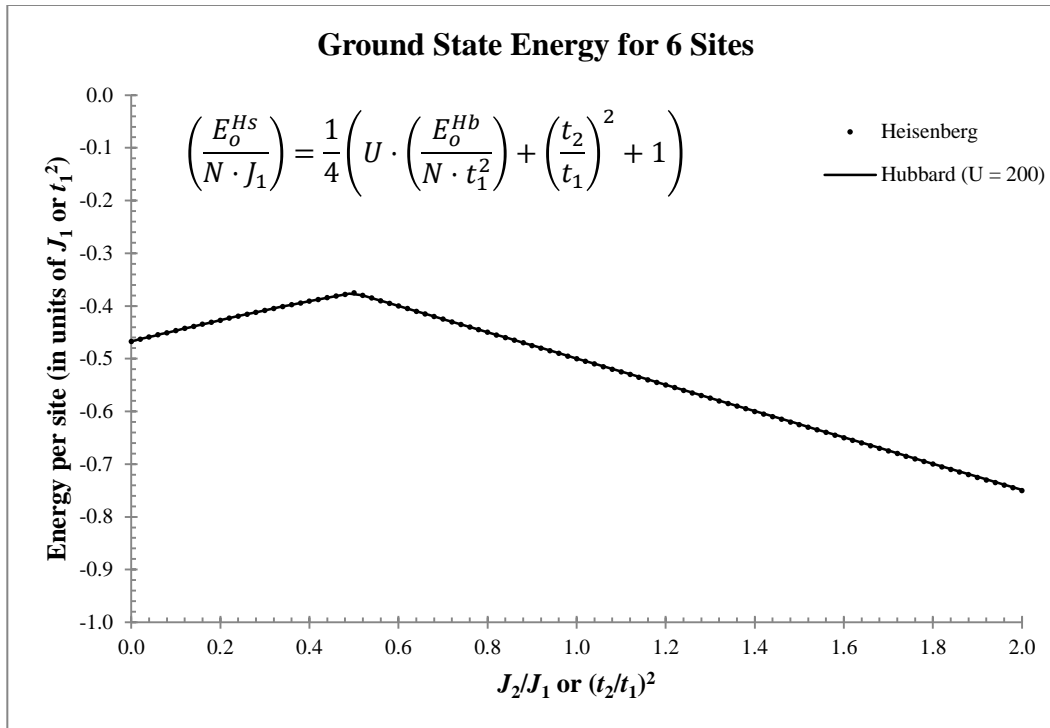


Figure 41 – For $N = 6$, there is one cusp at $J_2/J_1 = 0.5$ where there is a level crossing and there is complete agreement between the Heisenberg and Hubbard ground state energies.

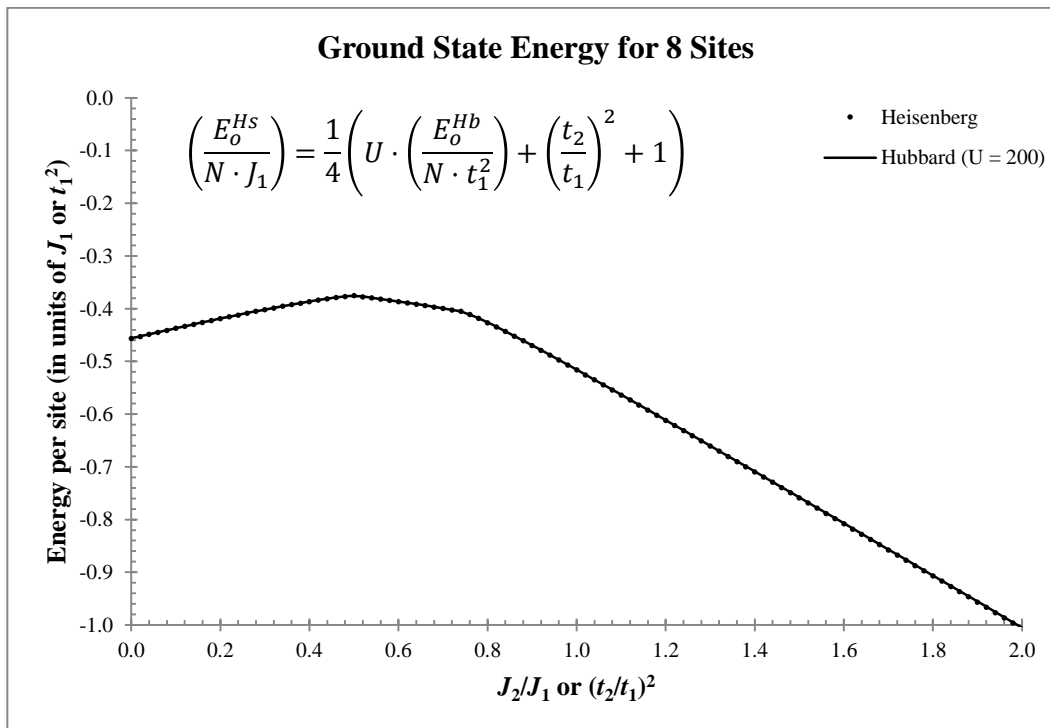


Figure 42 – This figure has two cusps, one at $J_2/J_1 = 0.5$ and the other at $J_2/J_1 = 0.75$. For $0 < J_2/J_1 < 0.5$ the ground state has $\uparrow\downarrow\uparrow\downarrow \dots$ antiferromagnetic ordering and for $J_2/J_1 > 0.75$, the ground state has $\uparrow\uparrow\downarrow\downarrow \dots$ antiferromagnetic ordering. Between the two cusps is when the ground state has the frustrated 1D VBC ordering (see **Figure 45**).

There are no discrepancies between the ground state energies of the Heisenberg and Hubbard models; thus, further supporting that my GVB basis rules are correct.

The three figures (**Figures 43 – 45**) show three spin correlation functions: staggered magnetization $S(\pi)$ (or M2), doubly staggered magnetization $S(\pi/2)$ (or M2D), and dimer order $\langle \hat{D}^2 \rangle$ (or D2). We expect $S(\pi)$ ordering ($\uparrow\downarrow\uparrow\downarrow \dots$) to dominate for small t_2/t_1 , $S(\pi/2)$ ordering ($\uparrow\uparrow\downarrow\downarrow \dots$) to dominate for large t_2/t_1 , and $\langle \hat{D}^2 \rangle$ to dominate in the frustrated regime in between (see **Figure 45**).

We nearly see complete agreement between the spin correlation functions calculated on the Heisenberg ground state and the Hubbard ground state at $U/t_1 = 200$. The only discrepancies occur around the cusp points because the exact diagonalization process is unstable at these level crossings where there are, often, many degenerate states. Also, some disagreement is seen because of resolution. The data points are equally space apart with respect to t_2/t_1 ($\Delta t_2/t_1 = 0.02$) and J_2/J_1 ($\Delta J_2/J_1 = 0.02$). However, I am plotting the Hubbard results with respect to $(t_2/t_1)^2$ and as a result the resolution is higher for small t_2/t_1 and lower for large t_2/t_1 .

Note the y-axis label “ O/N^2 ,” where O is the corresponding operator ($S(\pi)$, $S(\pi/2)$, or $\langle \hat{D}^2 \rangle$).

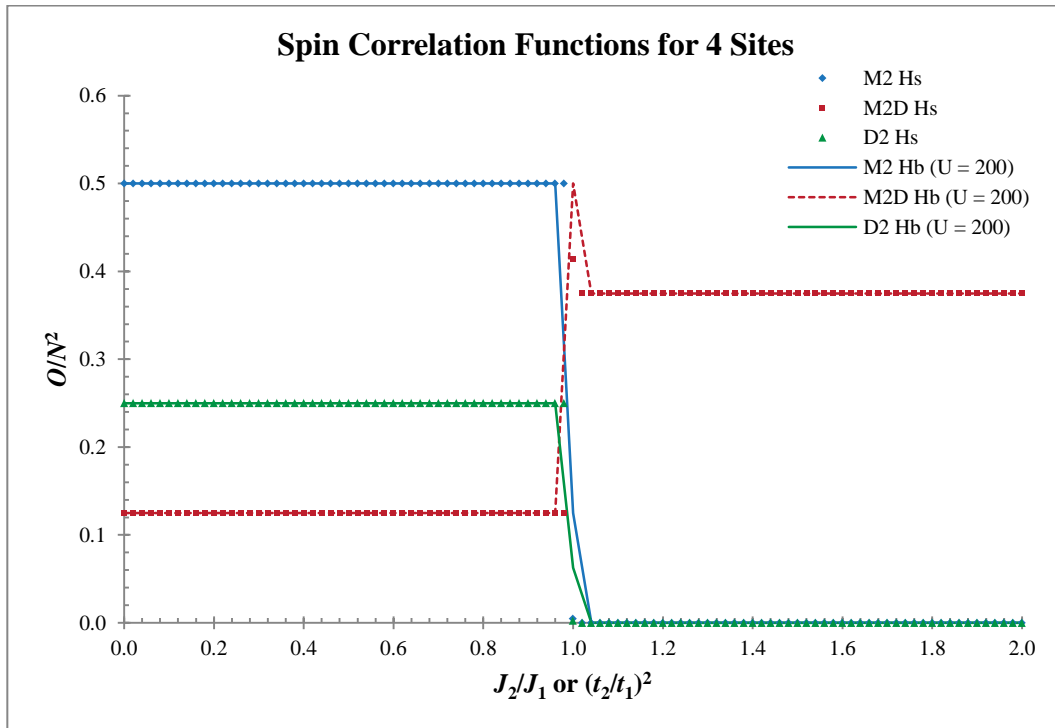


Figure 43 – Other than at the cusp points, there is complete agreement between the spin correlation functions calculated on the ground state of the Heisenberg model and the Hubbard model at $U/t_1 = 200$.

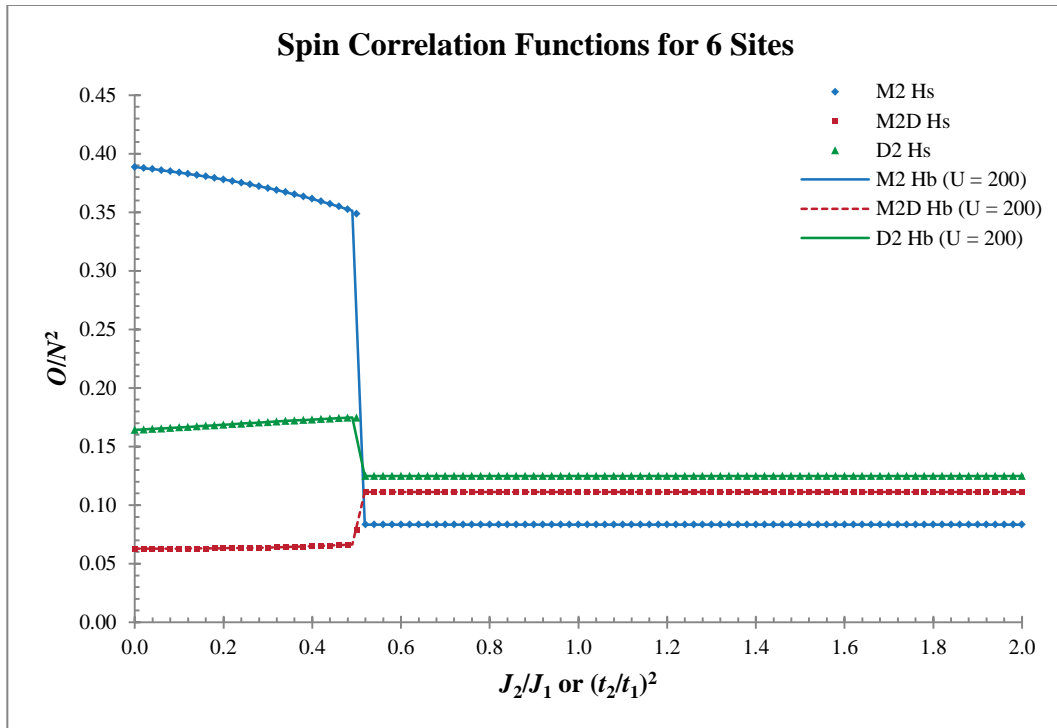


Figure 44 – Oddly enough dimer order is dominant for $J_2/J_1 > 0.5$ (with M2D close behind). This is most likely the cause of the increased frustration due to the periodic boundary conditions when next-nearest-neighbour antiferromagnetic interactions are large on odd $N/2$ 1D lattices.

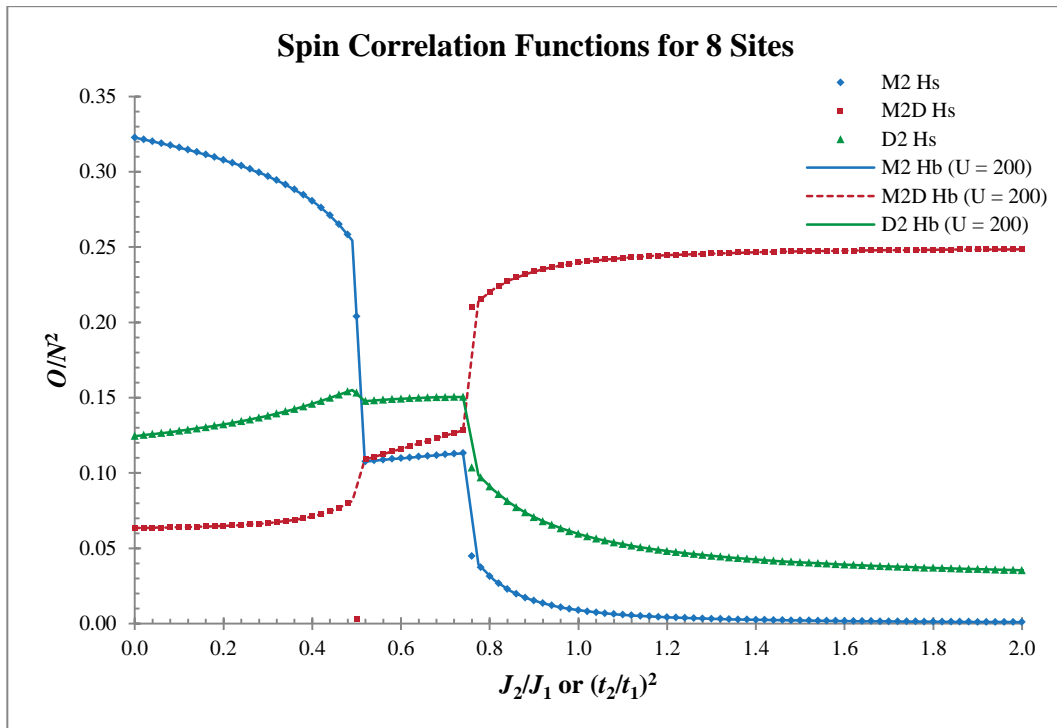


Figure 45 – There are three regions in which each of the spin correlation functions dominate. For small J_2/J_1 , M2 ($\uparrow\uparrow\downarrow\downarrow \dots$) order dominates, for large J_2/J_1 , M2D ($\uparrow\uparrow\downarrow\downarrow \dots$) order dominates, and in the frustrated regime in between, the dimer order dominates.

6.3 – Tight-binding model (analytical)

If we set $U = 0$ in our Hubbard Hamiltonian we obtain the following, so-called, tight-binding Hamiltonian

$$\hat{\mathcal{H}} = - \sum_{ij,\sigma} t_{ij} (c_{i\sigma}^\dagger c_{j\sigma} + c_{j\sigma}^\dagger c_{i\sigma}).$$

Restricting ourselves to nearest- and next-nearest-neighbour hopping only, we obtain

$$\hat{\mathcal{H}} = -t_1 \sum_{\substack{\langle i,j \rangle \\ \sigma}} (c_{i\sigma}^\dagger c_{j\sigma} + c_{j\sigma}^\dagger c_{i\sigma}) - t_2 \sum_{\langle\langle i,j \rangle\rangle} (c_{i\sigma}^\dagger c_{j\sigma} + c_{j\sigma}^\dagger c_{i\sigma}).$$

The tight-binding model can be solved analytically via taking the Fourier transform of each creation ($c_{i\sigma}^\dagger$) and annihilation ($c_{i\sigma}$) operator.

$$c_{i\sigma}^\dagger = \frac{1}{\sqrt{N}} \sum_{\vec{k}} e^{-i\vec{k}\cdot\vec{r}_i} c_{k\sigma}^\dagger$$

$$c_{i\sigma} = \frac{1}{\sqrt{N}} \sum_{\vec{k}} e^{i\vec{k}\cdot\vec{r}_i} c_{k\sigma}$$

After some work (shown in [Appendix C](#)), the tight-binding model is expressed in k -space and in diagonal form as

$$\hat{\mathcal{H}} = \sum_{k\sigma} \varepsilon_k c_{k\sigma}^\dagger c_{k\sigma}$$

with

$$\varepsilon_k = -2t_1 \cos(ka) - 2t_2 \cos(2ka)$$

as the tight-binding energy spectrum and where ‘ a ’ is the distance between nearest-neighbour atoms. The energy spectrum is plotted with respect to ‘ ka ’ in [Figure 46](#) for five different values of the parameter t_2/t_1 .

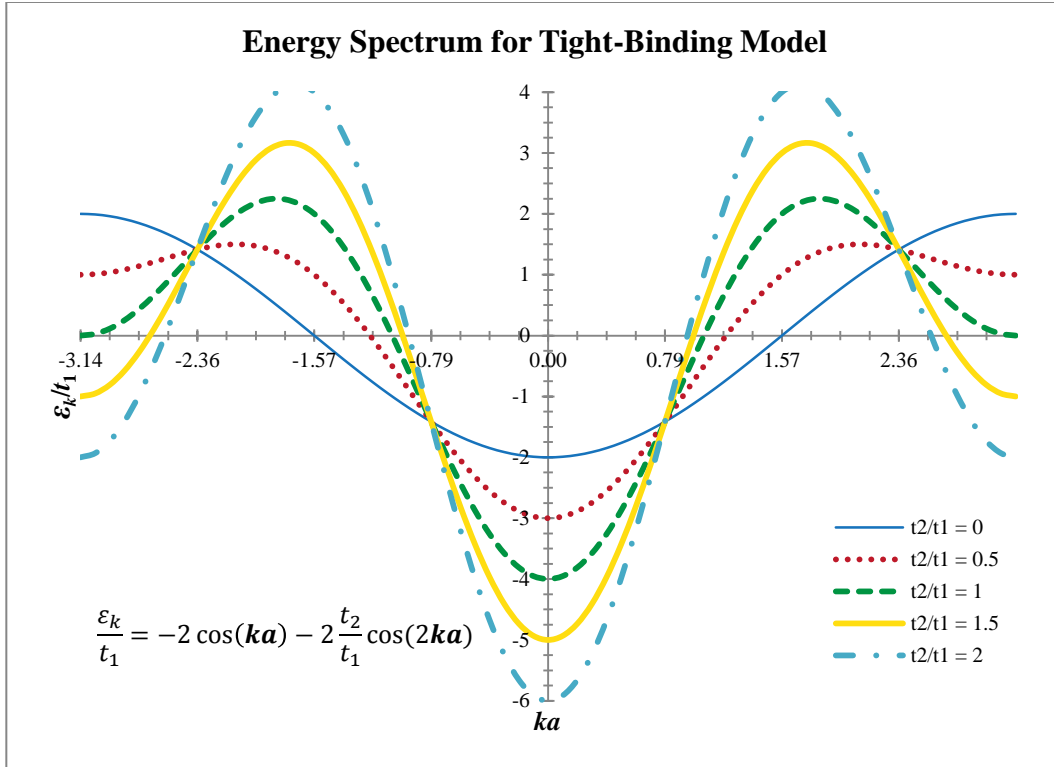


Figure 46 – The tight-binding energy spectrum is plotted with respect to ‘ ka ’ for five different values of the parameter t_2/t_1 .

The ground state energy for a half-filled N -site system is determined by assigning N electrons ($N/2$ spin up electrons and $N/2$ spin down electrons) to the lowest energy levels. Since we are dealing with a discrete lattice of N sites, the energy spectrum ε_k is divided equally into N divisions. For example, when $N = 8$ the energy spectrum is divided up into the 8 possible k -states $ka = 0, \pm \frac{\pi}{4}, \pm \frac{\pi}{2}, \pm \frac{3\pi}{4}, \pi$, and the states with the lowest energy levels are filled with the 8 electrons. It is easier to see the states of lowest energy when we plot these particular states as a function of t_2/t_1 (see **Figure 47**).

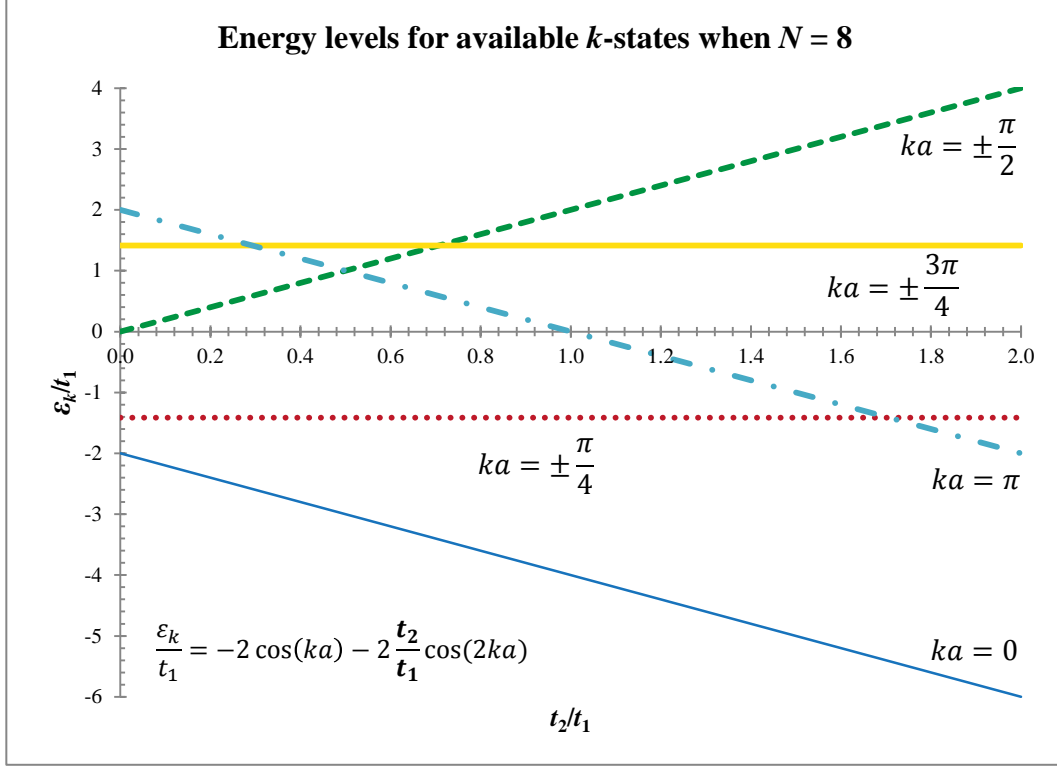


Figure 47 – This figure plots the energy levels for the 8 possible k -states when $N = 8$ with respect to t_2/t_1 . Each state can hold two electrons (one spin up and one spin down).

From **Figure 47** we can clearly see a level crossing at $t_2/t_1 = 0.5$ where the states $ka = \pm\pi/2$ cross the $ka = \pi$ state (there are other level crossings, but this one is particularly important to the ground state). For $t_2/t_1 < 0.5$ the lowest energy states are $ka = 0, \pm\pi/4$, and $\pm\pi/2$; however, there are a total of *ten* possible locations where the 8 electrons may be placed. Nevertheless, this does not affect the ground state energy; we just fill up the $ka = 0$ state with 2 electrons, the $ka = \pm\pi/4$ states with 4 electrons, and place the remaining 2 electrons in any of the four possible locations in states $ka = \pm\pi/2$. The ground state energy is obtained by summing the energies of the occupied states. Thus for 8 sites, the ground state energy is

$$\begin{aligned} \frac{E_o}{t_1} &= 2 \left(-2 - 2 \frac{t_2}{t_1} \right)_{ka=0} + 4(-\sqrt{2})_{ka=\pm\pi/4} + 2 \left(2 \frac{t_2}{t_1} \right)_{ka=\pm\pi/2} \\ &= -4(\sqrt{2} + 1) \approx -9.65685. \end{aligned}$$

The ground state energy written as energy per site is

$$\frac{E_o}{Nt_1} = -\frac{1}{2}(\sqrt{2} + 1) \approx -1.20711$$

and as seen in **Figure 48**, this is equivalent to my results obtained with the GVB basis and the Hubbard model (for $t_2/t_1 < 0.5$). For $\frac{t_2}{t_1} > 0.5$, the lowest energy states are $ka = 0, \pm\pi/4$, and π , and there are eight possible locations for the 8 electrons. All the ground state energies per site that I obtained using the GVB basis agree with the analytical ground state energies obtained from solving the tight-binding model for 4, 6, and 8 sites.

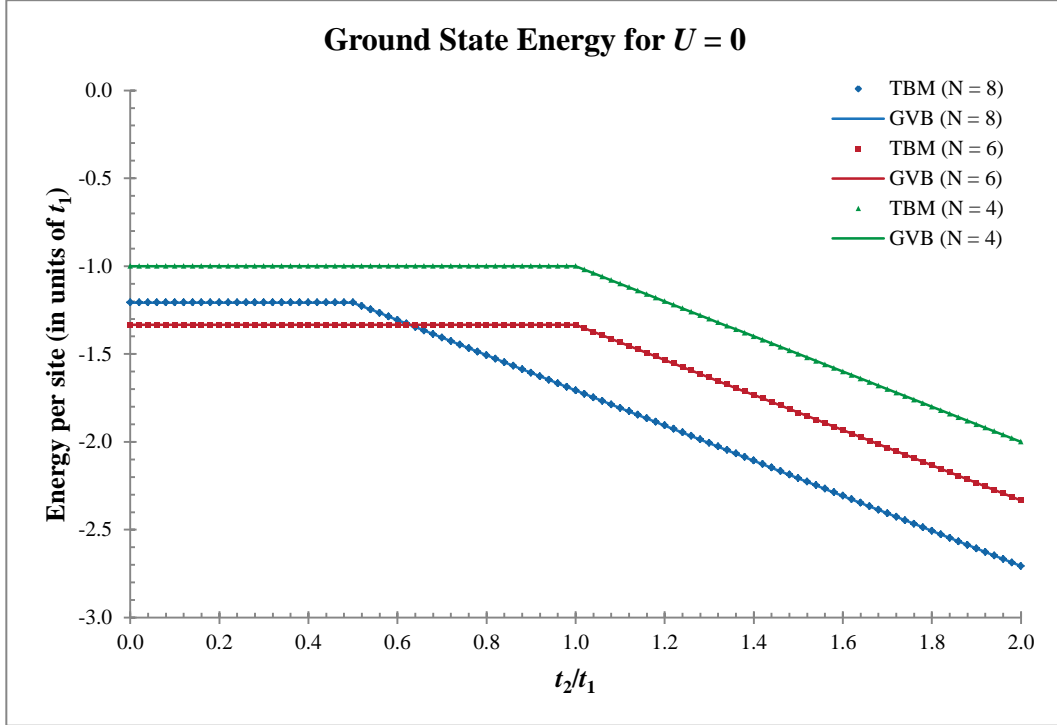


Figure 48 – This figure is a plot of the ground state energies per site for the tight-binding-model (TBM) and the Hubbard model (using the GVB basis).

All the cusps seen in **Figure 48** are a result of level crossings as seen with our $N = 8$ example. Note that, for 4 sites, the level crossing is at 1.0, not 0.5 like the $N = 8$ case. This is because there is a slight change in the energy spectrum function to account for double counting next-nearest-neighbours ($t_2/t_1 \rightarrow \frac{1}{2}t_2/t_1$).

Since the tight-binding-model has an analytical solution, we are not limited by the number of sites. Consider the ground state energy for large N ($N = 100$) in **Figure 49**.

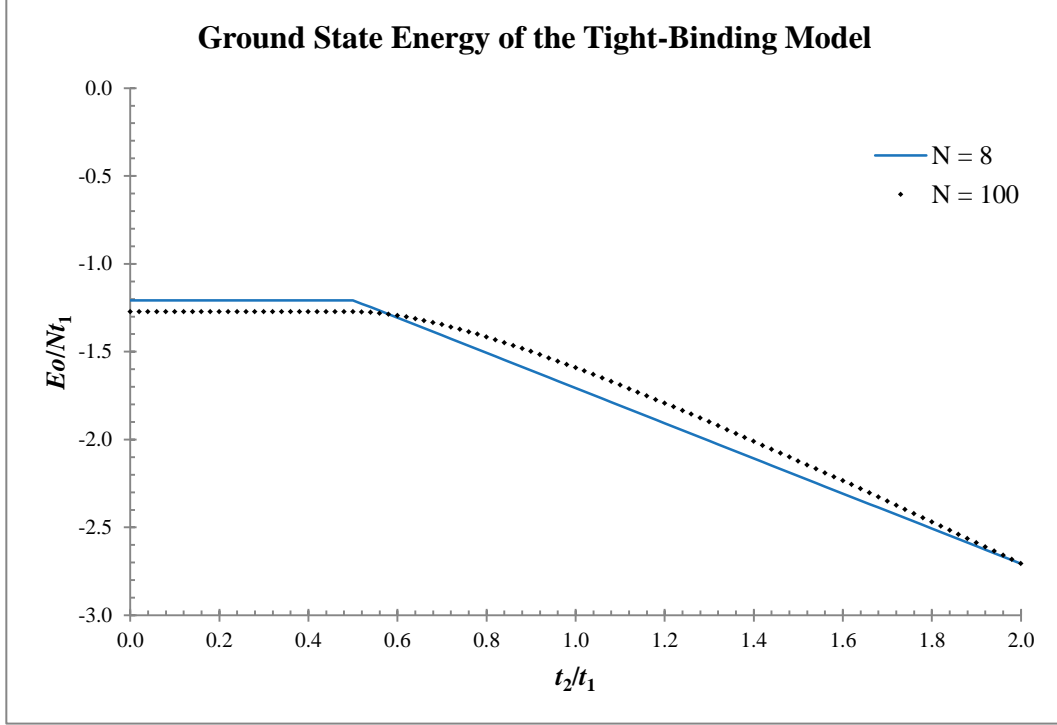


Figure 49 – The ground state energy of the tight-binding model for $N = 8$ and $N = 100$. The energy is constant with respect to t_2/t_1 for $t_2/t_1 < 0.5$ in the large- N limit, just as it was for $N = 8$. However, for large N and large t_2/t_1 , the slope of the energy is steeper. This suggests 8 sites is a decent approximation (in terms of capturing the ground state properties) for small t_2/t_1 , but not for larger t_2/t_1 .

Interestingly enough, the point $t_2/t_1 = 0.5$ is an important transition point even in the large- N limit and before this point the ground state is independent of t_2/t_1 .

As I mentioned in the $N = 8$ example, the case when $t_2/t_1 < 0.5$ and we need to place two electrons into the four locations provided by the states $ka = \pm\pi/2$ was not an issue with the ground state energy (as any arrangement has the same energy). However, this is not the case with the staggered magnetization $S(\pi)$. The 1D structure factor $S(q)$ can be determined by taking the Fourier transform of the creation and annihilation operators (see [Appendix C2](#)) and at the end can be expressed as

$$S(q) = \frac{1}{4} \sum_k \left(3 \sum_s f(\varepsilon_{k+q,s}) - 2 \sum_{st} f(\varepsilon_{ks}) f(\varepsilon_{k+q,t}) + \sum_s (f(\varepsilon_{ks}) f(\varepsilon_{k+q,s})) \right) + \frac{\delta_{q,0}}{4} \sum_{kl} \left(2 \sum_s f(\varepsilon_{ks}) f(\varepsilon_{ls}) - \sum_{st} f(\varepsilon_{ks}) f(\varepsilon_{lt}) \right)$$

where, s and t are spin indices (just like σ), k and l are k -state indices, and

$$f(\varepsilon_{ks}) = \begin{cases} 1, & \text{if there is an electron in state } k \text{ with spin } s, \\ 0, & \text{otherwise.} \end{cases}$$

The structure factor then depends on the arrangement of the electrons; thus, it is important to consider the possible arrangements. There is a *degeneracy* issue whenever there are more locations than electrons to fill them at the Fermi level. The next three figures (**Figures 50 – 52**) plotting $S(\pi)$ show that the arrangement of a double occupancy and a vacancy is possibly the correct arrangement for the ground state. However, since there is a stability issue with exact diagonalization at $U = 0$ exactly (see **Chapter 6.1**), I cannot say for certain.

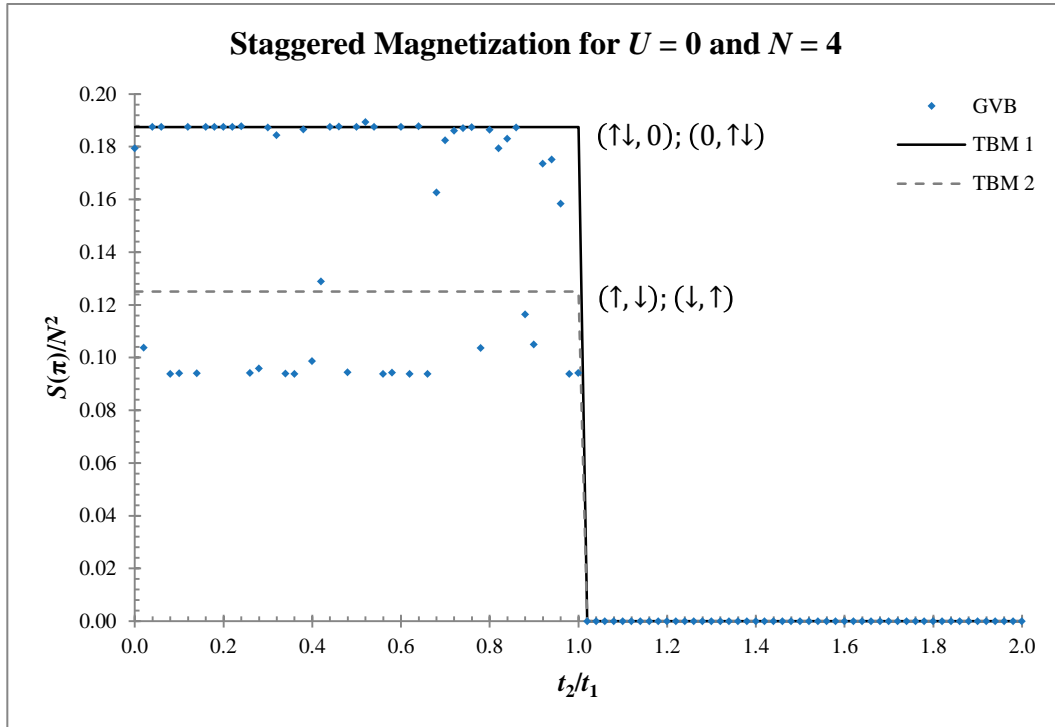


Figure 50 – Like the 8-site case, when $N = 4$, there is the degeneracy between states $\pm\pi/2$ at the Fermi level for $t_2/t_1 < 1$. It appears that the $(\uparrow\downarrow, 0)$ arrangement (TBM 1) in states $(+\pi/2, -\pi/2)$ agrees with the GVB results (TBM 2 is the staggered magnetization for the arrangement (\uparrow, \downarrow)). Unfortunately, because there definitely is an instability issue with the GVB results (recall that this instability issue is seen with the occupation basis results as well) I cannot state this conclusively. Note that the two degenerate states at the Fermi level is separated by π and I am measuring $S(\pi)$; I believe this relation to be important.

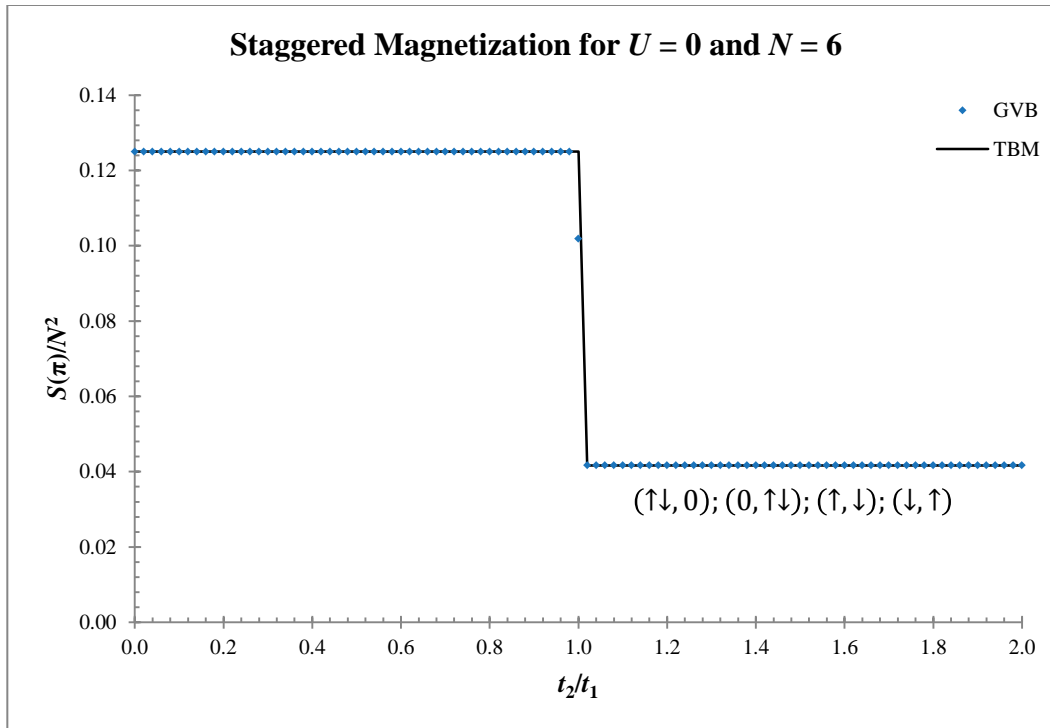


Figure 51 – For $N = 6$, there is no instability issue; however, there is a degeneracy between states $\pm\pi/3$ for $t_2/t_1 > 1$ (see **Figure 53**) but this does not alter the staggered magnetization $S(\pi)$. Note that in this case the degenerate states are separated by $2\pi/3$, not π .

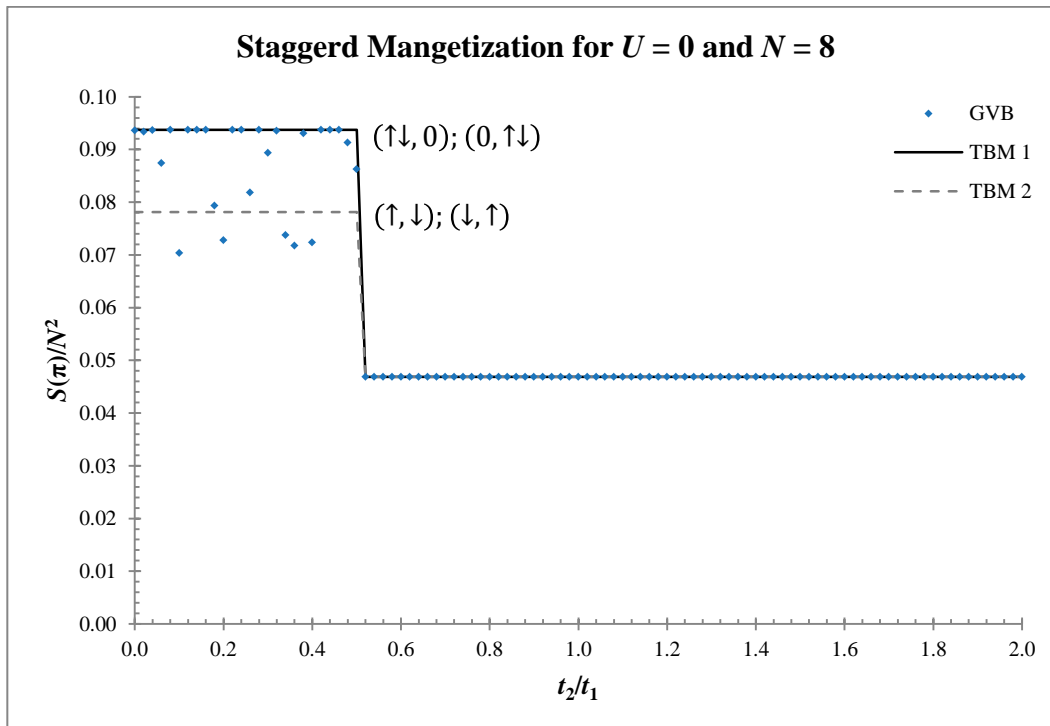


Figure 52 – We see the instability issue again, but only in the region where we have the $+\pi/2$ and $-\pi/2$ degeneracy at the Fermi level. And again, it appears that the $(\uparrow\downarrow, 0)$ arrangement (TBM 1) is the preferred arrangement.

I suspect that this instability, at $U = 0$ exactly, *only* occurs when we have this degeneracy issue at the Fermi level *and* the degenerate states are separated by π for measurements with $S(\pi)$. The 6-site case does have this degeneracy issue for $t_2/t_1 > 1$, but it involves two electrons filling the four locations provided by states $ka = \pm\pi/3$ (see **Figure 53**).

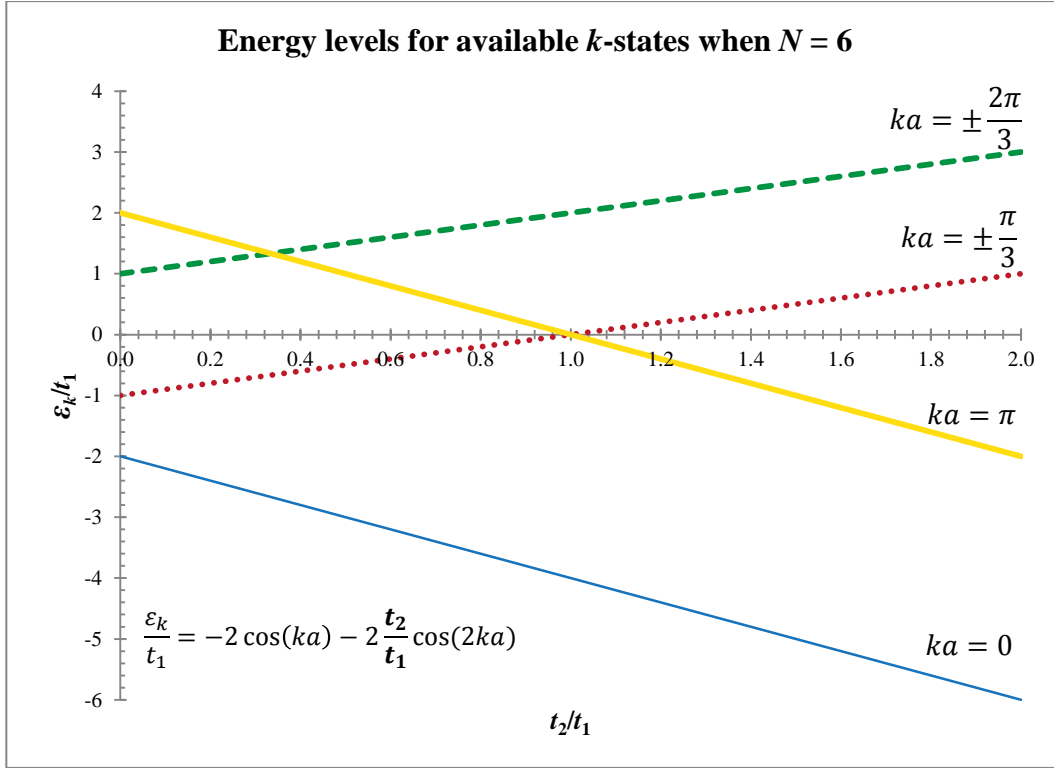


Figure 53 – For $t_2/t_1 < 1$, states $ka = 0$ and $ka = \pm\pi/3$ are filled completely with the six available electrons. For $t_2/t_1 > 1$, states $ka = 0$ and $ka = \pi$ are filled completely, and states $ka = \pm\pi/3$ are half-filled with only two electrons.

I mentioned in **Chapter 6.1** that the GVB and occupation basis results stabilize for small U . **Figures 54 – 56** show that the GVB results is stabilized for $U = 10^{-4}$, but the values are shifted from the tight-binding values. This shift is only seen with the $+\pi/2$ and $-\pi/2$ degeneracy. Unfortunately, I do not know why this shift occurs, but it is also seen with the occupation basis results; so I do not believe this to be an issue with the GVB basis.

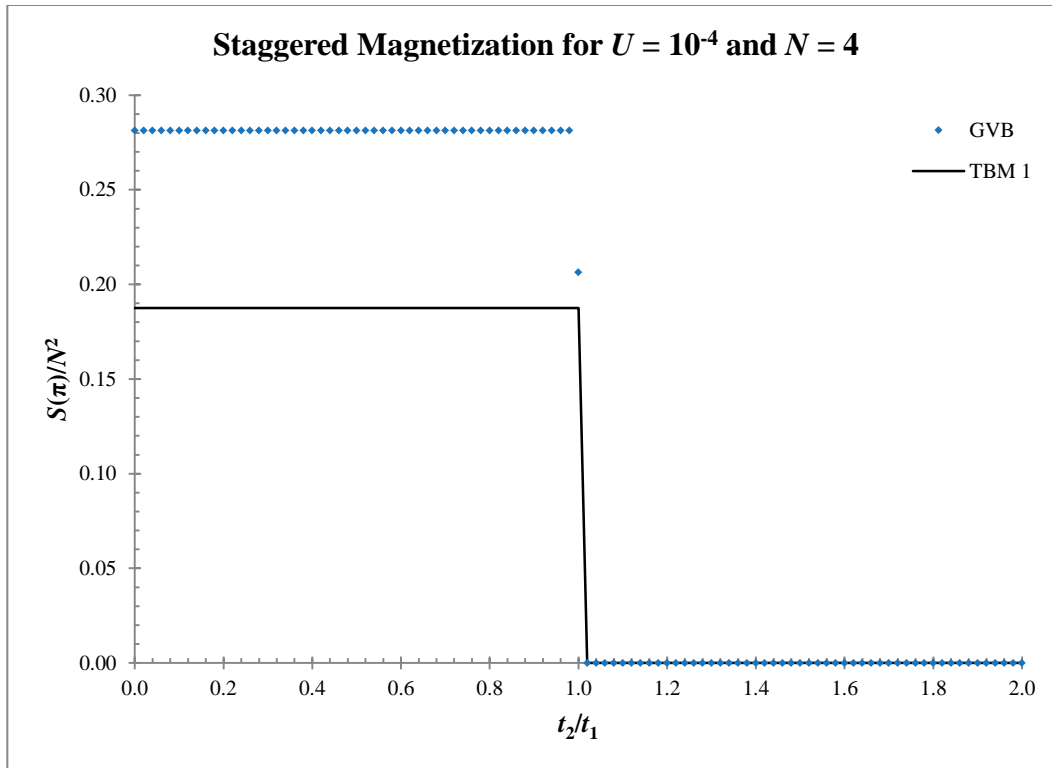


Figure 54 – For $U/t_1 = 10^{-4}$, there is a clear difference between the GVB results and the TBM results (TBM 1 is the $(\uparrow\downarrow, 0)$ electron arrangement for the degenerate $+\pi/2, -\pi/2$ states).

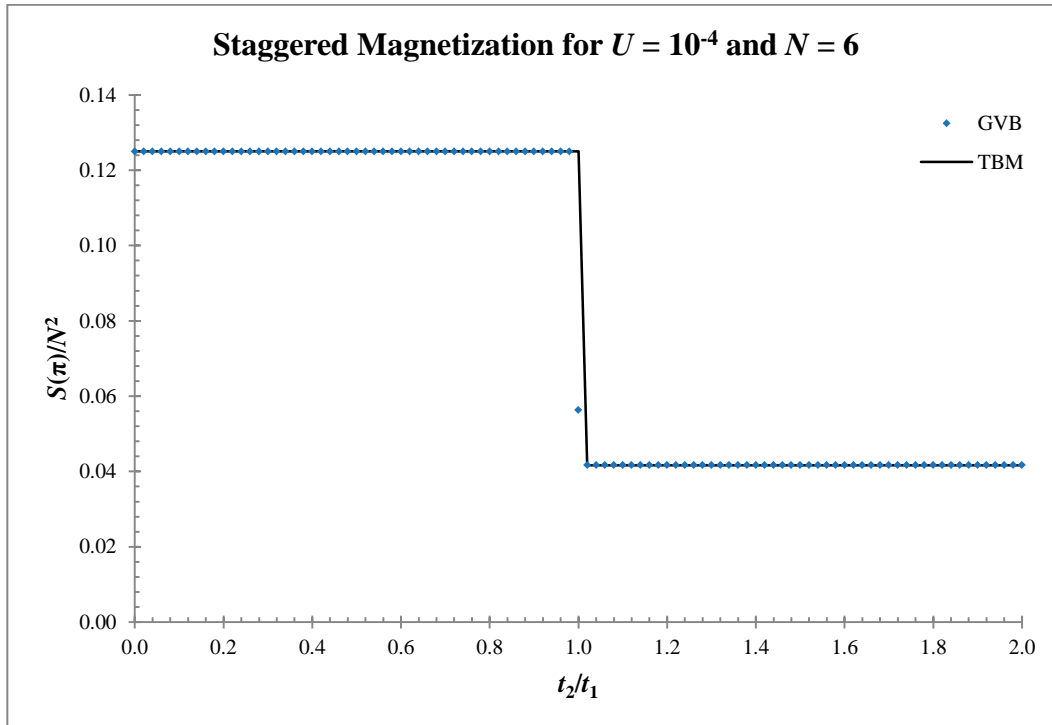


Figure 55 – No change with respect to **Figure 51** ($U = 0$ exactly) for $N = 6$.

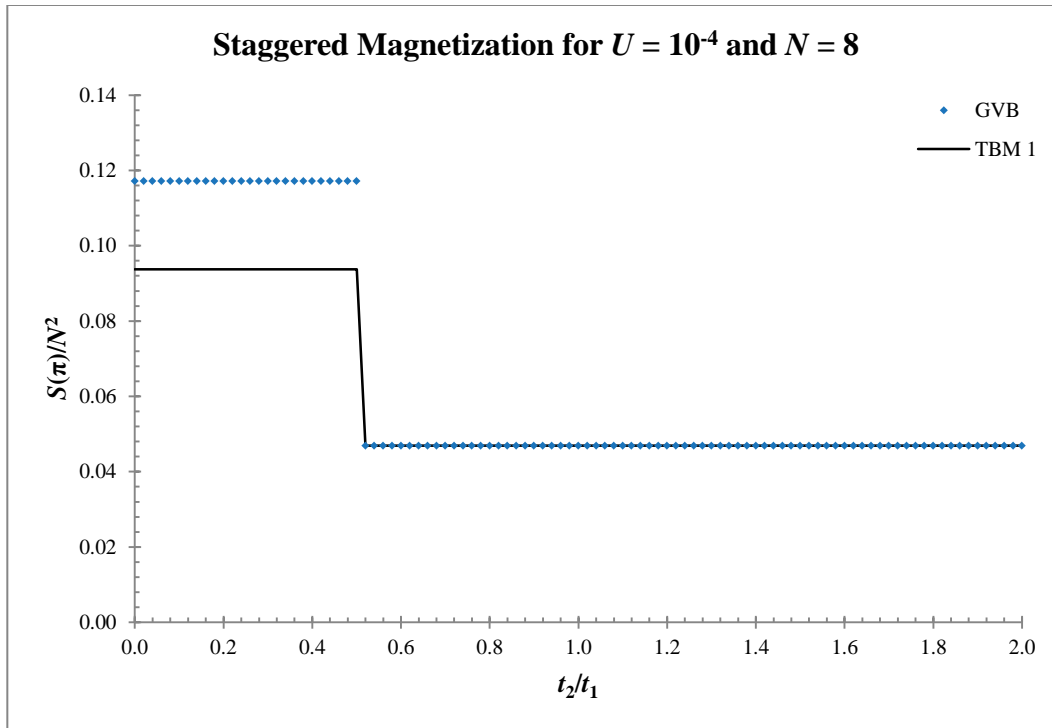


Figure 56 – Like the 4-site case, there is a clear shift in the $+\pi/2, -\pi/2$ degenerate region, otherwise the plot remains unchanged. The occupation basis shows the same shift as well.

Chapter 7

Results

In this chapter, I will present my results for an 8-site, one-dimensional chain and discuss the ground state magnetic order ([Chapter 7.1](#)) and structure ([Chapter 7.2](#)).

7.1 – Phase diagram

As discussed in previous chapters, the classical antiferromagnet has anti-aligned spins. With nearest-neighbour interactions only, we expect the antiferromagnetic ground state of the half-filled Hubbard model to favour anti-aligned neighbouring spins ($\uparrow\downarrow\uparrow\downarrow \dots$). With next-nearest-neighbouring interactions, we expect the antiferromagnetic ground state to favour anti-aligned next-nearest-neighbouring spins ($\uparrow\uparrow\downarrow\downarrow \dots$). In the frustrated regime there is a competition between the two types of antiferromagnetic ordering and the ground state is expected to be more of a valence bond crystal [[34](#)][[37](#)][[38](#)] (Majumdar-Ghosh chain in 1D).

[Figure 57](#) is the phase diagram of the ground state of the half-filled Hubbard model and shows the various magnetic phases which are dominant in each of the regions of the phase diagram. The phase diagram is plotted with respect to t_2/t_1 and U/t_1 and the solid lines represent the level crossings.

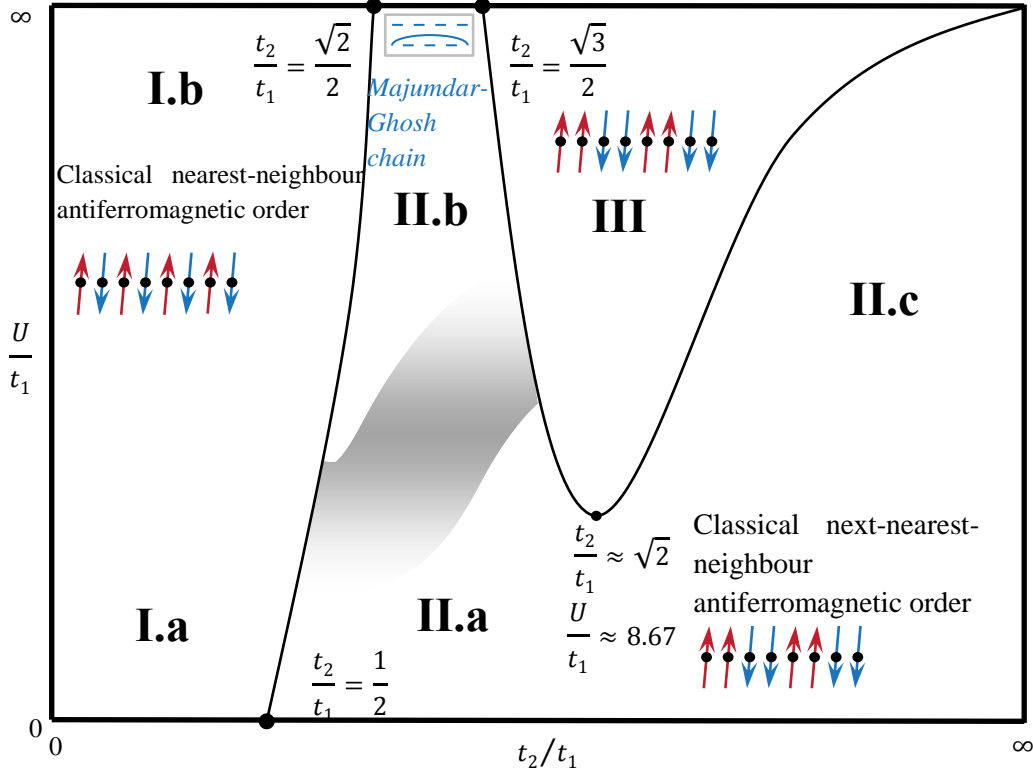


Figure 57 – Phase diagram for the ground state of the half-filled Hubbard model when $N = 8$. I divide the phase diagram into three main regions: I, II, and III.

In order to measure the nearest- and next-nearest-neighbour antiferromagnetic ordering of the ground state, I measured the structure factors $S(\pi)$ and $S(\pi/2)$ respectively (see [Chapter 5.1](#)). I also measured the dimer order $\langle \hat{D}^2 \rangle$ (see [Chapter 5.3](#)) to capture VBC ordering in the frustrated regime. These three spin correlation functions, $S(\pi)$ (labelled M2S in the following Figures), $S(\pi/2)$ (labelled M2D), and $\langle \hat{D}^2 \rangle$ (labelled D2), are plotted for six values of U/t_1 (10^{-4} , 2, 5, 8.8, 20, and 200) over the range $0 < t_2/t_1 < 2$ ([Figures 58 – 63](#)). From these figures we observe that the staggered magnetization $S(\pi)$, in region I, increases as U/t_1 increases. This is a natural result of the suppression of GVB states with charge bonds when U/t_1 is increased (as a result, singlet states contribute more). In this region, the staggered magnetization is always dominant; thus supporting our expectations that region I has nearest-neighbour antiferromagnetic ordering ($\uparrow\downarrow\uparrow\downarrow \dots$). When region III appears at $U/t_1 \approx 8.67$, it is dominated by next-nearest-neighbour antiferromagnetic ordering ($\uparrow\uparrow\downarrow\downarrow \dots$). In the frustrated regime of region II (between region I and III) and at large enough U/t_1 , the dimer order, favouring VBC states, is the dominant order of the ground state.

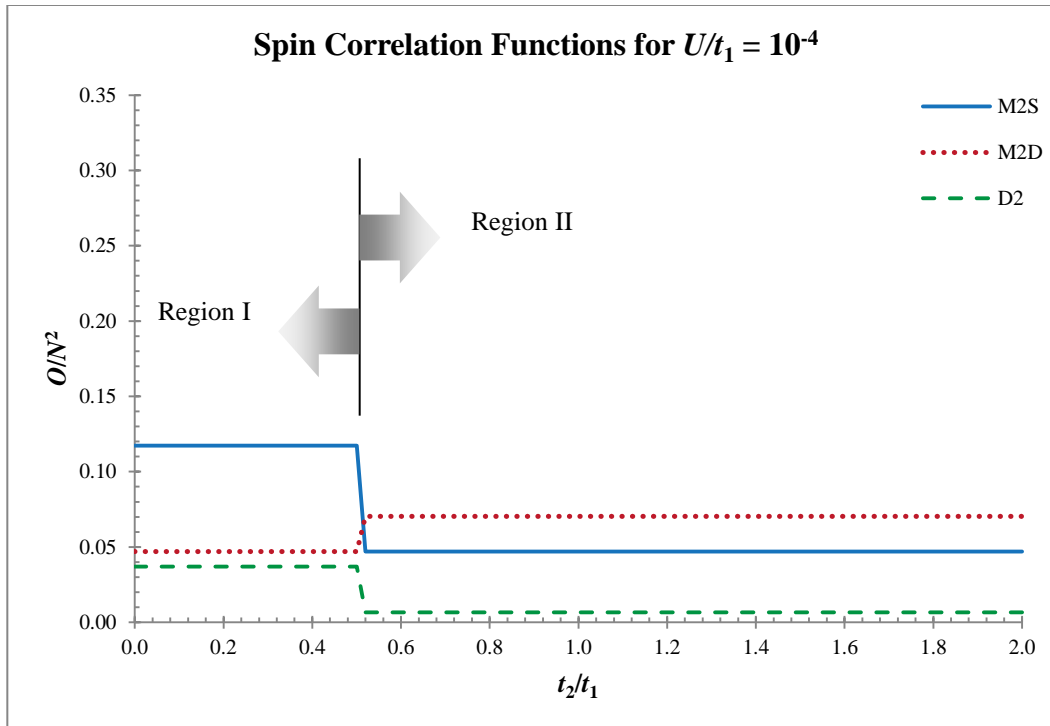


Figure 58 – The $\uparrow\downarrow\uparrow \dots$ ordering (M2S) is clearly dominant in region I when $U/t_1 = 10^{-4}$, with non-zero $\uparrow\uparrow\downarrow \dots$ (M2D) and dimer ordering (D2). In region II, $\uparrow\uparrow\downarrow \dots$ is the dominant ordering, but there is still a significant amount of M2S order. This suggests that for small U there are other types of order that the ground state has in region II—in particular I suspect some sort of order pertaining to charge bonds, since U is small (also see **Figures 64 – 66**).

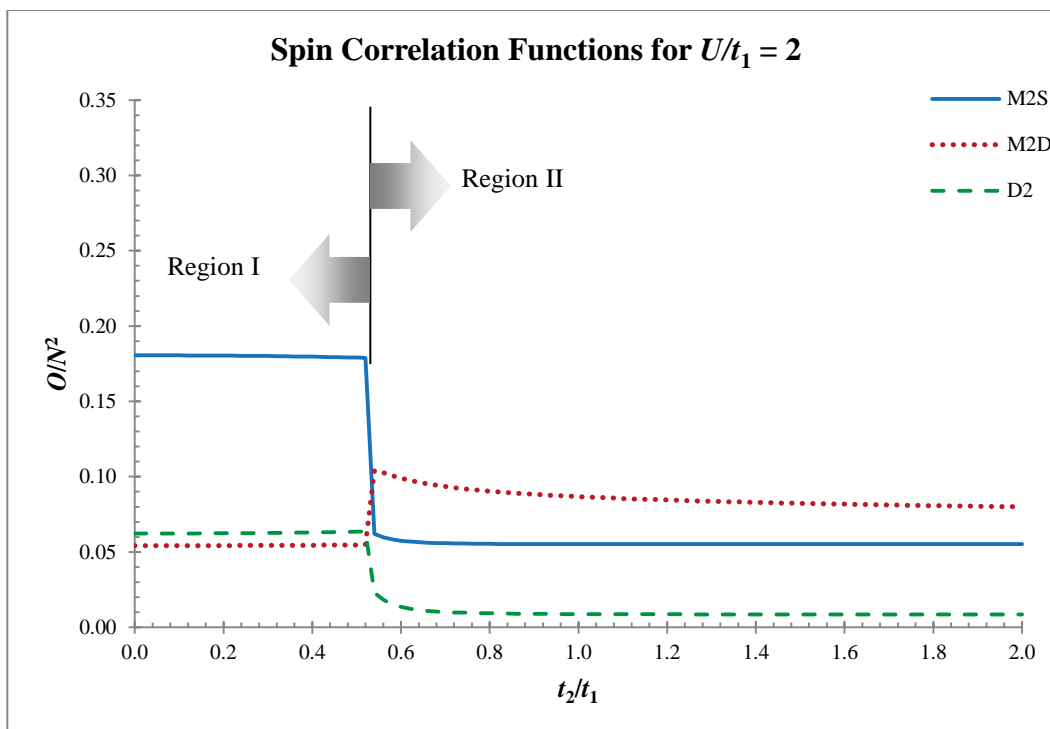


Figure 59 – This figure is similar to **Figure 58** ($U/t_1 = 10^{-4}$), but D2 begins to surpass M2D in region I.

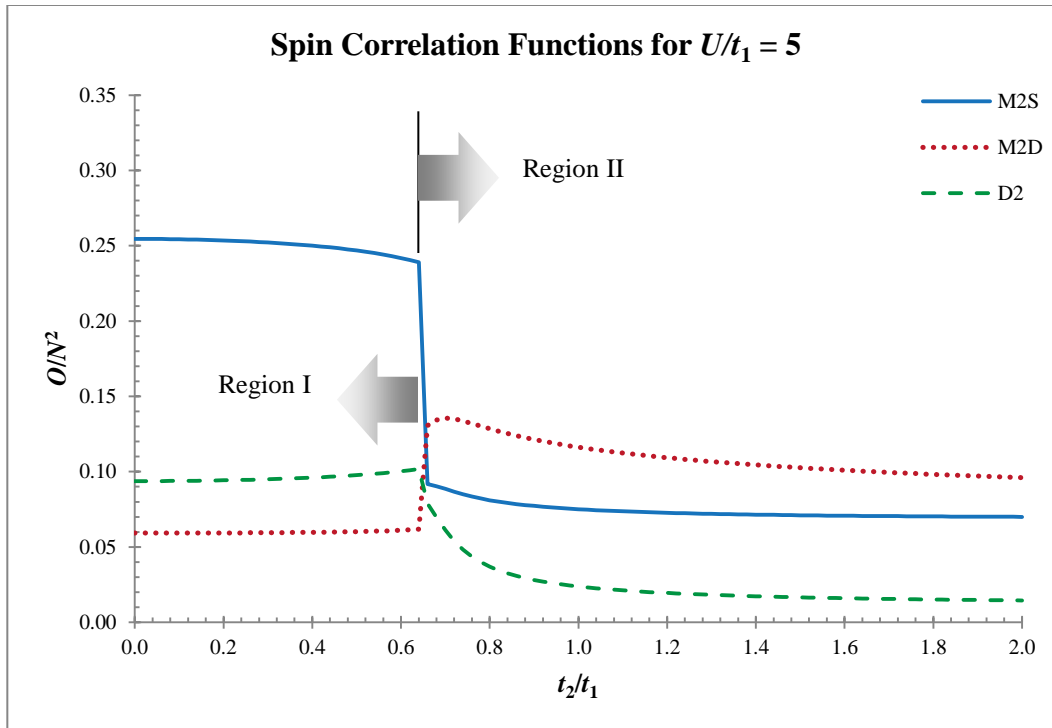


Figure 60 – We begin to see D2 contributing more in the frustrated regime of region II (next to region I).

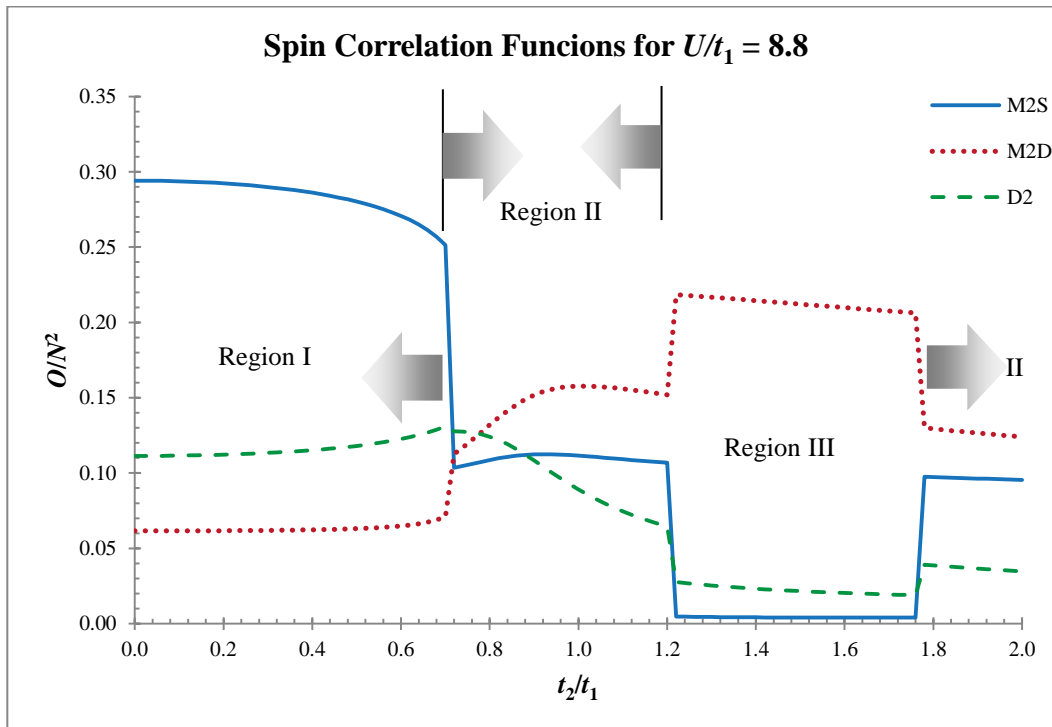


Figure 61 – Region III clearly has $\uparrow\uparrow\downarrow\downarrow \dots$ as its dominant ordering, with little to no M2S and D2 ordering. Region II, between region I and III, clearly has the competing order between M2S and M2D, but now with the dimer order as well.

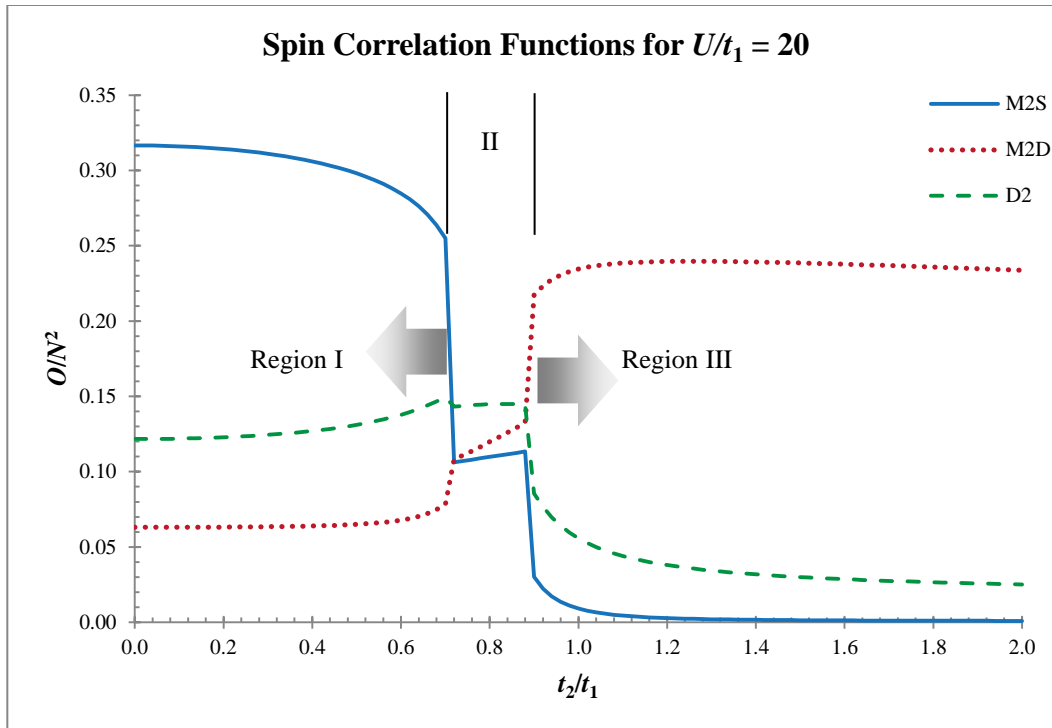


Figure 62 – With $U/t_1 = 20$, we are very near the large- U limit where we see $\uparrow\downarrow\uparrow \dots$ order in region I, $\uparrow\uparrow\downarrow \dots$ in region III, and dimer order in region II.

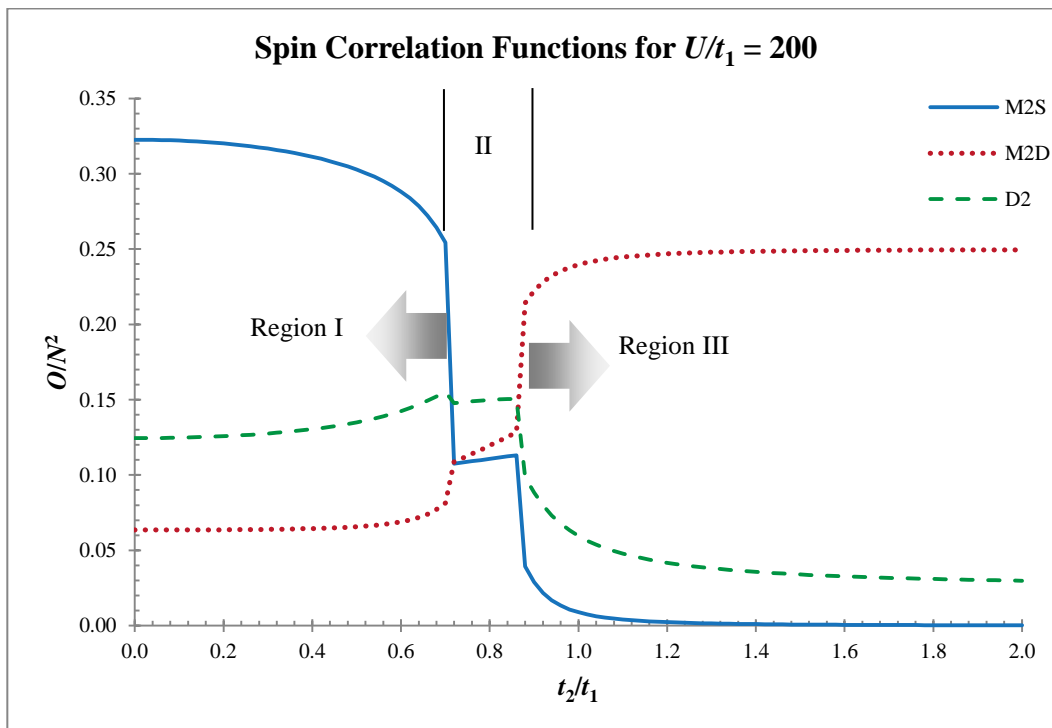


Figure 63 – Very similar behaviour to **Figure 62** ($U/t_1 = 20$).

For large U/t_1 , the magnetic order coincides with our expectations of nearest-neighbour antiferromagnetic order ($\uparrow\downarrow\uparrow \dots$) in region I (small t_2/t_1), next-nearest-neighbour

antiferromagnetic order ($\uparrow\downarrow\downarrow \dots$) in region III (large t_2/t_1), and dimer order (Majumdar-Ghosh chain) in the frustrated regime of region II. For small U/t_1 (before region III appears), there is still nearest-neighbour antiferromagnetic order ($\uparrow\downarrow\uparrow \dots$) in region I; however, region II does not appear to be completely dominated by next-nearest-neighbour antiferromagnetic order ($\uparrow\downarrow\downarrow \dots$). I believe there is also some sort of order in region II associated with double occupancies and vacancies (or charge bonds). Consider the following three figures (Figures 64 – 66) that show the fraction of bond types that make up the ground state for small values of U/t_1 (before the appearance of region III). For $U/t_1 = 0$ (Figure 64) and in region II, half of the bonds are singlets and the other half are charge bonds. And we can see that charge bonds contribute more to the ground state in region II than in region I for any value of U/t_1 . In fact, we can see that the charge bond contribution in region II always increases (for finite $U/t_1 > 0$) as t_2/t_1 increases. This is important, as in the region of very large t_2/t_1 , charge bonds are not as easily suppressed (e.g. Figure 91, shows that there is still a significant charge bond contribution to the ground state when $t_2/t_1 = 200$ and $U/t_1 = 200$).

The following three figures (Figures 67 – 69), show the fraction of bond types for values of U/t_1 , after region III first appears. In region III, charge bond contribution is clearly less for values of U/t_1 shortly after region III first appears (~ 8.67 to ~ 10). When U/t_1 is too large, the fraction of charge bonds is continuous between regions and increases as t_2/t_1 increases. It is clear that U/t_1 suppresses charge bond contribution as expected. Also note that NCBs always contribute less than PCBs.

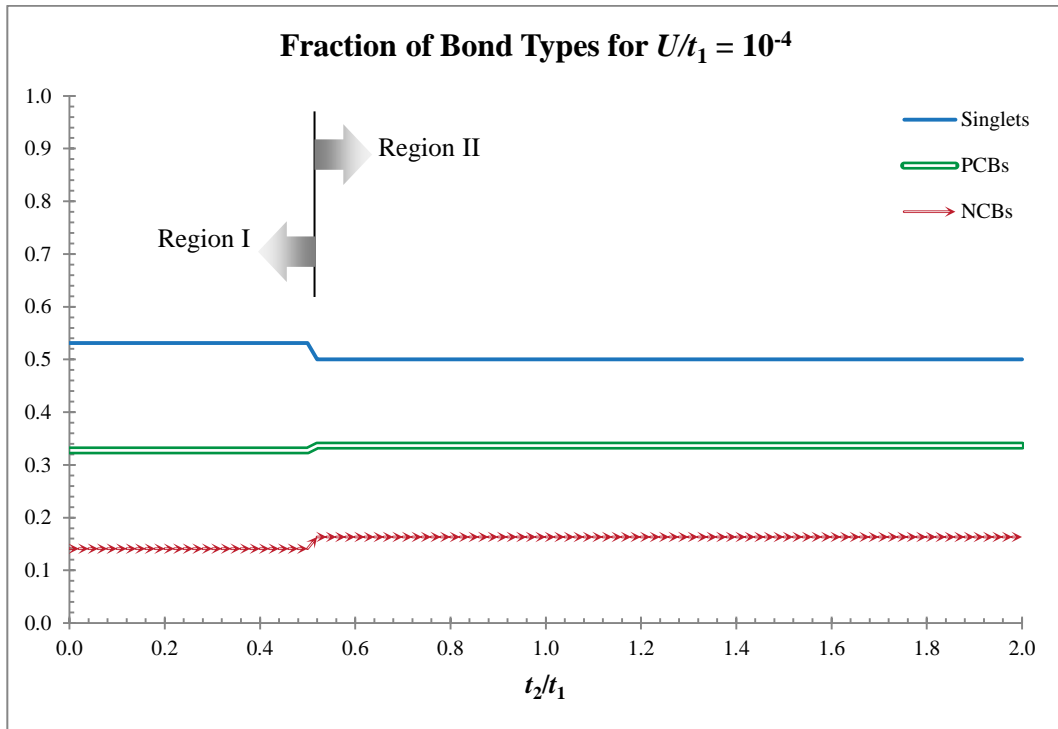


Figure 64 – Singlet bonds always contribute the most to the ground state, except in region II at $U/t_1 = 10^{-4}$, where the contribution from singlets and charge bonds (both PCBs and NCBs) are equal.

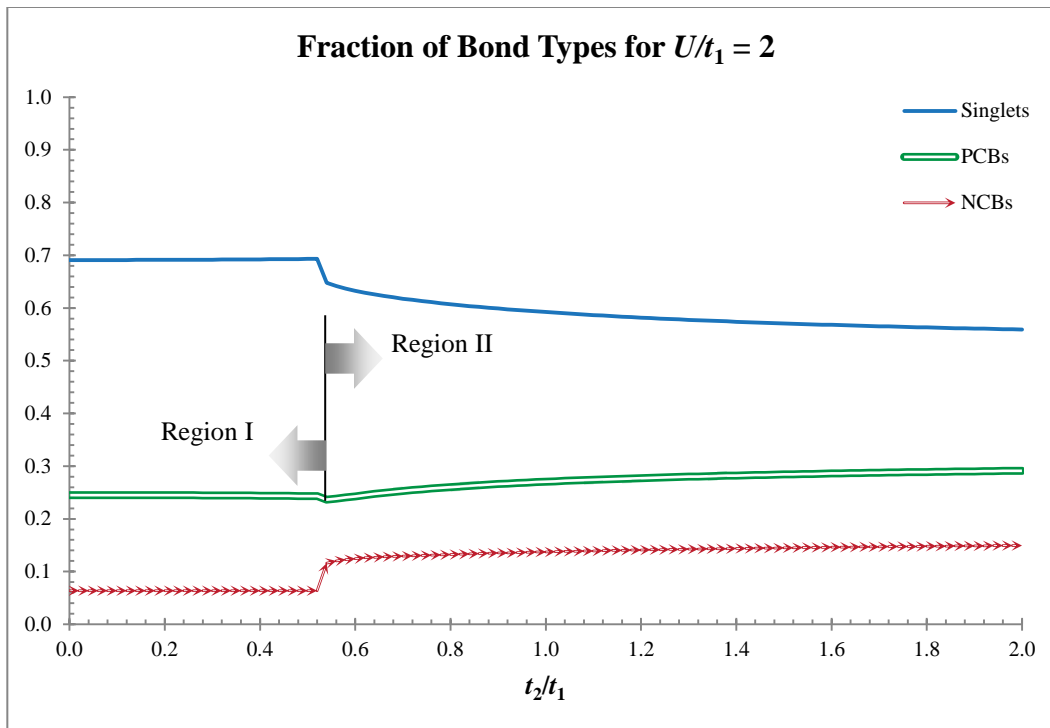


Figure 65 – For $U/t_1 = 2$, we begin to see an increase in charge bond contribution in region II as t_2/t_1 increases (however, singlet bonds always have over 50% contribution).

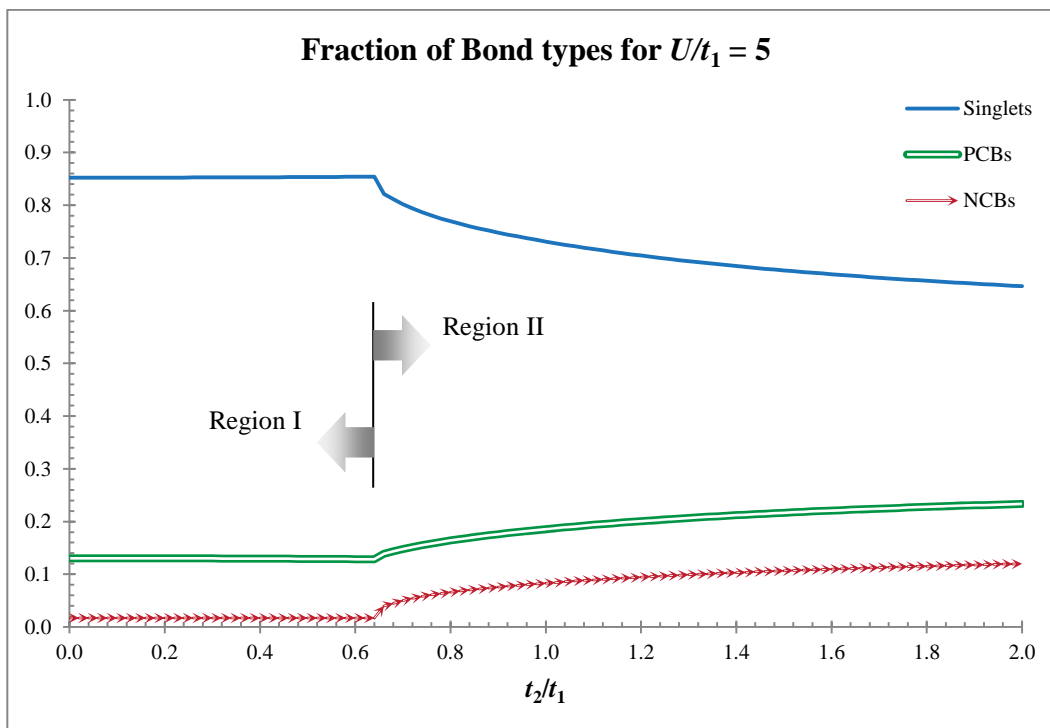


Figure 66 – With $U/t_1 = 5$, we see a more prominent increase in charge bond contribution with t_2/t_1 .

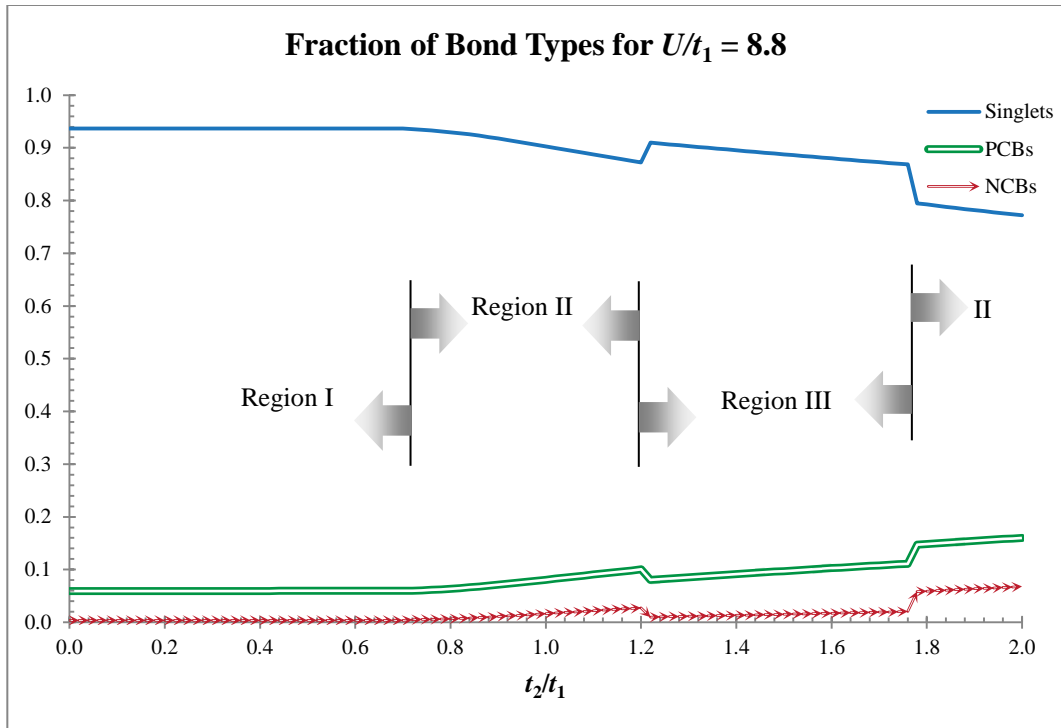


Figure 67 – Oddly enough, with the introduction of region III, the concavity of the charge bond contribution changes (though I believe the concavity changes back for large enough t_2/t_1 , suggesting that at some value of t_2/t_1 there is an inflection point). In region I, we see almost complete suppression of NCB contribution.

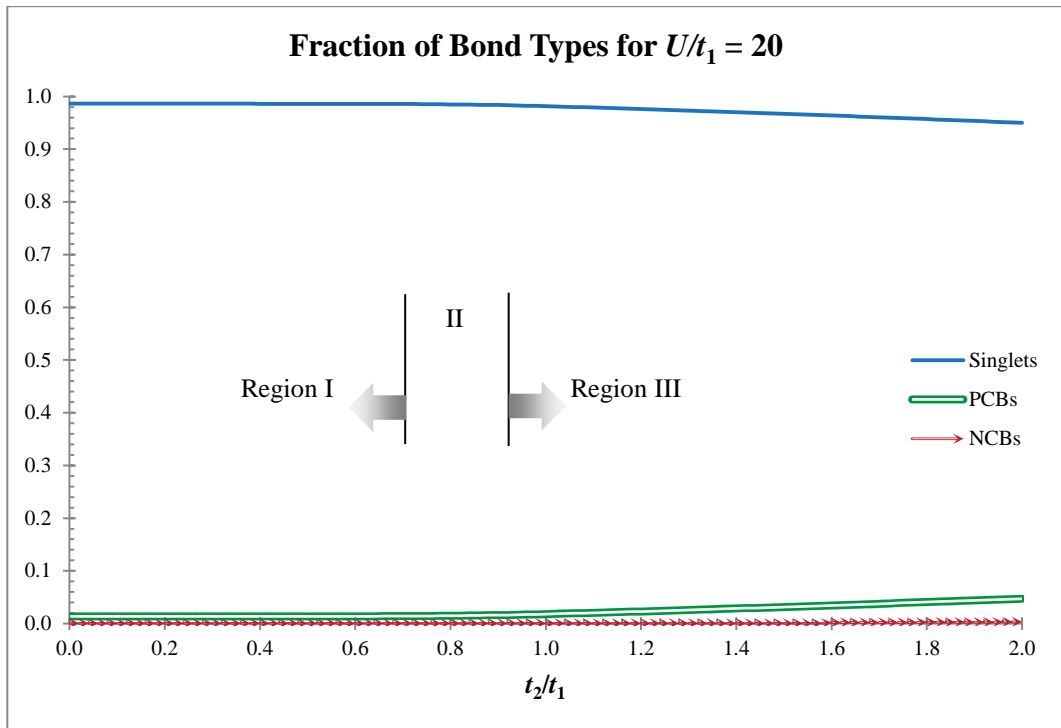


Figure 68 – There are no discontinuities in the fraction of bond type plots between regions.

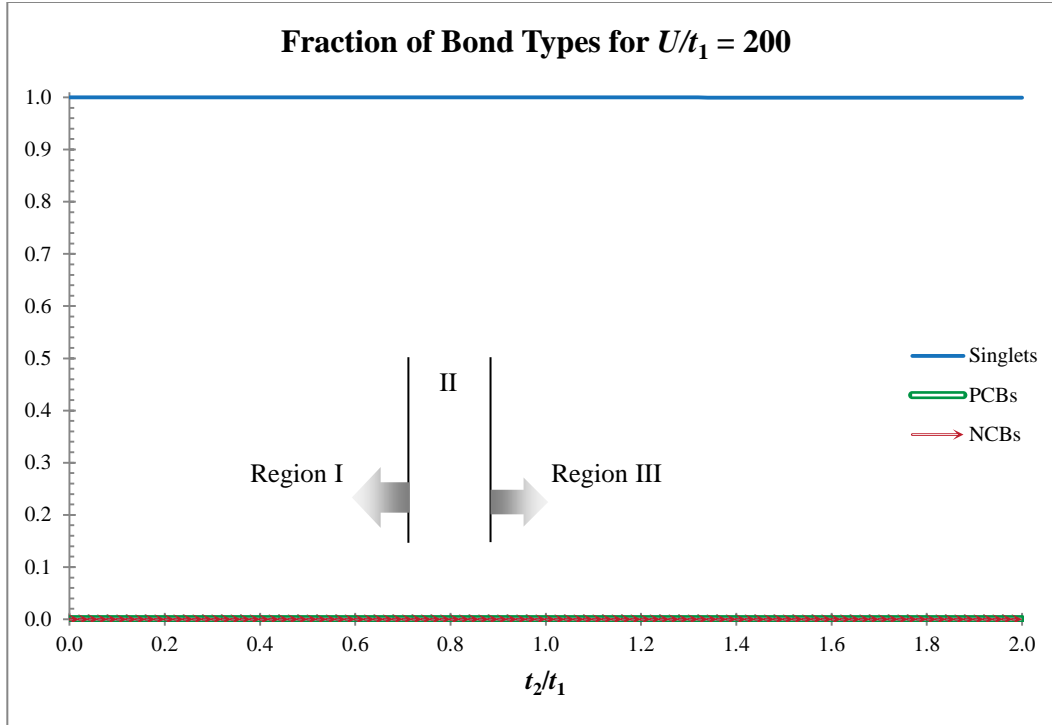


Figure 69 – At $U/t_1 = 200$, the charge bonds are completely suppressed in the range $0 < t_2/t_1 < 2$. As I show in [Chapter 7.2](#), the contribution does increase for larger values of t_2/t_1 (see [Figure 91](#)).

7.2 – Ground state structure

In this subchapter, I present results to show that structure exists in the ground state represented using the GVB basis—in particular, the ground state weights c_p (as in $|\psi\rangle = \sum c_p |P\rangle$) depend (albeit non-trivially) on the bond lengths and bond types. The VB basis displayed this bond-length dependence of the ground state for the non-frustrated Heisenberg model and was used to construct trial wave functions to variationally determine the ground state of larger systems [11].

The 1D non-frustrated ($J_2/J_1 = 0$) Heisenberg ground state represented using VB states shows a clear dependence on the product of the bond lengths for 16 sites (see [Figure 70](#)). On the y -axis, I plotted the *relative* magnitudes of the ground state weights c_p . The magnitude of each weight is divided by the magnitude of the weight of the state with the maximum number for the product of bond lengths (i.e. the state with the longest possible bonds). On the x -axis, I plotted the product of all the bond lengths in each state (so each point represents one state in our basis $|P\rangle$ with ground state weight c_p). The length of a bond is defined as the number of lattice sites in between the bond endpoints (including one of the end points). For a 1D chain, a bond connecting nearest-neighbours has length 1, a bond connecting next-nearest-neighbours has length 2, and etc.

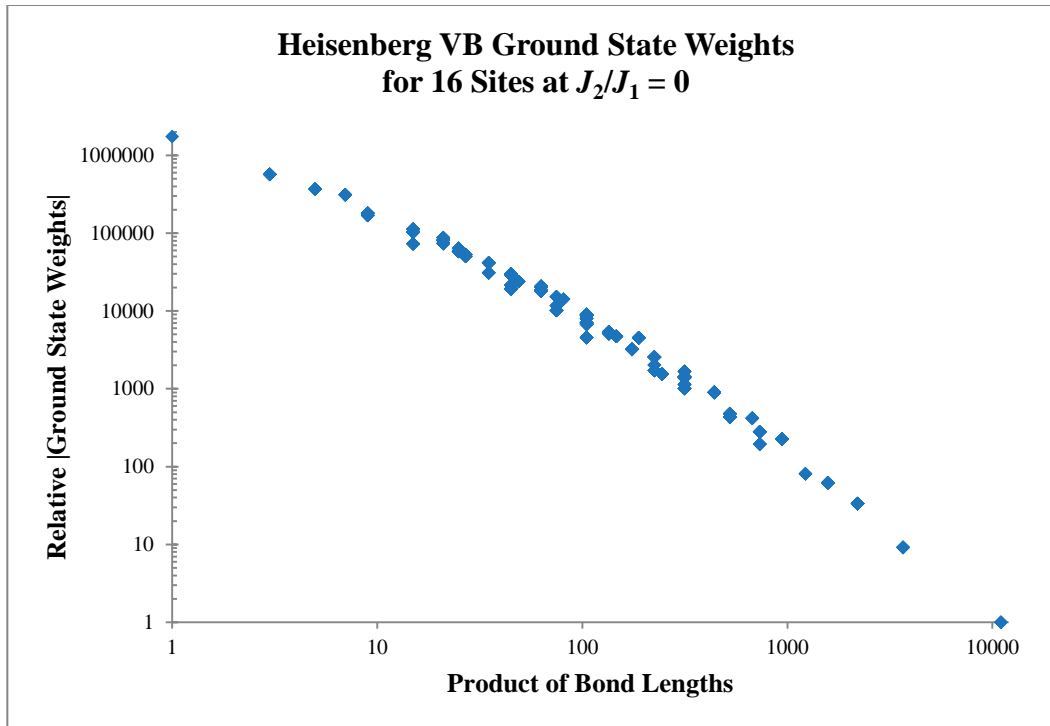


Figure 70 – With each axis with a logarithmic scale, the Heisenberg ground state is nearly linearly dependent on the product of bond lengths. This, in turn, implies that the ground state weights depend on the product of bond lengths according to some power law.

The following four figures (**Figures 71 – 74**) are similar plots as **Figure 70**; however, these figures plot the magnitude of the ground state weights (non-relative) of the Hubbard model at $U/t_1 = 10^{-4}$ (also only the x -axis has a logarithmic scale). Some of the GVB states with charge bonds do not display translational symmetry as we would expect (i.e. the ground state weights are not equal for translationally equivalent states). This issue remains unsolved, but once resolved we could effectively reduce the size of the basis by N .

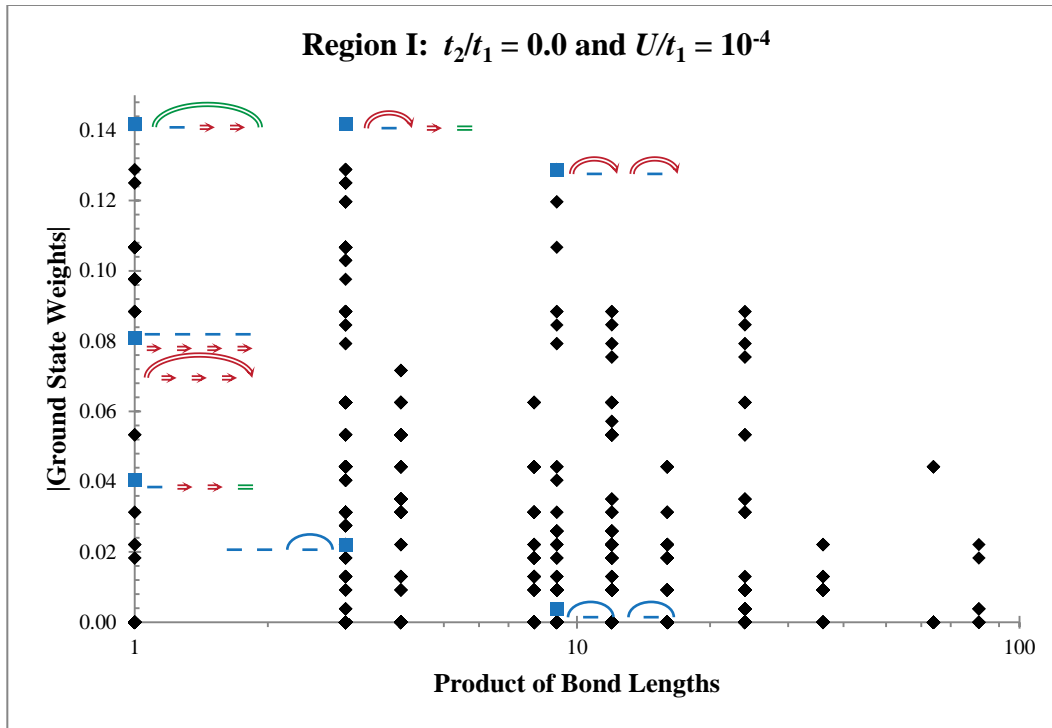


Figure 71 – The pure singlet states decay with the product of bond lengths. Note the *asymmetry* with translation of the most contributing state with only nearest-neighbour bonds (upper-left-most labelled state). Also note the translational *symmetry* of the pure NCB state indicated in the figure, as **Figures 73 and 74** show translational *asymmetry* in region II.

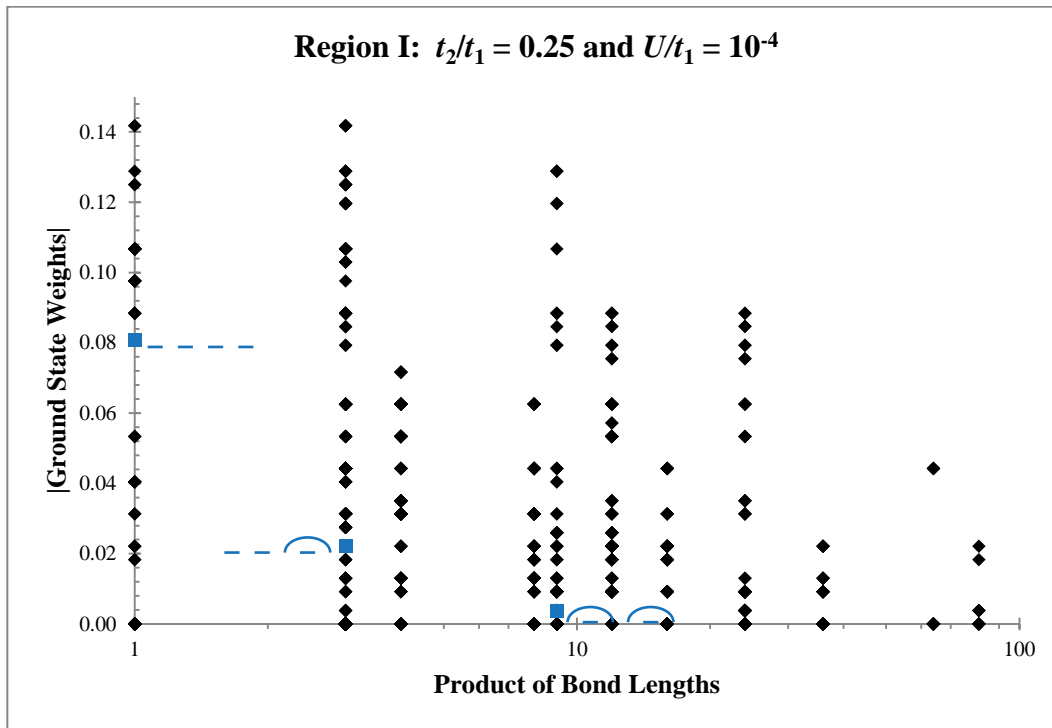


Figure 72 – Since we know the ground state does not change (in each region) in the tight-binding limit, this figure is exactly the same as **Figure 71**.

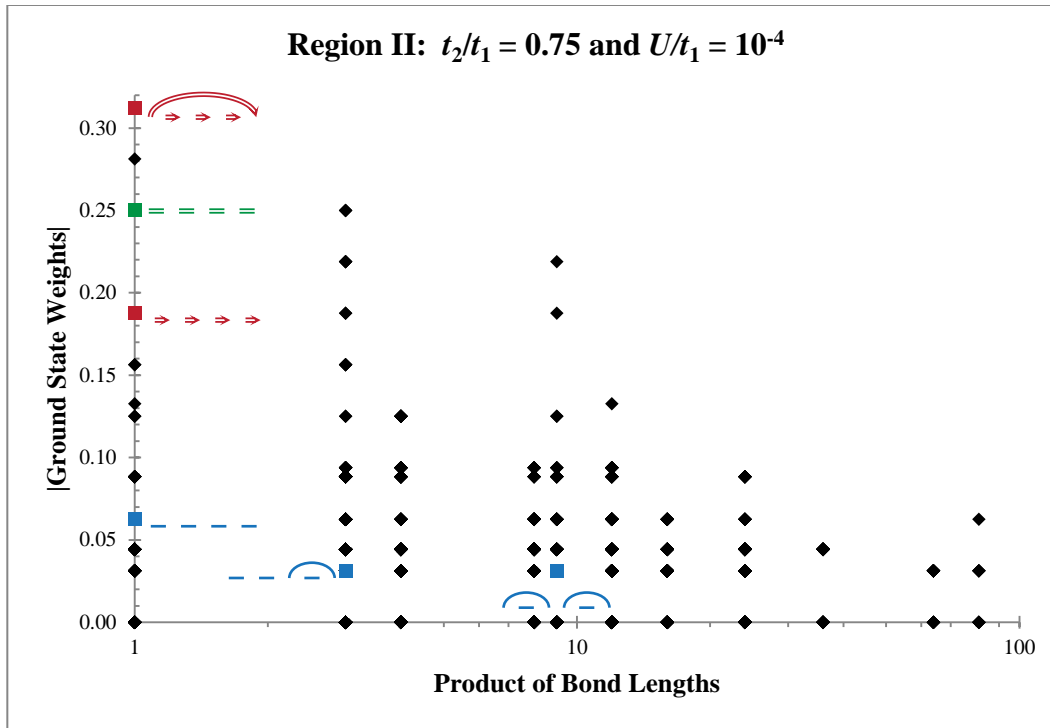


Figure 73 – In region II, we see the translational *asymmetry* between the pure NCB state indicated. Also, the pure PCB state indicated contributes significantly to the ground state, whereas, in region I, it did not contribute at all. Note the change in the pure singlet state weights, the two longer bond states have the same magnitude, with the nearest-neighbour pure singlet state having exactly twice that magnitude.

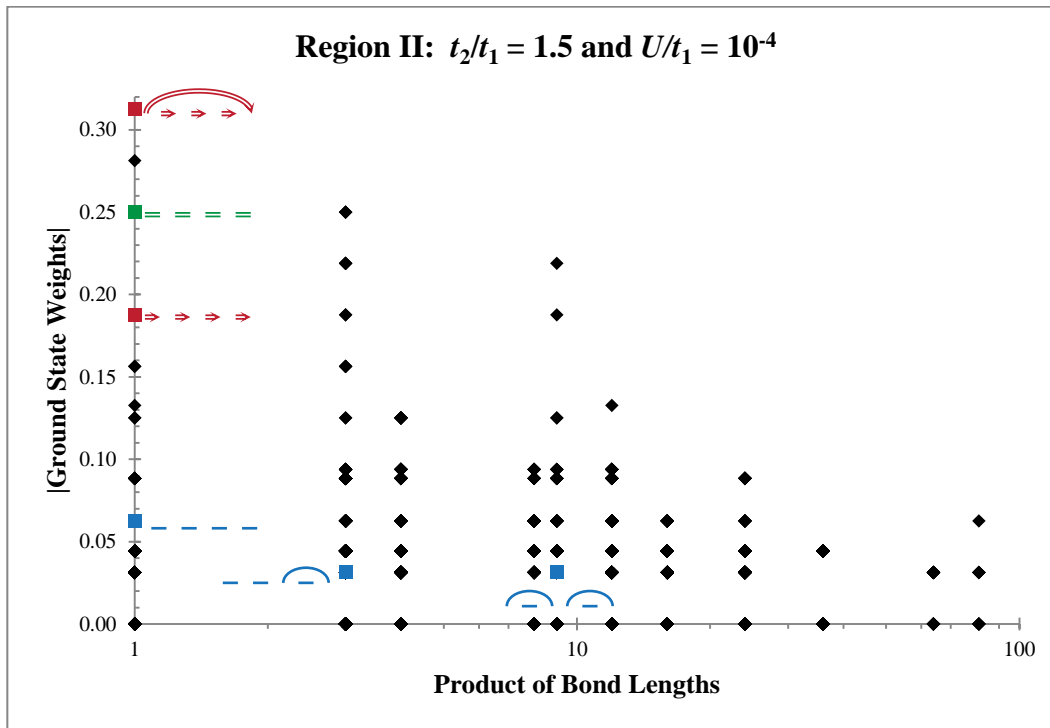


Figure 74 – The ground state weights are exactly the same as **Figure 73**, since we are in the same region and in the tight-binding limit.

The next set of four figures (**Figures 75 – 78**) show the ground state weights for $U/t_1 = 2$ and $t_2/t_1 = (0, 0.25, 0.75, \text{ and } 1.5)$. The following figures after show the ground state weights for larger values of U/t_1 and t_2/t_1 (**Figures 79 – 91**).

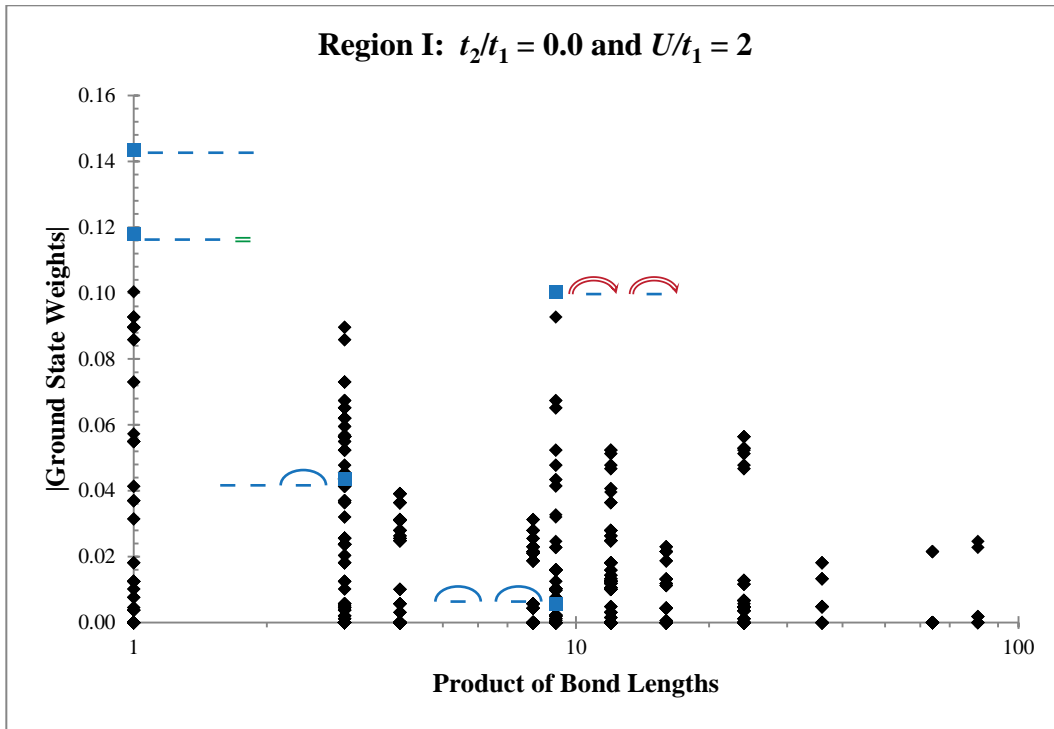


Figure 75 – Even with a small value of U/t_1 , the pure singlet states contribute more (and there is still a similar decay with bond length) than most of the mixed states. Many of the states that have many charge bonds do not contribute nearly as much as when $U/t_1 = 0$.

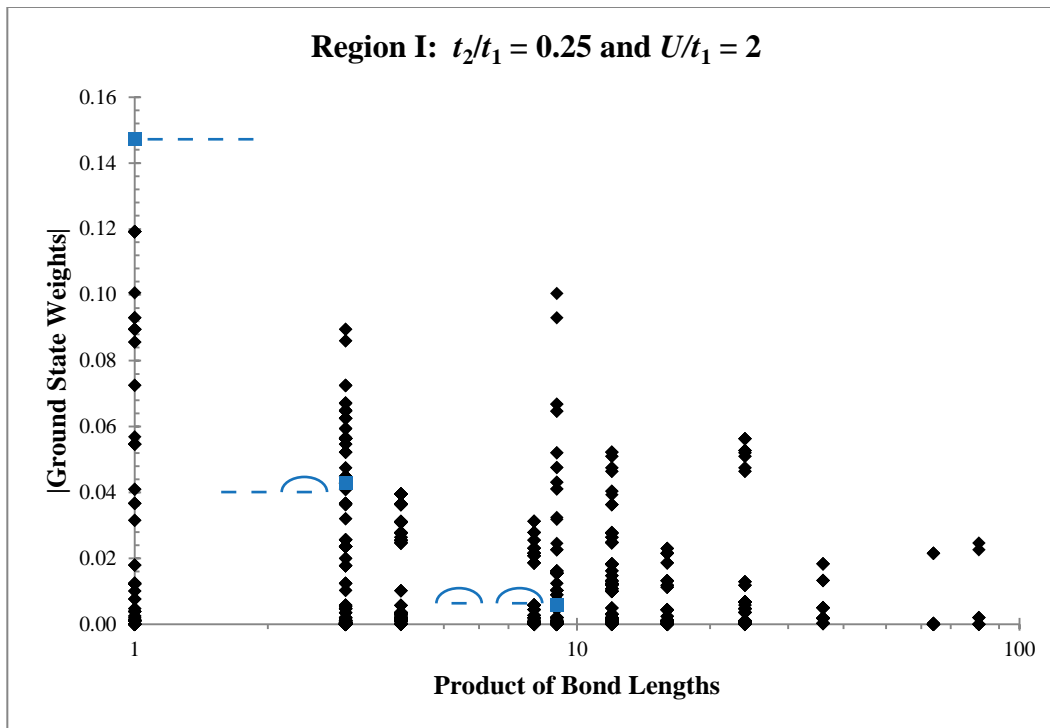


Figure 76 – This state is very similar to the one in the previous figure. This is because we are in the same region (region I).

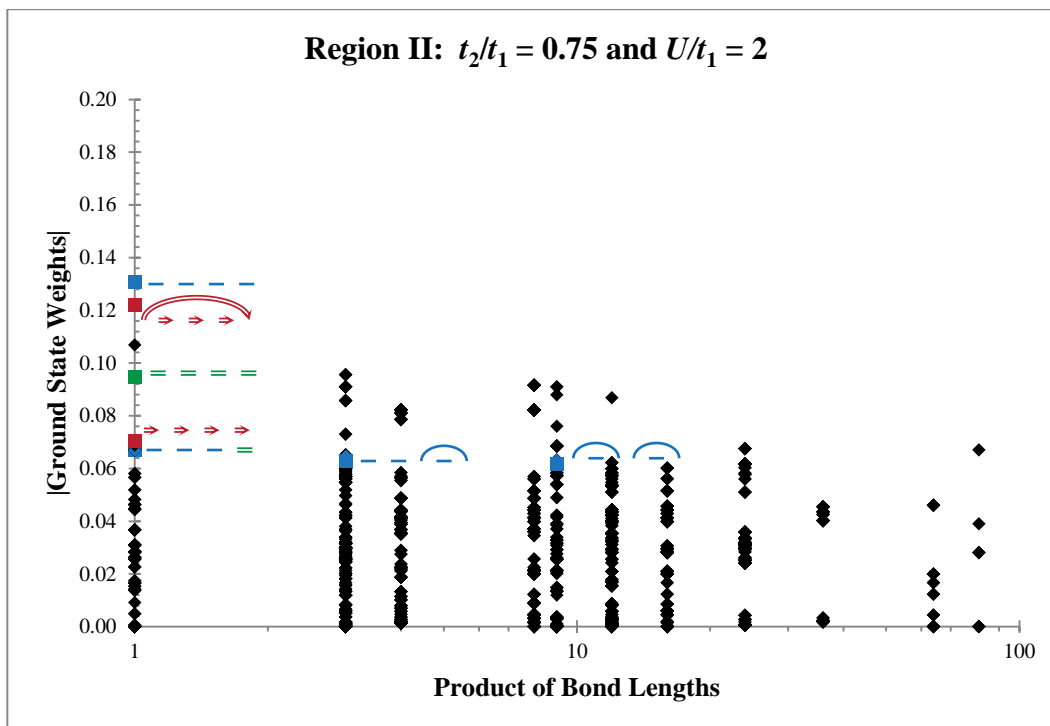


Figure 77 – Notice that the pure charge bond states indicated still significantly contribute to the ground state. This supports **Figure 65** where the charge bond contribution increases in region II.

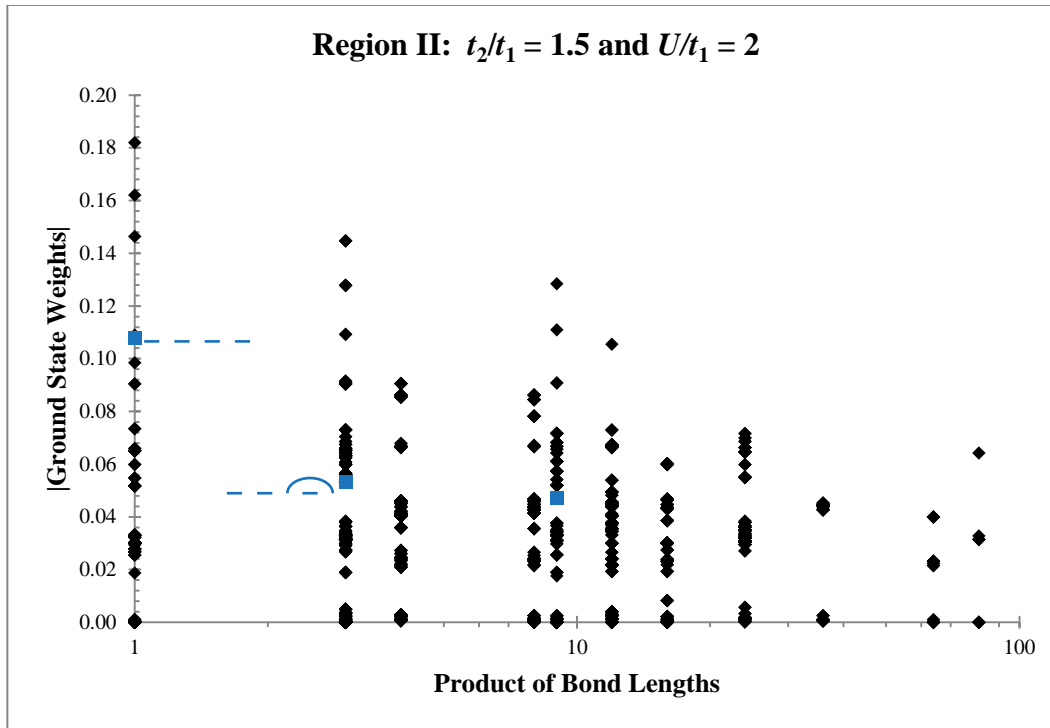


Figure 78 – Despite being in the same region as the previous figure, this state appears quite different than when $t_2/t_1 = 0.75$. For example, the nearest-neighbour pure singlet state no longer has the largest contribution. This also supports the fact that charge bonds are not as easily suppressed for large t_2/t_1 .

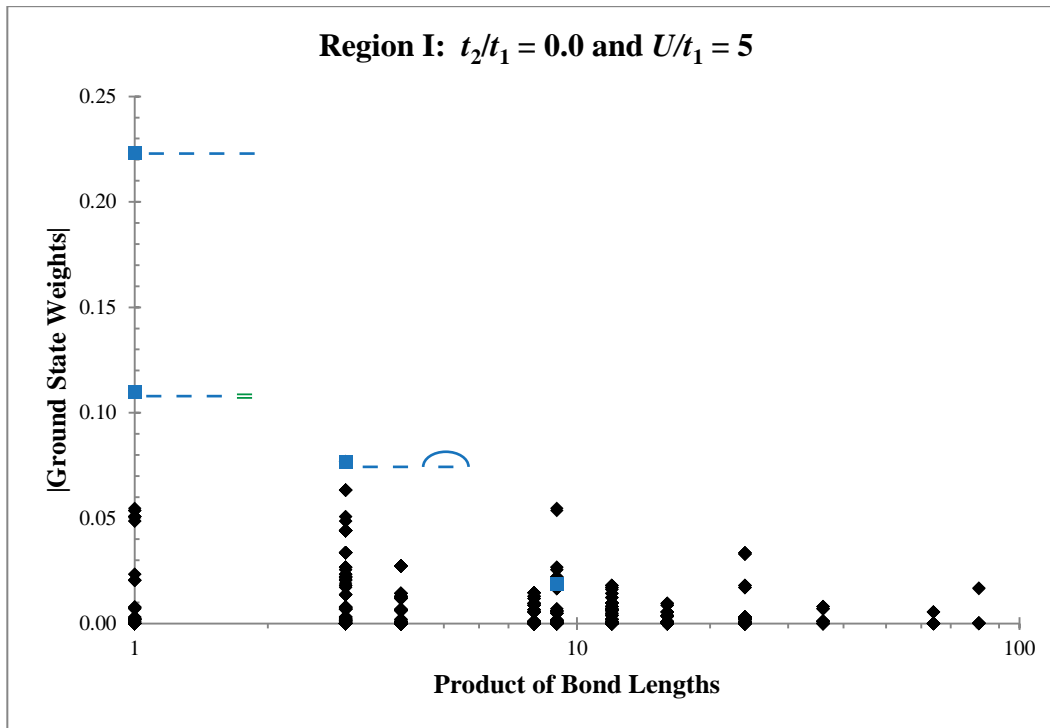


Figure 79 – The contribution of the states with charge bonds are further suppressed as U/t_1 is increased from 2 to 5. We still see, however, that the state with one PCB indicated still contributes a significant amount.

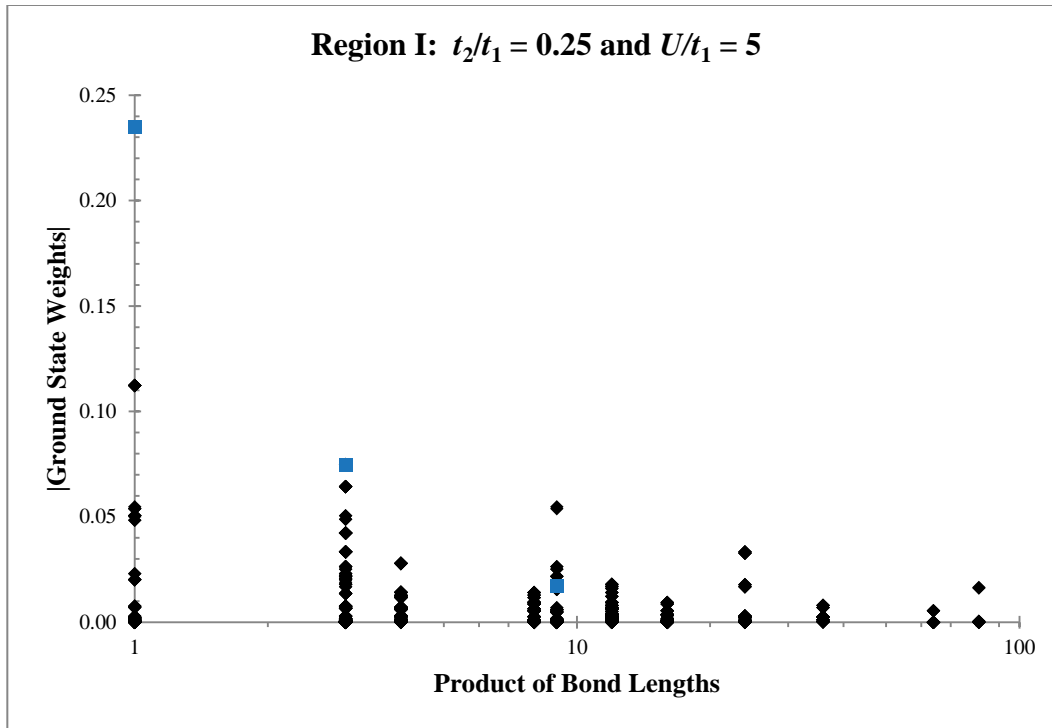


Figure 80 – Almost the same as the previous figure (the charge bond states are suppressed a little more, as the pure singlet states contribute a little more).

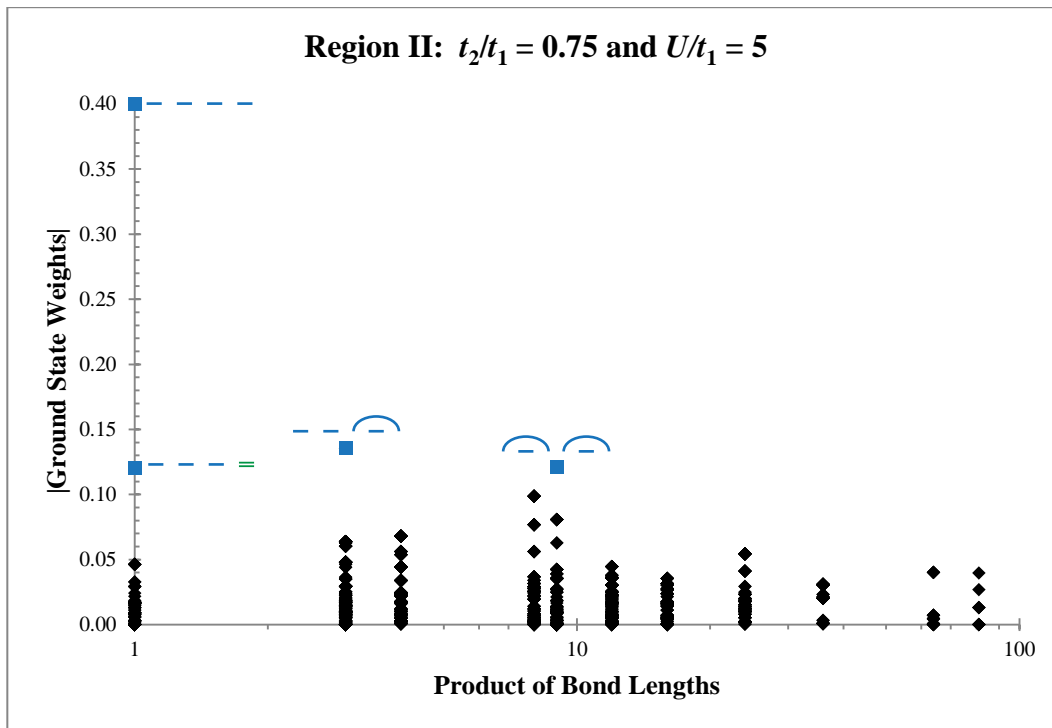


Figure 81 – With $U/t_1 = 5$, we now see more suppression of charge bond states in region II.

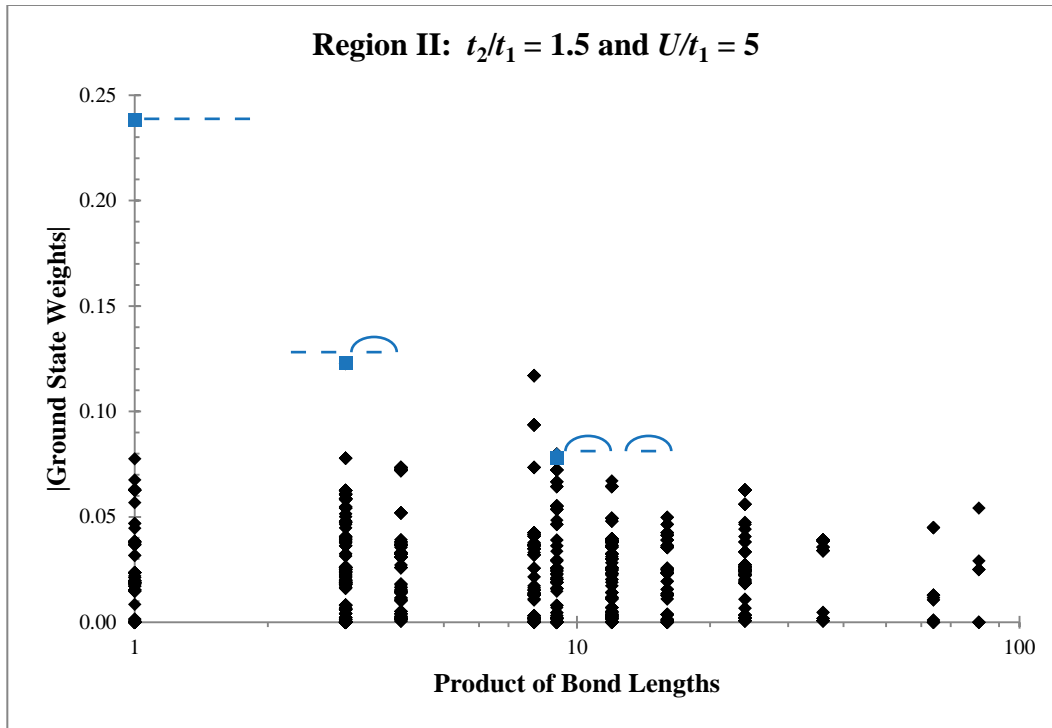


Figure 82 – As t_2/t_1 is increased from 0.75 to 1.5, the charge bond states contribute more to the ground state.

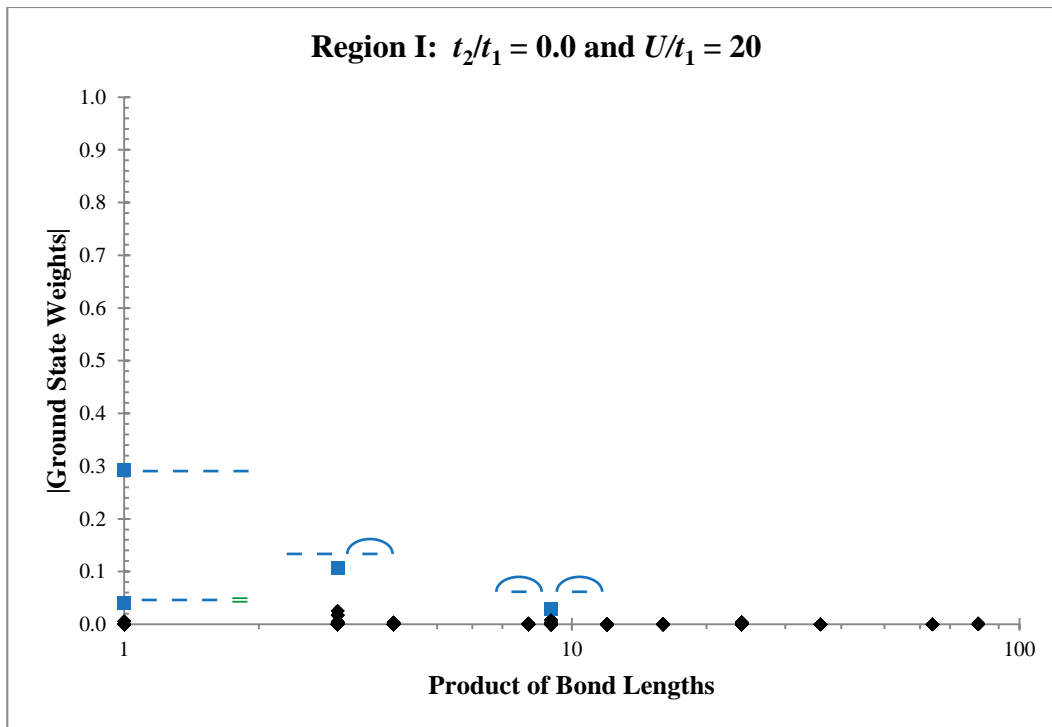


Figure 83 – With $U/t_1 = 20$, we expect almost all the charge bond states to be suppressed by this large on-site interaction.

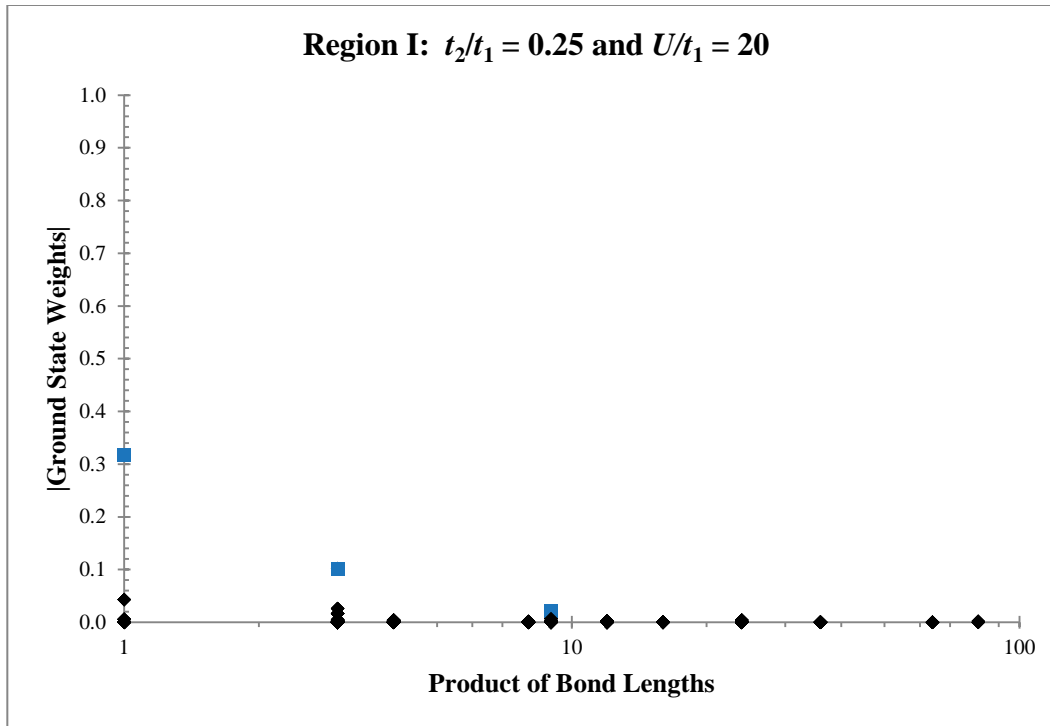


Figure 84 – Again, in region I, we do not much change to the ground state (the charge bond states are a little more suppressed again when changing t_2/t_1 from 0 to 0.25).

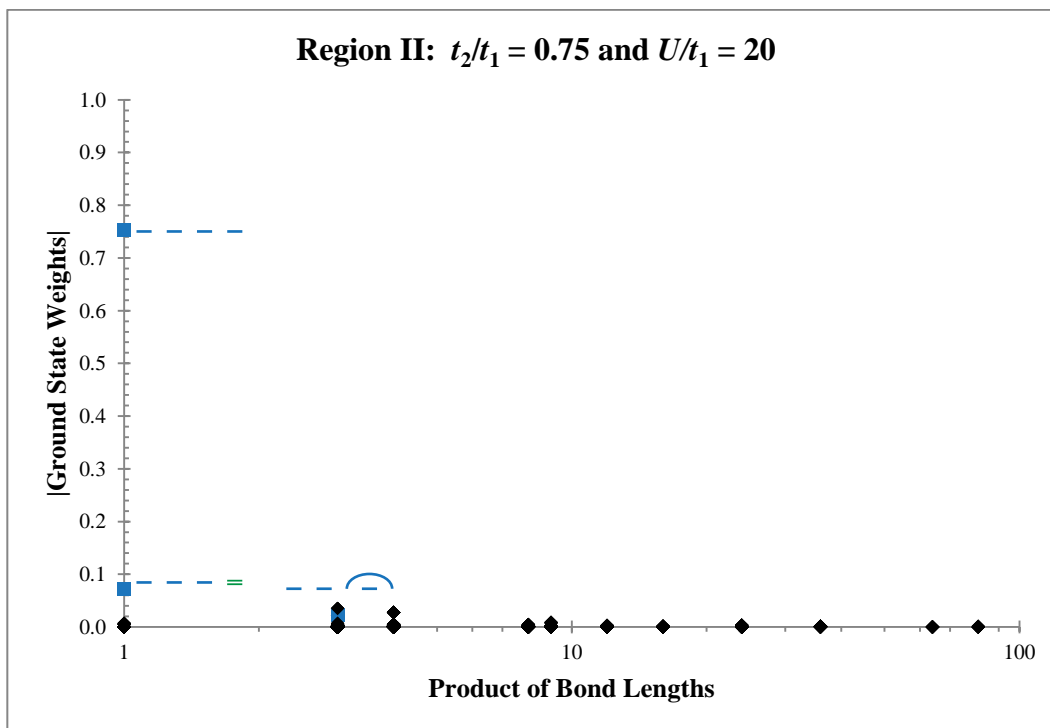


Figure 85 – This is the first time we take a look at region II in between regions I and III. There is a significant change to the ground state. The Majumdar-Ghosh chain (nearest-neighbour singlets) is nearly the only state that contributes to the ground state.

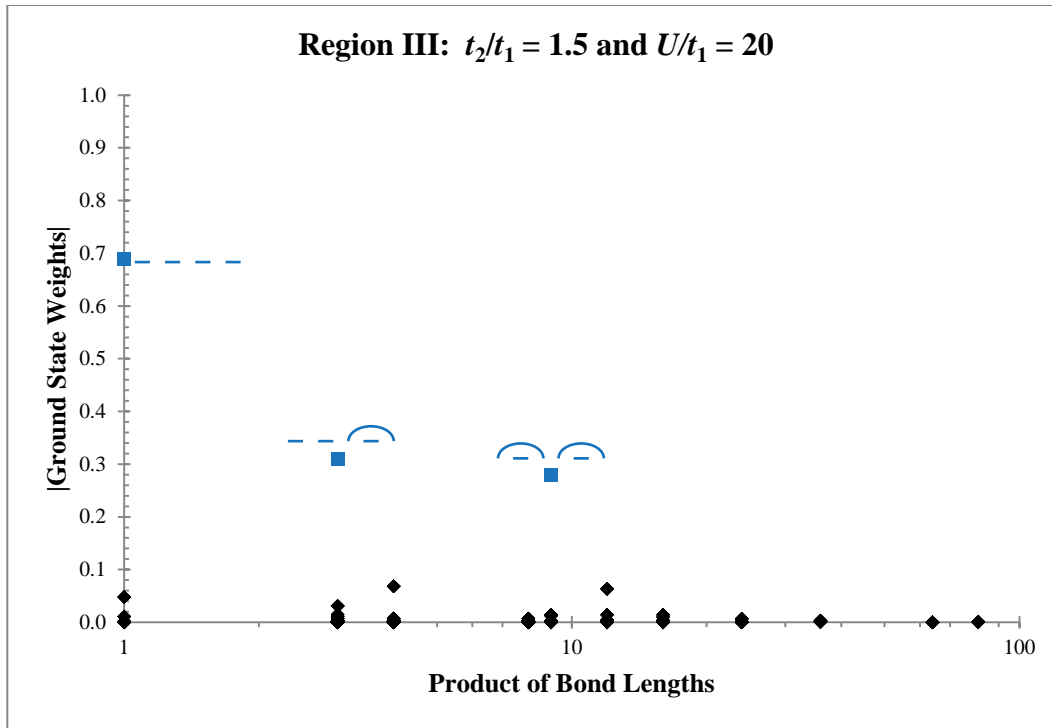


Figure 86 – In region III and at $U/t_1 = 20$, many of the charge bond states are suppressed. Also, the pure singlet states do not decay in the same fashion as region I.

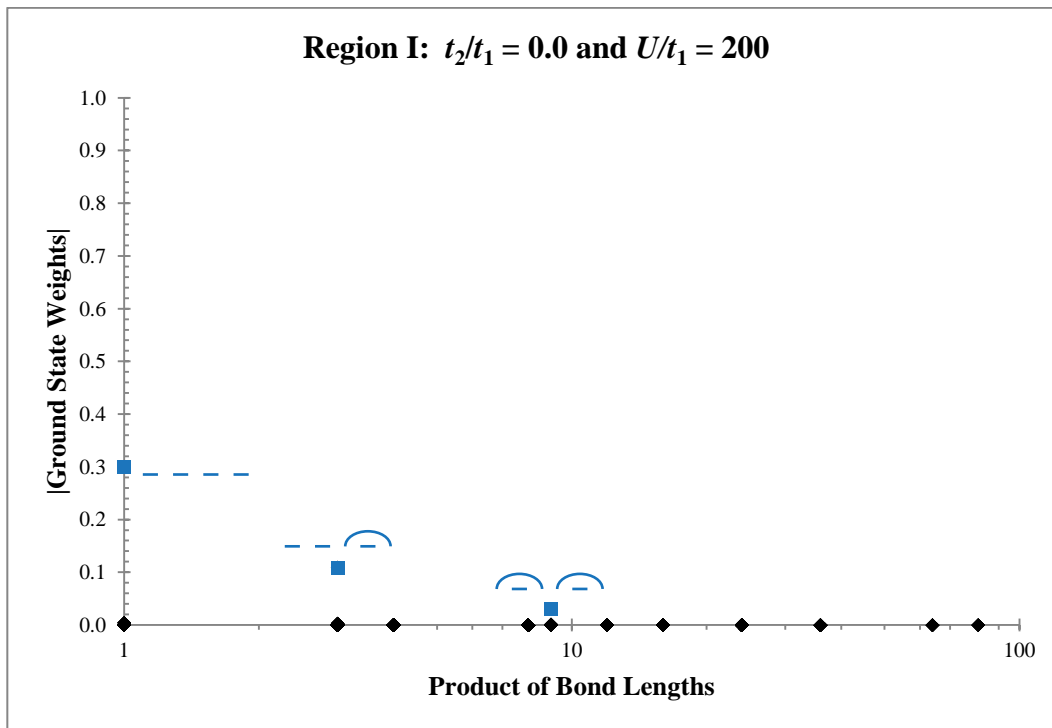


Figure 87 – We are now in the Heisenberg limit. We clearly see the full suppression of states with charge bonds as only the pure singlet states contribute to the ground state.

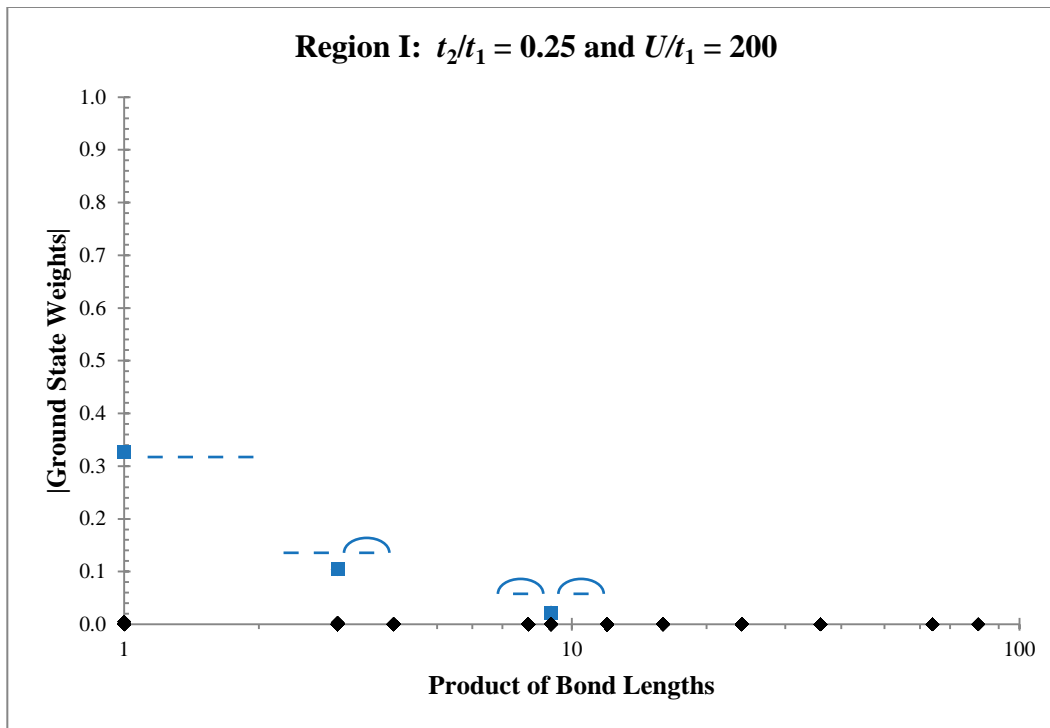


Figure 88 – Very similar, in shape to the previous figure.

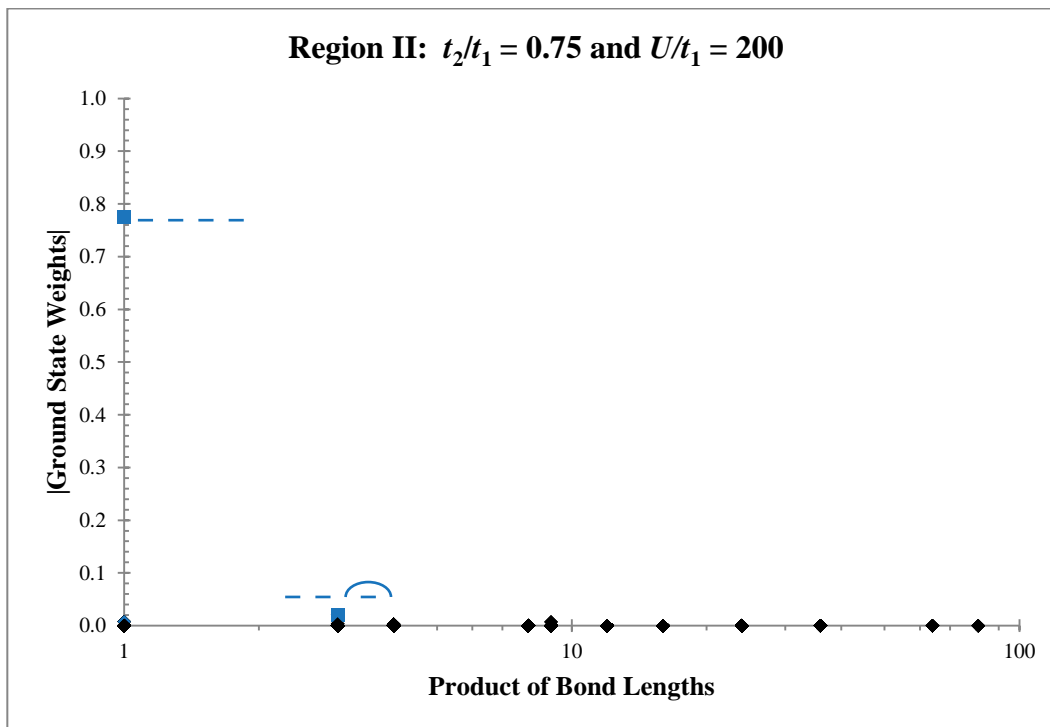


Figure 89 – In the frustrated regime of region II, we see that the Majumdar-Ghosh chain is nearly the only contributing state.

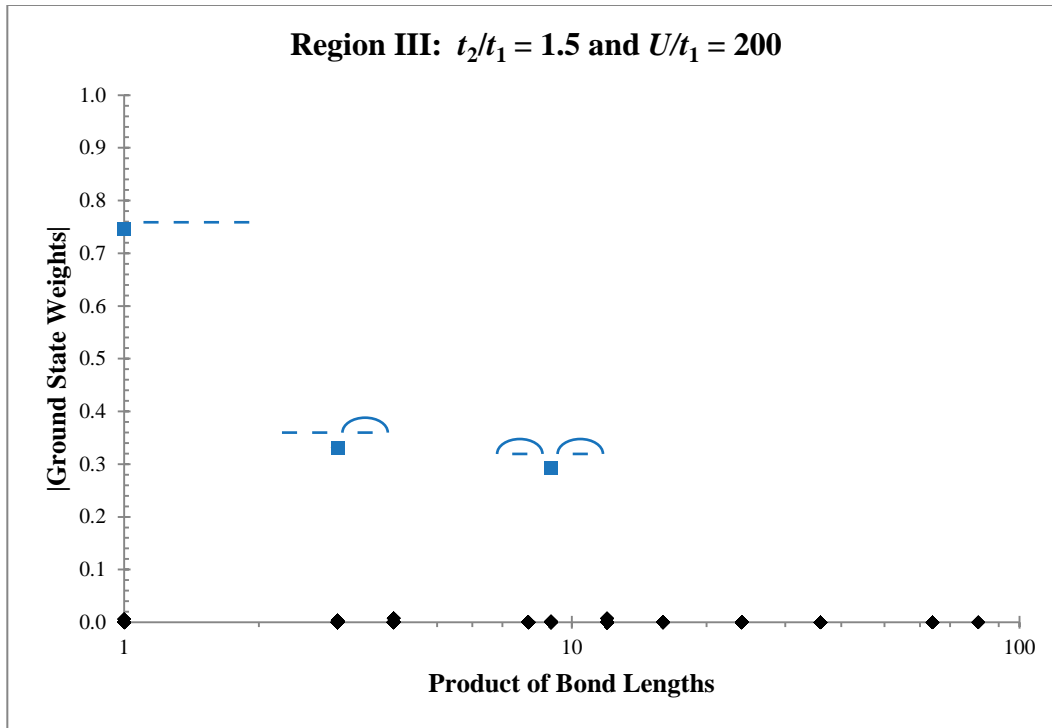


Figure 90 – In region III and at $t_2/t_1 = 1.5$, we see that most of the charge bond states are sufficiently suppressed.

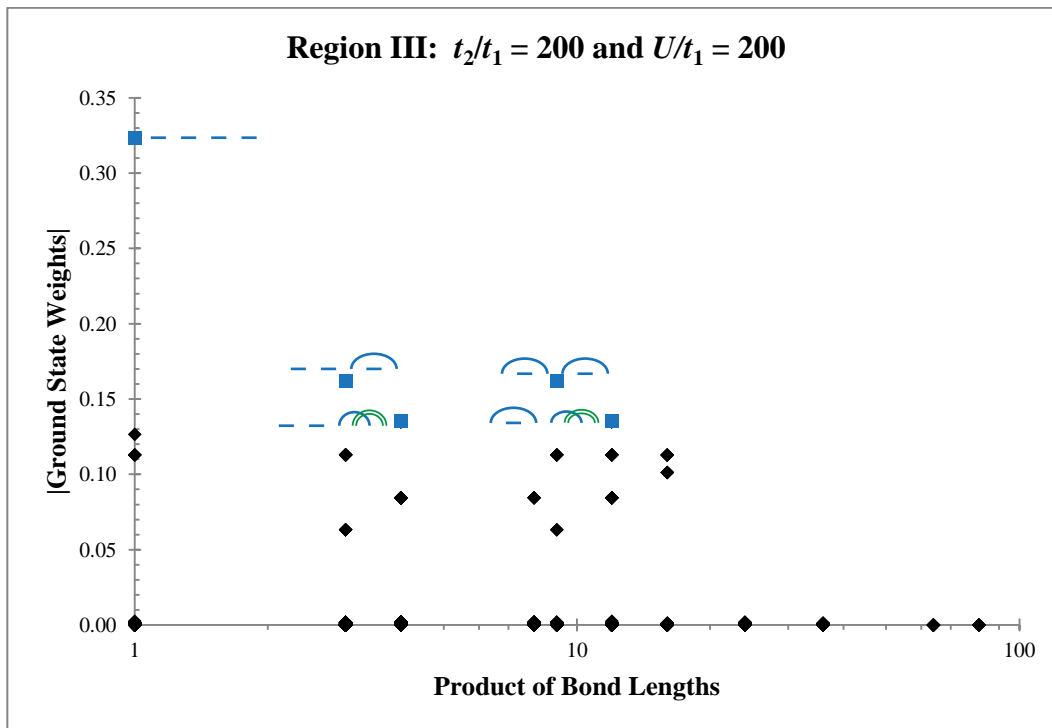


Figure 91 – This figure suggests that even at a large value of $U/t_1 = 200$, it is still very hard to suppress states with charge bonds for very large values of t_2/t_1 .

As **Figures 71 – 91** have shown us, the GVB states with charge bonds contribute less to the ground state as U/t_1 is increased (as expected), but they also contribute more as t_2/t_1 is increased.

The following two figures (**Figures 92 and 93**) show the ground state weights plotted with respect to the product of the bond lengths for 10 sites at $t_2/t_1 = 0$ and $U/t_1 = 10^{-4}$.

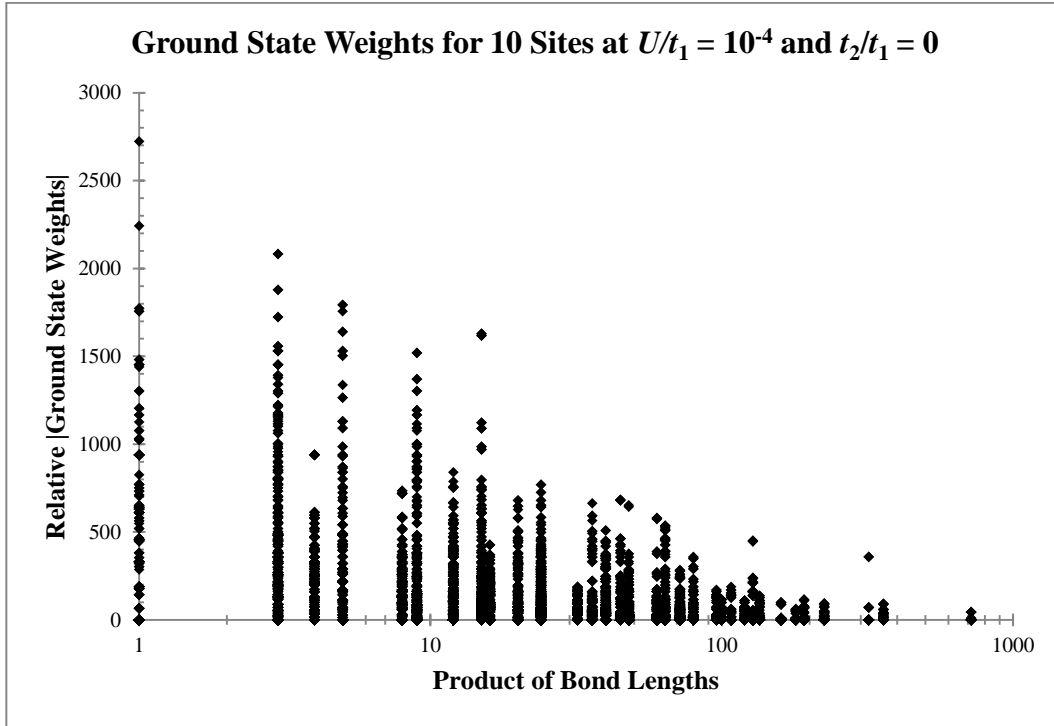


Figure 92 – With 10 sites, there are 19404 states in the GVB basis, and we can see a nice decay envelope as the product of bond lengths increases.

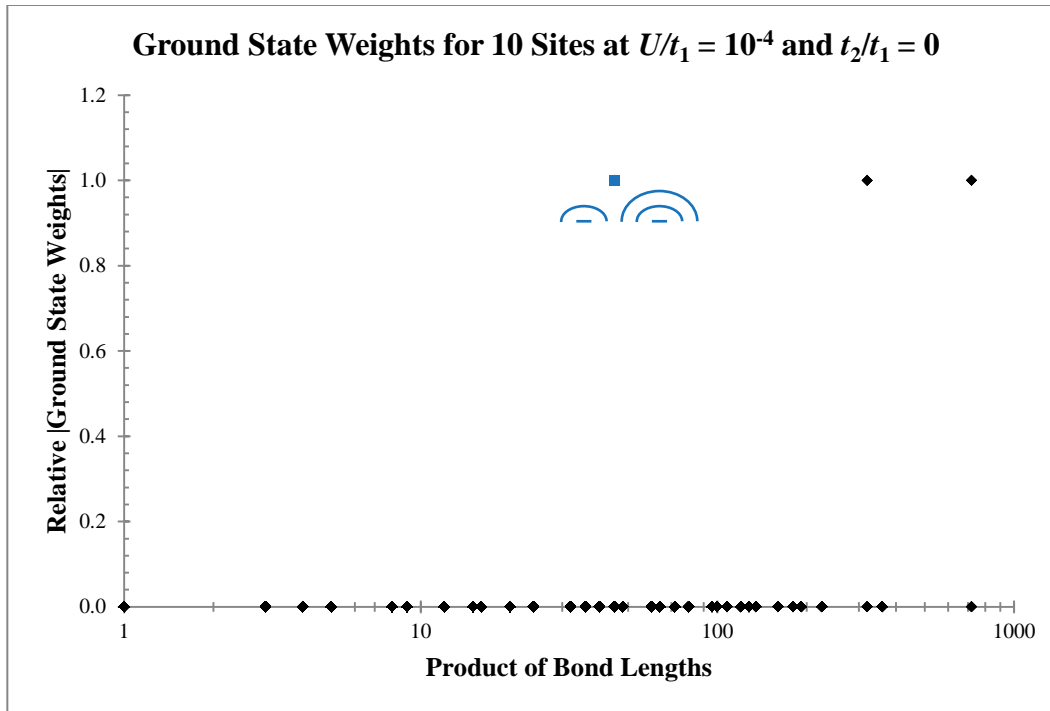


Figure 93 – Both this figure and the last, plotted the ground state weights on the y-axis relative to the ground state weight of the pure singlet state with the longest possible bonds (indicated in the figure). In the tight-binding limit, the pure singlet state with the longest possible bonds always has the lowest, non-zero contribution to the ground state. This can also be seen in **Figures 71 – 74** for $N = 8$ in the same limit.

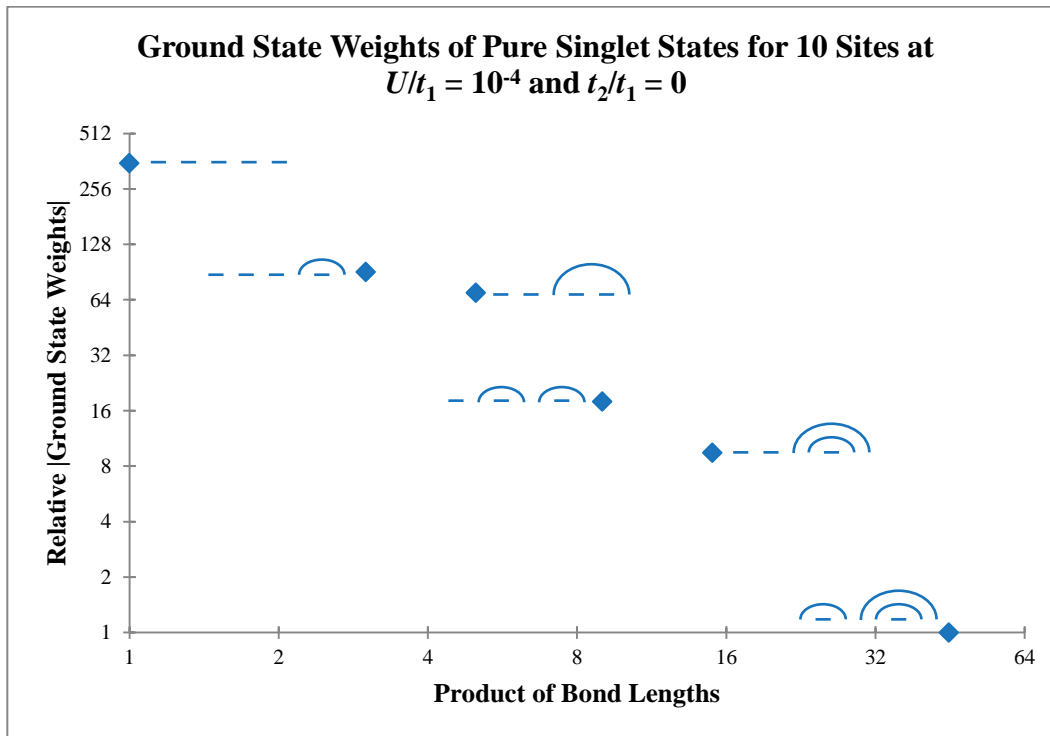


Figure 94 – This is a plot of only the pure singlet state weights. Notice that the pure singlet states follow the nice power law decay even in the tight-binding limit (we already know it will in the Heisenberg limit).

The ground state weights generally decrease with bond length for 8 sites; this is clearer for 10 sites. Pure singlet states in region I appear to have a similar weight distribution for small and large U/t_1 . For large U/t_1 and in region II, the ground state changes into the Majumdar-Ghosh chain.

Charge bond states (mixed or pure) do not always display this decay in as clear a fashion. However, consider the large U/t_1 and t_2/t_1 limit and pure singlet states. For these states, the weights when the product of the bond lengths $P(L)$ are 3 and 9 ($N = 8$), their weights are equal despite the differences in bond length. This happens to be seen in many cases with charge bond states. For example, consider the same limit, the two states in **Figure 91** that have three singlet bonds and one PCB with that PCB crossing one of the singlets, also have equal weights despite their bond lengths $P(L) = 4$ and 12. Another example, although not obvious from the above figures, is with states that have at least two NCBs. There are multiple circumstances in which these two NCB bonds configured in a $P(L) = 1$ for one state and a $P(L) = 3$ in another, with the rest of the state remaining unchanged between them, will have the same weights as well. There are many other circumstances with different bond configurations that display this type of behaviour (though not always; sometimes it depends on which region we are in, much like the pure singlet states). The following figure provides a few examples of states that are equivalent in *all* tested cases.

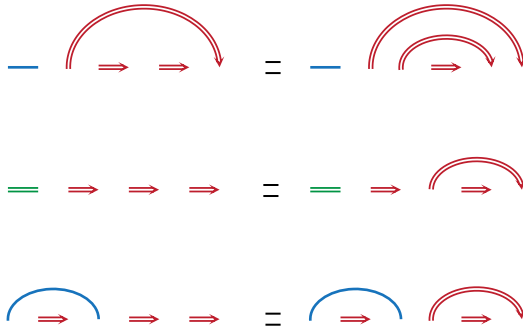


Figure 95 – Three examples of states with equivalent weights, but with different bond lengths. States are equivalent for all tested data points.

A commonly seen issue is with applying translational symmetries to reduce the size of the matrices that are to be diagonalized by LAPACK by a factor of N (approximately). By applying translational symmetry we can diagonalize each momentum block individually, such as $k = 0$ and $k = \pi$. With our GVB basis, applying translational symmetry to pure singlet states works as expected (there is an alternating negative sign since we use fermion operators in defining the singlet states and not boson operators, as in the VB basis). This is not always true when we add charge bonds. States with only one charge bond (the rest singlets) display translational symmetry as expected (their weights are always equal). However, as shown in **Figures 71 and 73**, some states display translational symmetry as expected in one region but not another. The example these two figures show is with the nearest neighbour pure NCB states; where (at $U = 10^{-4}$)

it displays “proper” translational symmetry in region I, but not in region II. The reason for this is unknown to me at this point, but it would certainly be helpful to solve this translational symmetry issue.

An interesting feature is seen when $U = 10^4$: all non-zero bond weights are equal to or larger than the weight of the pure singlet state with the longest possible bonds. For $N = 8$, it is the pure singlet state with $P(L) = 9$, and for 10 sites it is the pure singlet state with $P(L) = 45$. This is visible in **Figures 71 – 74** ($U = 10^4$) for 8 sites and **Figure 93** for 10 sites. When U/t_1 is increased this is no longer the case as the weights split apart as the charge bond states are suppressed.

What is not obvious from these diagrams is that there is a set of states which never contribute (weight $< 10^{-12}$) to the 8 site ground state for all test cases (as listed above as well as some other points). These states do have one thing in common, which is they all have an odd number of negative charge bonds. Although, not all states with an odd number of NCBs have zero weight. There also are a set of states which never contribute in one region of the phase diagram, but do contribute (usually significantly) in other regions. The state with nearest neighbour positive charge bonds is such a state. It has zero weight for regions I and III, but non-zero weight in region II. **Figure 73**, which is in region II, shows that the nearest neighbour PCB state is the second-most contributing state.

Chapter 8

Conclusion

In this thesis I presented a new basis to solve the half-filled Hubbard model. This new basis, the generalized valence bond (GVB) basis, is an extension of the non-orthogonal and overcomplete valence bond (VB) basis commonly used when solving the Heisenberg model in the singlet ($S_{tot} = 0$) sector. The Heisenberg model is a special case of the half-filled Hubbard model; when there is exactly one electron per site and double occupancies are disallowed. Hence one would expect that the VB basis could be extended to span the singlet sector of the Hilbert space for the Hubbard model. As shown in this thesis, this is indeed true.

The VB basis introduced two main advantages when working with the Heisenberg model. First, it spans the singlet sector of the Hilbert space, which is smaller than the $S_{tot}^z = 0$ sector that the orthogonal and complete S^z basis can trivially be reduced to span. This is useful when studying the ground state, as it is well known that the ground state lies in the singlet sector (and $S_{tot}^z = 0$) [9]. Since the $S_{tot} = 0$ spin sector is smaller, it is more useful for exact diagonalization techniques; as long as the VB basis is restricted to the subset of only “non-crossing” states as to ensure we are working with a complete basis (but still non-orthogonal). Since exact diagonalization techniques scale as $O(D^3)$ reducing the size D of the basis will improve the performance, even if we have to work with the inconvenience of a non-orthogonal basis. Second, the VB basis displays structure in the ground state that the S^z basis does not. The weights associated with each valence bond configuration depend only on the bond lengths, for the non-frustrated Heisenberg model [10]. One can use a master equation technique [11] for computing the bond amplitudes and a trial wave function approach to solve the model with little frustrating interactions.

The GVB basis, non-orthogonal and overcomplete as well, spans the singlet sector of the Hilbert space for the Hubbard model, by adding positive and negative charge bonds to the singlet bonds use in the VB basis. Whereas, the traditional occupation basis can only be trivially made to span the larger $S_{tot}^z = 0$ sector (see **Table 1** in **Chapter 1** for a comparison of the sizes for small lattices). A subset of the GVB states can be selected to form a complete basis that we can use to solve the Hubbard model via exact diagonalization. This complete basis is made up of states with the following three conditions: 1) singlets may not cross one another, 2) charge bonds may not cross one another, and 3) positive (or negative) charge bonds may not be enclosed by another charge bond.

Our results, obtained using the GVB basis to solve the Hubbard model, agreed with results of the Hubbard model solved using the occupation basis, with results of the Heisenberg model solved using the VB basis (in the large- U limit), and with results of the tight-binding model solved analytically in the micro-canonical ensemble (for $U/t_1 = 0$). Any discrepancies seen could be reasonably explained, thus we conclude that our results are correct. Furthermore, we conclude by this fact that our overlap rules and update rules are correct.

Without applying translational symmetry, solving the Hubbard model with the GVB basis outperforms the occupation basis (exact diagonalization) since the $S_{tot} = 0$ sector is smaller than the $S_{tot}^z = 0$ sector. With our GVB basis we could solve for the 10 site case, but with over 60 000 states spanning the $S_{tot}^z = 0$ sector, there is no hope of solving this model using the occupation basis (on any decent computer today), unless one applies translational symmetry. Translational symmetry can be trivially applied to the occupation basis to reduce the size of the basis by the number of lattice sites N . From our analysis of the ground state structure using GVB states, it appears that translational symmetry becomes non-trivial to implement with the introduction of charge bonds, as pure singlet states still display translational symmetry. Also, as shown by our plots of the ground state weights versus the product of the bond lengths, it is evident that there is some correlation between the weights and bond lengths. From this, perhaps a trial wave function approach could be used to solve the Hubbard model.

Bibliography

- [1] A. Auerbach, *Interacting Electrons and Quantum Magnetism* (Springer-Verlag, New York, 1994).
- [2] R.J. Baxter, *Exactly Solved Models in Statistical Mechanics* (Academic Press, San Diego, 1982).
- [3] N. Ashcroft and D. Mermin, *Solid State Physics* (Nelson Thomson, Toronto, 1976).
- [4] F. Essler et al., *The One-Dimensional Hubbard Model* (Cambridge University Press, New York, 2005).
- [5] M. Rasetti, *The Hubbard Model: Recent Results* (World Scientific, New Jersey, 1991).
- [6] G. Rumer, *Göttingen Nachr. Tech.* **1932**, 377 (1932).
- [7] L. Pauling, *J. Chem. Phys.* **1** (4), 280 (1933).
- [8] I. Affleck and E. Lieb, *Lett. Math. Phys.* **12** (1), 57 (1986).
- [9] E. Lieb, *Phys. Rev. Lett.* **62** (10), 1201 (1989).
- [10] S. Liang, B. Douçot, and P.W. Anderson, *Phys. Rev. Lett.* **61** (3), 365 (1988).
- [11] K.S.D. Beach, *Phys. Rev. B.* **79** (22), 224431 (2009).
- [12] E. Anderson et al., *LAPACK Users' Guide Third Edition* (Society for Industrial and Applied Mathematics, Philadelphia, 1999).
- [13] S.R. White, *Phys. Rev. Lett.* **69** (19), 2863 (1992).
- [14] S.R. White, *Phys. Rev. B.* **48** (14), 10345 (1993).
- [15] T. Xiang, J. Lou, and Z. Su, *Phys. Rev. B.* **64** (10), 104414 (2001).
- [16] R. Noack, S.R. White, and D. Scalapino, *Phys. Rev. B.* **270** (3-4), 281 (1996).
- [17] A. Georges and G. Kotliar, *Phys. Rev. B.* **45** (12), 6479 (1992).
- [18] A. Georges, G. Kotliar, W. Krauth, and M. Rozenberg, *Rev. Mod. Phys.* **68** (1), 13 (1996).
- [19] G. Kotliar, S. Savrasov, K. Haule, V. Oudovenko, O. Parcollet, and C. Marianetti, *Rev. Mod. Phys.* **78** (3), 865 (2006).
- [20] A. Georges and W. Krauth, *Phys. Rev. Lett.* **69** (8), 1240 (1992).

- [21] C. Lanczos, *J. Res. Nat. Bur. Stand.* **45** (4), 255 (1950).
- [22] A. Ruhe, *Math. Comp.* **33** (146), 680 (1979).
- [23] J. Cullum and R. Willoughby, *J. Comput. Phys.* **44** (2), 329 (1981).
- [24] E. Dagotto and A. Moreo, *Phys. Rev. Lett.* **63** (19), 2148 (1989).
- [25] F. Becca, A. Parola and S. Sorella, *Phys. Rev. B.* **61** (24), R16287 (2000).
- [26] K.S.D. Beach and A.W. Sandvik, *Nucl. Phys. B.* **750** (3), 142 (2006).
- [27] D. Griffiths, *Introduction to Quantum Mechanics* (Pearson Education, New Jersey, 2005).
- [28] S. Lang, *Linear Algebra* (Springer-Verlag, New York, 1987).
- [29] L. Molinari, *Linear Algebra Appl.* **429**, 2221 (2008).
- [30] H. Bowdler, R. Martin, C. Reinsch, and J. Wilkinson, *Numer. Math.* **11** (4), 293 (1968).
- [31] J. Cuppen, *Numer. Math.* **36** (2), 177 (1981).
- [32] I. Dhillon, Ph.D. dissertation, University of California, Berkeley, 1997.
- [33] D. Campbell, *Math. Mag.* **57** (4), 195 (1984).
- [34] I. Affleck, T. Kennedy, E. Lieb, and H. Tasaki, *Phys. Rev. Lett.* **59** (7), 799 (1987).
- [35] M. Zhitomirshy and K. Ueda, *Phys. Rev. B.* **54** (13), 9007 (1996).
- [36] M. Mambrini, A. Lauchli, D. Poilblanc and F. Mila, *Phys. Rev. B.* **74** (14), 144422 (2006).
- [37] C. Majumdar and D. Ghosh, *J. Math. Phys.* **10** (8), 1388 (1969).
- [38] C. Majumdar and D. Ghosh, *J. Math. Phys.* **10** (8), 1399 (1969).

Appendix A

A1 – Commutation Relations

I define the singlet (χ) and charge bond (η) creation and annihilation operators as

$$\begin{aligned}\chi_{ij}^\dagger &= \frac{1}{\sqrt{2}}(c_{i\uparrow}^\dagger c_{j\downarrow}^\dagger - c_{i\downarrow}^\dagger c_{j\uparrow}^\dagger) & \chi_{ij} &= \frac{1}{\sqrt{2}}(c_{j\downarrow} c_{i\uparrow} - c_{j\uparrow} c_{i\downarrow}) \\ \eta_{ij}^{u\dagger} &= \frac{1}{\sqrt{2}}(c_{i\uparrow}^\dagger c_{i\downarrow}^\dagger + u c_{j\uparrow}^\dagger c_{j\downarrow}^\dagger) & \eta_{ij}^u &= \frac{1}{\sqrt{2}}(c_{i\downarrow} c_{i\uparrow} + u c_{j\downarrow} c_{j\uparrow})\end{aligned}$$

Where $u = +1$ for a positive charge bond (PCB) and $u = -1$ for a negative charge bond (NCB). $c_{i\sigma}^\dagger$ is a fermion operator satisfying the anticommutation relation $\{c_{i\sigma}, c_{j\sigma'}^\dagger\} = \delta_{ij}\delta_{\sigma\sigma'}$.

There are commutation relations $[\hat{A}, \hat{B}]$ and anticommutation relations $\{\hat{A}, \hat{B}\}$ and each are defined as

$$[\hat{A}, \hat{B}] = \hat{A}\hat{B} - \hat{B}\hat{A}$$

$$\{\hat{A}, \hat{B}\} = \hat{A}\hat{B} + \hat{B}\hat{A}$$

A1.1 – Summary of commutation relations

The following is a comprehensive list of useful commutation relations involving operators χ_{ij}^\dagger and $\eta_{ij}^{u\dagger}$ ($|vac\rangle$ is the vacuum state with no electrons).

$$[\chi_{ij}, \chi_{kl}^\dagger] = 0 \quad \text{If } i \neq k, j \neq l \text{ or } i \neq l, j \neq k$$

$$[\eta_{ij}^u, \eta_{kl}^{v\dagger}] = 0 \quad \text{If } i \neq k, j \neq l \text{ or } i \neq l, j \neq k$$

$$[\chi_{ij}, \eta_{kl}^{u\dagger}] = 0 \quad \text{If } i \neq k, j \neq l \text{ or } i \neq l, j \neq k$$

$$[\eta_{ij}^u, \chi_{kl}^\dagger] = 0 \quad \text{If } i \neq k, j \neq l \text{ or } i \neq l, j \neq k$$

$$[\chi_{ij}^\dagger, \chi_{kl}^\dagger] = 0 \quad [\chi_{ij}, \chi_{kl}] = 0$$

$$[\eta_{ij}^{u\dagger}, \eta_{kl}^{v\dagger}] = 0 \quad [\eta_{ij}^u, \eta_{kl}^v] = 0$$

$$[\chi_{ij}, \chi_{ij}^\dagger] |vac\rangle = |vac\rangle$$

$$[\eta_{ij}^u, \eta_{ij}^{v\dagger}] |vac\rangle = \delta^{uv} |vac\rangle \quad [\eta_{ij}^u, \eta_{ji}^{v\dagger}] |vac\rangle = -\delta^{uv} |vac\rangle$$

$$[\chi_{ij}, \eta_{kl}^{u\dagger}] |vac\rangle = 0$$

$$[\eta_{ij}^u, \chi_{kl}^\dagger] |vac\rangle = 0$$

$$[\chi_{ij}, \chi_{il}^\dagger \chi_{kj}^\dagger] |vac\rangle = -\frac{1}{2} \chi_{kl}^\dagger |vac\rangle$$

$$\begin{aligned} [\eta_{ij}^u, \eta_{kj}^{v\dagger} \eta_{il}^{w\dagger}] |vac\rangle &= \frac{1}{2} (\eta_{kj}^{v\dagger} + uv \eta_{il}^{w\dagger}) |vac\rangle & [\eta_{ij}^u, \eta_{ik}^{v\dagger}] |vac\rangle &= \frac{1}{2} |vac\rangle \\ [\eta_{ij}^u, \eta_{kj}^{v\dagger} \eta_{li}^{w\dagger}] |vac\rangle &= \frac{1}{2} (w \eta_{kj}^{v\dagger} + uv \eta_{li}^{w\dagger}) |vac\rangle & [\eta_{ij}^u, \eta_{ki}^{v\dagger}] |vac\rangle &= \frac{v}{2} |vac\rangle \\ [\eta_{ij}^u, \eta_{jk}^{v\dagger} \eta_{il}^{w\dagger}] |vac\rangle &= \frac{1}{2} (\eta_{kj}^{v\dagger} + u \eta_{il}^{w\dagger}) |vac\rangle & [\eta_{ji}^u, \eta_{ik}^{v\dagger}] |vac\rangle &= \frac{u}{2} |vac\rangle \\ [\eta_{ij}^u, \eta_{jk}^{v\dagger} \eta_{li}^{w\dagger}] |vac\rangle &= \frac{1}{2} (w \eta_{kj}^{v\dagger} + u \eta_{li}^{w\dagger}) |vac\rangle & [\eta_{ji}^u, \eta_{ki}^{v\dagger}] |vac\rangle &= \frac{uv}{2} |vac\rangle \\ [\eta_{ji}^u, \eta_{kj}^{v\dagger} \eta_{il}^{w\dagger}] |vac\rangle &= \frac{1}{2} (u \eta_{kj}^{v\dagger} + v \eta_{il}^{w\dagger}) |vac\rangle \\ [\eta_{ji}^u, \eta_{kj}^{v\dagger} \eta_{li}^{w\dagger}] |vac\rangle &= \frac{1}{2} (u w \eta_{kj}^{v\dagger} + v \eta_{li}^{w\dagger}) |vac\rangle \\ [\eta_{ji}^u, \eta_{jk}^{v\dagger} \eta_{il}^{w\dagger}] |vac\rangle &= \frac{1}{2} (u \eta_{kj}^{v\dagger} + \eta_{il}^{w\dagger}) |vac\rangle \\ [\eta_{ji}^u, \eta_{jk}^{v\dagger} \eta_{li}^{w\dagger}] |vac\rangle &= \frac{1}{2} (u w \eta_{kj}^{v\dagger} + \eta_{li}^{w\dagger}) |vac\rangle \end{aligned}$$

$$\begin{aligned} [\chi_{ij}, \eta_{kj}^{u\dagger} \eta_{il}^{v\dagger}] |vac\rangle &= -\frac{u}{2} \chi_{ij}^\dagger |vac\rangle \\ [\chi_{ij}, \eta_{kj}^{u\dagger} \eta_{li}^{v\dagger}] |vac\rangle &= -\frac{uv}{2} \chi_{ij}^\dagger |vac\rangle \\ [\chi_{ij}, \eta_{jk}^{u\dagger} \eta_{il}^{v\dagger}] |vac\rangle &= -\frac{1}{2} \chi_{ij}^\dagger |vac\rangle \\ [\chi_{ij}, \eta_{jk}^{u\dagger} \eta_{li}^{v\dagger}] |vac\rangle &= -\frac{v}{2} \chi_{ij}^\dagger |vac\rangle \end{aligned}$$

$$[\eta_{ij}^u, \chi_{kj}^\dagger \chi_{il}^\dagger] |vac\rangle = 0$$

$$\begin{aligned} [\chi_{ij}, \chi_{kj}^\dagger \eta_{li}^{u\dagger}] |vac\rangle &= -\frac{1}{2} \chi_{ik}^\dagger |vac\rangle \\ [\chi_{ij}, \chi_{kj}^\dagger \eta_{li}^{u\dagger}] |vac\rangle &= -\frac{u}{2} \chi_{ik}^\dagger |vac\rangle \end{aligned}$$

$$\begin{aligned} [\eta_{ij}^u, \chi_{kj}^\dagger \eta_{li}^{v\dagger}] |vac\rangle &= \frac{1}{2} \chi_{kj}^\dagger |vac\rangle \\ [\eta_{ij}^u, \chi_{kj}^\dagger \eta_{li}^{v\dagger}] |vac\rangle &= \frac{v}{2} \chi_{kj}^\dagger |vac\rangle \\ [\eta_{ji}^u, \chi_{kj}^\dagger \eta_{li}^{v\dagger}] |vac\rangle &= \frac{u}{2} \chi_{kj}^\dagger |vac\rangle \\ [\eta_{ji}^u, \chi_{kj}^\dagger \eta_{li}^{v\dagger}] |vac\rangle &= \frac{uv}{2} \chi_{kj}^\dagger |vac\rangle \end{aligned}$$

A1.2 – Work for commutation relations

$$\begin{aligned}
 [\chi_{ij}, \chi_{ij}^\dagger] |vac\rangle &= \frac{1}{2} (c_{j\downarrow} c_{i\uparrow} - c_{j\uparrow} c_{i\downarrow}) (c_{i\uparrow}^\dagger c_{j\downarrow}^\dagger - c_{i\downarrow}^\dagger c_{j\uparrow}^\dagger) |vac\rangle \\
 &= \frac{1}{2} (c_{j\downarrow} c_{i\uparrow} c_{i\uparrow}^\dagger c_{j\downarrow}^\dagger - c_{j\downarrow} c_{i\uparrow} c_{i\downarrow}^\dagger c_{j\uparrow}^\dagger - c_{j\uparrow} c_{i\downarrow} c_{i\uparrow}^\dagger c_{j\downarrow}^\dagger + c_{j\uparrow} c_{i\downarrow} c_{i\downarrow}^\dagger c_{j\uparrow}^\dagger) |vac\rangle \\
 &= \frac{1}{2} (1 + 1) |vac\rangle = |vac\rangle
 \end{aligned}$$

$$\begin{aligned}
 [\eta_{ij}^u, \eta_{ij}^{v\dagger}] |vac\rangle &= \frac{1}{2} (c_{i\downarrow} c_{i\uparrow} + u c_{j\downarrow} c_{j\uparrow}) (c_{i\uparrow}^\dagger c_{i\downarrow}^\dagger + v c_{j\uparrow}^\dagger c_{j\downarrow}^\dagger) |vac\rangle \\
 &= \frac{1}{2} (1 + uv) |vac\rangle = \delta^{uv} |vac\rangle
 \end{aligned}$$

$$[\chi_{ij}, \eta_{ij}^{u\dagger}] |vac\rangle = \frac{1}{2} (c_{j\downarrow} c_{i\uparrow} - c_{j\uparrow} c_{i\downarrow}) (c_{i\uparrow}^\dagger c_{i\downarrow}^\dagger + u c_{j\uparrow}^\dagger c_{j\downarrow}^\dagger) |vac\rangle = 0$$

$$[\eta_{ij}^u, \chi_{kl}^\dagger] |vac\rangle = \frac{1}{2} (c_{i\downarrow} c_{i\uparrow} + u c_{j\downarrow} c_{j\uparrow}) (c_{i\uparrow}^\dagger c_{j\downarrow}^\dagger - c_{i\downarrow}^\dagger c_{j\uparrow}^\dagger) |vac\rangle = 0$$

$$\begin{aligned}
 [\chi_{ij}, \chi_{il}^\dagger \chi_{kj}^\dagger] |vac\rangle &= \frac{3}{\sqrt{2}} (c_{j\downarrow} c_{i\uparrow} - c_{j\uparrow} c_{i\downarrow}) (c_{i\uparrow}^\dagger c_{i\downarrow}^\dagger - c_{i\downarrow}^\dagger c_{i\uparrow}^\dagger) (c_{k\uparrow}^\dagger c_{j\downarrow}^\dagger - c_{k\downarrow}^\dagger c_{j\uparrow}^\dagger) |vac\rangle \\
 &= \frac{3}{\sqrt{2}} (c_{j\downarrow} c_{i\uparrow} c_{i\uparrow}^\dagger c_{i\downarrow}^\dagger c_{k\uparrow}^\dagger c_{j\downarrow}^\dagger - c_{j\uparrow} c_{i\downarrow} c_{i\downarrow}^\dagger c_{i\uparrow}^\dagger c_{k\downarrow}^\dagger c_{j\uparrow}^\dagger) |vac\rangle \\
 &= \frac{3}{\sqrt{2}} (c_{i\downarrow}^\dagger c_{k\uparrow}^\dagger - c_{i\uparrow}^\dagger c_{k\downarrow}^\dagger) |vac\rangle \\
 &= -\frac{1}{2} \chi_{kl}^\dagger |vac\rangle
 \end{aligned}$$

$$\begin{aligned}
 [\eta_{ij}^u, \eta_{kj}^{v\dagger} \eta_{il}^{w\dagger}] |vac\rangle &= \frac{3}{\sqrt{2}} (c_{i\downarrow} c_{i\uparrow} + u c_{j\downarrow} c_{j\uparrow}) (c_{k\uparrow}^\dagger c_{k\downarrow}^\dagger + v c_{j\uparrow}^\dagger c_{j\downarrow}^\dagger) (c_{i\uparrow}^\dagger c_{i\downarrow}^\dagger + w c_{i\uparrow}^\dagger c_{i\downarrow}^\dagger) |vac\rangle \\
 &= \frac{3}{\sqrt{2}} (c_{i\downarrow} c_{i\uparrow} (c_{k\uparrow}^\dagger c_{k\downarrow}^\dagger + v c_{j\uparrow}^\dagger c_{j\downarrow}^\dagger) c_{i\uparrow}^\dagger c_{i\downarrow}^\dagger + uv c_{j\downarrow} c_{j\uparrow} (c_{i\uparrow}^\dagger c_{i\downarrow}^\dagger + w c_{i\uparrow}^\dagger c_{i\downarrow}^\dagger) c_{j\uparrow}^\dagger c_{j\downarrow}^\dagger) |vac\rangle \\
 &= \frac{1}{2} (\eta_{kj}^{v\dagger} + uv \eta_{il}^{w\dagger}) |vac\rangle
 \end{aligned}$$

$$\begin{aligned}
[\eta_{ij}^u, \eta_{ik}^{v\dagger}]|vac\rangle &= \frac{1}{2}(c_{i\downarrow}c_{i\uparrow} + uc_{j\downarrow}c_{j\uparrow})(c_{i\uparrow}^\dagger c_{i\downarrow}^\dagger + vc_{k\uparrow}^\dagger c_{k\downarrow}^\dagger)|vac\rangle \\
&= \frac{1}{2}(c_{i\downarrow}c_{i\uparrow}c_{i\uparrow}^\dagger c_{i\downarrow}^\dagger)|vac\rangle = \frac{1}{2}|vac\rangle
\end{aligned}$$

$$\begin{aligned}
[\chi_{ij}, \eta_{kj}^{u\dagger} \eta_{il}^{v\dagger}]|vac\rangle &= \frac{3}{\sqrt{2}}(c_{j\downarrow}c_{i\uparrow} - c_{j\uparrow}c_{i\downarrow})(c_{k\uparrow}^\dagger c_{k\downarrow}^\dagger + uc_{j\uparrow}^\dagger c_{j\downarrow}^\dagger)(c_{i\uparrow}^\dagger c_{i\downarrow}^\dagger + vc_{l\uparrow}^\dagger c_{l\downarrow}^\dagger)|vac\rangle \\
&= \frac{3}{\sqrt{2}}(uc_{j\downarrow}c_{i\uparrow}c_{j\uparrow}^\dagger c_{j\downarrow}^\dagger c_{i\uparrow}^\dagger c_{i\downarrow}^\dagger - uc_{j\uparrow}c_{i\downarrow}c_{j\downarrow}^\dagger c_{j\uparrow}^\dagger c_{i\downarrow}^\dagger c_{i\uparrow}^\dagger)|vac\rangle \\
&= \frac{3u}{\sqrt{2}}(-c_{j\uparrow}^\dagger c_{i\downarrow}^\dagger + c_{j\downarrow}^\dagger c_{i\uparrow}^\dagger)|vac\rangle \\
&= -\frac{u}{2}\chi_{ij}^\dagger|vac\rangle
\end{aligned}$$

$$[\chi_{ij}, \chi_{kj}^\dagger \chi_{il}^\dagger]|vac\rangle = \frac{3}{\sqrt{2}}(c_{i\downarrow}c_{i\uparrow} + uc_{j\downarrow}c_{j\uparrow})(c_{k\uparrow}^\dagger c_{j\downarrow}^\dagger - c_{k\downarrow}^\dagger c_{j\uparrow}^\dagger)(c_{i\uparrow}^\dagger c_{i\downarrow}^\dagger - c_{i\downarrow}^\dagger c_{i\uparrow}^\dagger)|vac\rangle = 0$$

$$\begin{aligned}
[\chi_{ij}, \chi_{kj}^\dagger \eta_{il}^{u\dagger}]|vac\rangle &= \frac{3}{\sqrt{2}}(c_{j\downarrow}c_{i\uparrow} - c_{j\uparrow}c_{i\downarrow})(c_{k\uparrow}^\dagger c_{j\downarrow}^\dagger - c_{k\downarrow}^\dagger c_{j\uparrow}^\dagger)(c_{i\uparrow}^\dagger c_{i\downarrow}^\dagger + uc_{l\uparrow}^\dagger c_{l\downarrow}^\dagger)|vac\rangle \\
&= \frac{3}{\sqrt{2}}(c_{j\downarrow}c_{i\uparrow}c_{k\uparrow}^\dagger c_{j\downarrow}^\dagger c_{i\uparrow}^\dagger c_{i\downarrow}^\dagger + c_{j\uparrow}c_{i\downarrow}c_{k\downarrow}^\dagger c_{j\uparrow}^\dagger c_{i\downarrow}^\dagger c_{i\uparrow}^\dagger)|vac\rangle \\
&= \frac{3}{\sqrt{2}}(-c_{k\uparrow}^\dagger c_{i\downarrow}^\dagger + c_{k\downarrow}^\dagger c_{i\uparrow}^\dagger)|vac\rangle \\
&= -\frac{1}{2}\chi_{ik}^\dagger|vac\rangle
\end{aligned}$$

$$\begin{aligned}
[\eta_{ij}^u, \chi_{kj}^\dagger \eta_{il}^{v\dagger}]|vac\rangle &= \frac{3}{\sqrt{2}}(c_{i\downarrow}c_{i\uparrow} + uc_{j\downarrow}c_{j\uparrow})(c_{k\uparrow}^\dagger c_{j\downarrow}^\dagger - c_{k\downarrow}^\dagger c_{j\uparrow}^\dagger)(c_{i\uparrow}^\dagger c_{i\downarrow}^\dagger + vc_{l\uparrow}^\dagger c_{l\downarrow}^\dagger)|vac\rangle \\
&= \frac{3}{\sqrt{2}}(c_{i\downarrow}c_{i\uparrow}(c_{k\uparrow}^\dagger c_{j\downarrow}^\dagger - c_{k\downarrow}^\dagger c_{j\uparrow}^\dagger)c_{i\uparrow}^\dagger c_{i\downarrow}^\dagger)|vac\rangle \\
&= \frac{1}{2}\chi_{kj}^\dagger|vac\rangle
\end{aligned}$$

A2 – Linear dependence

$$\begin{aligned}
\chi_{ij}^\dagger \chi_{kl}^\dagger + \chi_{kj}^\dagger \chi_{il}^\dagger &= \frac{1}{2} \left((c_{i\uparrow}^\dagger c_{j\downarrow}^\dagger - c_{i\downarrow}^\dagger c_{j\uparrow}^\dagger) (c_{k\uparrow}^\dagger c_{l\downarrow}^\dagger - c_{k\downarrow}^\dagger c_{l\uparrow}^\dagger) \right. \\
&\quad \left. + (c_{k\uparrow}^\dagger c_{j\downarrow}^\dagger - c_{k\downarrow}^\dagger c_{j\uparrow}^\dagger) (c_{i\uparrow}^\dagger c_{l\downarrow}^\dagger - c_{i\downarrow}^\dagger c_{l\uparrow}^\dagger) \right) \\
&= \frac{1}{2} \left((c_{i\uparrow}^\dagger c_{j\downarrow}^\dagger c_{k\uparrow}^\dagger c_{l\downarrow}^\dagger - c_{i\uparrow}^\dagger c_{j\downarrow}^\dagger c_{k\downarrow}^\dagger c_{l\uparrow}^\dagger - c_{i\downarrow}^\dagger c_{j\uparrow}^\dagger c_{k\uparrow}^\dagger c_{l\downarrow}^\dagger + c_{i\downarrow}^\dagger c_{j\uparrow}^\dagger c_{k\downarrow}^\dagger c_{l\uparrow}^\dagger) \right. \\
&\quad \left. + (c_{k\uparrow}^\dagger c_{j\downarrow}^\dagger c_{i\uparrow}^\dagger c_{l\downarrow}^\dagger - c_{k\uparrow}^\dagger c_{j\downarrow}^\dagger c_{i\downarrow}^\dagger c_{l\uparrow}^\dagger - c_{k\downarrow}^\dagger c_{j\uparrow}^\dagger c_{i\uparrow}^\dagger c_{l\downarrow}^\dagger + c_{k\downarrow}^\dagger c_{j\uparrow}^\dagger c_{i\downarrow}^\dagger c_{l\uparrow}^\dagger) \right) \\
&= \frac{1}{2} (c_{i\uparrow}^\dagger c_{k\downarrow}^\dagger c_{j\downarrow}^\dagger c_{l\uparrow}^\dagger + c_{i\downarrow}^\dagger c_{k\uparrow}^\dagger c_{j\uparrow}^\dagger c_{l\downarrow}^\dagger - c_{i\downarrow}^\dagger c_{k\uparrow}^\dagger c_{j\downarrow}^\dagger c_{l\uparrow}^\dagger - c_{i\uparrow}^\dagger c_{k\downarrow}^\dagger c_{j\uparrow}^\dagger c_{l\downarrow}^\dagger) \\
&= \frac{1}{2} (c_{i\uparrow}^\dagger c_{k\downarrow}^\dagger (c_{j\downarrow}^\dagger c_{l\uparrow}^\dagger - c_{j\uparrow}^\dagger c_{l\downarrow}^\dagger) - c_{i\downarrow}^\dagger c_{k\uparrow}^\dagger (c_{j\downarrow}^\dagger c_{l\uparrow}^\dagger - c_{j\uparrow}^\dagger c_{l\downarrow}^\dagger)) \\
&= -\chi_{ik}^\dagger \chi_{jl}^\dagger
\end{aligned}$$

$$\begin{aligned}
\eta_{ij}^{u\dagger} \eta_{kl}^{v\dagger} - \eta_{kj}^{s\dagger} \eta_{il}^{t\dagger} &= \frac{1}{2} \left((c_{i\uparrow}^\dagger c_{i\downarrow}^\dagger + u c_{j\uparrow}^\dagger c_{j\downarrow}^\dagger) (c_{k\uparrow}^\dagger c_{k\downarrow}^\dagger + v c_{l\uparrow}^\dagger c_{l\downarrow}^\dagger) \right. \\
&\quad \left. - (c_{k\uparrow}^\dagger c_{k\downarrow}^\dagger + s c_{j\uparrow}^\dagger c_{j\downarrow}^\dagger) (c_{i\uparrow}^\dagger c_{i\downarrow}^\dagger + t c_{l\uparrow}^\dagger c_{l\downarrow}^\dagger) \right) \\
&= \frac{1}{2} (c_{i\uparrow}^\dagger c_{i\downarrow}^\dagger c_{k\uparrow}^\dagger c_{k\downarrow}^\dagger + v c_{i\uparrow}^\dagger c_{i\downarrow}^\dagger c_{l\uparrow}^\dagger c_{l\downarrow}^\dagger + u c_{j\uparrow}^\dagger c_{j\downarrow}^\dagger c_{k\uparrow}^\dagger c_{k\downarrow}^\dagger + u v c_{j\uparrow}^\dagger c_{j\downarrow}^\dagger c_{l\uparrow}^\dagger c_{l\downarrow}^\dagger - c_{k\uparrow}^\dagger c_{k\downarrow}^\dagger c_{i\uparrow}^\dagger c_{i\downarrow}^\dagger \\
&\quad - t c_{k\uparrow}^\dagger c_{k\downarrow}^\dagger c_{l\uparrow}^\dagger c_{l\downarrow}^\dagger - s c_{j\uparrow}^\dagger c_{j\downarrow}^\dagger c_{i\uparrow}^\dagger c_{i\downarrow}^\dagger - s t c_{j\uparrow}^\dagger c_{j\downarrow}^\dagger c_{l\uparrow}^\dagger c_{l\downarrow}^\dagger) \\
&= \frac{1}{2} \left((u v - s t) c_{j\uparrow}^\dagger c_{j\downarrow}^\dagger c_{l\uparrow}^\dagger c_{l\downarrow}^\dagger + c_{i\uparrow}^\dagger c_{i\downarrow}^\dagger (v c_{l\uparrow}^\dagger c_{l\downarrow}^\dagger - s c_{j\uparrow}^\dagger c_{j\downarrow}^\dagger) - c_{k\uparrow}^\dagger c_{k\downarrow}^\dagger (t c_{l\uparrow}^\dagger c_{l\downarrow}^\dagger - u c_{j\uparrow}^\dagger c_{j\downarrow}^\dagger) \right) \\
&= \frac{1}{2} (u v - s t) c_{j\uparrow}^\dagger c_{j\downarrow}^\dagger c_{l\uparrow}^\dagger c_{l\downarrow}^\dagger \\
&\quad + \frac{1}{2} \left(v c_{i\uparrow}^\dagger c_{i\downarrow}^\dagger (c_{l\uparrow}^\dagger c_{l\downarrow}^\dagger - s v c_{j\uparrow}^\dagger c_{j\downarrow}^\dagger) - t c_{k\uparrow}^\dagger c_{k\downarrow}^\dagger (c_{l\uparrow}^\dagger c_{l\downarrow}^\dagger - t u c_{j\uparrow}^\dagger c_{j\downarrow}^\dagger) \right)
\end{aligned}$$

Apply condition $uv = st$

$$\begin{aligned}
&= \frac{1}{2} (v c_{i\uparrow}^\dagger c_{i\downarrow}^\dagger - t c_{k\uparrow}^\dagger c_{k\downarrow}^\dagger) (c_{l\uparrow}^\dagger c_{l\downarrow}^\dagger - s v c_{j\uparrow}^\dagger c_{j\downarrow}^\dagger) \\
&= v \eta_{ik}^{\bar{t}v\dagger} \eta_{lj}^{\bar{s}v\dagger}
\end{aligned}$$

Appendix B

B1 – Update rules for Hubbard Hamiltonian

The Hubbard Hamiltonian is given by,

$$\hat{H} = - \sum_{ij,\sigma} t_{ij} (c_{i\sigma}^\dagger c_{j\sigma} + c_{j\sigma}^\dagger c_{i\sigma}) + U \sum_i n_{i\uparrow} n_{i\downarrow}$$

$$\hat{T}_{ij} \equiv \sum_{\sigma} (c_{i\sigma}^\dagger c_{j\sigma} + c_{j\sigma}^\dagger c_{i\sigma})$$

$$\hat{U}_i \equiv n_{i\uparrow} n_{i\downarrow}$$

B1.1 – Summary of update rules

$$\hat{U}_i(\chi_{ij}^\dagger | vac) = 0$$

$$(\hat{U}_i + \hat{U}_j)(\eta_{ij}^{u\dagger} | vac) = \eta_{ij}^{u\dagger} | vac$$

$$\hat{T}_{ij}(\chi_{ij}^\dagger | vac) = 2\eta_{ij}^{+\dagger} | vac$$

$$\hat{T}_{ij}(\eta_{ij}^{u\dagger} | vac) = (1 + u)\chi_{ij}^\dagger | vac$$

$$\hat{T}_{ij}(\chi_{kj}^\dagger \chi_{il}^\dagger | vac) = -\eta_{ij}^{+\dagger} \chi_{kl}^\dagger | vac$$

$$\hat{T}_{ij}(\eta_{kj}^{u\dagger} \eta_{il}^{v\dagger} | vac) = \chi_{ij}^\dagger \eta_{kl}^{uv\dagger} | vac$$

$$\hat{T}_{ij}(\eta_{kj}^{u\dagger} \eta_{il}^{v\dagger} | vac) = v \chi_{ij}^\dagger \eta_{kl}^{uv\dagger} | vac$$

$$\hat{T}_{ij}(\eta_{jk}^{u\dagger} \eta_{il}^{v\dagger} | vac) = u \chi_{ij}^\dagger \eta_{kl}^{uv\dagger} | vac$$

$$\hat{T}_{ij}(\eta_{jk}^{u\dagger} \eta_{il}^{v\dagger} | vac) = uv \chi_{ij}^\dagger \eta_{kl}^{uv\dagger} | vac$$

$$\hat{T}_{ij}(\chi_{kj}^\dagger \eta_{il}^{u\dagger} | vac) = \chi_{ik}^\dagger \eta_{jl}^{u\dagger} | vac$$

$$\hat{T}_{ij}(\chi_{kj}^\dagger \eta_{il}^{u\dagger} | vac) = u \chi_{ik}^\dagger \eta_{jl}^{u\dagger} | vac$$

B1.2 – Work for update rules

$$\hat{U}_i(\chi_{ij}^\dagger | vac) = \frac{1}{\sqrt{2}} c_{i\uparrow}^\dagger c_{i\uparrow} c_{i\downarrow}^\dagger c_{i\downarrow} (c_{i\uparrow}^\dagger c_{j\downarrow}^\dagger - c_{i\downarrow}^\dagger c_{j\uparrow}^\dagger) | vac \rangle = 0$$

$$\hat{U}_i(\eta_{ij}^{u\dagger} | vac) = \frac{1}{\sqrt{2}} c_{i\uparrow}^\dagger c_{i\uparrow} c_{i\downarrow}^\dagger c_{i\downarrow} (c_{i\uparrow}^\dagger c_{i\downarrow}^\dagger + u c_{j\uparrow}^\dagger c_{j\downarrow}^\dagger) | vac \rangle = \frac{1}{\sqrt{2}} c_{i\uparrow}^\dagger c_{i\downarrow}^\dagger | vac \rangle$$

$$\begin{aligned} \hat{T}_{ij}(\chi_{ij}^\dagger | vac) &= \frac{1}{\sqrt{2}} (c_{i\uparrow}^\dagger c_{j\uparrow}^\dagger + c_{j\uparrow}^\dagger c_{i\uparrow}^\dagger + c_{i\downarrow}^\dagger c_{j\downarrow}^\dagger + c_{j\downarrow}^\dagger c_{i\downarrow}^\dagger) (c_{i\uparrow}^\dagger c_{j\downarrow}^\dagger - c_{i\downarrow}^\dagger c_{j\uparrow}^\dagger) | vac \rangle \\ &= \frac{1}{\sqrt{2}} (-c_{i\uparrow}^\dagger c_{j\uparrow}^\dagger c_{i\downarrow}^\dagger c_{j\downarrow}^\dagger + c_{j\uparrow}^\dagger c_{i\uparrow}^\dagger c_{i\downarrow}^\dagger c_{j\downarrow}^\dagger + c_{i\downarrow}^\dagger c_{j\downarrow}^\dagger c_{i\uparrow}^\dagger c_{j\uparrow}^\dagger - c_{j\downarrow}^\dagger c_{i\downarrow}^\dagger c_{i\uparrow}^\dagger c_{j\uparrow}^\dagger) | vac \rangle \\ &= \frac{1}{\sqrt{2}} (c_{i\uparrow}^\dagger c_{i\downarrow}^\dagger + c_{j\uparrow}^\dagger c_{j\downarrow}^\dagger - c_{i\downarrow}^\dagger c_{i\uparrow}^\dagger - c_{j\downarrow}^\dagger c_{j\uparrow}^\dagger) | vac \rangle \\ &= 2\eta_{ij}^{+\dagger} | vac \rangle \end{aligned}$$

$$\begin{aligned} \hat{T}_{ij}(\eta_{ij}^{u\dagger} | vac) &= \frac{1}{\sqrt{2}} (c_{i\uparrow}^\dagger c_{j\uparrow}^\dagger + c_{j\uparrow}^\dagger c_{i\uparrow}^\dagger + c_{i\downarrow}^\dagger c_{j\downarrow}^\dagger + c_{j\downarrow}^\dagger c_{i\downarrow}^\dagger) (c_{i\uparrow}^\dagger c_{i\downarrow}^\dagger + u c_{j\uparrow}^\dagger c_{j\downarrow}^\dagger) | vac \rangle \\ &= \frac{1}{\sqrt{2}} (u c_{i\uparrow}^\dagger c_{j\uparrow}^\dagger c_{j\downarrow}^\dagger c_{i\downarrow}^\dagger + c_{j\uparrow}^\dagger c_{i\uparrow}^\dagger c_{i\downarrow}^\dagger c_{i\downarrow}^\dagger + u c_{i\downarrow}^\dagger c_{j\downarrow}^\dagger c_{j\uparrow}^\dagger c_{i\uparrow}^\dagger + c_{j\downarrow}^\dagger c_{i\downarrow}^\dagger c_{i\uparrow}^\dagger c_{i\downarrow}^\dagger) | vac \rangle \\ &= \frac{1}{\sqrt{2}} (u c_{i\uparrow}^\dagger c_{j\downarrow}^\dagger + c_{j\uparrow}^\dagger c_{i\downarrow}^\dagger - u c_{i\downarrow}^\dagger c_{j\uparrow}^\dagger - c_{j\downarrow}^\dagger c_{i\uparrow}^\dagger) | vac \rangle \\ &= \frac{1}{\sqrt{2}} ((1+u) c_{i\uparrow}^\dagger c_{j\downarrow}^\dagger - (1+u) c_{i\downarrow}^\dagger c_{j\uparrow}^\dagger) | vac \rangle \\ &= (1+u) \chi_{ij}^\dagger | vac \rangle \end{aligned}$$

$$\begin{aligned} \hat{T}_{ij}(\chi_{kj}^\dagger \chi_{il}^\dagger | vac) &= \frac{1}{2} (c_{i\uparrow}^\dagger c_{j\uparrow}^\dagger + c_{j\uparrow}^\dagger c_{i\uparrow}^\dagger + c_{i\downarrow}^\dagger c_{j\downarrow}^\dagger + c_{j\downarrow}^\dagger c_{i\downarrow}^\dagger) \\ &\quad \cdot (c_{k\uparrow}^\dagger c_{j\downarrow}^\dagger - c_{k\downarrow}^\dagger c_{j\uparrow}^\dagger) (c_{i\uparrow}^\dagger c_{i\downarrow}^\dagger - c_{i\downarrow}^\dagger c_{i\uparrow}^\dagger) | vac \rangle \\ &= \frac{1}{2} (c_{i\uparrow}^\dagger c_{j\uparrow}^\dagger c_{k\downarrow}^\dagger c_{j\downarrow}^\dagger c_{i\downarrow}^\dagger c_{i\uparrow}^\dagger + c_{j\uparrow}^\dagger c_{i\uparrow}^\dagger c_{k\uparrow}^\dagger c_{j\downarrow}^\dagger c_{i\uparrow}^\dagger c_{i\downarrow}^\dagger + c_{i\downarrow}^\dagger c_{j\downarrow}^\dagger c_{k\uparrow}^\dagger c_{j\downarrow}^\dagger c_{i\uparrow}^\dagger c_{i\downarrow}^\dagger \\ &\quad + c_{j\downarrow}^\dagger c_{i\downarrow}^\dagger c_{k\downarrow}^\dagger c_{j\uparrow}^\dagger c_{i\downarrow}^\dagger c_{i\uparrow}^\dagger) | vac \rangle \end{aligned}$$

$$\begin{aligned}
&= \frac{1}{2}(-c_{i\uparrow}^\dagger c_{k\downarrow}^\dagger c_{i\downarrow}^\dagger c_{i\uparrow}^\dagger + c_{j\uparrow}^\dagger c_{k\uparrow}^\dagger c_{j\downarrow}^\dagger c_{i\downarrow}^\dagger - c_{i\downarrow}^\dagger c_{k\uparrow}^\dagger c_{i\uparrow}^\dagger c_{i\downarrow}^\dagger + c_{j\downarrow}^\dagger c_{k\downarrow}^\dagger c_{j\uparrow}^\dagger c_{i\uparrow}^\dagger)|vac\rangle \\
&= \frac{1}{2}(c_{i\uparrow}^\dagger c_{i\downarrow}^\dagger (c_{k\downarrow}^\dagger c_{i\uparrow}^\dagger - c_{k\uparrow}^\dagger c_{i\downarrow}^\dagger) + c_{j\uparrow}^\dagger c_{j\downarrow}^\dagger (c_{k\downarrow}^\dagger c_{i\uparrow}^\dagger - c_{k\uparrow}^\dagger c_{i\downarrow}^\dagger))|vac\rangle \\
&= -\eta_{ij}^{++} \chi_{kl}^\dagger |vac\rangle
\end{aligned}$$

$$\begin{aligned}
\hat{T}_{ij}(\eta_{kj}^{u\dagger} \eta_{il}^{v\dagger} |vac\rangle) &= \frac{1}{2}(c_{i\uparrow}^\dagger c_{j\uparrow}^\dagger + c_{j\uparrow}^\dagger c_{i\uparrow}^\dagger + c_{i\downarrow}^\dagger c_{j\downarrow}^\dagger + c_{j\downarrow}^\dagger c_{i\downarrow}^\dagger) \\
&\quad \cdot (c_{k\uparrow}^\dagger c_{k\downarrow}^\dagger + u c_{j\uparrow}^\dagger c_{j\downarrow}^\dagger)(c_{i\uparrow}^\dagger c_{i\downarrow}^\dagger + v c_{i\uparrow}^\dagger c_{i\downarrow}^\dagger)|vac\rangle \\
&= \frac{1}{2}(u v c_{i\uparrow}^\dagger c_{j\uparrow}^\dagger c_{j\downarrow}^\dagger c_{i\uparrow}^\dagger c_{i\downarrow}^\dagger + c_{j\uparrow}^\dagger c_{i\uparrow}^\dagger c_{k\uparrow}^\dagger c_{k\downarrow}^\dagger c_{i\uparrow}^\dagger c_{i\downarrow}^\dagger + u v c_{i\downarrow}^\dagger c_{j\downarrow}^\dagger c_{j\uparrow}^\dagger c_{i\downarrow}^\dagger c_{i\uparrow}^\dagger \\
&\quad + c_{j\downarrow}^\dagger c_{i\downarrow}^\dagger c_{k\uparrow}^\dagger c_{k\downarrow}^\dagger c_{i\uparrow}^\dagger c_{i\downarrow}^\dagger)|vac\rangle \\
&= \frac{1}{2}(u v c_{i\uparrow}^\dagger c_{j\downarrow}^\dagger c_{i\uparrow}^\dagger c_{i\downarrow}^\dagger + c_{j\uparrow}^\dagger c_{k\uparrow}^\dagger c_{k\downarrow}^\dagger c_{i\downarrow}^\dagger - u v c_{i\downarrow}^\dagger c_{j\uparrow}^\dagger c_{i\uparrow}^\dagger c_{i\downarrow}^\dagger - c_{j\downarrow}^\dagger c_{k\uparrow}^\dagger c_{k\downarrow}^\dagger c_{i\uparrow}^\dagger)|vac\rangle \\
&= \frac{1}{2}(c_{i\uparrow}^\dagger c_{j\downarrow}^\dagger (u v c_{i\uparrow}^\dagger c_{i\downarrow}^\dagger + c_{k\uparrow}^\dagger c_{k\downarrow}^\dagger) - c_{i\downarrow}^\dagger c_{j\uparrow}^\dagger (u v c_{i\uparrow}^\dagger c_{i\downarrow}^\dagger + c_{k\uparrow}^\dagger c_{k\downarrow}^\dagger))|vac\rangle \\
&= \chi_{ij}^\dagger \eta_{kl}^{uv\dagger} |vac\rangle
\end{aligned}$$

$$\begin{aligned}
\hat{T}_{ij}(\chi_{kj}^\dagger \eta_{il}^{u\dagger} |vac\rangle) &= \frac{1}{2}(c_{i\uparrow}^\dagger c_{j\uparrow}^\dagger + c_{j\uparrow}^\dagger c_{i\uparrow}^\dagger + c_{i\downarrow}^\dagger c_{j\downarrow}^\dagger + c_{j\downarrow}^\dagger c_{i\downarrow}^\dagger) \\
&\quad \cdot (c_{k\uparrow}^\dagger c_{j\downarrow}^\dagger - c_{k\downarrow}^\dagger c_{j\uparrow}^\dagger)(c_{i\uparrow}^\dagger c_{i\downarrow}^\dagger + u c_{i\uparrow}^\dagger c_{i\downarrow}^\dagger)|vac\rangle \\
&= \frac{1}{2}(-u c_{i\uparrow}^\dagger c_{j\uparrow}^\dagger c_{k\downarrow}^\dagger c_{j\uparrow}^\dagger c_{i\uparrow}^\dagger c_{i\downarrow}^\dagger + c_{j\uparrow}^\dagger c_{i\uparrow}^\dagger c_{k\uparrow}^\dagger c_{j\downarrow}^\dagger c_{i\uparrow}^\dagger c_{i\downarrow}^\dagger + u c_{i\downarrow}^\dagger c_{j\downarrow}^\dagger c_{k\uparrow}^\dagger c_{j\downarrow}^\dagger c_{i\uparrow}^\dagger c_{i\downarrow}^\dagger \\
&\quad - c_{j\downarrow}^\dagger c_{i\downarrow}^\dagger c_{k\downarrow}^\dagger c_{j\uparrow}^\dagger c_{i\uparrow}^\dagger c_{i\downarrow}^\dagger)|vac\rangle \\
&= \frac{1}{2}(u c_{i\uparrow}^\dagger c_{k\downarrow}^\dagger c_{i\uparrow}^\dagger c_{i\downarrow}^\dagger + c_{j\uparrow}^\dagger c_{k\uparrow}^\dagger c_{j\downarrow}^\dagger c_{i\downarrow}^\dagger - u c_{i\downarrow}^\dagger c_{k\uparrow}^\dagger c_{i\uparrow}^\dagger c_{i\downarrow}^\dagger + c_{j\downarrow}^\dagger c_{k\downarrow}^\dagger c_{j\uparrow}^\dagger c_{i\uparrow}^\dagger)|vac\rangle \\
&= \frac{1}{2}(c_{i\uparrow}^\dagger c_{k\downarrow}^\dagger (u c_{i\uparrow}^\dagger c_{i\downarrow}^\dagger + c_{j\uparrow}^\dagger c_{j\downarrow}^\dagger) - c_{i\downarrow}^\dagger c_{k\uparrow}^\dagger (u c_{i\uparrow}^\dagger c_{i\downarrow}^\dagger + c_{j\uparrow}^\dagger c_{j\downarrow}^\dagger))|vac\rangle \\
&= \chi_{ik}^\dagger \eta_{jl}^{u\dagger} |vac\rangle
\end{aligned}$$

B2 – Update rules for $\vec{S}_i \cdot \vec{S}_j$

Update Rules for $\vec{S}_i \cdot \vec{S}_j$ acting on our basis states. $\vec{S}_i \cdot \vec{S}_j$ can be rewritten as

$$\vec{S}_i \cdot \vec{S}_j = \frac{1}{4}n_i n_j - \chi_{ij}^\dagger \chi_{ij} + \delta_{ij} n_i.$$

B2.1 – Summary of update rules

$$\vec{S}_i \cdot \vec{S}_j(\chi_{ij}^\dagger |vac\rangle) = -\frac{3}{4}\chi_{ij}^\dagger |vac\rangle$$

$$\vec{S}_i \cdot \vec{S}_j(\chi_{kj}^\dagger \chi_{il}^\dagger |vac\rangle) = \frac{1}{4}\chi_{kj}^\dagger \chi_{il}^\dagger |vac\rangle + \frac{1}{2}\chi_{ij}^\dagger \chi_{kl}^\dagger |vac\rangle$$

$$\vec{S}_i \cdot \vec{S}_j(\eta_{ij}^{u\dagger} |vac\rangle) = 0$$

$$\vec{S}_i \cdot \vec{S}_j(\eta_{kj}^{u\dagger} \eta_{il}^{v\dagger} |vac\rangle) = 0$$

$$\vec{S}_i \cdot \vec{S}_j(\chi_{kj}^\dagger \eta_{il}^{u\dagger} |vac\rangle) = 0$$

B2.2 – Work for update rules

Some useful update rules needed to show work.

$$n_i(\chi_{ij}^\dagger |vac\rangle) = \frac{1}{\sqrt{2}}(c_{i\uparrow}^\dagger c_{i\uparrow} + c_{i\downarrow}^\dagger c_{i\downarrow})(c_{i\uparrow}^\dagger c_{j\downarrow}^\dagger - c_{i\downarrow}^\dagger c_{j\uparrow}^\dagger) |vac\rangle = \chi_{ij}^\dagger |vac\rangle$$

$$n_i(\eta_{ij}^{u\dagger} |vac\rangle) = \frac{1}{\sqrt{2}}(c_{i\uparrow}^\dagger c_{i\uparrow} + c_{i\downarrow}^\dagger c_{i\downarrow})(c_{i\uparrow}^\dagger c_{i\downarrow}^\dagger + u c_{j\uparrow}^\dagger c_{j\downarrow}^\dagger) |vac\rangle = \frac{2}{\sqrt{2}}c_{i\uparrow}^\dagger c_{i\downarrow}^\dagger |vac\rangle$$

$$n_j(\eta_{ij}^{u\dagger} |vac\rangle) = \frac{2u}{\sqrt{2}}c_{j\uparrow}^\dagger c_{j\downarrow}^\dagger |vac\rangle$$

$$n_i n_j(\chi_{ij}^\dagger |vac\rangle) = \chi_{ij}^\dagger |vac\rangle$$

$$n_i n_j(\eta_{ij}^{u\dagger} |vac\rangle) = 0$$

$$\chi_{ij}^\dagger \chi_{ij}^\dagger |vac\rangle = \frac{1}{2}(c_{i\uparrow}^\dagger c_{j\downarrow}^\dagger - c_{i\downarrow}^\dagger c_{j\uparrow}^\dagger)(c_{i\uparrow}^\dagger c_{j\downarrow}^\dagger - c_{i\downarrow}^\dagger c_{j\uparrow}^\dagger) |vac\rangle$$

$$= \frac{1}{2}(-c_{i\uparrow}^\dagger c_{j\downarrow}^\dagger c_{i\downarrow}^\dagger c_{j\uparrow}^\dagger - c_{i\downarrow}^\dagger c_{j\uparrow}^\dagger c_{i\uparrow}^\dagger c_{j\downarrow}^\dagger) |vac\rangle$$

$$= -c_{i\uparrow}^\dagger c_{i\downarrow}^\dagger c_{j\uparrow}^\dagger c_{j\downarrow}^\dagger |vac\rangle$$

$$\begin{aligned}
\chi_{ij}^\dagger \chi_{ik}^\dagger |vac\rangle &= \frac{1}{2} (c_{i\uparrow}^\dagger c_{j\downarrow}^\dagger - c_{i\downarrow}^\dagger c_{j\uparrow}^\dagger) (c_{i\uparrow}^\dagger c_{k\downarrow}^\dagger - c_{i\downarrow}^\dagger c_{k\uparrow}^\dagger) |vac\rangle \\
&= \frac{1}{2} (-c_{i\uparrow}^\dagger c_{j\downarrow}^\dagger c_{i\downarrow}^\dagger c_{k\uparrow}^\dagger - c_{i\downarrow}^\dagger c_{j\uparrow}^\dagger c_{i\uparrow}^\dagger c_{k\downarrow}^\dagger) |vac\rangle \\
&= \frac{1}{2} c_{i\uparrow}^\dagger c_{i\downarrow}^\dagger (-c_{k\uparrow}^\dagger c_{j\downarrow}^\dagger + c_{k\downarrow}^\dagger c_{j\uparrow}^\dagger) |vac\rangle = -\frac{1}{\sqrt{2}} c_{i\uparrow}^\dagger c_{i\downarrow}^\dagger \chi_{kj}^\dagger |vac\rangle
\end{aligned}$$

$$\begin{aligned}
\vec{S}_i \cdot \vec{S}_j (\chi_{ij}^\dagger |vac\rangle) &= \left(\frac{1}{4} n_i n_j - \chi_{ij}^\dagger \chi_{ij} \right) (\chi_{ij}^\dagger |vac\rangle) \\
&= \left(\frac{1}{4} \chi_{ij}^\dagger - \chi_{ij}^\dagger \right) |vac\rangle = -\frac{3}{4} \chi_{ij}^\dagger |vac\rangle
\end{aligned}$$

$$\begin{aligned}
\vec{S}_i \cdot \vec{S}_j (\chi_{kj}^\dagger \chi_{il}^\dagger |vac\rangle) &= \left(\frac{1}{4} n_i n_j - \chi_{ij}^\dagger \chi_{ij} \right) \chi_{kj}^\dagger \chi_{il}^\dagger |vac\rangle \\
&= \left(\frac{1}{4} \chi_{kj}^\dagger \chi_{il}^\dagger - \left(-\frac{1}{2} \right) \chi_{ij}^\dagger \chi_{kl}^\dagger \right) |vac\rangle = \frac{1}{4} \chi_{kj}^\dagger \chi_{il}^\dagger |vac\rangle + \frac{1}{2} \chi_{ij}^\dagger \chi_{kl}^\dagger |vac\rangle
\end{aligned}$$

$$\vec{S}_i \cdot \vec{S}_j (\eta_{ij}^{u\dagger} |vac\rangle) = \left(\frac{1}{4} n_i n_j - \chi_{ij}^\dagger \chi_{ij} \right) \eta_{ij}^{u\dagger} |vac\rangle = 0 - 0 = 0$$

$$\begin{aligned}
\vec{S}_i \cdot \vec{S}_j (\eta_{kj}^{u\dagger} \eta_{il}^{v\dagger} |vac\rangle) &= \left(\frac{1}{4} n_i n_j - \chi_{ij}^\dagger \chi_{ij} \right) \eta_{kj}^{u\dagger} \eta_{il}^{v\dagger} |vac\rangle \\
&= \frac{1}{4} \left(\frac{2u}{\sqrt{2}} \right) \left(\frac{2}{\sqrt{2}} \right) c_{j\uparrow}^\dagger c_{j\downarrow}^\dagger c_{i\uparrow}^\dagger c_{i\downarrow}^\dagger |vac\rangle - \left(-\frac{u}{2} \right) \chi_{ij}^\dagger \chi_{ij}^\dagger |vac\rangle \\
&= \frac{u}{4} \left(\frac{2}{\sqrt{2}} \right)^2 c_{j\uparrow}^\dagger c_{j\downarrow}^\dagger c_{i\uparrow}^\dagger c_{i\downarrow}^\dagger |vac\rangle - \frac{u}{2} c_{i\uparrow}^\dagger c_{i\downarrow}^\dagger c_{j\uparrow}^\dagger c_{j\downarrow}^\dagger |vac\rangle = 0
\end{aligned}$$

$$\begin{aligned}
\vec{S}_i \cdot \vec{S}_j (\chi_{kj}^\dagger \eta_{il}^{u\dagger} |vac\rangle) &= \left(\frac{1}{4} n_i n_j - \chi_{ij}^\dagger \chi_{ij} \right) \chi_{kj}^\dagger \eta_{il}^{u\dagger} |vac\rangle \\
&= \frac{1}{4} \chi_{kj}^\dagger \left(\frac{2}{\sqrt{2}} \right) c_{i\uparrow}^\dagger c_{i\downarrow}^\dagger |vac\rangle - \chi_{ij}^\dagger \left(-\frac{1}{2} \right) \chi_{ik}^\dagger |vac\rangle \\
&= \frac{1}{2\sqrt{2}} c_{i\uparrow}^\dagger c_{i\downarrow}^\dagger \chi_{kj}^\dagger |vac\rangle - \frac{1}{2\sqrt{2}} c_{i\uparrow}^\dagger c_{i\downarrow}^\dagger \chi_{kj}^\dagger |vac\rangle = 0
\end{aligned}$$

B3 – Other update rules

$$(n_i - 1)\chi_{ij}^\dagger |vac\rangle = 0$$

$$(n_i - 1)\eta_{ij}^{u\dagger} |vac\rangle = \eta_{ij}^{\bar{u}\dagger} |vac\rangle$$

$$(n_j - 1)\eta_{ij}^{u\dagger} |vac\rangle = -\eta_{ij}^{\bar{u}\dagger} |vac\rangle$$

$$(n_i - 1)(n_j - 1)\eta_{ij}^{u\dagger} |vac\rangle = -\eta_{ij}^{u\dagger} |vac\rangle$$

$$(n_i - 1)(n_j - 1)\eta_{kj}^{u\dagger}\eta_{il}^{v\dagger} |vac\rangle = -\eta_{kj}^{\bar{u}\dagger}\eta_{il}^{\bar{v}\dagger} |vac\rangle$$

$$(n_i - 1)\chi_{ij}^\dagger |vac\rangle = \frac{1}{\sqrt{2}}(\chi_{ij}^\dagger - \chi_{ij}^\dagger) |vac\rangle = 0$$

$$\begin{aligned} (n_i - 1)\eta_{ij}^{u\dagger} |vac\rangle &= \left(\frac{2}{\sqrt{2}}c_{i\uparrow}^\dagger c_{i\downarrow}^\dagger - \eta_{ij}^{u\dagger} \right) |vac\rangle \\ &= \left(\frac{2}{\sqrt{2}}c_{i\uparrow}^\dagger c_{i\downarrow}^\dagger - \frac{1}{\sqrt{2}}(c_{i\uparrow}^\dagger c_{i\downarrow}^\dagger + uc_{j\uparrow}^\dagger c_{j\downarrow}^\dagger) \right) |vac\rangle \\ &= \left(\frac{1}{\sqrt{2}}(c_{i\uparrow}^\dagger c_{i\downarrow}^\dagger - uc_{j\uparrow}^\dagger c_{j\downarrow}^\dagger) \right) |vac\rangle \\ &= \eta_{ij}^{\bar{u}\dagger} |vac\rangle \end{aligned}$$

$$n_i(2 - n_i)\chi_{ij}^\dagger |vac\rangle = n_i(2\chi_{ij}^\dagger - \chi_{ij}^\dagger) |vac\rangle = \chi_{ij}^\dagger |vac\rangle$$

$$\begin{aligned} n_i(2 - n_i)\eta_{ij}^{u\dagger} |vac\rangle &= n_i \left(2\eta_{ij}^{u\dagger} - \frac{2}{\sqrt{2}}c_{i\uparrow}^\dagger c_{i\downarrow}^\dagger \right) |vac\rangle \\ &= \left(2 \left(\frac{2}{\sqrt{2}} \right) c_{i\uparrow}^\dagger c_{i\downarrow}^\dagger - \left(\frac{2}{\sqrt{2}} \right) 2c_{i\uparrow}^\dagger c_{i\downarrow}^\dagger \right) |vac\rangle = 0 \end{aligned}$$

Appendix C

The tight-binding model is the Hubbard model with no on site interaction term ($U = 0$). Hence, the tight-binding Hamiltonian for nearest and next-nearest neighbour interactions is given by,

$$\hat{\mathcal{H}} = -t_1 \sum_{\substack{\langle ij \rangle \\ \sigma}} (c_{i\sigma}^\dagger c_{j\sigma} + c_{j\sigma}^\dagger c_{i\sigma}) - t_2 \sum_{\langle\langle ij \rangle\rangle} (c_{i\sigma}^\dagger c_{j\sigma}^\dagger + c_{j\sigma}^\dagger c_{i\sigma}^\dagger)$$

We can diagonalize this expression by taking the Fourier transform of each operator.

$$c_{i\sigma}^\dagger = \frac{1}{\sqrt{N}} \sum_{\vec{k}} e^{-i\vec{k}\cdot\vec{r}_i} c_{k\sigma}^\dagger$$

$$c_{i\sigma} = \frac{1}{\sqrt{N}} \sum_{\vec{k}} e^{i\vec{k}\cdot\vec{r}_i} c_{k\sigma}$$

In 1D, nearest neighbours of i are given by $i + 1$ and next-nearest neighbours are $i + 2$. Also, $\vec{r}_{i+1} = r_i + a$ and $\vec{r}_{i+2} = r_i + 2a$, where a is the lattice spacing. Hence,

$$\begin{aligned} \hat{\mathcal{H}} &= -t_1 \sum_{i\sigma} \left(\left(\frac{1}{\sqrt{N}} \sum_k e^{-ikr_i} c_{k\sigma}^\dagger \right) \left(\frac{1}{\sqrt{N}} \sum_{k'} e^{ik'r_{i+1}} c_{k'\sigma} \right) \right. \\ &\quad \left. + \left(\frac{1}{\sqrt{N}} \sum_k e^{-ik\cdot r_{i+1}} c_{k\sigma}^\dagger \right) \left(\frac{1}{\sqrt{N}} \sum_{k'} e^{ikr_i} c_{k'\sigma} \right) \right) \\ &\quad - t_2 \sum_{i\sigma} \left(\left(\frac{1}{\sqrt{N}} \sum_k e^{-ikr_i} c_{k\sigma}^\dagger \right) \left(\frac{1}{\sqrt{N}} \sum_{k'} e^{ik'r_{i+2}} c_{k'\sigma} \right) \right. \\ &\quad \left. + \left(\frac{1}{\sqrt{N}} \sum_k e^{-ik\cdot r_{i+2}} c_{k\sigma}^\dagger \right) \left(\frac{1}{\sqrt{N}} \sum_{k'} e^{ikr_i} c_{k'\sigma} \right) \right) \\ &= -t_1 \sum_{kk'\sigma} \left(\left(\frac{1}{N} \sum_i e^{-i(k-k')r_i} \right) e^{ik'a} c_{k\sigma}^\dagger c_{k'\sigma} + \left(\frac{1}{N} \sum_i e^{-i(k-k')r_i} \right) e^{-ika} c_{k\sigma}^\dagger c_{k'\sigma} \right) \\ &\quad - t_2 \sum_{kk'\sigma} \left(\left(\frac{1}{N} \sum_i e^{-i(k-k')r_i} \right) e^{i2k'a} c_{k\sigma}^\dagger c_{k'\sigma} \right. \\ &\quad \left. + \left(\frac{1}{N} \sum_i e^{-i(k-k')r_i} \right) e^{-i2ka} c_{k\sigma}^\dagger c_{k'\sigma} \right) \end{aligned}$$

$$\begin{aligned}
&= -t_1 \sum_{kk'\sigma} (\delta_{kk'} e^{ik'a} c_{k\sigma}^\dagger c_{k'\sigma} + \delta_{kk'} e^{-ika} c_{k\sigma}^\dagger c_{k'\sigma}) \\
&\quad - t_2 \sum_{kk'\sigma} (\delta_{kk'} e^{i2k'a} c_{k\sigma}^\dagger c_{k'\sigma} + \delta_{kk'} e^{-i2ka} c_{k\sigma}^\dagger c_{k'\sigma}) \\
&= -t_1 \sum_{k\sigma} (e^{ika} + e^{-ika}) c_{k\sigma}^\dagger c_{k\sigma} - t_2 \sum_{k\sigma} (e^{i2ka} + e^{-i2ka}) c_{k\sigma}^\dagger c_{k\sigma} \\
&= -2t_1 \sum_{k\sigma} \cos(ka) c_{k\sigma}^\dagger c_{k\sigma} - 2t_2 \sum_{k\sigma} \cos(2ka) c_{k\sigma}^\dagger c_{k\sigma} \\
&= \sum_{k\sigma} \varepsilon_k c_{k\sigma}^\dagger c_{k\sigma}
\end{aligned}$$

Where, $\varepsilon_k = -2t_1 \cos(ka) - 2t_2 \cos(2ka)$ is the tight-binding energy spectrum.

C1 – Ground state energy

To obtain the ground state energy, equivalent to the one we obtain from solving the Hubbard model, we must work in the micro-canonical ensemble. That is, for a system of N sites, the possible values of ka between $-\pi$ and π are discretized uniformly into N values. For example, if $N = 4$, then the possible values of ka are $(0, \pm \frac{\pi}{2}, \pi)$. To obtain the ground state energy, we assign the N electrons (half-filling) into the states which have the lowest energy ε_k , provided that there are a maximum of two electrons per state with opposite spin (Pauli exclusion principle). The ground state energy is then the sum of the energies ε_k of the occupied states.

For example, when $N = 4$, the available states are $(0, \pm \frac{\pi}{2}, \pi)$ and the occupied (or partially occupied) states are $(0, \pm \frac{\pi}{2})$ for $\frac{t_2}{t_1} < 1$ and $(0, \pi)$ for $\frac{t_2}{t_1} > 1$. For 4 sites we need to correct ε_k to eliminate double counting in the next-nearest neighbour term. We do this by dividing t_2 by 2; hence, $\varepsilon_k = -2t_1 \cos(ka) - t_2 \cos(2ka)$. For $\frac{t_2}{t_1} < 1$ we can see that there is a degeneracy in states $ka = \pm \frac{\pi}{2}$, so we can have an electron in each state or both electrons in one of the states. Either configuration will give the same energy. The ground state energy per site can then be expressed as,

$$\begin{aligned}
\frac{E_o}{Nt_1} &= \frac{1}{N} (2\varepsilon_0 + 2\varepsilon_{\pi/2}) \theta\left(1 - \frac{t_2}{t_1}\right) + \frac{1}{N} (2\varepsilon_0 + 2\varepsilon_\pi) \theta\left(\frac{t_2}{t_1} - 1\right) \\
&= \frac{1}{4} \left(2\left(-2 - \frac{t_2}{t_1}\right) + 2\left(\frac{t_2}{t_1}\right) \right) \theta\left(1 - \frac{t_2}{t_1}\right) + \frac{1}{4} \left(2\left(-2 - \frac{t_2}{t_1}\right) + 2\left(2 - \frac{t_2}{t_1}\right) \right) \theta\left(\frac{t_2}{t_1} - 1\right)
\end{aligned}$$

$$= -\theta\left(1 - \frac{t_2}{t_1}\right) - \frac{t_2}{t_1}\theta\left(\frac{t_2}{t_1} - 1\right)$$

Where $\theta(x)$ is the Heaviside step function.

C2 – Structure factor

The structure factor is given by the following expression,

$$S(\vec{q}) = \sum_{ij} e^{i\vec{q}\cdot\vec{r}_{ij}} \langle \vec{S}_i \cdot \vec{S}_j \rangle$$

$$\vec{S}_i = \frac{1}{2} \sum_{ss'} c_{is}^\dagger \vec{\sigma}_{ss'} c_{is'}$$

In 1-D, $\vec{q} = q$ and $\vec{r}_{ij} = \vec{r}_j - \vec{r}_i = r_j - r_i$, therefore;

$$S(q) = \frac{1}{4} \sum_{ij} \sum_{ss'tt'} e^{iq(r_j - r_i)} \vec{\sigma}_{ss'} \cdot \vec{\sigma}_{tt'} \langle c_{is}^\dagger c_{is'} c_{jt}^\dagger c_{jt'} \rangle$$

Taking the Fourier transform of the creation and annihilation operators,

$$\langle c_{is}^\dagger c_{is'} c_{jt}^\dagger c_{jt'} \rangle$$

$$= \left\langle \left(\frac{1}{\sqrt{N}} \sum_k e^{-ikr_i} c_{ks}^\dagger \right) \left(\frac{1}{\sqrt{N}} \sum_{k'} e^{ik'r_i} c_{k's'} \right) \left(\frac{1}{\sqrt{N}} \sum_l e^{-ilr_j} c_{lt}^\dagger \right) \left(\frac{1}{\sqrt{N}} \sum_{l'} e^{il'r_j} c_{l't'} \right) \right\rangle$$

$$= \frac{1}{N^2} e^{-i(k-k')r_i} e^{-i(l-l')r_j} \langle c_{ks}^\dagger c_{k's'} c_{lt}^\dagger c_{l't'} \rangle$$

$$S(q) = \frac{1}{4N^2} \sum_{kk'll'} \sum_{ij} e^{iq(r_j - r_i)} e^{-i(k-k')r_i} e^{-i(l-l')r_j} \sum_{ss'tt'} \vec{\sigma}_{ss'} \cdot \vec{\sigma}_{tt'} \langle c_{ks}^\dagger c_{k's'} c_{lt}^\dagger c_{l't'} \rangle$$

$$= \frac{1}{4} \sum_{kk'll'} \frac{1}{N} \sum_i e^{-i(k-k'+q)r_i} \cdot \frac{1}{N} \sum_j e^{-i(l-l'-q)r_j} \sum_{ss'tt'} \vec{\sigma}_{ss'} \cdot \vec{\sigma}_{tt'} \langle c_{ks}^\dagger c_{k's'} c_{lt}^\dagger c_{l't'} \rangle$$

$$S(q) = \frac{1}{4} \sum_{kk'll'} \delta(k - k' + q) \delta(l - l' - q) \sum_{ss'tt'} (2\delta_{st'} \delta_{s't} - \delta_{ss'} \delta_{tt'}) \langle c_{ks}^\dagger c_{k's'} c_{lt}^\dagger c_{l't'} \rangle$$

$$= \frac{1}{4} \sum_{kl} \sum_{ss'tt'} (2\delta_{st'} \delta_{s't} - \delta_{ss'} \delta_{tt'}) \langle c_{ks}^\dagger c_{k+q,s'} c_{lt}^\dagger c_{l-q,t'} \rangle$$

$$\begin{aligned}
\langle c_{ks}^\dagger c_{k's'} c_{lt}^\dagger c_{l't'} \rangle &= \langle (\delta_{kk'} \delta_{ss'} - c_{k's'} c_{ks}^\dagger) (\delta_{ll'} \delta_{tt'} - c_{l't'} c_{lt}^\dagger) \rangle \\
&= \langle \delta_{kk'} \delta_{ss'} \delta_{ll'} \delta_{tt'} - \delta_{kk'} \delta_{ss'} c_{l't'} c_{lt}^\dagger - \delta_{ll'} \delta_{tt'} c_{k's'} c_{ks}^\dagger + c_{k's'} c_{ks}^\dagger c_{l't'} c_{lt}^\dagger \rangle \\
&= \delta_{kk'} \delta_{ss'} \delta_{ll'} \delta_{tt'} - \delta_{kk'} \delta_{ss'} \langle c_{l't'} c_{lt}^\dagger \rangle - \delta_{ll'} \delta_{tt'} \langle c_{k's'} c_{ks}^\dagger \rangle \\
&\quad + \langle c_{k's'} (\delta_{kl'} \delta_{st'} - c_{l't'} c_{ks}^\dagger) c_{lt}^\dagger \rangle \\
&= \delta_{kk'} \delta_{ss'} \delta_{ll'} \delta_{tt'} - \delta_{kk'} \delta_{ss'} \langle c_{l't'} c_{lt}^\dagger \rangle - \delta_{ll'} \delta_{tt'} \langle c_{k's'} c_{ks}^\dagger \rangle + \delta_{kl'} \delta_{st'} \langle c_{k's'} c_{lt}^\dagger \rangle \\
&\quad - \langle c_{k's'} c_{l't'} c_{ks}^\dagger c_{lt}^\dagger \rangle \\
&= \delta_{kk'} \delta_{ss'} \delta_{ll'} \delta_{tt'} - \delta_{kk'} \delta_{ss'} \langle c_{l't'} c_{lt}^\dagger \rangle - \delta_{ll'} \delta_{tt'} \langle c_{k's'} c_{ks}^\dagger \rangle + \delta_{kl'} \delta_{st'} \langle c_{k's'} c_{lt}^\dagger \rangle \\
&\quad - \langle c_{k's'} c_{lt}^\dagger \rangle \langle c_{l't'} c_{ks}^\dagger \rangle + \langle c_{k's'} c_{ks}^\dagger \rangle \langle c_{l't'} c_{lt}^\dagger \rangle
\end{aligned}$$

Using, $\langle c_{k's'} c_{l't'} c_{ks}^\dagger c_{lt}^\dagger \rangle = \langle c_{k's'} c_{lt}^\dagger \rangle \langle c_{l't'} c_{ks}^\dagger \rangle - \langle c_{k's'} c_{ks}^\dagger \rangle \langle c_{l't'} c_{lt}^\dagger \rangle$

$$\begin{aligned}
S(q) &= \frac{1}{4} \sum_{kl} \sum_{ss'tt'} (2\delta_{st'} \delta_{s't} - \delta_{ss'} \delta_{tt'}) (\delta_{k,k+q} \delta_{ss'} \delta_{l,l-q} \delta_{tt'} - \delta_{k,k+q} \delta_{ss'} \langle c_{l-q,t'} c_{lt}^\dagger \rangle \\
&\quad - \delta_{l,l-q} \delta_{tt'} \langle c_{k+q,s'} c_{ks}^\dagger \rangle + \delta_{k,l-q} \delta_{st'} \langle c_{k+q,s'} c_{lt}^\dagger \rangle \\
&\quad - \langle c_{k+q,s'} c_{lt}^\dagger \rangle \langle c_{l-q,t'} c_{ks}^\dagger \rangle + \langle c_{k+q,s'} c_{ks}^\dagger \rangle \langle c_{l-q,t'} c_{lt}^\dagger \rangle) \\
&= \frac{1}{4} \sum_{kl} \left(2 \sum_{st} (\delta_{q,0} \delta_{st} - \delta_{q,0} \delta_{st} \langle c_{l-q,s} c_{lt}^\dagger \rangle - \delta_{q,0} \delta_{ts} \langle c_{k+q,t} c_{ks}^\dagger \rangle + \delta_{k,l-q} \langle c_{k+q,t} c_{lt}^\dagger \rangle \right. \\
&\quad - \langle c_{k+q,t} c_{lt}^\dagger \rangle \langle c_{l-q,s} c_{ks}^\dagger \rangle + \langle c_{k+q,t} c_{ks}^\dagger \rangle \langle c_{l-q,s} c_{lt}^\dagger \rangle) \\
&\quad - \sum_{st} (\delta_{q,0} - \delta_{q,0} \langle c_{l-q,t} c_{lt}^\dagger \rangle - \delta_{q,0} \langle c_{k+q,s} c_{ks}^\dagger \rangle + \delta_{k,l-q} \delta_{st} \langle c_{k+q,s} c_{lt}^\dagger \rangle \\
&\quad \left. - \langle c_{k+q,s} c_{lt}^\dagger \rangle \langle c_{l-q,t} c_{ks}^\dagger \rangle + \langle c_{k+q,s} c_{ks}^\dagger \rangle \langle c_{l-q,t} c_{lt}^\dagger \rangle) \right) \\
&= \frac{1}{4} \sum_{kl} \left(\delta_{q,0} \left(2 \sum_s 1 - 2 \sum_s \langle c_{l-q,s} c_{ls}^\dagger \rangle - 2 \sum_s \langle c_{k+q,s} c_{ks}^\dagger \rangle - \sum_{st} 1 + \sum_{st} \langle c_{l-q,t} c_{lt}^\dagger \rangle \right. \right. \\
&\quad \left. \left. + \sum_{st} \langle c_{k+q,s} c_{ks}^\dagger \rangle \right) + \delta_{k,l-q} \left(2 \sum_{st} \langle c_{k+q,t} c_{lt}^\dagger \rangle - \sum_s \langle c_{k+q,s} c_{ls}^\dagger \rangle \right) \right. \\
&\quad \left. - 2 \sum_{st} \langle c_{k+q,t} c_{lt}^\dagger \rangle \langle c_{l-q,s} c_{ks}^\dagger \rangle + 2 \sum_{st} \langle c_{k+q,t} c_{ks}^\dagger \rangle \langle c_{l-q,s} c_{lt}^\dagger \rangle \right. \\
&\quad \left. + \sum_{st} \langle c_{k+q,s} c_{lt}^\dagger \rangle \langle c_{l-q,t} c_{ks}^\dagger \rangle - \sum_{st} \langle c_{k+q,s} c_{ks}^\dagger \rangle \langle c_{l-q,t} c_{lt}^\dagger \rangle \right)
\end{aligned}$$

$$\begin{aligned}
&= \frac{1}{4} \sum_{kl} \left(\delta_{q,0}(0) + 3\delta_{k,l-q} \sum_s \langle c_{k+q,s} c_{ls}^\dagger \rangle - 2 \sum_{st} \langle c_{k+q,t} c_{lt}^\dagger \rangle \langle c_{l-q,s} c_{ks}^\dagger \rangle \right. \\
&\quad + 2 \sum_{st} \langle c_{k+q,t} c_{ks}^\dagger \rangle \langle c_{l-q,s} c_{lt}^\dagger \rangle + \sum_{st} \langle c_{k+q,s} c_{lt}^\dagger \rangle \langle c_{l-q,t} c_{ks}^\dagger \rangle \\
&\quad \left. - \sum_{st} \langle c_{k+q,s} c_{ks}^\dagger \rangle \langle c_{l-q,t} c_{lt}^\dagger \rangle \right)
\end{aligned}$$

Using, $\langle c_{ks} c_{lt}^\dagger \rangle = \delta_{kl} \delta_{st} (1 - f(\varepsilon_{ks}))$; $f(\varepsilon_{ks}) = 1$ if state ks is occupied and 0 if it is not.

$$\begin{aligned}
S(q) &= \frac{1}{4} \sum_{kl} \left(3\delta_{k+q,l} \sum_s (1 - f(\varepsilon_{ks})) - 2\delta_{k+q,l} \sum_{st} (1 - f(\varepsilon_{k+q,t})) (1 - f(\varepsilon_{ks})) \right. \\
&\quad + 2\delta_{q,0} \sum_s (1 - f(\varepsilon_{ks})) (1 - f(\varepsilon_{ls})) \\
&\quad + \delta_{k+q,l} \sum_s (1 - f(\varepsilon_{k+q,s})) (1 - f(\varepsilon_{ks})) \\
&\quad \left. - \delta_{q,0} \sum_{st} (1 - f(\varepsilon_{ks})) (1 - f(\varepsilon_{lt})) \right)
\end{aligned}$$

$$\begin{aligned}
&= \frac{1}{4} \sum_k \left(-3 \sum_s f(\varepsilon_{ks}) + 6 - 2 \sum_{st} (1 - f(\varepsilon_{ks}) - f(\varepsilon_{k+q,t}) + f(\varepsilon_{ks})f(\varepsilon_{k+q,t})) \right. \\
&\quad + \sum_s (1 - f(\varepsilon_{ks}) - f(\varepsilon_{k+q,s}) + f(\varepsilon_{ks})f(\varepsilon_{k+q,s})) \\
&\quad + \frac{\delta_{q,0}}{4} \sum_{kl} \left(2 \sum_s (1 - f(\varepsilon_{ks}) - f(\varepsilon_{ls}) + f(\varepsilon_{ks})f(\varepsilon_{ls})) \right. \\
&\quad \left. - \sum_{st} (1 - f(\varepsilon_{ks}) - f(\varepsilon_{lt}) + f(\varepsilon_{ks})f(\varepsilon_{lt})) \right)
\end{aligned}$$

$$\begin{aligned}
&= \frac{1}{4} \sum_k \left((6 - 8 + 2) + (4 - 3 - 1) \sum_s f(\varepsilon_{ks}) + (4 - 1) \sum_s f(\varepsilon_{k+q,s}) \right. \\
&\quad \left. - 2 \sum_{st} f(\varepsilon_{ks})f(\varepsilon_{k+q,t}) + \sum_s f(\varepsilon_{ks})f(\varepsilon_{k+q,s}) \right) \\
&\quad + \frac{\delta_{q,0}}{4} \sum_{kl} \left((4 - 4) + (2 - 2) \sum_s f(\varepsilon_{ks}) + (2 - 2) \sum_s f(\varepsilon_{ls}) \right. \\
&\quad \left. + 2 \sum_s f(\varepsilon_{ks})f(\varepsilon_{ls}) - \sum_{st} f(\varepsilon_{ks})f(\varepsilon_{lt}) \right)
\end{aligned}$$

$$\begin{aligned}
&= \frac{1}{4} \sum_k \left(3 \sum_s f(\varepsilon_{k+q,s}) - 2 \sum_{st} f(\varepsilon_{ks}) f(\varepsilon_{k+q,t}) + \sum_s f(\varepsilon_{ks}) f(\varepsilon_{k+q,s}) \right) \\
&\quad + \frac{\delta_{q,0}}{4} \sum_{kl} \left(2 \sum_s f(\varepsilon_{ks}) f(\varepsilon_{ls}) - \sum_{st} f(\varepsilon_{ks}) f(\varepsilon_{lt}) \right)
\end{aligned}$$